Distribution Agreement

In presenting this thesis or dissertation as a partial fulfillment of the requirements for an advanced degree from Emory University, I hereby grant to Emory University and its agents the non-exclusive license to archive, make accessible, and display my thesis or dissertation in whole or in part in all forms of media, now or hereafter known, including display on the world wide web. I understand that I may select some access restrictions as part of the online submission of this thesis or dissertation. I retain all ownership rights to the copyright of the thesis or dissertation. I also retain the right to use in future works (such as articles or books) all or part of this thesis or dissertation.

Signature:

_____ _____

Colin Swenson Date

Harnessing the Dual Nature of Peptide Nucleic Acids

By

Colin S. Swenson
Doctor of Philosophy

Chemistry

Prof. Jennifer M. Heemstra
Advisor

Prof. David G. Lynn
Committee Member

Prof. William M. Wuest
Committee Member

Accepted:

Lisa A. Tedesco, Ph.D.
Dean of the James T. Laney School of Graduate Studies

Date

Harnessing the Dual Nature of Peptide Nucleic Acids

By

Colin S. Swenson
B.S., University of Utah, 2015

Advisor: Jennifer M. Heemstra, Ph.D.

An abstract of
A dissertation submitted to the Faculty of the
James. T. Laney School of Graduate Studies of Emory University
in partial fulfillment of the requirements for the degree of
Doctor of Philosophy
in Chemistry
2020

Abstract

Harnessing the Dual Nature of Peptide Nucleic Acids
By Colin S. Swenson

Peptide nucleic acid is a unique synthetic nucleic acid analogue wherein the canonical negatively charged phosphate backbone has been replaced by a neutral pseudopeptide backbone. This peptide-like backbone imparts significant properties such as stronger affinity and specificity for base pairing with DNA and RNA as well as increased hydrolase resistance and stability in complex environments. These properties have made PNA a prime candidate to improve hybridization-based applications such as antisense interactions, nucleic acid detection, and gene editing by taking advantage of the nucleic acid nature. However, the ability to incorporate complex amino acid functional groups within the PNA backbone remains a less explored avenue for utilizing PNA as a peptide mimic. This thesis aims to highlight the dual nature of PNA, to be useful as both a nucleic acid and peptide mimic. In Chapter 1, I provide a literature review to introduce the concepts of PNA with amino acid functionality and applications therein. In Chapter 2, I describe a “bilingual” PNA wherein a complex amphiphilic amino acid sequence embedded in the backbone drives self-assembly into micellar architectures similar to peptide amphiphiles. The nucleic acid code can then be accessed sequence-specifically, resulting in disassembly and highlighting the first example of a PNA acting as both nucleic acid and peptide. In Chapter 3, I explore the use of forced-intercalation PNA probes (FIT-PNA) for detection of an adenosine to inosine modification in nucleic acids. I show the synthesis of a novel malachite green PNA monomer and the fluorescence properties of three individual FIT-PNAs when hybridized to RNA and DNA targets. I determine that the surrogate base dye thiazole orange is a viable candidate for future studies. In Chapter 4, I evaluate the effect of ionic strength on PNA:DNA hybridization and determine that the association rate is significantly affected whereas the dissociation rate is less affected. I then describe the use of a small molecule, glyoxal, to thermoreversibly cage and decage the Franklin-Watson-Crick face to disrupt and restore duplex formation, respectfully. Finally, in Chapter 5 I discuss the practical implications of the presented studies and consider avenues for future directions and applications.

Harnessing the Dual Nature of Peptide Nucleic Acids

By

Colin S. Swenson
B.S., University of Utah, 2015

Advisor: Jennifer M. Heemstra, Ph.D.

A dissertation submitted to the Faculty of the
James. T. Laney School of Graduate Studies of Emory University
in partial fulfillment of the requirements for the degree of
Doctor of Philosophy
in Chemistry
2020

Acknowledgements

Graduate school has been a time for unreal growth through a variety of hurdles, relationships, and adversity. I believe my doctoral experience was unique: beginning graduate school with no prior research experience, moving across the country halfway through the program, and completing the requirements through a pandemic. For these reasons, I feel there is a long list of people to whom I must give my gratitude, for I would not have made it this far without a lot of help.

First off, I need to thank my advisor Prof. Jennifer M. Heemstra. I will be forever grateful for her belief in me and the opportunities she provided. She gave me a chance to perform research and ultimately to attend graduate school. Her enthusiasm for science, leadership, mentoring, and personal growth is extremely contagious and I am thankful that I was able to study in the collaborative, interdisciplinary, and congenial environment she created.

I would also like to thank my committee members at Emory University, Prof. David G. Lynn and Prof. William (Bill) M. Wuest for their support and guidance, as well as the faculty and staff of the Department of Chemistry, especially Kira Walsh, Ana Velez, and Todd Polley for making our transition to Emory smooth and simple.

I am thankful for all of my colleagues in the Heemstra Lab, past and present. I want to extend my personal gratitude to Hector S. Argueta-Gonzalez for his patience and hard work on the PNA amphiphiles project and for putting up with me through my growth as a mentor. I also want to thank Dr. Hershel H. Lackey and our collaborators at the University of Utah, Prof. Joel M. Harris, Dr. Eric M. Petersen, and Eric J. Reece for their contribution to the investigation of PNA:DNA hybridization, through collecting all of the single-molecule kinetics data and analyses. I am extremely grateful towards my roommates over the past years, Dr. Tewoderos M. Ayele (“T”) and Steve D. Knutson. Our nights discussing research on the couch over a few beers (or a bit

more than a few) served as a stress deterrent as well as a fountain of knowledge and ideas that we were able to bring with us into the lab. Steve also greatly contributed to the glyoxal caging of PNA by providing the data on the caging, decaging, and DNA binding assays for which I am thankful.

Finally, I want to thank all of my friends and family. Thank you to my father and mother, Matt and Janelle Swenson, for continually providing unconditional love and support in anything I want to accomplish, be it a Ph.D. program or making enchiladas. Thank you to my older sister, Brittney Kettwich, for always being around for a fun chat while teaching me kindness and selflessness. Thank you to my grandparents, Stu and Joyce Swenson and Paul and Birdie Williams, for always expressing their interest and pride in everything I do. Lastly, thank you to my partner, Hayley Ann Bunn, for being my best friend, biggest supporter, and pushing me to keep trying and working hard even when I'm at my lowest.

Table of Contents

List of Tables and Figures:

Chapter 1

Peptide Nucleic Acids Harness Dual Information Codes in a Single Molecule[1*]

1.1 Abstract:

Nature encodes the information required for life in two fundamental biopolymers: nucleic acids and proteins. Peptide nucleic acid (PNA), a synthetic analog comprised of nucleobases arrayed along a pseudopeptide backbone, has the ability to combine the power of nucleic acids to encode information with the versatility of amino acids to encode structure and function. Historically, PNA has been perceived as a simple nucleic acid mimic having desirable properties such as high biostability and strong affinity for complementary nucleic acids. The aim of this thesis is to adjust this perception by highlighting the ability of PNA to act as a peptide mimic and showing the largely untapped potential to encode information in the amino acid sequence. First, we provide an introduction to PNA and discuss the use of conjugation to impart tunable properties to the biopolymer. Next, we describe the integration of functional groups directly into the PNA backbone to impart specific physical properties. We then highlight the use of these integrated amino acid side chains to encode peptide-like sequences in the PNA backbone, imparting novel activity and function and demonstrating the ability of PNA to simultaneously mimic both a peptide and a nucleic acid. Finally, we summarize and highlight the objectives of the chapters found in this dissertation.

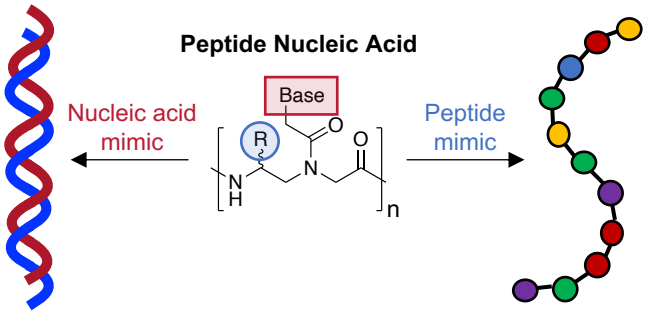

[*] Adapted from Ref. 1 with permission from The Royal Society of Chemistry.

1.2 Introduction:

Proteins and nucleic acids are two of the essential building blocks of life, necessary for both cellular information storage and biological function. Nature has evolved these biopolymers over millions of years to create and refine their properties. The amino acid sequences in peptides and proteins encode intricate structural information that enables complex functions, and researchers have investigated and probed these codes in order to appropriate their function for a wide range of applications.[2–4] In parallel, nucleic acids are virtually unmatched in their capacity to store retrievable information necessary for life and the nucleotide code offers exceptionally predictable and precise molecular recognition properties. Scientists have extensively studied and utilized this recognition ability for naturally occurring nucleic acids,[5,6] and many different forms of unnatural nucleic acids have been developed to improve upon the physical properties of canonical DNA and RNA.[7,8]

Peptide nucleic acid (PNA) is an interesting and powerful nucleic acid analogue developed by Nielsen and coworkers in which the negatively charged phosphate backbone is replaced with a neutral pseudopeptide backbone (**Figure 1.1**).[9] This peptide-like backbone, combined with the ability to undergo complementary Franklin-Watson-Crick hybridization, is responsible for a number of desirable properties such as improved binding affinity, enhanced specificity, and strong resistance to chemical and enzymatic degradation.[9–13] Therefore, it is not surprising that PNA has garnered significant interest in a number of research areas. For example, as a tool in medicine and biology, therapeutic and antimicrobial PNAs can be designed to regulate gene expression through antisense interactions or nuclease-like activity.[14–19] PNA has been used as a delivery vehicle for nucleic acid therapeutics and PNA-based approaches to gene editing have also been described.[20–24] In molecular imaging and diagnostics, the enhanced recognition properties of PNA are promising for the development

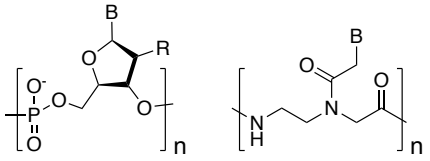

DNA, R = H
RNA, R = OH

PNA

Figure 1.1: Chemical structures of DNA, RNA, and PNA.

of methods for detection and in situ visualization of DNA and RNA.[25] Each of these uses for PNA have been extensively reviewed and rely solely upon the ability of PNA to function as a nucleic acid analogue.[26–32] Looking beyond the ability of PNA to undergo Franklin-Watson-Crick base pairing, the pseudopeptide nature of the PNA backbone also allows for direct inclusion of amino acid functionality, and researchers have utilized this capability to introduce side chains that enhance solubility or cellular uptake.[33,34] We recognized that the amino acid sequence could also be used to encode information to direct assembly, opening the door to the use of PNA as both a nucleic acid and a peptide analogue.

In this thesis introduction, ways in which the structure of PNA has been synthetically altered to afford increased functionality and structural information are discussed. Specifically, we first highlight examples of PNA conjugates that include terminally appended amino acids or lipids to create peptide-like mimics or impart structural changes. We then focus on modifications that have allowed the insertion of amino acid-like side chains in the PNA backbone, including their design, synthesis, characterization, and functional properties. We also describe the hybridization properties of PNA and the changes upon modification. Finally, we discuss examples of PNA as peptide mimics and describe the objectives of this dissertation in relation to the included chapters.

1.3 Conjugation of PNA:

PNA suffers from inherent weaknesses such as low solubility and cell permeability, which hinder its use in many biomedical applications.[35,36] In order to overcome these limitations, researchers have developed strategies for conjugating a variety of functional groups to the termini. PNA benefits from high chemical stability and is synthesized through standard solid-phase peptide synthesis (SPPS) procedures employing Fmoc- or Boc-based strategies.[36] Therefore, it is relatively easy to functionalize the termini with modifiers that can be added using the same amino acid chemistry, including peptides and hydrophobic moieties such as lipids or alkyl chains.[37]

1.3.1 PNA conjugated to peptides

A simple method to increase the solubility of PNA is to include charged amino acid residues through the solid-phase synthesis procedure.[36] Incorporating one or more lysine or arginine residues at either terminus results in enhanced solubility, presumably due to an increase in charge and therefore hydrophilicity. The simplicity of adding additional amino acids during synthesis has led to a number of PNA-amino acid conjugates having improved solubility.

Several molecules having potential biological applications lack inherent cell permeability, and a common approach for improving the cellular uptake is to attach cell penetrating peptides (CPPs).[38] These cationic peptides facilitate movement across cell and tissue barriers that would otherwise prevent uptake. Covalent attachment of these peptides to PNA results in CPP-PNA conjugates that have improved cellular uptake, and thus increased efficacy in biological applications such as antisense gene regulation (**Figure 1.2**).[39] As an example, Nielsen and coworkers observed the uptake of PNA conjugated to pAnt (a 17-residue fragment of the protein antennapedia) and pTat (a 14-residue fragment of HIV Tat protein) in five cell types (SK-BR-3, HeLa, IMR-90, U937, and H9), whereas unmodified PNA showed no uptake.[40] However, in these cases the PNA primarily localized to vesicular compartments and did not escape endosomal entrapment.

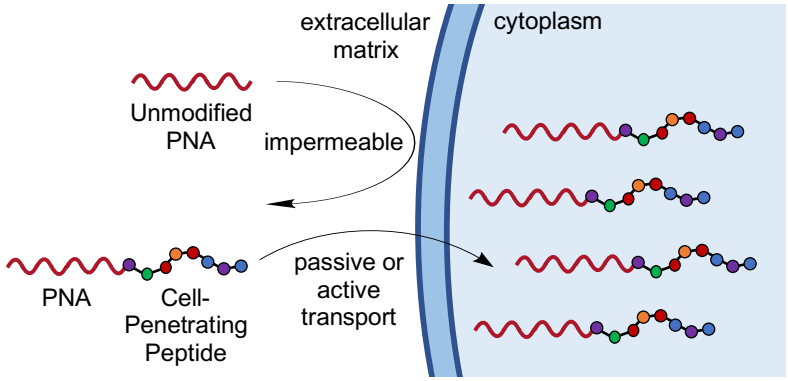

Figure 1.2: Modification of PNA with a cell-penetrating peptide increases cell permeability via passive or active transport.

In order to ascertain the cellular internalization of PNA, Bendifallah et. al. employed a luciferase-based activity assay for CPP-PNAs.[41] Using a series of unique conjugation techniques, they examined seven distinctive CPPs including a nuclear localization sequence (NLS) and a simple stretch of positively charged arginine residues (R7-9). Transportan-conjugated PNA as well as the arginine-based conjugates displayed increased activity. Interestingly, delivery efficacy was dependent on the chemical nature and position of the covalent linker. An NLS sequence had previously been shown to increase uptake, likely due to the increased positive charge.[42] However, in the aforementioned study, the NLS-PNA conjugates showed minimal or no activity. This could be explained by the difference in cell types and targets used for each study. An expanded number of CPP-PNAs and their delivery efficiency in different cell types have been studied and reported but further investigation is required to fully elucidate the relationship between identity and efficacy.[43–45]

The attachment of CPPs to PNA resulted in an abundance of knowledge regarding methods to fuse peptides to PNA to enhance the properties of this nucleic acid analogue for biomedical applications. However, in these examples the peptide and PNA portions are designed to act autonomously, each imparting their own chemical and biological properties independent of the other. Looking beyond this, researchers envisioned PNA conjugates in which the properties of each segment modulate and enhance the properties of the architecture as a whole, and to this end developed amphiphiles in which the PNA and appended functionality serve to direct assembly.

1.3.2 Amphiphilic PNA conjugates

Peptide amphiphiles are an attractive class of molecules that are capable of assembling into supramolecular architectures at the nanoscale.[46,47] These typically consist of a short hydrophilic peptide sequence ligated to a hydrophobic domain such as a lipid or alkyl chain.[48] PNA comprised of a neutral polyamide backbone and canonical nucleobases is inherently hydrophobic, but strategic placement of amino acids and hydrophobic lipid or alkyl domains can

induce amphiphilic behavior and promote controlled assembly analogous to that of peptide amphiphiles (**Figure 1.3A**).[49] Stupp and coworkers demonstrated this phenomenon through the synthesis of an amphiphilic PNA-peptide conjugate.[50] A β-sheet promoting peptide sequence (KGGGAAAK) followed by a palmitoyl alkyl chain was conjugated to the C-terminus of a polythymine PNA heptamer using SPPS methods. Transmission electron microscopy (TEM) and circular dichroism (CD) revealed the formation of uniform nanofibers under aqueous conditions (pH > 7), consistent with similar peptide amphiphiles. Thermal denaturation experiments revealed a significant increase in affinity and specificity for the fully matched polyadenine DNA when self-assembled into nanostructures as opposed to acting as free PNA in solution. Taken together, these results are promising for applications such as biosensing and purification, which require high specificity and strong binding to oligonucleotide targets.[50]

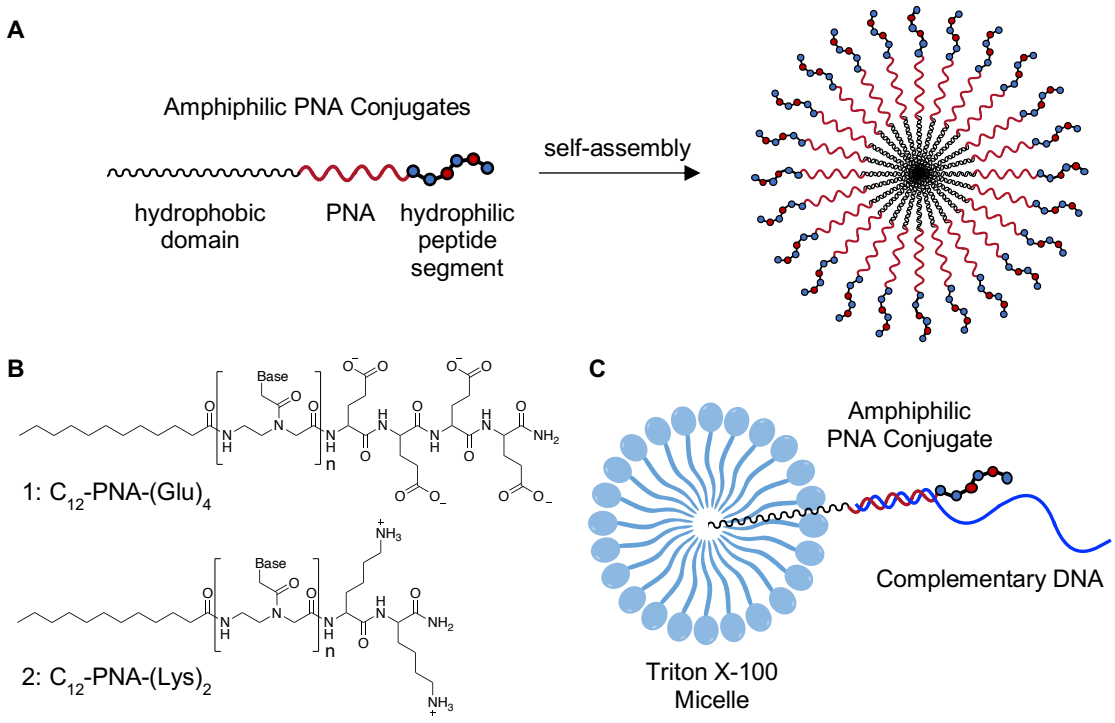

Figure 1.3: Examples of amphiphilic PNA conjugates. A) Structure and self-assembly of amphiphilic PNA conjugates having a PNA segment between a hydrophobic domain and a hydrophilic peptide. B) Chemical structures of (1) negatively charged and (2) positively charged PNA amphiphiles. C) TX-100/PNA micelles can be used for purification of DNA PCR products. Adapted from Ref. 54 with permission from Grosser, S.T. et al. *Anal. Chem.* 2007, *79* (24), 9513–9519. Copyright 2007 American Chemical Society.

Amphiphiles wherein the PNA oligomer is positioned between a hydrophilic peptide segment and a hydrophobic domain have also been described (**Figure 1.3A**). Schneider and coworkers produced a series of PNA amphiphiles having varied PNA sequences, hydrophilic peptides, and alkyl chains.[51,52] Specifically, they explored the use of positively charged lysine and negatively charged glutamic acid as the hydrophilic head groups (**Figure 1.3B**). As expected, the longer the PNA sequence and alkyl chain, the greater the number of charged amino acids required for solubility. Inclusion of negatively charged glutamic acids produced PNA amphiphiles having a lower critical micelle concentration (CMC) compared to the positively charged lysines. Additionally, the position of PNA in the center of the constructs did not affect the binding stability or selectivity for a complementary DNA sequence.[51] These studies guided the design of DNA-binding liposomes through the use of a di-alkyl PNA amphiphile.[53] Incorporating the di-alkyl hydrophobic domain allowed co-extrusion of amphiphiles with phospholipids, enabling the PNA sequence to hybridize to target DNA for the development of highly sensitive bioanalytical devices. Later work showed that through co-assembly with a common surfactant, Triton X-100, micelles capable of binding to specific nucleic acid oligomers are formed (**Figure 1.3C**).[54] Utilizing this design, purification of single-stranded PCR products of varying lengths was accomplished by micellar electrokinetic chromatography in which the PNA-surfactant micelle acts as a “drag-tag” to shift the mobility, providing a rapid and gel-free DNA separation method.

In more recent work, Zhang and coworkers explored the assembly properties of semi-self-complementary PNA amphiphiles equipped with a hydrophobic alkyl chain and a negatively charged glutamic acid head group.[55] Their results indicated the ability of PNA:PNA duplexes to exist within a micellar architecture, presumably the result of a stabilizing or “cross-linking” effect through hybridization and stronger base stacking interactions. Although applications for this structural phenomenon are less immediately apparent, the authors suggest potential uses for this technology in oligonucleotide purification, gene-related therapeutics, and biomedical detection devices.

The chemical stability and synthetic versatility of PNA make it a promising candidate for the design of myriad conjugates having unique physical and structural characteristics. To this extent, researchers have taken advantage of the ease of covalent modification to install amino acids and lipids within PNA constructs. However, these designs require the addition of information-poor hydrophobic domains and long strings of charged amino acids that act independently of the inherently information-rich PNA segment. Furthermore, current strategies focus on utilizing the nucleic acid information of PNA while ignoring its peptide-like properties. A design that incorporates functional groups similar to amino acid side chains to alter the properties of the PNA oligomer itself would benefit from the dual identity of PNA as both a nucleic acid and a peptide.

1.4 Functional modifications to the PNA backbone:

The PNA scaffold is highly versatile, allowing the addition of many different functional groups through post-synthetic conjugation. Alternatively, functional groups may also be incorporated into the backbone through the use of modified PNA monomers in oligomer synthesis, and this approach offers the benefit of incorporating these modifications along the full length of PNA rather than solely at the termini.

1.4.1 Synthesis and properties of backbone modified PNA

PNA monomers can be synthesized in a few steps and on a large scale using relatively inexpensive starting materials.[56] Typically, the amine-protected backbone portion of the monomer is synthesized and then coupled to a nucleobase acetic acid to produce monomers compatible with SPPS. The PNA backbone presents a desirable location for modifications, as it can be synthesized using amino acid precursors, allowing a number of different functional

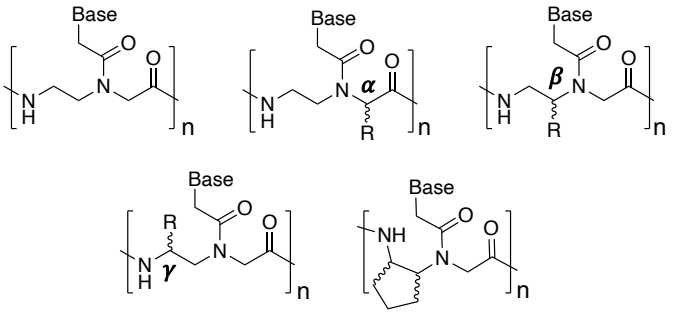

Figure 1.4: Chemical structures of unmodified PNA, α-PNA, β-PNA, γ-PNA, and cyclic PNA.

groups to be included.[57] For this reason, the PNA backbone has intrigued researchers and inspired the design of many modified PNA monomers. Specifically, chiral PNA monomers have been developed to include modifications at the α-, β-, and γ-positions, each with unique synthetic routes and resulting oligomer properties (**Figure 1.4**).[58]

α-Modified PNA (α-PNA) was the first backbone-modified PNA analogue to be designed and was reported by Nielsen et. al. In this initial example, glycine was replaced with L- or D-alanine during monomer synthesis.[59] The D-form was discovered to hybridize to complementary DNA with slightly higher affinity than the L-form, displaying a preference for a specific stereochemistry. Later functional groups incorporated at the α-position included lysine, serine, and arginine, the latter of which showed enhanced cellular uptake compared to unmodified PNA, similar to that of the TAT transduction domain peptide.[34,60,61] Bulky hydrophobic groups such as phenylalanine, tryptophan, valine, and leucine have also been incorporated at this position, displaying the versatility of α-PNA for functionalization.[62]

The development of β-modified PNA (β-PNA) is a relatively new field, likely due to the significant synthetic barriers compared to that of α-PNA. However, monomers containing methyl groups at the β-position have been produced and their hybridization properties explored.[63] Cyclic PNA monomers containing chiral centers at both the β- and γ-positions have also been synthesized.[64–69] Cyclopentane-derived PNAs have been shown to be promising diagnostic agents because of their improved binding affinity and selectivity for DNA or RNA.[64,65,68,69]

γ-Modified PNA (γ-PNA) is perhaps the most widely explored and promising candidate for including functional groups in the backbone, and modifications have been explored to improve a range of physicochemical properties such as solubility, cell permeability, and hybridization stability. The first γ-PNA monomer was synthesized by reacting an alanine amino acid aldehyde with glycine through reductive amination.[70] Similar to α-PNA, the identity of the stereocenter was found to be important for hybridization affinity to complementary DNA. γ-PNA synthesized from L-

amino acids exhibited a significantly higher affinity than those produced from D-amino acids, indicating that stereochemical purity is important for binding affinity.[71] Understanding this significance, Ly and coworkers developed a synthetic route based on a Mitsunobu coupling reaction to produce optically pure γ-PNA for improvements towards antigene applications.[72] Regardless of the route, γ-PNA has been produced containing a variety of hydrophilic and hydrophobic side chains, including lysine, guanidine, mercaptomethyl, hydroxymethyl, sulfate, aspartic acid, miniPEG, valine, leucine, and phenylalanine.[33,34,73–78] This structurally diverse range of functional groups able to be incorporated at this position enables researchers to fine-tune specific physical characteristics for many applications.

1.4.2 Hybridization properties of PNA

PNA hybridizes to single- or double-stranded DNA in different arrangements depending on the sequence and backbone modifications (**Figure 1.5**).[9,11,79–84] Cytosine-rich homopyrimidine PNAs have been shown to bind double-stranded DNA in a triple helix, or triplex, configuration through Hoogsteen base pairing.[79] Alternatively, thymine-rich homopyrimidine PNA was shown to bind in a triplex wherein two PNAs hybridize to a single homopurine DNA strand by Franklin-Watson-Crick and Hoogsteen base pairing.[80,81] This occurs through a strand invasion process in which one DNA strand in the duplex is displaced by the competing PNA strands.[9,81] It was later discovered that single mixed purine and pyrimidine PNA strands are also capable of forming stable Franklin-Watson-Crick duplexes with complementary DNA in a 1:1 ratio.[11] However, a single unmodified PNA of mixed purine and pyrimidines is incapable of invading double stranded linear DNA.[82] It is

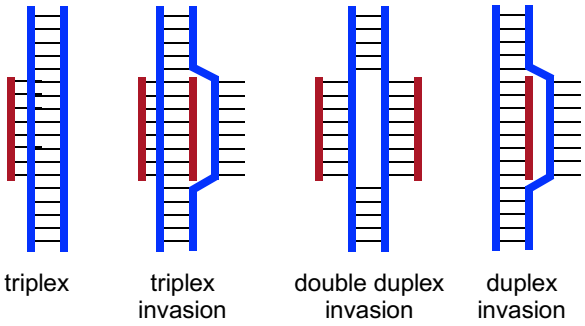

Figure 1.5: Hybridization modes of PNA (red) to complementary nucleic acids (blue). Adapted from Lohse, J. et al. *Proc. Natl. Acad. Sci. U. S. A.* 1999, *96* (21), 11804–11808. Copyright 1999 National Academy of Sciences.

possible to form double duplexes through the use of two PNA strands targeting separate DNA strands in the duplex, but this approach requires the use of pseudocomplementary nucleobases and multiple PNA strands, complicating synthesis and design.[83] Including modifications in the backbone significantly increases binding affinity and allows a single PNA to target double stranded DNA or RNA in a sequence-specific manner through a strand invasion mechanism. As an example of this, incorporating a methyl group at the γ-position in the PNA scaffold revealed the formation of PNA:DNA duplexes by strand invasion.[84] Interestingly, the backbone modified PNA hybridized to the DNA solely in a double helix arrangement, and no evidence of triplex or double duplexes was observed.

In contrast to unmodified PNA, which is flexible and can bind complementary nucleic acids in a parallel or anti-parallel fashion (with the N terminus of PNA being defined as equivalent to the 5' terminus of DNA or RNA),[11] chiral modified PNA pre-organizes into a left- or right-handed helix depending on the position and stereochemistry of the side chain (**Figure 1.6**).[85,86] This effect can stabilize or destabilize hybridization, presumably due to the entropic cost associated with rearrangement, and in cases of stabilization is likely responsible for the increased strand invasion capability.[84]

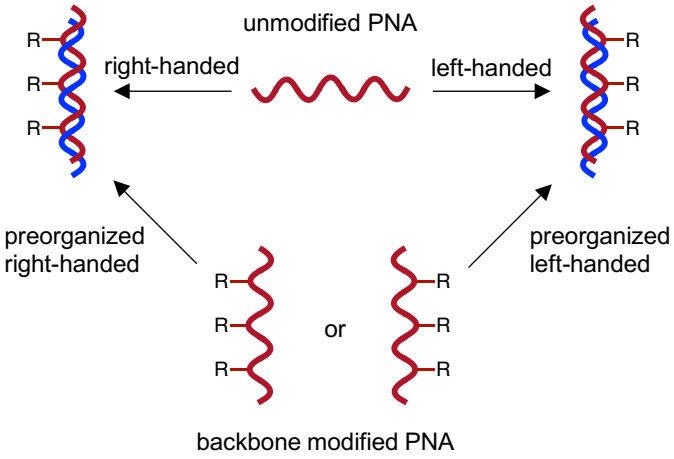

Figure 1.6: Backbone-modified PNA pre-organizes into left- or right-handed helices, dictating the helicity of the corresponding duplex.

Interestingly, a longstanding hypothesis in the field had been that the increased hybridization stability of PNA with DNA or RNA could be attributed to the lack of charge repulsion with the neutral backbone. However, our group explored the incorporation of negatively charged side chains into the PNA backbone and found that while affinity to DNA and RNA was dependent upon ionic strength, PNAs having negatively or positively charged side chains had similar affinities

at physiological ionic strength. From these data, we hypothesize that it is pre-organization of the backbone through hydrogen bonding interactions rather than the lack of charge that is responsible for the strong binding affinity of PNA to complementary nucleic acids.[77] This finding is important for applications such as charged-based delivery methods and the development of PNA therapeutics or materials, as it suggests that PNA can be synthesized to electrostatically mimic DNA and RNA and thus take advantage of the cellular delivery methods that are rapidly being developed for these nucleic acids.

1.4.3 Applications of backbone modified PNA

The exploration of structurally diverse backbone-modified PNAs has allowed researchers to gain a better understanding of structure-function relationships for this artificial biopolymer and expand the repertoire of applications that are possible. For example, the enhanced affinity and specificity afforded to modified PNAs increases their capacity to function as biosensors and capture probes. Marchelli et al. described the use of α-PNA containing a chiral D-lysine box to develop a method using capillary electrophoresis to detect a single point mutation in DNA related to cystic fibrosis.[87] Including the lysine functional groups increased the specificity and allowed researchers to distinguish between healthy, mutated homozygous, and heterozygous individuals. In a different example, rational design of a cyclopentane-derived cyclic β-PNA to adopt a pre-organized structure led to higher affinity and sequence specificity,[64,65] which was then used to detect pag anthrax DNA through a sandwich-based assay using two β-PNA probes.[69]

Backbone-modified PNAs have also shown significant potential for use in antisense and imaging applications. Incorporating arginine side chains in α-PNA or γ-PNA increases the solubility, hybridization, and cell permeability of PNA probes.[34,88] Manicardi et al. synthesized a series of 18-mer PNA probes containing eight arginine side chains at varying positions (α or γ) along the backbone (consecutive or alternating) that target miRNA-210 (**Figure 1.7A**).[89] Fluorescence-activated cell sorting revealed that each modified probe was internalized by cells,

with γ-modified probes exhibiting the highest level of uptake. Real-time quantitative PCR demonstrated the ability to inhibit the target miRNA-210 in leukemic K562 cells, presenting the first example of anti-miR activity using backbone-modified PNA. Importantly, resistance to enzymatic degradation was increased in the backbone-modified PNAs over an arginine-rich CPP-PNA conjugate, highlighting the advantage of internal side chain inclusion for in vivo applications. Similarly, Ly and coworkers decorated an α-PNA with arginine side chains to generate what they call guanidinium peptide nucleic acid (GPNA) and

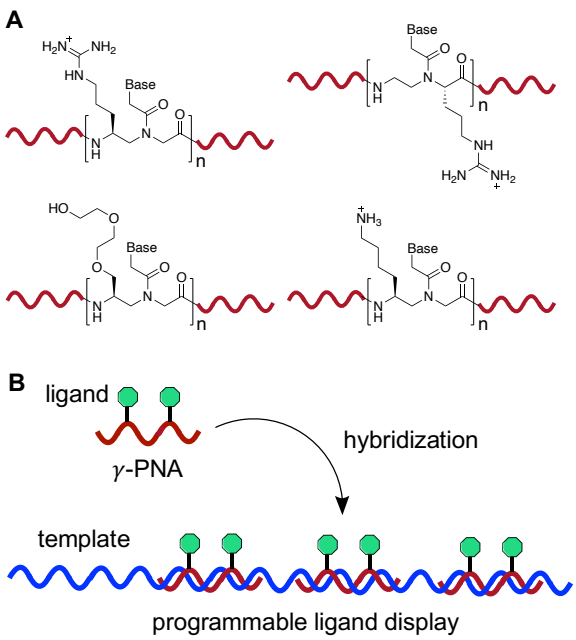

Figure 1.7: Examples of γ-modified PNAs. A) Chemical representations of α-PNA containing a guanidinium side chain and γ-PNA containing a guanidinium, miniPEG, or lysine side chains. B) γ-PNA can be functionalized for programmable multivalent ligand display.

demonstrated the ability to sequence-specifically inhibit transcription of the E-cadherin gene in live cells (**Figure 1.7A**).[90] Notably, they found that including the arginine side chains within the PNA backbone resulted in less cytotoxicity than conjugation of unfunctionalized PNA to an arginine-rich CPP. This group has also pioneered the invention of miniPEG PNA, the first example of a charge-neutral yet strongly hydrophilic modification in the PNA backbone (**Figure 1.7A**).[33] This modification was shown to allow the direct Franklin-Watson-Crick recognition of double helical B-DNA through a strand invasion mechanism, desirable for in vivo applications.[91] Gupta et al. used a γ-PNA containing miniPEG side chains to silence the activity of miR-210 and observed anti-tumor activity in mouse models.[92] Additionally, miniPEG γ-PNAs showed promise as imaging agents for intracellular staining of telomeric DNA.[93] The improved physicochemical

properties of backbone-modified PNA greatly augments its use for each of these in vivo applications.

Beyond typical hybridization-based applications, backbone-modified PNAs have been used as well-defined scaffolds for multivalent ligand display (**Figure 1.7B**).[94–97] For example, Appella and coworkers first synthesized a γ-PNA containing lysine side chains and found that it was a convenient position to attach bulky modifications without disrupting DNA and RNA binding (**Figure 1.7A and 1.7B**).[73,94] Using this technology, they demonstrated programmable multivalent display of a cyclic RGD analogue to block metastatic melanoma cell attachment, and modulated dopamine D_2 receptor activity by displaying a known agonist, (±)-PPHT.[95,96] These examples highlight the power of modifying the side chain sequence of PNA to display specific amino acid functional groups at precise spatial locations on the biopolymer.

In each of the examples presented, the inclusion of amino acid-like side chains into the PNA backbone resulted in a change of internal properties and the ability to adopt a pre-organized structure or spatially present functional groups in unique ways. Thus, addition of amino acid side chains to the backbone has benefitted PNA in numerous applications. However, the design and application of these modifications has largely been to enhance the nucleic acid recognition capability by increasing solubility, hybridization efficiency, or cellular uptake. In contrast, the abundant diversity of functional groups that can be included at multiple defined positions in the PNA scaffold represents a yet unrealized potential and underexplored avenue to encode information for activity, assembly, or structure analogous to peptides.

1.5 Encoding Amino Acid Information in the PNA Backbone:

The development of backbone-modified PNA revealed the underlying potential of PNA to act as both a peptide and nucleic acid mimic. By combining the information derived from PNA-peptide conjugates with the invention of functionally customized monomers, new information-rich constructs can be designed and investigated for a wide range of biological applications.

The use of PNA as a peptide mimic is still in its infancy and there are very few examples where the embedded amino acid sequence information is the main driver for structure or function. Marchelli and coworkers pioneered the consideration of PNA as a "peptide" through the first known example of inserting an amino acid sequence into the PNA backbone to promote activity.[98] Using a submonomeric synthetic strategy, a model PNA trimer conjugated to a rhodamine dye was synthesized containing an NLS sequence (PKKKRKV) at alternating α- and γ-positions in the backbone (**Figure 1.8**). Fluorescence microscopy images revealed high intracellular and nuclear localized levels of the modified PNA in Rhabdomyosarcoma cells, similar to that of the canonical NLS peptide. Unmodified PNA was not detected within the nuclei, providing evidence that the embedded amino acid information was responsible for the uptake and nuclear localization. The authors speculated that the amino acid sequence is able to interact with the receptor protein importin, resulting in importin-mediated nuclear transport. While further experimentation is required to ascertain the effects of both protein and nucleic acid binding to the PNA peptide mimic, this work demonstrated the feasibility of utilizing a complex peptide sequence for function, opening the doors to numerous applications in bioorganic chemistry and molecular biology.

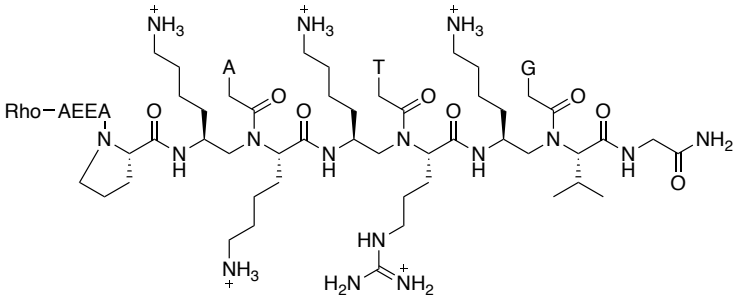

Figure 1.8: Chemical structure of PNA trimer with embedded NLS peptide sequence PKKKRKV. Side chains alternate between γ- and α-positions. "Rho" indicates a rhodamine dye.

1.6 Summary and Objectives of this Dissertation:

Chapter 2: Building upon the concept that PNA can be interpreted as a peptide mimic, our lab imagined the possibility of deriving controlled structural behavior through complex amino acid sequences. By combining the information-rich nucleic acid sequences with structurally diverse amino acid sequences into a single biopolymer, a tremendously programmable scaffold can be created for information storage and processing. The work presented in this thesis

describes our exploration of integrating defined codes of nucleic acids and amino acids in order to create a “bilingual” PNA. Inspired by peptide amphiphiles, we hypothesized that integrating a defined sequence of hydrophobic and hydrophilic amino acids along the PNA backbone would impart amphiphilic character and promote self-assembly analogous to folding or quaternary assembly of proteins. We present in Chapter 2 the design, synthesis, and characterization of “bilingual” PNA amphiphiles through incorporation of γ-PNA monomers derived from aliphatic alanine and positively charged lysine amino acid building blocks. We demonstrate that the amino acid code in these γ-PNA amphiphiles is responsible for promoting self-assembly into discrete micellar architectures, while the nucleic acid code can be accessed to support stimuli-responsive disassembly (**Figure 1.9**). These results provide the first example of a “bilingual biopolymer” using the PNA scaffold to simultaneously encode amino acid and nucleotide information to convey complex structural properties with specific molecular recognition. This design overcomes the inherent limitations of using the two codes separately and can serve as inspiration for a plethora of user-defined constructs for myriad applications in therapeutics, diagnostics, bioinspired materials, and biotechnology.[99]

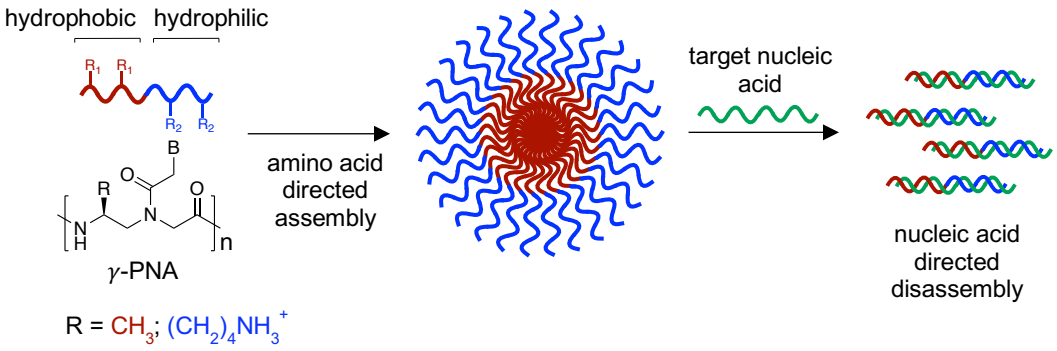

Figure 1.9: ”Bilingual” PNA. Amino acid side-chains direct self-assembly and disassembly is driven by recognition of a nucleobase sequence by a complementary target.

Chapter 3: In order to characterize our γ-PNA amphiphiles, I synthesized a novel fluorogenic PNA monomer based on the solvatochromic 4-dimethylamino(naphthalimide) (4-DMN) dye. This dye displays an enhanced fluorescence in hydrophobic environments, allowing a

turn-on signal upon self-assembly. We recognized this potential for use in forced-intercalation PNA (FIT-PNA) probes to image and detect single nucleotide polymorphisms. These probes selectively bind targets *via* complementary Franklin-Watson-Crick hybridization, prompting a fluorescent response from the dye.[100] We hypothesized that incorporating the 4-DMN dye, as well as another fluorogenic dye based on malachite green, into PNA oligomers that we could elicit a fluorescence response in the presence of a fully complementary target nucleic acid. In Chapter 3, We present the design and synthesis of FIT-PNA probes derived from 4-DMN, thiazole orange, and malachite green fluorogenic dyes to detect and image the deamination of adenosine to inosine (A → I) modification (**Figure 1.10**).[101] We further discuss the inherent characteristics of PNA as well as the ease of modifying the nucleobase portion to install desirable properties. We explore the effect on hybridization caused by dye incorporation, as well as the effect of temperature and adjacent nucleobase identity on fluorescence signal. We demonstrate that FIT-PNA probes containing thiazole orange are viable candidates for detecting this particular single nucleotide polymorphism in target nucleic acids and can be a useful tool for elucidating ADAR activity and mechanistic importance for *in vitro* and *in cellulo* applications.

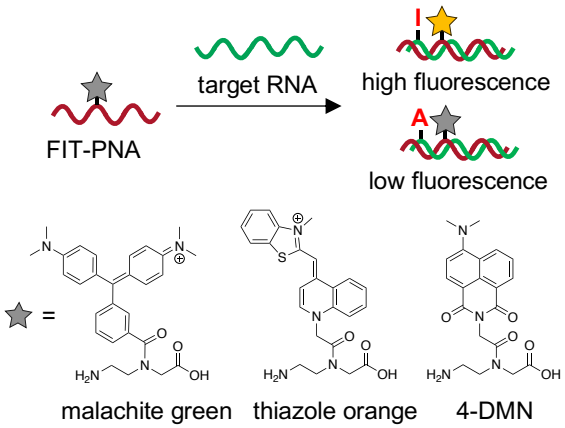

Figure 1.10: FIT-PNA probes enable detection of inosine-containing transcripts by enhanced fluorescence upon binding.

Chapter 4: Recognizing the tremendous potential of PNA for use in hybridization-based assays, we also wanted to further explore the properties of PNA:DNA hybridization. Previously, we used γ-PNA to determine the effect of charge on duplex affinity, noting that negatively and positively charged PNAs bound with similar affinities at physiological pH.[77] We wanted to expand our understanding of this relationship to elucidate how ionic strength governs the mechanism of duplex formation. In Chapter 4 we describe the design and synthesis of PNAs for use in single-

molecule kinetic experiments by total internal reflectance (TIRF) spectroscopy (**Figure 1.11A**). We developed a strategy to capture and hybridize PNA to a surface using a DNA target to measure the rates of association and dissociation at differing ionic strengths. Using this approach, we found that changes in ionic strength primarily affected the association rate of PNA, resulting in faster rates at lower ionic strengths, while the dissociation rate remained unaffected. Conversely, the association and dissociation rates of a comparable DNA sequence decreased and increased, respectively. We postulate that the increase in affinity of PNA:DNA duplexes compared to DNA:DNA stems from a considerable difference in the dissociation rate. These results provide important information for understanding PNA hybridization interactions for optimizing new and existing applications. We then sought to reversibly control hybridization by caging through reaction with glyoxal. Glyoxal is a small molecule that reacts with the Franklin-Watson-Crick face of guanine, adenine, and cytosine to disrupt hybridization.[102] Increasing temperature under mild alkaline conditions removes the glyoxal adducts, decaging targets to restore binding and duplex formation.[103] We demonstrate the thermoreversible interaction of glyoxal with PNA, effectively eliminating and restoring hybridization ability (**Figure 1.11B**). These results show the first example of chemically caging non-canonical nucleic acid substrates and support the use of glyoxal to thermally control PNA:DNA binding for potential in reversibly modulating antisense interactions and studying PNA hybridization interactions.

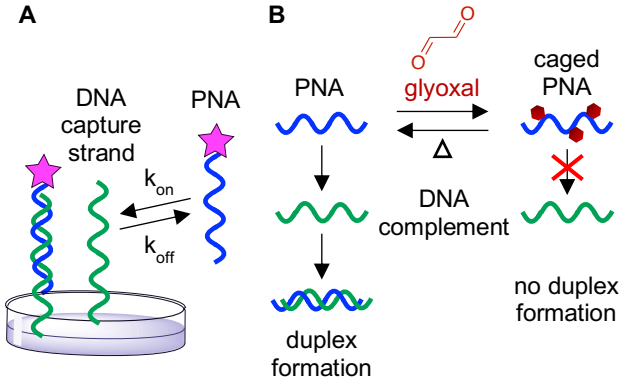

Figure 1.11: Techniques to study and control PNA hybridization. A) TIRF allows monitoring of single-molecule hybridization events. B) Thermally reversible glyoxal treatment inhibits hybridization of PNA:DNA duplexes.

1.7 Conclusions:

PNA is a highly programmable synthetic molecule with desirable properties such as chemical and enzymatic stability, increased specificity and affinity for complementary nucleic

acids, and the ability to fine-tune physical aspects through modification of the backbone and nucleobase portions. We are interested in harnessing this ability to explore constructs encoding the languages of both nucleic acids and proteins simultaneously in a single biopolymer, create tools for visualizing single nucleotide polymorphisms, and develop technologies for investigating PNA:DNA hybridization. In this thesis, we describe a “bilingual” PNA capable of amino acid-directed self-assembly and nucleobase-directed disassembly (Chapter 2). we demonstrate the design of a FIT-PNA probe capable of distinguishing between inosine and adenosine containing nucleic acid targets (Chapter 3). we explore the ionic strength-dependence of PNA:DNA hybridization kinetics and provide a technology to reversibly control duplex formation (Chapter 4). Finally, in Chapter 5 we discuss the broader implications of the work presented in this thesis as well as the future directions and applications of the present explorations.

1.8 References:

(1) Swenson, C. S.; Heemstra, J. M. Peptide Nucleic Acids Harness Dual Information Codes in a Single Molecule. *Chem. Commun.* **2020**, *56* (13), 1926–1935. https://doi.org/10.1039/c9cc09905k.

(2) Lee, A. C. L.; Harris, J. L.; Khanna, K. K.; Hong, J. H. A Comprehensive Review on Current Advances in Peptide Drug Development and Design. *Int. J. Mol. Sci.* **2019**, *20* (10), 1–21. https://doi.org/10.3390/ijms20102383.

(3) Huang, P. S.; Boyken, S. E.; Baker, D. The Coming of Age of de Novo Protein Design. *Nature* **2016**, *537* (7620), 320–327. https://doi.org/10.1038/nature19946.

(4) Sato, K.; Hendricks, M. P.; Palmer, L. C.; Stupp, S. I. Peptide Supramolecular Materials for Therapeutics. *Chem. Soc. Rev.* **2018**, *47* (20), 7539–7551. https://doi.org/10.1039/C7CS00735C.

(5) Seeman, N. C.; Sleiman, H. F. DNA Nanotechnology. *Nat. Rev. Mater.* **2018**, *3* (1), 17068. https://doi.org/10.1038/natrevmats.2017.68.

(6) Agrawal, S.; Gait, M. J. CHAPTER 1 History and Development of Nucleotide Analogues in Nucleic Acids Drugs. In *Advances in Nucleic Acid Therapeutics*; The Royal Society of Chemistry, 2019; pp 1–21. https://doi.org/10.1039/9781788015714-00001.

(7) Morihiro, K.; Kasahara, Y.; Obika, S. Biological Applications of Xeno Nucleic Acids. *Mol. Biosyst.* **2017**, *13* (2), 235–245. https://doi.org/10.1039/c6mb00538a.

(8) Ma, Q.; Lee, D.; Tan, Y. Q.; Wong, G.; Gao, Z. Synthetic Genetic Polymers: Advances and Applications. *Polym. Chem.* **2016**, *7* (33), 5199–5216. https://doi.org/10.1039/c6py01075j.

(9) Nielsen, P. E.; Egholm, M.; Berg, R. H.; Buchardt, O. Sequence-Selective Recognition of DNA by Strand Displacement with a Thymine-Substituted Polyamide. *Science (80-.).* **1991**, *254* (5037), 1497–1500. https://doi.org/10.1126/science.1962210.

(10) Demidov, V. V; Potaman, V. N.; Frank-Kamenetskii, M. D.; Egholm, M.; Buchardt, O.; Sonnichsen, S. H.; Nlelsen, P. E. Stability of Peptide Nucleic Acids in Human Serum and Cellular Extracts. *Biochem. Pharmacol.* **1994**, *48* (6), 1310–1313.

(11) Egholm, M.; Buchardt, O.; Christensen, L.; Behrens, C.; Freier, S. M.; Driver, D. A.; Berg, R. H.; Kim, S. K.; Norden, B.; Nielsen, P. E. PNA Hybridizes to Complementary Oligonucleotides Obeying the Watson–Crick Hydrogen-Bonding Rules. *Nature* **1993**, *365*, 566–568. https://doi.org/10.1038/365566a0.

(12) Uhlmann, E.; Peyman, A.; Breipohl, G.; Will, D. W. PNA: Synthetic Polyamide Nucleic Acids with Unusual Binding Properties. *Angew. Chemie Int. Ed.* **1998**, *37* (20), 2796–2823. https://doi.org/10.1002/chin.199909294.

(13) Nielsen, P. E.; Egholm, M.; Buchardt, O. Peptide Nucleic Acid (PNA). A DNA Mimic with a Peptide Backbone. *Bioconjug. Chem.* **1994**, *5* (1), 3–7. https://doi.org/10.1021/bc00025a001.

(14) Whitney, A.; Gavory, G.; Balasubramanian, S. Site-Specific Cleavage of Human Telomerase RNA Using PNA-Neocuproine·Zn(II) Derivatives. *Chem. Commun.* **2003**, *9* (1), 36–37. https://doi.org/10.1039/b210135a.

(15) Murtola, M.; Wenska, M.; Strömberg, R. PNAzymes That Are Artificial RNA Restriction Enzymes. *J. Am. Chem. Soc.* **2010**, *132* (26), 8984–8990. https://doi.org/10.1021/ja1008739.

(16) Gaglione, M.; Milano, G.; Chambery, A.; Moggio, L.; Romanelli, A.; Messere, A. PNA-Based Artificial Nucleases as Antisense and Anti-MiRNA Oligonucleotide Agents. *Mol. Biosyst.* **2011**, *7* (8), 2490–2499. https://doi.org/10.1039/c1mb05131h.

(17) Petersen, L.; de Koning, M. C.; van Kuik-Romeijn, P.; Weterings, J.; Pol, C. J.; Platenburg, G.; Overhand, M.; van der Marel, G. A.; van Boom, J. H. Synthesis and in Vitro Evaluation of PNA−Peptide−DETA Conjugates as Potential Cell Penetrating Artificial Ribonucleases. *Bioconjug. Chem.* **2004**, *15* (3), 576–582. https://doi.org/10.1021/bc034219p.

(18) Ghosal, A.; Nielsen, P. E. Potent Antibacterial Antisense Peptide-Peptide Nucleic Acid Conjugates against Pseudomonas Aeruginosa. *Nucleic Acid Ther.* **2012**, *22* (5), 323–334. https://doi.org/10.1089/nat.2012.0370.

(19) Narenji, H.; Teymournejad, O.; Rezaee, M. A.; Taghizadeh, S.; Mehramuz, B.; Aghazadeh, M.; Asgharzadeh, M.; Madhi, M.; Gholizadeh, P.; Ganbarov, K.; Yousefi, M.; Pakravan, A.; Dal, T.; Ahmadi, R.; Samadi Kafil, H. Antisense Peptide Nucleic Acids AgainstftsZ AndefaA Genes Inhibit Growth and Biofilm Formation of Enterococcus Faecalis. *Microb. Pathog.* **2020**, *139*, 103907. https://doi.org/10.1016/j.micpath.2019.103907.

(20) Nielsen, P. E.; Shiraishi, T. Peptide Nucleic Acid (PNA) Cell Penetrating Peptide (CPP) Conjugates as Carriers for Cellular Delivery of Antisense Oligomers. *Artif. DNA PNA XNA* **2011**, *2* (3), 90–99. https://doi.org/10.4161/adna.18739.

(21) Svahn, M. G.; Lundin, K. E.; Ge, R.; Törnquist, E.; Simonson, E. O.; Oscarsson, S.; Leijon, M.; Brandén, L. J.; Smith, C. I. E. Adding Functional Entities to Plasmids. *J. Gene Med.* **2004**, *6* (S1), S36–S44. https://doi.org/10.1002/jgm.510.

(22) Brandén, L. J.; Mohamed, A. J.; Smith, C. I. E. A Peptide Nucleic Acid-Nuclear Localization Signal Fusion That Mediates Nuclear Transport of DNA. *Nat. Biotechnol.* **1999**, *17* (8),

784–787. https://doi.org/10.1038/11726.

(23) Faruqi, A. F.; Egholm, M.; Glazer, P. M. Peptide Nucleic Acid-Targeted Mutagenesis of a Chromosomal Gene in Mouse Cells. *Proc. Natl. Acad. Sci. U. S. A.* **1998**, *95* (4), 1398–1403. https://doi.org/10.1073/pnas.95.4.1398.

(24) Bahal, R.; Ali McNeer, N.; Quijano, E.; Liu, Y.; Sulkowski, P.; Turchick, A.; Lu, Y. C.; Bhunia, D. C.; Manna, A.; Greiner, D. L.; Brehm, M. A.; Cheng, C. J.; López-Giráldez, F.; Ricciardi, A.; Beloor, J.; Krause, D. S.; Kumar, P.; Gallagher, P. G.; Braddock, D. T.; Mark Saltzman, W.; Ly, D. H.; Glazer, P. M. In Vivo Correction of Anaemia in β-Thalassemic Mice by Γ3PNA-Mediated Gene Editing with Nanoparticle Delivery. *Nat. Commun.* **2016**, *7*, 13304. https://doi.org/10.1038/ncomms13304.

(25) Nielsen, P. E.; Egholm, M. An Introduction to Peptide Nucleic Acid. *Curr. Issues Molec. Biol.* **1999**, *1* (2), 89–104.

(26) Pellestor, F.; Paulasova, P. The Peptide Nucleic Acids (PNAs), Powerful Tools for Molecular Genetics and Cytogenetics. *European Journal of Human Genetics*. **2004**, *12*(9), 697-700. https://doi.org/10.1038/sj.ejhg.5201226.

(27) D'Agata, R.; Giuffrida, M. C.; Spoto, G. Peptide Nucleic Acid-Based Biosensors for Cancer Diagnosis. *Molecules*. **2017**, *22*(11), 1951. https://doi.org/10.3390/molecules22111951.

(28) Gambari, R. Peptide Nucleic Acids: A Review on Recent Patents and Technology Transfer. *Expert Opin. Ther. Pat.* **2014**, *24* (3), 267–294. https://doi.org/10.1517/13543776.2014.863874.

(29) Gupta, A.; Mishra, A.; Puri, N. Peptide Nucleic Acids: Advanced Tools for Biomedical Applications. *J. Biotechnol.* **2017**, *259*, 148–159. https://doi.org/10.1016/j.jbiotec.2017.07.026.

(30) Wu, J.-C.; Meng, Q.-C.; Ren, H.-M.; Wang, H.-T.; Wu, J.; Wang, Q. Recent Advances in Peptide Nucleic Acid for Cancer Bionanotechnology. *Acta Pharmacol. Sin.* **2017**, *38*, 798–805. https://doi.org/10.1038/aps.2017.33.

(31) Narenji, H.; Gholizadeh, P.; Aghazadeh, M.; Rezaee, M. A.; Asgharzadeh, M.; Kafil, H. S. Peptide Nucleic Acids (PNAs): Currently Potential Bactericidal Agents. *Biomed. Pharmacother.* **2017**, *93*, 580–588. https://doi.org/10.1016/j.biopha.2017.06.092.

(32) Saarbach, J.; Sabale, P. M.; Winssinger, N. Peptide Nucleic Acid (PNA) and Its Applications in Chemical Biology, Diagnostics, and Therapeutics. *Curr. Opin. Chem. Biol.* **2019**, *52*, 112–124. https://doi.org/10.1016/j.cbpa.2019.06.006.

(33) Sahu, B.; Sacui, I.; Rapireddy, S.; Zanotti, K. J.; Bahal, R.; Armitage, B. A.; Ly, D. H. Synthesis and Characterization of Conformationally Preorganized, MiniPEG-Containing γ-PNAs with Superior Hybridization Properties and Water Solubility. *J. Org. Chem.* **2011**, *76* (14), 5614–5627. https://doi.org/10.1021/jo200482d.

(34) Zhou, P.; Wang, M.; Du, L.; Fisher, G. W.; Waggoner, A.; Ly, D. H. Novel Binding and Efficient Cellular Uptake of Guanidine-Based Peptide Nucleic Acids (GPNA). *J. Am. Chem. Soc* **2003**, *125* (23), 6878–6879. https://doi.org/10.1021/JA029665M.

(35) Wittung, P.; Kajanus, J.; Edwards, K.; Nielsen, P.; Nordén, B.; Malmström, B. G. Phospholipid Membrane Permeability of Peptide Nucleic Acid. *FEBS Lett.* **1995**, *365* (1), 27–29. https://doi.org/10.1016/0014-5793(95)00409-3.

(36) Braasch, D. A.; Corey, D. R. Synthesis, Analysis, Purification, and Intracellular Delivery of Peptide Nucleic Acids. *Methods* **2001**, *23* (2), 97–107. https://doi.org/10.1006/meth.2000.1111.

(37) Ljungstrøm, T.; Knudsen, H.; Nielsen, P. E. Cellular Uptake of Adamantyl Conjugated Peptide Nucleic Acids. *Bioconjug. Chem.* **1999**, *10* (6), 965–972. https://doi.org/10.1021/BC990053+.

(38) Guidotti, G.; Brambilla, L.; Rossi, D. Cell-Penetrating Peptides: From Basic Research to Clinics. *Trends in Pharmacological Sciences*. **2017**, *38*(4), 406-424. https://doi.org/10.1016/j.tips.2017.01.003.

(39) Díaz-Mochón, J. J.; Bialy, L.; Watson, J.; Sánchez-Martín, R. M.; Bradley, M. Synthesis

and Cellular Uptake of Cell Delivering PNA-Peptide Conjugates. *Chem. Commun.* **2005**, No. 26, 3316–3318. https://doi.org/10.1039/b503777h.

(40) Koppelhus, U.; Awasthi, S. K.; Zachar, V.; Holst, H. U.; Ebbesen, P.; Nielsen, P. E. Cell-Dependent Differential Cellular Uptake of PNA, Peptides, and PNA-Peptide Conjugates. *Antisense Nucleic Acid Drug Dev.* **2002**, *12* (2), 51–63.

(41) Bendifallah, N.; Rasmussen, F. W.; Zachar, V.; Ebbesen, P.; Nielsen, P. E.; Koppelhus, U. Evaluation of Cell-Penetrating Peptides (CPPs) as Vehicles for Intracellular Delivery of Antisense Peptide Nucleic Acid (PNA). *Bioconjug. Chem.* **2006**, *17* (3), 750–758. https://doi.org/10.1021/bc050283q.

(42) Cutrona, G.; Carpaneto, E. M.; Ulivi, M.; Roncella, S.; Landt, O.; Ferrarini, M.; Boffa, L. C. Effects in Live Cells of a C-Myc Anti-Gene PNA Linked to a Nuclear Localization Signal. *Nat. Biotechnol.* **2000**, *18* (3), 300–303. https://doi.org/10.1038/73745.

(43) Ndeboko, B.; Ramamurthy, N.; Lemamy, G. J.; Jamard, C.; Nielsen, P. E.; Cova, L. Role of Cell-Penetrating Peptides in Intracellular Delivery of Peptide Nucleic Acids Targeting Hepadnaviral Replication. *Mol. Ther. - Nucleic Acids* **2017**, *9*, 162–169. https://doi.org/10.1016/j.omtn.2017.09.003.

(44) Barkowsky, G.; Lemster, A. L.; Pappesch, R.; Jacob, A.; Krüger, S.; Schröder, A.; Kreikemeyer, B.; Patenge, N. Influence of Different Cell-Penetrating Peptides on the Antimicrobial Efficiency of PNAs in Streptococcus Pyogenes. *Mol. Ther. - Nucleic Acids* **2019**, *18*, 444–454. https://doi.org/10.1016/j.omtn.2019.09.010.

(45) Turner, Y.; Wallukat, G.; Säälik, P.; Wiesner, B.; Pritza, S.; Oehlke, J. Cellular Uptake and Biological Activity of Peptide Nucleic Acids Conjugated with Peptides with and without Cell-Penetrating Ability. *J. Pept. Sci.* **2010**, *16* (1), 71–80. https://doi.org/10.1002/psc.1198.

(46) Cui, H.; Webber, M. J.; Stupp, S. I. Self-Assembly of Peptide Amphiphiles: From Molecules to Nanostructures to Biomaterials. *Biopolymers* **2010**, *94* (1), 1–18. https://doi.org/10.1002/bip.21328.

(47) Hendricks, M. P.; Sato, K.; Palmer, L. C.; Stupp, S. I. Supramolecular Assembly of Peptide Amphiphiles. *Acc. Chem. Res.* **2017**, *50* (10), 2440–2448. https://doi.org/10.1021/acs.accounts.7b00297.

(48) Dasgupta, A.; Das, D. Designer Peptide Amphiphiles: Self-Assembly to Applications. *Langmuir* **2019**, *35* (33), 10704–10724. https://doi.org/10.1021/acs.langmuir.9b01837.

(49) Berger, O.; Gazit, E. Molecular Self-Assembly Using Peptide Nucleic Acids. *Biopolymers* **2017**, *108* (1), e22930. https://doi.org/10.1002/bip.22930.

(50) Guler, M. O.; Pokorski, J. K.; Appella, D. H.; Stupp, S. I. Enhanced Oligonucleotide Binding to Self-Assembled Nanofibers. *Bioconjug. Chem.* **2005**, *16* (3), 501–503. https://doi.org/10.1021/bc050053b.

(51) Vernille, J. P.; Kovell, L. C.; Schneider, J. W. Peptide Nucleic Acid (PNA) Amphiphiles: Synthesis, Self-Assembly, and Duplex Stability. *Bioconjug. Chem.* **2004**, *15* (6), 1314–1321. https://doi.org/10.1021/BC049831A.

(52) Lau, C.; Bitton, R.; Bianco-Peled, H.; Schultz, D. G.; Cookson, D. J.; Grosser, S. T.; Schneider, J. W. Morphological Characterization of Self-Assembled Peptide Nucleic Acid Amphiphiles. *J. Phys. Chem. B* **2006**, *110* (18), 9027–9033. https://doi.org/10.1021/JP057049H.

(53) Marques, B. F.; Schneider, J. W. Sequence-Specific Binding of DNA to Liposomes Containing Di-Alkyl Peptide Nucleic Acid (PNA) Amphiphiles. *Langmuir* **2005**, *21* (6), 2488–2494. https://doi.org/10.1021/LA047962U.

(54) Grosser, S. T.; Savard, J. M.; Schneider, J. W. Identification of PCR Products Using PNA Amphiphiles in Micellar Electrokinetic Chromatography. *Anal. Chem.* **2007**, *79* (24), 9513–9519. https://doi.org/10.1021/ac7016376.

(55) Liu, L.-H.; Li, Z.-Y.; Rong, L.; Qin, S.-Y.; Lei, Q.; Cheng, H.; Zhou, X.; Zhuo, R.-X.; Zhang, X.-Z. Self-Assembly of Hybridized Peptide Nucleic Acid Amphiphiles. *ACS Macro Lett.* **2014**, *3* (5), 467–471. https://doi.org/10.1021/mz5001916.

(56) Feagin, T. A.; Shah, N. I.; Heemstra, J. M. Convenient and Scalable Synthesis of Fmoc-Protected Peptide Nucleic Acid Backbone. *J. Nucleic Acids* **2012**, *2012*, 354549. https://doi.org/10.1155/2012/354549.

(57) Sharma, C.; Awasthi, S. K. Versatility of Peptide Nucleic Acids (PNAs): Role in Chemical Biology, Drug Discovery, and Origins of Life. *Chem. Biol. Drug Des.* **2017**, *89* (1), 16–37. https://doi.org/10.1111/cbdd.12833.

(58) Moccia, M.; Adamo, M. F. A.; Saviano, M. Insights on Chiral, Backbone Modified Peptide Nucleic Acids: Properties and Biological Activity. *Artif. DNA PNA XNA* **2016**, *5* (3), e1107176. https://doi.org/10.1080/1949095X.2015.1107176.

(59) Dueholm, K. L.; Peterson, K. H.; Jensen, D. K.; Egholm, M.; Nielsen, P. E.; Buchardt, O. Peptide Nucleic Acid (PNA) with a Chiral Backbone Based on Alanine. *Bioorg. Med. Chem. Lett.* **1994**, *4* (8), 1077–1080. https://doi.org/10.1016/S0960-894X(01)80684-3.

(60) Nielsen, P. E.; Haaima, G.; Lohse, A.; Buchardt, O. Peptide Nucleic Acids (PNAs) Containing Thymine Monomers Derived from Chiral Amino Acids: Hybridization and Solubility Properties OfD-Lysine PNA. *Angew. Chemie Int. Ed. English* **1996**, *35* (17), 1939–1942. https://doi.org/10.1002/anie.199619391.

(61) Katritzky, A. R.; Narindoshvili, T. Chiral Peptide Nucleic Acid Monomers (PNAM) with Modified Backbones. *Org. Biomol. Chem.* **2008**, *6* (17), 3171–3176. https://doi.org/10.1039/b806141f.

(62) Püschl, A.; Sforza, S.; Haaima, G.; Dahl, O.; Nielsen, P. E. Peptide Nucleic Acids (PNAs) with a Functional Backbone. *Tetrahedron Lett.* **1998**, *39* (26), 4707–4710. https://doi.org/10.1016/S0040-4039(98)00862-4.

(63) Sugiyama, T.; Imamura, Y.; Demizu, Y.; Kurihara, M.; Takano, M.; Kittaka, A. β-PNA: Peptide Nucleic Acid (PNA) with a Chiral Center at the β-Position of the PNA Backbone. *Bioorganic Med. Chem. Lett.* **2011**, *21* (24), 7317–7320. https://doi.org/10.1016/j.bmcl.2011.10.017.

(64) Myers, M. C.; Witschi, M. A.; Larionova, N. V.; Franck, J. M.; Haynes, R. D.; Hara, T.; Grajkowski, A.; Appella, D. H. A Cyclopentane Conformational Restraint for a Peptide Nucleic Acid: Design, Asymmetric Synthesis, and Improved Binding Affinity to DNA and RNA. *Org. Lett.* **2003**, *5* (15), 2695–2698. https://doi.org/10.1021/ol0348811.

(65) Pokorski, J. K.; Witschi, M. A.; Purnell, B. L.; Appella, D. H. (S,S)-Trans-Cyclopentane-Constrained Peptide Nucleic Acids. A General Backbone Modification That Improves Binding Affinity and Sequence Specificity. *J. Am. Chem. Soc.* **2004**, *126* (46), 15067–15073. https://doi.org/10.1021/ja046280q.

(66) Pokorski, J. K.; Myers, M. C.; Appella, D. H. Cyclopropane PNA: Observable Triplex Melting in a PNA Constrained with a 3-Membered Ring. *Tetrahedron Lett.* **2005**, *46* (6), 915–917. https://doi.org/10.1016/j.tetlet.2004.12.061.

(67) Lagriffoule, P.; Eriksson, M.; Jensen, K. K.; Nielsen, P. E.; Wittung, P.; Nordén, B.; Buchardt, O. Peptide Nucleic Acids with a Conformationally Constrained Chiral Cyclohexyl-Derived Backbone. *Chem. - A Eur. J.* **1997**, *3* (6), 912–919. https://doi.org/10.1002/chem.19970030613.

(68) Govindaraju, T.; Kumar, V. A.; Ganesh, K. N. Cis-Cyclopentyl PNA (CpPNA) as Constrained Chiral PNA Analogues: Stereochemical Dependence of DNA/RNA Hybridization. *Chem. Commun.* **2004**, *10* (7), 860–861. https://doi.org/10.1039/b317000d.

(69) Micklitsch, C. M.; Oquare, B. Y.; Zhao, C.; Appella, D. H. Cyclopentane-Peptide Nucleic Acids for Qualitative, Quantitative, and Repetitive Detection of Nucleic Acids. *Anal. Chem.* **2013**, *85* (1), 251–257. https://doi.org/10.1021/ac3026459.

(70) Kosynkina, L.; Wang, W.; Liang, T. C. A Convenient Synthesis of Chiral Peptide Nucleic Acid (PNA) Monomers. *Tetrahedron Lett.* **1994**, *35* (29), 5173–5176. https://doi.org/10.1016/S0040-4039(00)77056-0.

(71) Tedeschi, T.; Sforza, S.; Corradini, R.; Marchelli, R. Synthesis of New Chiral PNAs Bearing a Dipeptide-Mimic Monomer with Two Lysine-Derived Stereogenic Centres. *Tetrahedron*

Lett. **2005**, *46* (48), 8395–8399. https://doi.org/10.1016/j.tetlet.2005.09.157.

(72) Manna, A.; Rapireddy, S.; Sureshkumar, G.; Ly, D. H. Synthesis of Optically Pure ΓPNA Monomers: A Comparative Study. *Tetrahedron* **2015**, *71* (21), 3507–3514. https://doi.org/10.1016/j.tet.2015.03.052.

(73) Englund, E. A.; Appella, D. H. Synthesis of γ-Substituted Peptide Nucleic Acids: A New Place to Attach Fluorophores without Affecting DNA Binding. *Org. Lett.* **2005**, *7* (16), 3465–3467. https://doi.org/10.1021/OL051143Z.

(74) de Koning, M. C.; Petersen, L.; Weterings, J. J.; Overhand, M.; van der Marel, G. A.; Filippov, D. V. Synthesis of Thiol-Modified Peptide Nucleic Acids Designed for Post-Assembly Conjugation Reactions. *Tetrahedron* **2006**, *62* (14), 3248–3258. https://doi.org/10.1016/j.tet.2006.01.065.

(75) Pensato, S.; Saviano, M.; Bianchi, N.; Borgatti, M.; Fabbri, E.; Gambari, R.; Romanelli, A. γ-Hydroxymethyl PNAs: Synthesis, Interaction with DNA and Inhibition of Protein/DNA Interactions. *Bioorg. Chem.* **2010**, *38* (5), 196–201. https://doi.org/10.1016/j.bioorg.2010.06.002.

(76) Avitabile, C.; Moggio, L.; Malgieri, G.; Capasso, D.; Di Gaetano, S.; Saviano, M.; Pedone, C.; Romanelli, A. γ Sulphate PNA (PNA S): Highly Selective DNA Binding Molecule Showing Promising Antigene Activity. *PLoS One* **2012**, *7* (5), e35774. https://doi.org/10.1371/journal.pone.0035774.

(77) De Costa, N. T. S.; Heemstra, J. M. Evaluating the Effect of Ionic Strength on Duplex Stability for PNA Having Negatively or Positively Charged Side Chains. *PLoS One* **2013**, *8* (3), e58670. https://doi.org/10.1371/journal.pone.0058670.

(78) Crawford, M. J.; Rapireddy, S.; Bahal, R.; Sacui, I.; Ly, D. H. Effect of Steric Constraint at the γ-Backbone Position on the Conformations and Hybridization Properties of PNAs. *J. Nucleic Acids* **2011**, *2011*, 652702. https://doi.org/10.4061/2011/652702.

(79) Wittung, P.; Nielsen, P.; Nordén, B. Extended DNA-Recognition Repertoire of Peptide

Nucleic Acid (PNA): PNA−dsDNA Triplex Formed with Cytosine-Rich Homopyrimidine PNA. *Biochemistry* **1997**, *36* (26), 7973–7979. https://doi.org/10.1021/bi963136b.

(80) Egholm, M.; Buchardt, O.; Nielsen, P. E.; Berg, R. H. Peptide Nucleic Acids (PNA). Oligonucleotide Analogs with an Achiral Peptide Backbone. *J. Am. Chem. Soc.* **1992**, *114* (5), 1895–1897. https://doi.org/10.1021/ja00031a062.

(81) Nielsen, P. E.; Egholm, M.; Buchardt, O. Evidence for (PNA)2/DNA Triplex Structure upon Binding of PNA to DsDNA by Strand Displacement. *J. Mol. Recognit.* **1994**, *7* (3), 165–170. https://doi.org/10.1002/jmr.300070303.

(82) Rapireddy, S.; He, G.; Roy, S.; Armitage, B. A.; Ly, D. H. Strand Invasion of Mixed-Sequence B-DNA by Acridine-Linked, γ-Peptide Nucleic Acid (γ-PNA). *J. Am. Chem. Soc.* **2007**, *129* (50), 15596–15600. https://doi.org/10.1021/ja074886j.

(83) Lohse, J.; Dahl, O.; Nielsen, P. E. Double Duplex Invasion by Peptide Nucleic Acid: A General Principle for Sequence-Specific Targeting of Double-Stranded DNA. *Proc. Natl. Acad. Sci. U. S. A.* **1999**, *96* (21), 11804–11808. https://doi.org/10.1073/pnas.96.21.11804.

(84) He, G.; Rapireddy, S.; Bahal, R.; Sahu, B.; Ly, D. H. Strand Invasion of Extended, Mixed-Sequence B-DNA by ΓPNAs. *J. Am. Chem. Soc.* **2009**, *131* (34), 12088–12090. https://doi.org/10.1021/ja900228j.

(85) Dragulescu-Andrasi, A.; Rapireddy, S.; Frezza, B. M.; Gayathri, C.; Gil, R. R.; Ly, D. H. A Simple γ-Backbone Modification Preorganizes Peptide Nucleic Acid into a Helical Structure. *J. Am. Chem. Soc* **2006**, *128* (31), 10258–10267. https://doi.org/10.1021/JA0625576.

(86) Verona, M. D.; Verdolino, V.; Palazzesi, F.; Corradini, R. Focus on PNA Flexibility and RNA Binding Using Molecular Dynamics and Metadynamics. *Sci. Rep.* **2017**, *7*, 42799. https://doi.org/10.1038/srep42799.

(87) Tedeschi, T.; Chiari, M.; Galaverna, G.; Sforza, S.; Cretich, M.; Corradini, R.; Marchelli, R. Detection of the R553X DNA Single Point Mutation Related to Cystic Fibrosis by a “Chiral

Box”D-Lysine-Peptide Nucleic Acid Probe by Capillary Electrophoresis. *Electrophoresis* **2005**, *26* (22), 4310–4316. https://doi.org/10.1002/elps.200410390.

(88) Zhou, P.; Dragulescu-Andrasi, A.; Bhattacharya, B.; O’Keefe, H.; Vatta, P.; Hyldig-Nielsen, J. J.; Ly, D. H. Synthesis of Cell-Permeable Peptide Nucleic Acids and Characterization of Their Hybridization and Uptake Properties. *Bioorganic Med. Chem. Lett.* **2006**, *16* (18), 4931–4935. https://doi.org/10.1016/j.bmcl.2006.06.052.

(89) Manicardi, A.; Fabbri, E.; Tedeschi, T.; Sforza, S.; Bianchi, N.; Brognara, E.; Gambari, R.; Marchelli, R.; Corradini, R. Cellular Uptakes, Biostabilities and Anti-MiR-210 Activities of Chiral Arginine-PNAs in Leukaemic K562 Cells. *ChemBioChem* **2012**, *13* (9), 1327–1337. https://doi.org/10.1002/cbic.201100745.

(90) Dragulescu-Andrasi, A.; Rapireddy, S.; He, G.; Bhattacharya, B.; Hyldig-Nielsen, J. J.; Zon, G.; Ly, D. H. Cell-Permeable Peptide Nucleic Acid Designed to Bind to the 5′-Untranslated Region of E-Cadherin Transcript Induces Potent and Sequence-Specific Antisense Effects. *J. Am. Chem. Soc.* **2006**, *128* (50), 16104–16112. https://doi.org/10.1021/ja063383v.

(91) Bahal, R.; Sahu, B.; Rapireddy, S.; Lee, C.-M.; Ly, D. H. Sequence-Unrestricted, Watson-Crick Recognition of Double Helical B-DNA by (R)-MiniPEG-ΓPNAs. *ChemBioChem.* **2012**, *13* (1), 56–60. https://doi.org/10.1002/cbic.201100646.

(92) Gupta, A.; Quijano, E.; Liu, Y.; Bahal, R.; Scanlon, S. E.; Song, E.; Hsieh, W. C.; Braddock, D. E.; Ly, D. H.; Saltzman, W. M.; Glazer, P. M. Anti-Tumor Activity of MiniPEG-γ-Modified PNAs to Inhibit MicroRNA-210 for Cancer Therapy. *Mol. Ther. Nucleic Acids* **2017**, *9*, 111–119. https://doi.org/10.1016/j.omtn.2017.09.001.

(93) Orenstein, A.; Berlyoung, A.; Rastede, E.; Pham, H.; Fouquerel, E.; Murphy, C.; Leibowitz, B.; Yu, J.; Srivastava, T.; Armitage, B.; Opresko, P. ΓPNA FRET Pair Miniprobes for Quantitative Fluorescent In Situ Hybridization to Telomeric DNA in Cells and Tissue. *Molecules* **2017**, *22* (12), 2117. https://doi.org/10.3390/molecules22122117.

(94) Englund, E. A.; Appella, D. H. γ-Substituted Peptide Nucleic Acids Constructed FromL-

Lysine Are a Versatile Scaffold for Multifunctional Display. *Angew. Chemie Int. Ed.* **2007**, *46* (9), 1414–1418. https://doi.org/10.1002/anie.200603483.

(95) Englund, E. A.; Wang, D.; Fujigaki, H.; Sakai, H.; Micklitsch, C. M.; Ghirlando, R.; Martin-Manso, G.; Pendrak, M. L.; Roberts, D. D.; Durell, S. R.; Appella, D. H. Programmable Multivalent Display of Receptor Ligands Using Peptide Nucleic Acid Nanoscaffolds. *Nat. Commun.* **2012**, *3* (1), 614. https://doi.org/10.1038/ncomms1629.

(96) Dix, A. V; Conroy, J. L.; Rosenker, K. M. G.; Sibley, D. R.; Appella, D. H. PNA-Based Multivalent Scaffolds Activate the Dopamine D2 Receptor. *ACS Med. Chem. Lett.* **2015**, *6* (4), 425–429. https://doi.org/10.1021/ml500478m.

(97) Gupta, P.; Rastede, E. E.; Appella, D. H. Multivalent LKγ-PNA Oligomers Bind to a Human Telomere DNA G-Rich Sequence to Form Quadruplexes. *Bioorganic Med. Chem. Lett.* **2015**, *25* (21), 4757–4760. https://doi.org/10.1016/j.bmcl.2015.07.075.

(98) Sforza, S.; Tedeschi, T.; Calabretta, A.; Corradini, R.; Camerin, C.; Tonelli, R.; Pession, A.; Marchelli, R. A Peptide Nucleic Acid Embedding a Pseudopeptide Nuclear Localization Sequence in the Backbone Behaves as a Peptide Mimic. *European J. Org. Chem.* **2010**, *2010* (13), 2441–2444. https://doi.org/10.1002/ejoc.201000123.

(99) Swenson, C. S.; Velusamy, A.; Argueta-Gonzalez, H. S.; Heemstra, J. M. Bilingual Peptide Nucleic Acids: Encoding the Languages of Nucleic Acids and Proteins in a Single Self-Assembling Biopolymer. *J. Am. Chem. Soc.* **2019**, *141* (48), 19038–19047. https://doi.org/10.1021/jacs.9b09146.

(100) Köhler, O.; Jarikote, D. V.; Seitz, O. Forced Intercalation Probes (FIT Probes): Thiazole Orange as a Fluorescent Base in Peptide Nucleic Acids for Homogeneous Single-Nucleotide-Polymorphism Detection. *ChemBioChem* **2005**, *6* (1), 69–77. https://doi.org/10.1002/cbic.200400260.

(101) Meier, J. C.; Kankowski, S.; Krestel, H.; Hetsch, F. RNA Editing—Systemic Relevance and Clue to Disease Mechanisms? *Front. Mol. Neurosci.* **2016**, *9*, 124.

https://doi.org/10.3389/fnmol.2016.00124.

(102) Nakaya, K.; Takenaka, O.; Horinishi, H.; Shibata, K. Reactions of Glyoxal with Nucleic Acids, Nucleotides and Their Component Bases. *BBA Sect. Nucleic Acids Protein Synth.* **1968**, *161* (1), 23–31. https://doi.org/10.1016/0005-2787(68)90290-6.

(103) Burnett, W. V. Northern Blotting of RNA Denatured in Glyoxal without Buffer Recirculation. *Biotechniques* **1997**, *22* (4), 668–671. https://doi.org/10.2144/97224st01.

Chapter 2

Bilingual Peptide Nucleic Acids: Encoding the Languages of Nucleic Acids and Proteins in a Single Self-Assembling Biopolymer[1*]

2.1 Abstract:

Nucleic acids and proteins are the fundamental biopolymers that support all life on Earth. Nucleic acids store large amounts of information in nucleobase sequences while peptides and proteins utilize diverse amino acid functional groups to adopt complex structures and perform wide-ranging activities. Although Nature has evolved machinery to read the nucleic acid code and translate it into amino acid code, the extant biopolymers are restricted to encoding amino acid or nucleotide sequences separately, limiting their potential applications in medicine and biotechnology. Here we describe the design, synthesis, and stimuli-responsive assembly behavior of a bilingual biopolymer that integrates both amino acid and nucleobase sequences into a single peptide nucleic acid (PNA) scaffold to enable tunable storage and retrieval of tertiary structural behavior and programmable molecular recognition capabilities. Incorporation of a defined sequence of amino acid side chains along the PNA backbone yields amphiphiles having a "protein code" that directs self-assembly into micellar architectures in aqueous conditions. However, these amphiphiles also carry a "nucleotide code" such that subsequent introduction of a complementary RNA strand induces a sequence-specific disruption of assemblies through hybridization. Together, these properties establish bilingual PNA as a powerful biopolymer that combines two information systems to harness structural responsiveness and sequence recognition. The PNA scaffold and our synthetic system are highly generalizable, enabling

[*]Adapted from Ref. 1 with permission from Swenson, C. S; Velusamy, A.; Argueta-Gonzalez, H. S.; Heemstra, J. M. *Journal of the American Chemical Society*. **2019**, *141*(48), 19038-19047. Copyright 2019 American Chemical Society.

fabrication of a wide array of user-defined peptide and nucleotide sequence combinations for diverse future biomedical and nanotechnology applications.

2.2 Introduction:

Nature encodes information, structure, and function in two basic forms of biopolymers: nucleic acids and proteins. Nucleotide sequences in DNA or RNA encode both genetic information and complementary molecular recognition properties, while amino acid sequences in peptides and proteins convey complex information for structure and function. The robust and adaptable performance of both of these biopolymer structures has been a fundamental driving force for evolution on Earth and explains their continued ubiquitous presence in Nature. Moreover, the straightforward design principles and privileged physicochemical properties of both nucleic acids and proteins position them as attractive materials to leverage and integrate in applications beyond their canonical roles.[2–4] For example, combining the high density of negative charge of DNA molecules with hydrophobic lipids or organic polymers enables assembly and formation of complex nanostructures including micelles, tubes, and vesicles.[5–7] While these DNA-polymer conjugates successfully integrate structural responsiveness and can perform sequence-specific recognition, they are difficult to control in biological systems and are limited to anionic backbones. Conversely, peptides are able to express myriad biophysical characteristics through programmable amino acid side-chain functionalities but lack the vast information storage and highly modular molecular recognition capabilities of nucleic acids. The ability to combine the functional properties of nucleic acids and proteins into a single biomolecule would largely overcome these material limitations. A “bilingual” biopolymer, able to simultaneously speak both amino acid and base-pairing languages, would allow for both the information processing capability of nucleobase sequence recognition as well as the structural and functional versatility afforded to peptides and proteins, together creating a powerful tool for biomedical and nanotechnology applications.

Despite these clear advantages, uniting these two chemical functionalities presents a significant logistical challenge. We recognized that peptide nucleic acid (PNA) offered an ideal scaffold for the design of a bilingual biopolymer, as is it capable of storing sequence-specific nucleotide code along a neutral pseudopeptide backbone.[8–10] This backbone imparts a number of desirable properties including extremely high affinity for complementary nucleic acids, enhanced stability in complex biological environments, and most significantly, the ability to incorporate amino acid side-chains at sequence-defined positions.[11–13] Researchers have used the latter capability to impact properties such as solubility, cell permeability, enhanced base-pairing, and bioconjugation.[14–23] Additionally, PNA-polymer conjugates have been constructed and shown to self-assemble.[24–26] While these are capable of binding to complementary nucleic acids, the hydrophobic portion and nucleic acid code exist in different blocks of the polymer and thus hybridization cannot be used to control assembly. In contrast to these previous examples, integrating a complex amino acid sequence in the PNA backbone to encode assembly or conformational information has yet to be explored. We hypothesized that strategically placing hydrophobic or hydrophilic amino acid side chains would enable us to controllably induce self-assembly of amphiphilic structures (**Figure 2.1**). We further speculated that addition of a complementary DNA or RNA strand would result in duplex formation with the PNA strand and a dramatic change in amphiphilicity, effectively harnessing the nucleic acid code to direct disruption

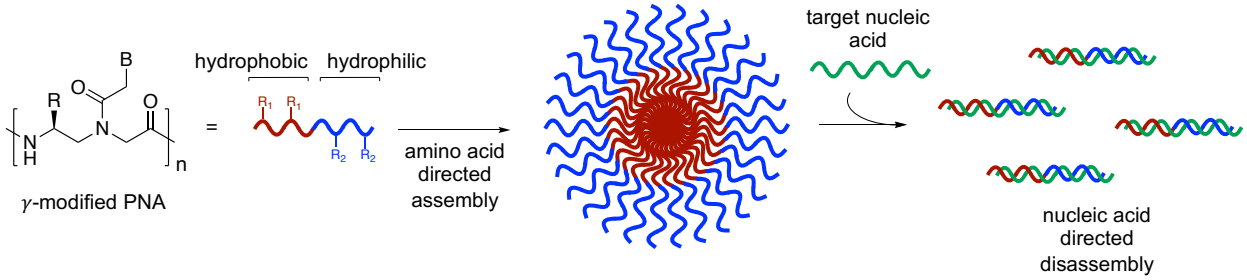

Figure 2.1: Schematic representation of bilingual PNA biopolymer. Amino acid side chains at the γ-position direct assembly, and disassembly is triggered by recognition of the nucleobase code by a complementary DNA or RNA strand.

of the assemblies. Here we demonstrate the design, synthesis, and characterization of such an amphiphilic PNA sequence and show assembly into micellar architectures under aqueous conditions. We also show stimuli-responsive disassembly using miRNA-21, a disease-related RNA target.[27] Together, these results represent the first example of a bilingual biopolymer capable of simultaneously encoding both amino acid and nucleotide information for utilization in controlled assembly and sequence-specific recognition.

2.3 Results and Discussion:

2.3.1 Design and Synthesis of Amphiphilic PNA

To demonstrate the ability of PNA to function as a bilingual biopolymer, we aimed to create a strand having a nucleobase sequence capable of specific RNA recognition and an amino acid sequence to impart amphiphilic behavior to drive assembly, analogous to folding or quaternary assembly of proteins. As a biologically relevant target, we designed a 12-nucleotide sequence complementary to miRNA-21, a well characterized oncomiR that is upregulated in almost all cancer types.[27] Conveniently, this complementary sequence exhibits low overall purine content and contains a single guanine nucleobase, averting sequence motifs that are known to be problematic in PNA synthesis and hybridization (**Table 2.1, Figure 2.2A**).[28] To impart hydrophobic properties in our amino acid sequence, we selected an alanine side-chain, as we previously observed aggregation of PNA having three methyl side-chains. For the hydrophilic portion of the

Table 2.1: Sequences of amphiphilic PNA-A, control PNA-C, and amino acid containing PNA-aa. "D" (orange) denotes the 4-DMN dye monomer. Subscripts denote the amino acid single letter code. Alanine monomers are in red. Lysine monomers are in blue. Masses were confirmed by ESI-TOF mass spectrometry.

Strand	Sequence	Mass $(M+3)^{3+}$	Found $(M+3)^{3+}$
PNA-A	C – D C T_A G A C_A T A C A_K A C T_K – N	1254.8752	1255.5583
PNA-C	C – Lys^+ D C T G A C T A C A A C T – N	1240.8474	1241.5322
PNA-aa	C – Ala Ala D C T G A C T A C A A C T Lys^+ Lys^+ – N	1330.9038	1331.6610

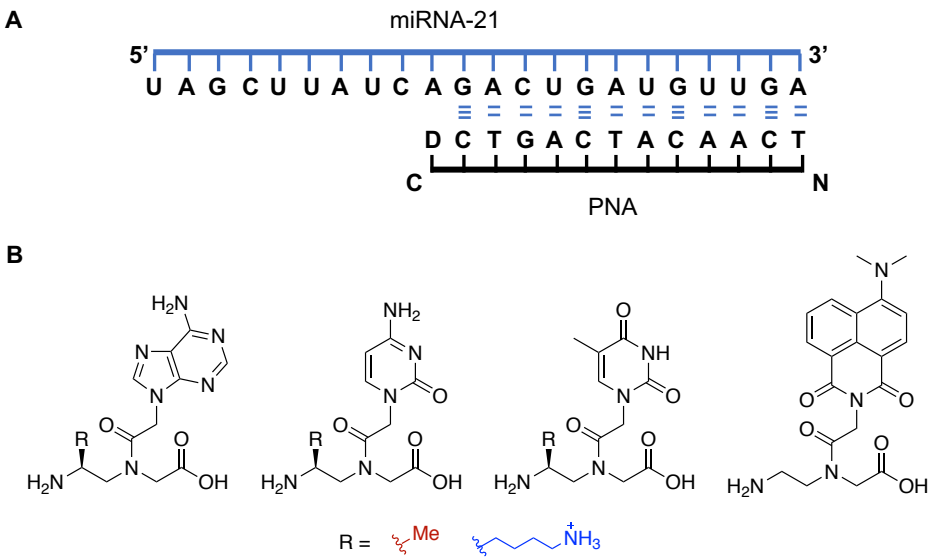

Figure 2.2: PNA monomers and miRNA-21 target. A) Hybridization site of PNA oligomers to the miRNA-21 target used in this study. B) PNA monomers synthesized in this study: γ-methyl monomers of cytosine and thymine, γ-lysyl monomers of adenine and thymine, and a solvatochromic 4-DMN monomer.

sequence, we chose a positively-charged lysine side-chain, which afforded convenient synthetic access and is known to impart favorable solubility properties.[13,29] The side-chains were placed at the γ-position along the PNA backbone using L-amino acids, as this enables installation of the side-chains using amino acid precursors, and this location and stereochemistry have been shown to confer increased binding affinity of PNA with complementary nucleic acids (**Figure 2.1**).[13,14] Lastly, we integrated a solvatochromic fluorophore, 4-dimethylamino-naphthalimide (4-DMN), at the hydrophobic terminus of the PNA (**Figure 2.2B**). This dye exhibits an enhancement in fluorescence intensity in increasingly hydrophobic environments,[30] and we envisioned that such an arrangement in the hydrophobic portion would allow us to visualize assembly formation by fluorescence spectroscopy.

We first synthesized the necessary γ-modified PNA monomers according to previously reported procedures.[23,29,31–33] Starting from Fmoc-protected L-amino acids, PNA backbones containing lysine and alanine side chains were produced. The γ-modified backbones were coupled to bis(Boc)-protected nucleobase acetic acids using HATU in the presence of *N*-*N*-

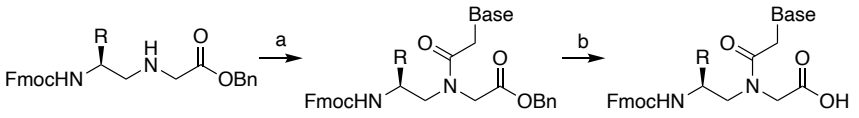

1: R = Lysyl; Base = A **3:** R = Me; Base = C

2: R = Lysyl; Base = T **4:** R = Me; Base = T

Scheme 2.1: General coupling procedure for the synthesis of γ-modified PNA monomers. (a) Nucleobase acetic acid, HATU, DIPEA, DMF; (b) H_2, Pd/C, MeOH.

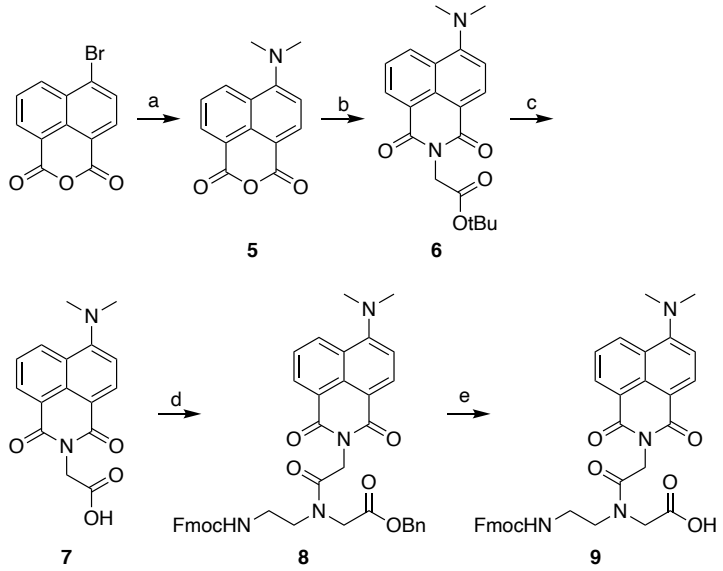

Scheme 2.2: Synthesis of 4-DMN PNA monomer. (a) 3-(dimethylamino)propionitrile, isoamyl alcohol, reflux, quant. (b) Glycine tert-butyl ester hydrochloride, DIPEA, DMF, 78%. (c) H2, Pd/C, methanol, 94%. (d) Fmoc (aminoethyl)glycine benzyl ester, HATU, DIPEA, DMF, 72%. (e) H2, Pd/C, methanol, quantitative.

diisopropylethylamine (DIPEA) to produce γ-modified monomers of A, T, and C (**Scheme 2.1**). Synthesis of the 4-DMN PNA monomer was performed using a protocol adapted from that of Saito and coworkers.[34] First, 4-dimethylamino-naphthalic anhydride was generated by reaction of 4-bromo-1,8-naphthalic anhydride with 3-dimethylamino-propionitrile in isoamyl alcohol.[35] The imide was then produced by condensation with glycine *tert*-butyl ester hydrochloride in the presence of DIPEA.[36] Removal of the tert-butyl protecting group by hydrolysis afforded the 4-DMN acetic acid. Unmodified (glycine) PNA backbone was synthesized according to previously

reported procedure,[37] and the 4-DMN acetic acid was coupled to the unmodified backbone using HATU/DIPEA conditions to afford the 4-DMN PNA monomer (**Scheme 2.2**).

Amphiphilic PNA and control PNA oligomers were then produced using solid-phase synthesis employing HATU/DIPEA coupling conditions on a semi-automatic synthesizer with microwave assistance. Initially, we sought to place three hydrophobic side chains and three hydrophilic side chains equally spaced along the backbone. However, we were unable to obtain full-length product with this design. We hypothesized that this was due to the close proximity of semi-consecutive γ-modified monomers, which could severely lower the efficiency of the coupling reactions, resulting in little to no product formation. With this in mind, we reduced the number of γ-modified monomers to two alanine and two lysine side chains. This design allowed placement of at least two unmodified monomers between each γ-modified residue, thereby mitigating otherwise poor coupling yields due to steric strain. Using this design, we produced an amphiphilic PNA sequence, PNA-A, as well as an unmodified control strand, PNA-C, containing a single C-terminal lysine, as is typically used in PNA strands to ensure solubility. In order to demonstrate the importance of using γ-modified monomers to encode the amino acid sequence along the PNA backbone, we also synthesized a control amphiphilic PNA, PNA-aa. This PNA has two alanine amino acids and two lysine amino acids on the C- and N-termini, respectively, and thus represents a sequence that is amphiphilic, but not bilingual, as the nucleotide and amino acid codes exist in separate blocks of the polymer (**Table 2.1).** The strands were purified via reverse-phase HPLC and characterized by ESI-TOF mass spectrometry to confirm identity (**Appendix A**).

After synthesis and characterization of the PNA sequences, we performed UV melting experiments to analyze the hybridization of each sequence to a complementary DNA or the miRNA-21 target. The presence of side chains at the γ-position is known to increase the duplex stability of PNA to complementary nucleic acids.[14,15,22] Thus, we were not surprised to find that the complementary DNA exhibits a melting temperature (T_m) of 69.5 °C with PNA-A, compared to

63.0 °C and 64.5 °C for PNA-C and PNA-aa, respectively (**Figure A1A**). miRNA-21 also displays a higher T_m of 68.6 °C with PNA-A, compared to 65.8 °C and 67.5 °C for PNA-C and PNA-aa, respectively, demonstrating that our γ-modifications improve the binding stability to complementary sequences (**Figure A1B**).

2.3.2 Characterization of Amphiphilic PNA Assembly

The ability of proteins to form tertiary and quaternary structures based on the information encoded in their primary amino acid sequence is a powerful tool. We envisioned that we could mimic this characteristic of proteins by encoding an amphiphilic amino acid sequence into the PNA backbone. After synthesis and characterization of the PNA strands, we sought to analytically confirm assembly formation and determine the critical micelle concentration (CMC) of PNA-A. To achieve this, we leveraged the ability of the 4-DMN dye to respond to changes in solvation, and we hypothesized that the dye's placement at the hydrophobic portion of the amphiphile should result in enhanced fluorescence upon assembly (**Figure 2.3A**).[30] CMC values determined using fluorescence-based methods often utilize a constant concentration of dye to visualize an inflection point where fluorescence increases. However, in our case the 4-DMN dye acts as an internal reporter, and thus changes in concentration as the concentration of amphiphile is varied. Given this approach, we instead quantified the relative fluorescence of PNA-A compared to the non-assembling dye monomer in solution. Indeed, we observed a concentration-dependent increase in fluorescence of amphiphile PNA-A over that of the 4-DMN monomer alone, suggesting the formation of assemblies having the dye sequestered in their hydrophobic core. Specifically, we observe a discontinuous change in slope with increasing concentration, as is typical of micelle formation. In contrast, the control strand, PNA-C, displayed very little fluorescence enhancement with increasing concentrations, as it does not have an amino acid code to direct assembly (**Figure A2**). While PNA-C does show a small amount of fluorescence signal over the 4-DMN monomer alone, we surmise that this is attributable to the solvation state of the dye when placed near a

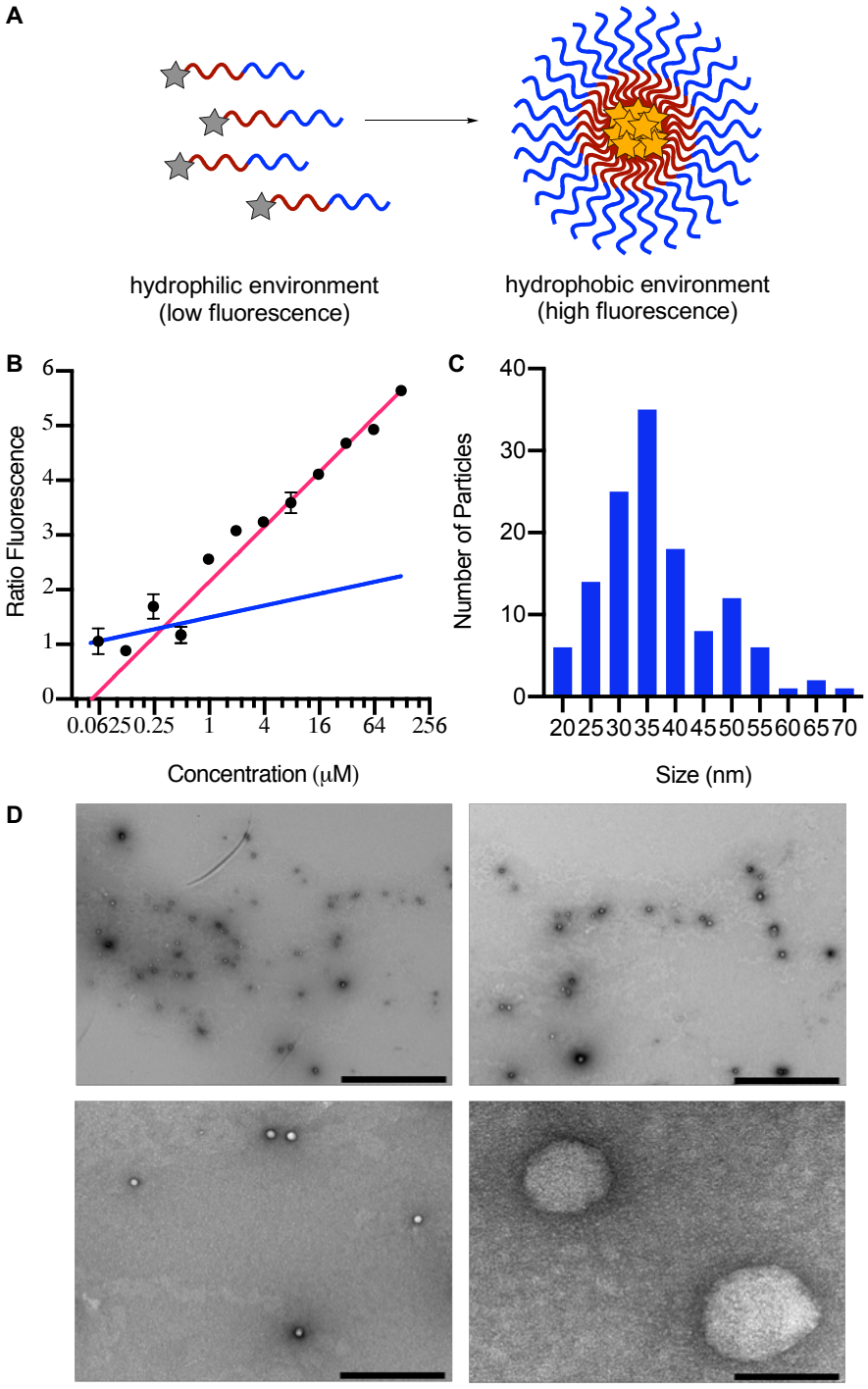

Figure 2.3: Characterization of amphiphilic PNA assembly. (A) Schematic representation of assembly and subsequent 4-DMN fluorescence response upon encapsulation. (B) Plot of the fluorescence ratio of PNA-A to the 4-DMN monomer as a function of concentration. Error bars represent SEM (n=3). (C) Histogram of the size distribution of particles as measured by ImageJ using TEM images. (D) TEM images of PNA-A at 100 μM. Scale bars = 2000 nm (top left), 1000 nm (top right), 500 nm (bottom left) and 50 nm (bottom right.)

hydrophobic nucleobase in the PNA strand, as opposed to the complete solvation of the free monomer. In any case, by observing the interception of the horizontal lower concentration and vertical upper concentration portions, we were able to estimate a CMC of ~317 nM, which is sufficiently low for a broad range of stimuli-responsive biological applications (**Figure 2.3B**).

We next aimed to visually confirm the formation of assemblies and characterize their morphology using transmission electron microscopy (TEM). Amphiphile PNA-A was first dissolved in ultrapure water and diluted to a concentration of 100 μM. This solution was spotted onto formvar/carbon-coated copper grids and stained using a 1% uranyl acetate solution for TEM visualization. As expected, we observed the presence of spherical assemblies having an average diameter of 36.9 ± 9.9 nm, consistent with the formation of micelles (**Figure 2.3C and 2.3D**). Conversely, the PNA-C control strand displayed only a small number of amorphous assemblies, likely due to uncontrolled aggregation of PNA at this high of concentration or drying effects during sample preparation (**Figure A3**). The amino acid amphiphile, PNA-aa, displayed a heterogeneous mixture of amorphous assemblies, some having a similar size as the amphiphile PNA-A, but others being significantly larger, and all lacking discrete and uniform shapes (**Figure A4**). This may be explained by the flexibility of PNA-aa compared to PNA-A, as installing amino acid side-chains directly onto the PNA backbone at the γ-position results in the oligomer adopting a right-handed helical secondary structure that can be visualized via circular dichroism,[15] whereas including them outside of the nucleobases retains the flexibility of the backbone (**Figure A6**). Irrespective of the explanation, the ability of PNA-A, but not PNA-aa, to form well-defined assemblies demonstrates the unique capabilities of our bilingual biopolymers compared to other amphiphilic PNA conjugate designs.

In order to gain a better understanding of the assembly properties in solution, we also carried out analysis using dynamic light scattering (DLS). Samples of PNA were prepared at 500 μM, as lower concentrations failed to provide sufficient signal intensity for validated

measurements. For the PNA-A assemblies, we observed a hydrodynamic diameter of 110.2 ± 31.9 nm according to the number distribution (**Figure A7**). This is larger than observed by TEM, but this difference is not entirely unexpected, as DLS has been shown to overestimate the sizes of particles in solution because it is a measure of the hydrodynamic diameter as opposed to actual size.[38–40] Additionally, in TEM the sample is dried onto a surface during preparation, which may cause the assemblies to decrease in size. Finally, the high concentrations required for DLS may lead to the formation of some larger particles, increasing the average size observed. DLS analysis of PNA-aa reveals a similar trend, showing assemblies having a hydrodynamic diameter of 344.7 ± 92.3 nm (**Figure A7**), which is larger than the assemblies observed by TEM. The non-amphiphilic PNA-C shows two populations in DLS, with a significant population at 2.4 ± 0.5 nm and a small population at 54.9 ± 15.4 nm (**Figure A7**). The smaller sized population is consistent with single-stranded PNA while the larger may represent uncontrolled aggregation. This is in agreement with the TEM data, as only sparse and amorphous assemblies were visualized for the control PNA-C. Together, these results demonstrate our ability to encode amino acid information into a PNA sequence to direct the formation of organized nanostructures under aqueous conditions.

2.3.3 Stimuli-Responsive Switching of Amphiphilic PNA Assembly

Assembly of our PNA amphiphiles is driven by the amino acid code, and we envisioned that disassembly could be driven by the nucleotide code (**Figure 2.4A**). While we designed the amphiphilic PNA sequence to be responsive to miRNA-21, we used a complementary 12-nucleotide DNA strand in our initial disassembly studies owing to greater ease of use and lower cost. First, we sought to confirm the ability of the complementary DNA to bind to the amphiphilic PNA using circular dichroism (CD). Incorporating γ-modifications into PNA oligomers imparts chirality and orients the strand into a helical secondary structure, which can be observed by CD spectroscopy at concentrations relevant to assembly formation.[15] In order to detect PNA:DNA

hybridization and subsequent disassembly, we first prepared PNA-A assemblies at 100 μM in 1x phosphate buffered saline (PBS), pH 7.4, as this concentration has previously displayed assemblies by TEM (**Figure 2.3D**). A range of concentrations of complementary or scrambled

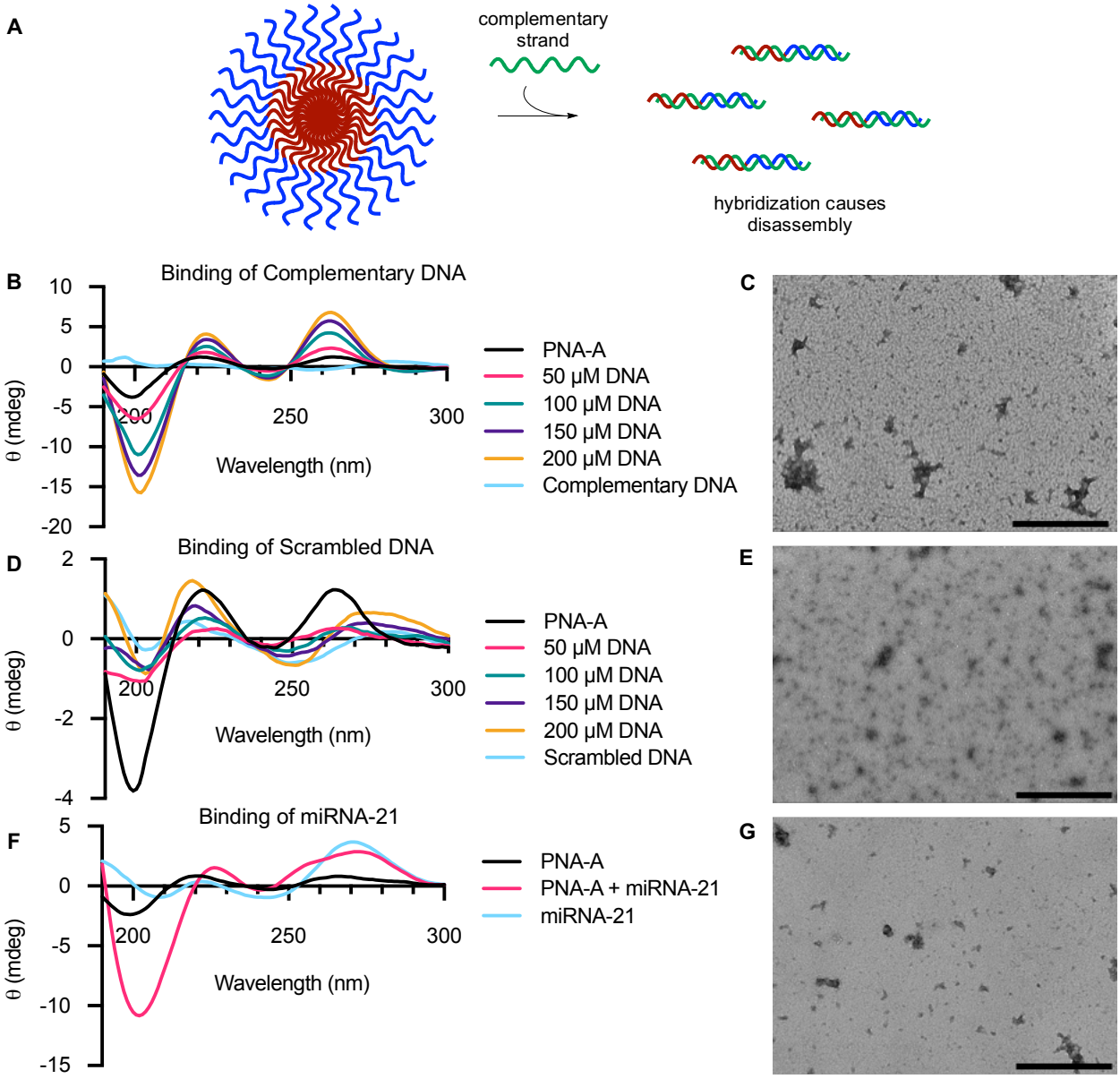

Figure 2.4: Binding and disassembly of amphiphilic structures by complementary nucleic acids. (A) Schematic representation of disassembly by hybridization of a complementary DNA or RNA strand. (B) CD plot confirming hybridization of complementary DNA to PNA-A in 1x PBS at 100 μM. (C) TEM image showing disappearance of spherical structures in the presence of complementary DNA. (D) CD plot showing inability of a scrambled DNA sequence to hybridize to PNA-A in 1x PBS at 100 μM. (E) TEM image showing retention of spherical assemblies in the presence of scrambled DNA. (F) CD plot confirming binding of full target miRNA-21 to PNA-A in water at 100 μM. (G) TEM image showing disappearance of spherical structures in the presence of complementary RNA. Scale bars in all TEM images = 500 nm.

DNA was added to the samples and CD signatures were recorded. We observed signals recording maxima near 263 nm and 222 nm, with minima occurring near 244 nm and 201 nm, which are indicative of a right-handed PNA:DNA duplex (**Figure 2.4B**).[15,41] As the concentration of complementary DNA in the samples was increased, the CD signal also increased while maintaining isosbestic points, suggesting a continuous increase in PNA:DNA duplex formation. Free DNA alone at 100 μM displayed maxima at 282 nm and 217 nm with minima occurring at 256 nm, further indicating that the increasing signal is caused by increased PNA:DNA duplex formation. As expected, we observed no increase in signal when PNA-A was exposed to the scrambled DNA sequence (**Figure 2.4D**). In fact, we observed a slight decrease in CD signal for PNA-A in the presence of scrambled DNA, which we speculate could be caused by minor electrostatic interference between the positively charged assemblies and the negatively charged DNA. We also confirmed that the control, PNA-C, and amino acid-containing amphiphile, PNA-aa, are capable of binding to complementary DNA at this concentration (**Figure A8**). Having established the ability of PNA-A to decode complementary DNA, we next aimed to explore whether similar decoding could be achieved using the full miRNA-21 target. Samples for CD spectroscopy were prepared as previously described at 100 μM but using only a single equivalent of RNA. We observed a significant change in CD signal, in particular a large increase in intensity at the 202 nm minima over that of PNA or miRNA alone, strongly suggesting the ability of the full target miRNA-21 to hybridize with PNA-A in water at concentrations relevant to assembly (**Figure 2.4F**).

Since our amphiphile is equipped with an internal fluorogenic dye, we sought to visualize disassembly via fluorescence response. Samples of PNA-A at 10 μM were prepared and mixed with increasing amounts of complementary and scrambled DNA. As expected, increasing amounts of complementary DNA caused the fluorescent signal to decrease (**Figure A9**). The change in fluorescence was not as significant as that observed via concentration-dependent

disassembly, likely because the dye can undergo base stacking with the hybridized DNA, still creating a somewhat hydrophobic environment. However, these data still provide evidence for DNA-induced disassembly. Interestingly, addition of the scrambled DNA sequence leads to an increase in fluorescence signal. We hypothesize that this may result from non-specific interactions between the negatively charged DNA and the positively charged micelles, and that the resulting charge repulsion screening leads to compaction of the assemblies and thus a more hydrophobic environment in the micelle core.

While the fluorescence data are promising, we wanted to further validate and confirm disassembly using TEM. In order to visualize stimuli-responsiveness to DNA, amphiphile PNA-A assemblies were prepared at a concentration of 200 μM in 1x PBS. To these samples was added one equivalent of the complementary or scrambled DNA sequence to a final concentration of 100 μM. The samples were spotted onto grids and stained with uranyl acetate for TEM analysis. As expected, we observed the disappearance of spherical assemblies upon addition of the complementary DNA sequence, indicating stimuli-responsive disruption of the micelles (**Figure 2.4C**). As a control, we observed retention of small spherical nanostructures in the presence of non-targeting scrambled DNA, strongly indicating that sequence-specific binding is required for disassembly (**Figure 2.4E**). These assemblies appear to be slightly smaller than PNA-A alone, supporting our hypothesis for the fluorescence increase described above. We also detected some dark aggregates in the presence of both DNA sequences and speculate this is likely due to the negative stain, uranyl acetate, which non-specifically interacts with phosphate ions present in the DNA backbone and PBS buffer, leading to precipitation. In any case, after confirming binding and stimuli-responsive disassembly by target DNA, we sought to also demonstrate responsiveness to the miRNA target of interest. Based on our previous results showing that one equivalent of DNA was sufficient for binding and disruption of assemblies, we challenged our PNA-A amphiphile constructs with a similar amount of miRNA-21. Assemblies were prepared in water and miRNA-

21 was added to give final concentrations of 100 μM for both PNA and RNA. The samples were then spotted onto grids and stained with uranyl acetate for TEM visualization. As expected, we observed the disappearance of spherical assemblies in the presence of miRNA-21 (**Figure 2.4G**). Consistent with our DNA studies, we observed similar staining precipitation patterns with miRNA-21, further suggesting that these objects are the result of non-specific artifactual precipitation between the uranyl acetate stain and phosphate-rich oligomers.

We had intended to also characterize disassembly using DLS, as this technique was successful for characterizing the assemblies in solution. However, as previously stated, this technique requires high concentrations (≥ 500 μM) of assemblies in order to obtain a reliable signal intensity.[38–40] At these concentrations, we observed the formation of a precipitate upon addition of the complementary target or a scrambled sequence. This is likely due to nonspecific electrostatic interactions which caused uncontrolled and catastrophic aggregation, resulting in the presence of larger assemblies rather than the expected disappearance of assemblies. While lower concentrations do show the expected lack of assemblies, this may be attributable to insufficient signal and cannot necessarily be attributed to disassembly.

Together, the T_m, CD, fluorescence, and TEM results demonstrate that both DNA and RNA can bind sequence-specifically to PNA-A and disrupt assembly. Thus, even in the assembled state, the nucleotide code of our bilingual PNA constructs can be accessed and used to decode nucleic acid sequence information into supramolecular conformational changes. This property is similar to that shown in other PNA amphiphile systems.[24–26] However, these systems rely upon the addition of a hydrophobic alkyl chain and hydrophilic amino acids on opposite ends of the PNA oligomer to impart amphiphilic properties. While those designs are advantageous for ease of synthesis, our design is fundamentally different in that the entire portion of the amphiphile is capable of nucleobase-specific recognition. This allows greater control over the assembly and

disassembly properties imparted by the amino acid and nucleobase codes, thus providing a truly modular bilingual biopolymer.

2.4 Conclusion:

Nature has evolved two languages for encoding the instructions and functions needed for life. While extant biopolymers are limited to encoding a single language, we introduce here a non-natural biopolymer that is able to simultaneously encode both. We report the synthesis and characterization of a PNA strand having amino acid-like side chains comprised of hydrophobic alanine and hydrophilic lysine, which when arrayed in a specific pattern are able to direct assembly in a manner analogous to peptide aggregation or quaternary protein assembly. The PNA strand also carries a specific nucleotide code, which is able to be decoded by complementary DNA or RNA to direct stimuli-responsive disassembly. These assembly and disassembly events can be observed both spectroscopically and using TEM, enabling characterization of the CMC and morphology of the assemblies and the sequence-specific nature of the disassembly process. The PNA scaffold is highly generalizable, allowing for the programming of both nucleotide and amino acid sequences to impart unique biological and physicochemical properties.[42] Thus, the ability of this information-rich bilingual biopolymer motif to undergo ordered self-assembly and conformationally respond to a variety of nucleic acid targets offers significant potential for applications in nanomedicine and biotechnology. While our initial exploration focused on micellar architectures, we envision that the bilingual biopolymer motif can be harnessed to recapitulate many of the structural motifs found in proteins, such as sheets and coils. Moreover, we anticipate that the ability to simultaneously interpret both of the biological codes can be extended beyond the creation of stimuli-responsive assemblies to also enable the construction of custom adaptors able to mediate precise interactions between specific protein and nucleic acid targets.

2.5 Materials and Methods:

Abbreviations: Fmoc, fluorenylmethyloxycarbonyl; DMF, dimethylformamide; HATU, 1-[Bis(dimethylamino)methylene]-1*H*-1,2,3-triazolo[4,5-*b*]pyridinium 3-oxid hexafluorophosphate; DIPEA, diisopropylethylamine; TFA, trifluoroacetic acid; DCM, dichloromethane; Boc, tert-butyloxycarbonyl; NMP, N-methyl-2-pyrrolidone.

PNA monomer synthesis

Unmodified PNA monomers were purchased from PolyOrg, Inc. Fmoc γ-lysyl and γ-methyl modified PNA backbones and nucleobase acetic acids of adenosine, thymine, and cytosine were prepared by previously published procedures.[23,29,31–33] Fmoc-L-amino acids and nucleobase starting materials were purchased from Chem-Impex International, Inc. All other reagents and solvents were purchased from Chem-Impex, Sigma-Aldrich, or Fisher Scientific and used without further purification unless otherwise stated. All dry solvents were distilled and collected from a J. C. Meyer solvent dispensing system prior to use to ensure dryness. Small molecule synthesis was monitored by thin layer chromatography (TLC) on Merck silica gel 60 F254 glass plates and visualized using UV light and staining with a ninhydrin solution followed by heating. Flash chromatography was performed using SiliaFlash F60 grade silica purchased from SiliCycle Inc. Compounds were characterized by proton magnetic resonance (^{1}H) and carbon nuclear magnetic resonance (^{13}C) NMR using a Varian Inova 400 MHz spectrometer containing a Bore Oxford magnet. Spectra were analyzed using the MestReNova software. The mass of compounds was confirmed by the use of an Agilent 6230 electrospray ionization time-of-flight (ESI-TOF) mass spectrometer.

General coupling procedure for PNA monomer synthesis

Nucleobase acetic acid (1 eq) was dissolved in dry DMF under N_2 in a round bottom flask. To the flask was added HATU (1 eq) in dry DMF and DIPEA (2 eq). The mixture was stirred at

room temperature for 10 min before addition of γ-modified PNA backbone (0.67 eq) in dry DMF. The mixture was stirred overnight or until consumption of the backbone as confirmed by TLC using ninhydrin staining. Upon completion, the reaction was quenched with H_2O, extracted with ethyl acetate and washed with 1M hydrochloric acid (HCl), saturated aqueous sodium bicarbonate ($NaHCO_3$), H_2O, and brine. The organic layer was dried with anhydrous sodium sulfate (Na_2SO_4) and concentrated with rotary evaporation. The crude solid was purified by flash column chromatography (hexane to ethyl acetate gradient) to give the protected PNA monomer. The purified benzyl-protected monomer was re-dissolved in methanol under N_2. To the solution was added palladium on activated charcoal (7%/wt.) and the N_2 was replaced with a balloon of H_2. The reaction was stirred until complete deprotection as confirmed by TLC. Upon completion, the solution was filtered through celite and concentrated with rotary evaporation to produce the final γ-modified PNA monomer.

Fmoc Lysyl Adenine Monomer (**1**). (43% yield) ^{1}H NMR (400 MHz, DMSO-d6, two rotamers) δ 8.75 (rotamer one, s, 1H) 8.73 (rotamer two, s, 1H) 8.45 (rotamer one, s, 1H) 8.43 (rotamer two, s, 1H) 7.88 (d, 2H) 7.69 (t, 2H) 7.26-7.43 (m, 4H) 6.81 (s, 1H) 6.76 (s, 1H) 5.40 (m, 2H) 5.18 (m, 2H) 4.18-4.36 (m, 3H) 3.81 (m, 1H) 3.49 (m, 2H) 2.87 (m, 2H) 1.00-1.60 (m, 6H) 1.38 (s, 9H) 1.36 (s, 18H). ^{13}C NMR (400 MHz, DMSO-d6) δ 170.78, 170.26, 167.04, 166.58, 156.25, 156.03, 155.64, 153.53, 150.10, 150.02, 148.96, 144.04, 143.91, 140.80, 140.79, 127.80, 127.52, 127.29, 126.94, 125.30, 120.19, 120.14, 83.31, 77.39, 46.95, 29.44, 28.40, 28.22, 27.40, 27.22. HRMS (ESI-TOF) *m/z* 887.3907 (calc'd $[M + H]^+$ = 887.4298).

Fmoc Lysyl Thymine Monomer (**2**). (49% yield) ^{1}H NMR (400 MHz, DMSO-d6, two rotamers) δ 11.30 (rotamer one, s, 1H) 11.28 (rotamer two, s, 1H) 7.88 (d, 2H) 7.68 (t, 2H) 7.41 (t, 2H) 7.32 (t, 2H) 7.21 (s, 1H) 6.77 (m, 1H) 4.63 (m, 2H) 4.45 (s, 1H) 4.30 (m, 2H) 4.21 (m, 2H) 3.92 (m, 2H)

3.35 (m, 2H) 2.88 (m, 2H) 1.72 (rotamer one, s, 3H) 1.69 (rotamer two, s, 3H) 1.19-1.44 (m, 6H) 1.36 (s, 9H). ^{13}C NMR (400 MHz, DMSO-d6) δ 170.32, 167.81, 167.45, 164.43, 156.14, 156.00, 155.62, 151.01, 143.91, 143.83, 140.79, 140.76, 127.66, 127.11, 125.24, 120.17, 108.14, 77.38, 65.34, 47.75, 46.87, 38.29, 29.33, 28.30, 22.90, 22.82, 11.96. HRMS (ESI-TOF) *m/z* 678.3166 (calc'd $[M + H]^+$ = 678.3134).

Fmoc Methyl Cytosine Monomer (**3**). (43% yield) ^{1}H NMR (400 MHz, DMSO-d6) δ 7.95 (d, 1H) 7.87 (d, 2H) 7.68 (d, 2H) 7.40 (m, 3H) 7.33 (t, 2H) 6.79 (t, 1H) 4.84 (m, 1H) 4.67 (m, 1H) 4.26 (m, 4H) 3.93 (m, 2H) 3.48 (m, 2H) 1.48 (s, 18H) 1.01 (d, 3H). ^{13}C NMR (400 MHz, DMSO-d6) δ 168.03, 162.30, 162.22, 155.98, 165.63, 162.11, 149.70, 144.32, 141.14, 128.02, 127.48, 125.65, 120.53, 95.61, 84.92, 64.92, 52.48, 50.41, 48.89, 47.15, 45.68, 27.66, 18.76 HRMS (ESI-TOF) *m/z* 706.3113 (calc'd $[M + H]^+$ = 706.3083).

Fmoc Methyl Thymine Monomer (**4**). (85% yield) ^{1}H NMR (400 MHz, DMSO-d6) δ 11.25 (s, broad, 1H) 7.87 (d, 2H) 7.68 (d, 2H) 7.41 (m, 3H) 7.32 (t, 2H) 7.22 (s, 1H) 4.63 (m, 1H) 4.44 (m, 2H) 4.25 (m, 3H) 3.83 (s, 2H) 3.44 (m, 2H) 1.70 (s, 3H) 0.99 (d, 3H) ^{13}C NMR (400 MHz, DMSO-d6) δ 168.36, 167.50, 164.86, 155.97, 151.46, 144.40, 144.29, 142.63, 141.13, 128.03, 127.51, 125.68, 120.52, 110.00, 108.37, 65.71, 48.26, 47.17, 45.76, 18.87, 12.32. HRMS (ESI-TOF) *m/z* 521.2051 (calc'd $[M + H]^+$ = 521.2031).

Synthesis of 4-(dimethylamino)naphthalimide monomer:

The 4-DMN monomer was synthesized according to an adapted procedure from Saito, et. al.[34]

4-dimethylamino-napthalic anhydride (**5**). 4-bromo-1,8-naphthalic anhydride (1 eq) dissolved in isoamyl alcohol was brought to reflux in an oil bath. 3-Dimethylamino-proprionitrile (4 eq) was

added and the mixture was refluxed overnight. The reaction was cooled to room temperature and the precipitate filtered. The precipitate was washed with water and cold hexane and dried under reduced pressure to yield a brown solid in quantitative yield. ^{1}H NMR (400 MHz, $CDCl_3$) δ 8.50 (d, 1H) 8.46 (d, 1H) 8.37 (d, 1H) 7.65 (t, 1H) 7.06 (d, 1H) 3.18 (s, 6H). ^{13}C NMR (400 MHz, $CDCl_3$) δ 161.76, 160.78, 157.98, 135.03, 133.20, 133.00, 125.02, 124.83, 119.19, 113.18, 109.30, 44.69. HRMS (ESI-TOF) *m/z* 242.0834 (calc'd $[M + H]^+$ = 242.0812).

4-dimethylamino-naphthalimide tert-butyl acetate (**6**). To a solution of 4-dimethylamino-napthalic anhydride **5** (36 mmol) and glycine tert-butyl ester (54 mmol) in 180 mL of dry DMF was added DIPEA (108 mmol). The turbid solution was brought to 80 °C and stirred overnight or until full consumption of the anhydride by TLC. Upon completion, the reaction was quenched by addition of 250 mL water and extracted with ethyl acetate (3x250 mL). The organic layer was washed with water and brine, dried with anhydrous sodium sulfate, and concentrated using rotary evaporation. The crude solid was purified by flash column chromatrography (1:1 ethyl acetate:hexane) to yield a yellow solid (78%). ^{1}H NMR (400 MHz, $CDCl_3$) δ 8.50 (d, 1H) 8.40 (d, 1H) 8.36 (d, 1H) 7.59 (t, 1H) 7.02 (d, 1H) 4.80 (s, 2H) 3.05 (s, 6H) 1.46 (9H). ^{13}C NMR (400 MHz, $CDCl_3$) δ 167.40, 164.28, 163.63, 157.20, 133.01, 132.93, 130.45, 125.25, 125.17, 122.58, 114.28, 113.21, 113.11, 81.98, 44.72, 41.96, 28.15. HRMS (ESI-TOF) *m/z* 355.16595 (calc'd $[M + H]^+$ = 355.1652).

4-dimethylamino-naphthalimide acetic acid (**7**). 4-dimethylamino-naphthalimide tert-butyl acetate **6** (18 mmol) was dissolved in a 50% mixture of TFA in DCM (90 mL). After stirring for 3 hours, TLC indicated reaction completion. The reaction was concentrated using rotary evaporation and azeotroped with toluene (3x). The solid was triturated with hexane/DCM, filtered, and the collected solid was dried under reduced pressure to yield the final product as a yellow solid (94%). ^{1}H NMR (400 MHz, DMSO-d6) δ 13.02 (s, broad, 1H) 8.40 (d, 1H) 8.35 (d, 1H) 8.21 (d, 1H) 7.66 (t, 1 H)

7.08 (d, 1H) 4.67 (s, 2H) 3.04 (s, 6H). ^{13}C NMR (400 MHz, DMSO-d6) δ 169.59, 163.31, 162.53, 156.76, 132.53, 131.96, 130.77, 129.66, 124.84, 123.98, 121.67, 112.76, 112.35, 44.34, 40.94. HRMS (ESI-TOF) *m/z* 299.10318 (calc'd $[M + H]^+$ = 299.1026).

Fmoc 4-dimethylamino-naphthalimide (aminoethyl)glycine benzyl ester (**8**). 4-dimethylamino-naphthalimide acetic acid **7** (2.67 mmol) was dissolved in dry DMF (15 mL) under N_2 in a round bottom flask. The flask was charged with HATU (2.67 mmol) and DIPEA (4.46 mmol). The reaction was stirred for 15 min before addition of Fmoc(aminoethyl)glycine benzyl ester PNA backbone (1.78 mmol) in dry DMF (5 mL). The reaction was stirred for 2.5 h, at which time TLC showed complete consumption of the backbone. Upon completion, the reaction was quenched with H_2O, extracted with ethyl acetate and washed with 1M HCl, saturated $NaHCO_3$, H_2O and brine. The organic layer was dried with anhydrous sodium sulfate and concentrated by rotary evaporation. The crude yellow solid was purified by flash column chromatography (hexane to ethyl acetate gradient) to provide the product as a yellow solid (72%). ^{1}H NMR (400 MHz, $CDCl_3$) δ 8.51 (d, 1H) 8.38 (m, 2H) 7.69 (m, 3H) 7.57 (m, 2H) 7.31 (m, 9H) 7.01 (d, 1H) 6.23 (t, 1H) 5.15 (s, 2H) 5.10 (s, 2H) 4.40 (d, 1H) 4.30 (t, 2H) 4.13 (s, 2H) 3.40-3.70 (m, 4H) 3.05 (s, 6H) ^{13}C NMR (400 MHz, $CDCl_3$) δ 169.81, 168.08, 164.43, 163.83, 157.23, 157.09, 144.20, 141.29, 135.23, 133.12, 131.56, 131.46, 130.57, 128.81, 128.68, 128.46, 128.39, 127.64, 127.13, 125.45, 125.20, 124.80, 122.68, 119.90, 114.41, 113.22, 67.89, 67.34, 49.32, 49.11, 47.29, 44.79, 40.98, 39.66. HRMS (ESI-TOF) *m/z* 711.2901 (calc'd $[M + H]^+$ = 711.2813).

Fmoc 4-dimethylamino-naphthalimide PNA monomer (**9**). Fmoc 4-dimethylamino-naphthalimide (aminoethyl)glycine benzyl ester **8** (1.49 mmol) was dissolved in methanol (25 mL) under N_2. Palladium on activated charcoal (7%/wt.) was added to the solution. The N_2 was replaced by H_2 and the reaction was stirred overnight, after which TLC showed full conversion to product. The

reaction was filtered through celite and concentrated using rotary evaporation to provide the product as a yellow solid in quantitative yield. ^{1}H NMR (400 MHz, DMSO-d6, two rotamers) δ 8.52 (rotamer one, d, 1H) 8.46 (rotamer two, d, 1H) 8.42 (rotamer one, d, 1H) 8.37 (rotamer two, d, 1H) 8.31 (rotamer one, d, 1H) 8.24 (rotamer two, d, 1H) 7.87 (rotamer one, t, 3H with Fmoc) 7.76 (rotamer two, t, 1H) 7.70 (d, 2H) 7.66 (d, 2H) 7.54 (t, 1H) 7.20 (rotamer one, d, 1H) 7.14 (rotamer two, d, 1H) 4.98 (s, 2H) 4.80 (s, 2H) 4.34 (d, 2H) 4.27 (t, 1H) 3.56 (t, 2H) 3.15 (m, 2H) 3.10 (rotamer one, s, 6H) 3.07 (rotamer two, s, 6H). ^{13}C NMR (400 MHz, DMSO-d6) δ 167.39, 166.82, 136.39, 162.67, 156.75, 156.46, 156.13, 143.94, 140.75, 132.41, 131.85, 130.70, 129.75, 127.62, 127.09, 125.20, 124.99, 124.19, 122.05, 120.13, 112.88, 65.64, 46.77, 46.39, 44.39, 44.36, 38.26. HRMS (ESI-TOF) *m/z* 621.2399 (calc'd $[M + H]^+$ = 621.2344).

PNA oligomer synthesis

PNA was synthesized on a Biotage SP Wave semi-automatic peptide synthesizer. Synthesis began by down-loading 50mg of a rink amide MBHA resin (0.52 mmol/g) with 5 µmols of the first Fmoc PNA monomer or Fmoc-Lys(Boc)-OH using HATU (1.2 eq), DIPEA (1.2 eq), and 2,6-lutidine (1.2 eq) in 200 µL dry NMP for 1 hour at room temperature followed by 1 hour of capping using a solution of 9% acetic anhydride/13% 2,6-lutidine in DMF. Successive couplings were performed using microwave assistance at 75 °C for 6 min with Fmoc PNA monomer (5 eq), HATU (5eq), DIPEA (5 eq) and 2,6-lutidine (5 eq) in 400 µL dry NMP. After coupling, capping (2x5 min with 1mL capping solution), washing (3x1.1 mL DMF, 3x1.1 mL DCM, then 3x1.1 mL DMF), deprotection (3x2 min with 1mL 25% piperidine/DMF), and washing (same as previous) completed a coupling cycle. All steps were monitored for completion by Kaiser test. Monomer coupling efficiency was monitored by absorbance at 301 nm of the dibenzofulvene-piperidine adduct using a Nanodrop 2000 spectrophotometer. Upon completion of synthesis, cleavage was performed twice using 500 µL of cleavage solution (95% TFA/2.5% triisopropylsilane/2.5% H_2O)

for 1 h. The crude oligomer was collected by ether precipitation and purified by reverse-phase HPLC using an Agilent Eclipse XDB-C18 5 μm, 9.4 x 250 mm column at 60°C with a flow rate of 2 mL/min, monitored at 260 nm using a linear gradient (10-40%) of 0.1% TFA/acetonitrile in 0.1% TFA/water. Identity was confirmed by ESI-TOF mass spectrometry.

Melting Temperature Analysis of PNA Strands

Samples containing 5 μM PNA and 5 μM complementary DNA or miRNA-21 were prepared from stock solutions in 1x PBS. The samples were transferred to an 8-cell quartz microcuvette with a 1 cm pathlength. A Shimadzu UV-1800 spectrophotometer equipped with a temperature controller and Julabo CORIO CD water circulator was used for the measurement. Absorbance was monitored at 260 nm from 25-95 °C at a rate of 0.5 °C/min. Melting temperatures were calculated by the first derivative method using a total of three independent trials.

Preparation of PNA amphiphile assemblies

In order to form uniform assemblies, samples of PNA dissolved in water or 1x PBS were heated to 95 °C for 30 min. The samples were then cooled to room temperature and incubated for at least 1 h before analysis.

PNA amphiphile CMC determination using internal 4-DMN monomer

The critical micelle concentration (CMC) of PNA-A was determined by the fluorescence response of the internal 4-DMN monomer. Samples of PNA-A, control PNA-C, and fully deprotected 4-DMN monomer ranging in concentration from 125 μM–0.0.061 μM in 1%DMSO/H_2O were prepared from stock solutions. DMSO was used to initially dissolve the monomer, then stock solutions were prepared in H_2O to a final DMSO content of 1% in each sample. Each sample was treated for amphiphile assembly as previously stated. Samples were

then transferred to a 384-well clear-bottom plate for analysis on a Biotek Cytation5 plate reader (higher concentrations) or to a 50 μL quartz cuvette for analysis by a Horiba Scientific Dual-FL fluorometer (lower concentrations). Fluorescence measurements at 550 nm were collected using an excitation of 458 nm. Absorbance was also measured at 458 nm to correct for any changes in concentration between PNA samples and the monomer. A plot of the fluorescence enhancement of the PNA samples over the monomer versus concentration was created using GraphPad Prism software and used to estimate the CMC. A semi-logarithmic fit to the data provided equations for the upper and lower portions of the curve, which were then compared to determine a CMC value of 317 nM.

Characterization of assemblies by TEM

Samples of PNA at 1mM and 100 μM were prepared in H_2O from stock solutions. Assemblies were formed as previously stated. 3.5 μL of sample was spotted onto a 200-mesh formvar/carbon-coated copper grid for 2 min before wicking with filter paper. 3.5 μL of a fresh 1% uranyl acetate stain solution was then spotted onto the grids for 30 sec before wicking with filter paper. The grids were allowed to dry at room temperature for 30 min before imaging using a Hitachi HT7700 transmission electron microscope.

Size distribution determination from TEM

Images were analyzed using the NIH ImageJ software. Particle diameters were measured manually by setting the scale of the image to the scale bar. Lines were drawn and measured in triplicate for each particle that had clear boundaries without overlap in order to accurately determine an average diameter for each particle. A total of 128 particles were measured and a histogram of the data using 12 bins for size was produced using the GraphPad Prism software.

Determination of size using dynamic light scattering

Samples of PNA were prepared in water to a concentration of 500 μM. The samples were heated to 95°C for 30 min, followed by sonication at 50°C for 10 min and incubation at RT for 1 hour to create uniform assemblies. Sizes were measured using a Particulate Systems NanoPlus DLS nano particle analyzer and automically generated by the NanoPlus software.

Confirmation of binding of complementary DNA to PNA-A by CD

DNA and RNA samples were purchased from Integrated DNA Technologies. Circular dichroism was used to confirm binding and therefore disruption of PNA amphiphile assemblies. Samples of PNA were prepared at 200 μM in 1x PBS. Assemblies were formed as previously stated. DNA stocks at concentrations of 100 μM, 200 μM, 300 μM, and 400 μM were prepared in 1x PBS. 30 μL of PNA was mixed with 30 μL of DNA stocks to a final concentration of 100 μM PNA and DNA concentrations of 50 μM, 100 μM, 150 μM, and 200 μM in 1x PBS. Samples were incubated for 1 h before being analyzed by a JASCO J-1500 circular dichroism spectrometer. Data points were collected every 1 nm from 190-300 nm using a continuous scanning mode of 200 nm/min at 23.5°C. Samples containing a scrambled DNA sequence were prepared in the same manner and analyzed simultaneously.

Confirmation of binding of miRNA-21 to PNA-A by CD

Samples were prepared similarly to analysis by DNA. PNA-A samples of 200 μM in water were prepared as previously described. A 200 μM stock of miRNA-21 was added to the samples in water to a final concentration of 100 μM PNA and 100 μM miRNA-21. The samples were incubated for 1 h before being analyzed.

PNA amphiphile disassembly by 4-DMN fluorescence

Samples of PNA-A at 11.11 μM in 1.1xPBS were prepared and the assemblies formed as previously stated. Complementary and scrambled DNA stocks ranging from 25 μM–200 μM were prepared and 5 μL of each was added to the appropriate PNA sample to a final concentration of 10 μM PNA and 2.5 μM-20 μM DNA in 1xPBS. After addition, samples were incubated for 1 hour before being transferred to a 384-well plate and analyzed using a Biotek Cytation5 plate reader. Fluorescence measurements at 550 nm were collected using an excitation of 458 nm.

PNA amphiphile disassembly by complementary DNA on TEM

Samples of 400 μM PNA-A in 1x PBS were prepared from stock solutions. Assemblies were formed as previously stated. To the samples was added complementary DNA or a scrambled DNA sequence in 1x PBS for a final concentration of 200 μM PNA-A and 200 μM DNA. Samples were incubated at room temperature for 1 h before preparation for TEM using the same procedure described above.

PNA amphiphile disassembly by complementary RNA on TEM

Samples of 200 μM PNA-A in water were prepared from stock solutions. Assemblies were formed as previously stated. To the samples was added a 200 μM stock of miRNA-21 in water to a final concentration of 100 μM PNA-A and 100 μM miRNA-21. The samples were incubated at room temperature for 1 h before preparation for TEM.

References:

(1) Swenson, C. S.; Velusamy, A.; Argueta-Gonzalez, H. S.; Heemstra, J. M. Bilingual Peptide Nucleic Acids: Encoding the Languages of Nucleic Acids and Proteins in a Single Self-Assembling Biopolymer. *J. Am. Chem. Soc.* **2019**, *141* (48), 19038–19047.

https://doi.org/10.1021/jacs.9b09146.

(2) Seeman, N. C.; Sleiman, H. F. DNA Nanotechnology. *Nat. Rev. Mater.* **2018**, *3* (1), 17068. https://doi.org/10.1038/natrevmats.2017.68.

(3) Sato, K.; Hendricks, M. P.; Palmer, L. C.; Stupp, S. I. Peptide Supramolecular Materials for Therapeutics. *Chem. Soc. Rev.* **2018**, *47* (20), 7539–7551. https://doi.org/10.1039/C7CS00735C.

(4) Habibi, N.; Kamaly, N.; Memic, A.; Shafiee, H. Self-Assembled Peptide-Based Nanostructures: Smart Nanomaterials toward Targeted Drug Delivery. *Nano Today* **2016**, *11* (1), 41–60. https://doi.org/10.1016/j.nantod.2016.02.004.

(5) Peterson, A. M.; Heemstra, J. M. Controlling Self-Assembly of DNA-Polymer Conjugates for Applications in Imaging and Drug Delivery. *Wiley Interdiscip. Rev. Nanomedicine Nanobiotechnology* **2015**, *7* (3), 282–297. https://doi.org/10.1002/wnan.1309.

(6) Kwak, M.; Herrmann, A. Nucleic Acid Amphiphiles: Synthesis and Self-Assembled Nanostructures. *Chem. Soc. Rev.* **2011**, *40* (12), 5745. https://doi.org/10.1039/c1cs15138j.

(7) Zhang, F.; Nangreave, J.; Liu, Y.; Yan, H. Structural DNA Nanotechnology: State of the Art and Future Perspective. *J. Am. Chem. Soc.* **2014**, *136* (32), 11198–11211. https://doi.org/10.1021/ja505101a.

(8) Egholm, M.; Buchardt, O.; Nielsen, P. E.; Berg, R. H. Peptide Nucleic Acids (PNA). Oligonucleotide Analogs with an Achiral Peptide Backbone. *J. Am. Chem. Soc.* **1992**, *114* (5), 1895–1897. https://doi.org/10.1021/ja00031a062.

(9) Nielsen, P. E. Peptide Nucleic Acid. A Molecule with Two Identities. *Acc. Chem. Res.* **1999**, *32* (7), 624–630. https://doi.org/10.1021/ar980010t.

(10) Dueholm, K. L.; Peterson, K. H.; Jensen, D. K.; Egholm, M.; Nielsen, P. E.; Buchardt, O. Peptide Nucleic Acid (PNA) with a Chiral Backbone Based on Alanine. *Bioorg. Med. Chem. Lett.* **1994**, *4* (8), 1077–1080. https://doi.org/10.1016/S0960-894X(01)80684-3.

(11) Egholm, M.; Buchardt, O.; Christensen, L.; Behrens, C.; Freier, S. M.; Driver, D. A.; Berg,

R. H.; Kim, S. K.; Norden, B.; Nielsen, P. E. PNA Hybridizes to Complementary Oligonucleotides Obeying the Watson–Crick Hydrogen-Bonding Rules. *Nature* **1993**, *365*, 566–568. https://doi.org/10.1038/365566a0.

(12) Demidov, V. V; Potaman, V. N.; Frank-Kamenetskii, M. D.; Egholm, M.; Buchardt, O.; Sonnichsen, S. H.; Nlelsen, P. E. Stability of Peptide Nucleic Acids in Human Serum and Cellular Extracts. *Biochem. Pharmacol.* **1994**, *48* (6), 1310–1313.

(13) Nielsen, P. E.; Haaima, G.; Lohse, A.; Buchardt, O. Peptide Nucleic Acids (PNAs) Containing Thymine Monomers Derived from Chiral Amino Acids: Hybridization and Solubility Properties OfD-Lysine PNA. *Angew. Chemie Int. Ed. English* **1996**, *35* (17), 1939–1942. https://doi.org/10.1002/anie.199619391.

(14) Sforza, S.; Tedeschi, T.; Corradini, R.; Marchelli, R. Induction of Helical Handedness and DNA Binding Properties of Peptide Nucleic Acids (PNAs) with Two Stereogenic Centres. *European J. Org. Chem.* **2007**, *2007* (35), 5879–5885. https://doi.org/10.1002/ejoc.200700644.

(15) Dragulescu-Andrasi, A.; Rapireddy, S.; Frezza, B. M.; Gayathri, C.; Gil, R. R.; Ly, D. H. A Simple γ-Backbone Modification Preorganizes Peptide Nucleic Acid into a Helical Structure. *J. Am. Chem. Soc* **2006**, *128* (31), 10258–10267. https://doi.org/10.1021/JA0625576.

(16) Yeh, J. I.; Shivachev, B.; Rapireddy, S.; Crawford, M. J.; Gil, R. R.; Du, S.; Madrid, M.; Ly, D. H. Crystal Structure of Chiral ΓPNA with Complementary DNA Strand: Insights into the Stability and Specificity of Recognition and Conformational Preorganization. *J. Am. Chem. Soc.* **2010**, *132* (31), 10717–10727. https://doi.org/10.1021/ja907225d.

(17) Zhou, P.; Wang, M.; Du, L.; Fisher, G. W.; Waggoner, A.; Ly, D. H. Novel Binding and Efficient Cellular Uptake of Guanidine-Based Peptide Nucleic Acids (GPNA). *J. Am. Chem. Soc* **2003**, *125* (23), 6878–6879. https://doi.org/10.1021/JA029665M.

(18) Sahu, B.; Chenna, V.; Lathrop, K. L.; Thomas, S. M.; Zon, G.; Livak, K. J.; Ly, D. H.

Synthesis of Conformationally Preorganized and Cell-Permeable Guanidine-Based γ-Peptide Nucleic Acids (ΓGPNAs). *J. Org. Chem.* **2009**, *74* (4), 1509–1516. https://doi.org/10.1021/jo802211n.

(19) Manicardi, A.; Fabbri, E.; Tedeschi, T.; Sforza, S.; Bianchi, N.; Brognara, E.; Gambari, R.; Marchelli, R.; Corradini, R. Cellular Uptakes, Biostabilities and Anti-MiR-210 Activities of Chiral Arginine-PNAs in Leukaemic K562 Cells. *ChemBioChem* **2012**, *13* (9), 1327–1337. https://doi.org/10.1002/cbic.201100745.

(20) Dose, C.; Seitz, O. Single Nucleotide Specific Detection of DNA by Native Chemical Ligation of Fluorescence Labeled PNA-Probes. *Bioorg. Med. Chem.* **2008**, *16* (1), 65–77. https://doi.org/10.1016/J.BMC.2007.04.059.

(21) Englund, E. A.; Wang, D.; Fujigaki, H.; Sakai, H.; Micklitsch, C. M.; Ghirlando, R.; Martin-Manso, G.; Pendrak, M. L.; Roberts, D. D.; Durell, S. R.; Appella, D. H. Programmable Multivalent Display of Receptor Ligands Using Peptide Nucleic Acid Nanoscaffolds. *Nat. Commun.* **2012**, *3* (1), 614. https://doi.org/10.1038/ncomms1629.

(22) Englund, E. A.; Appella, D. H. Synthesis of γ-Substituted Peptide Nucleic Acids: A New Place to Attach Fluorophores without Affecting DNA Binding. *Org. Lett.* **2005**, *7* (16), 3465–3467. https://doi.org/10.1021/OL051143Z.

(23) De Costa, N. T. S.; Heemstra, J. M. Evaluating the Effect of Ionic Strength on Duplex Stability for PNA Having Negatively or Positively Charged Side Chains. *PLoS One* **2013**, *8* (3), e58670. https://doi.org/10.1371/journal.pone.0058670.

(24) Vernille, J. P.; Kovell, L. C.; Schneider, J. W. Peptide Nucleic Acid (PNA) Amphiphiles: Synthesis, Self-Assembly, and Duplex Stability. *Bioconjug. Chem.* **2004**, *15* (6), 1314–1321. https://doi.org/10.1021/BC049831A.

(25) Marques, B. F.; Schneider, J. W. Sequence-Specific Binding of DNA to Liposomes Containing Di-Alkyl Peptide Nucleic Acid (PNA) Amphiphiles. *Langmuir* **2005**, *21* (6), 2488–2494. https://doi.org/10.1021/LA047962U.

(26) Lau, C.; Bitton, R.; Bianco-Peled, H.; Schultz, D. G.; Cookson, D. J.; Grosser, S. T.; Schneider, J. W. Morphological Characterization of Self-Assembled Peptide Nucleic Acid Amphiphiles. *J. Phys. Chem. B* **2006**, *110* (18), 9027–9033. https://doi.org/10.1021/JP057049H.

(27) Kumarswamy, R.; Volkmann, I.; Thum, T. Regulation and Function of MiRNA-21 in Health and Disease. *RNA Biol.* **2011**, *8* (5), 706–713. https://doi.org/10.4161/rna.8.5.16154.

(28) Nielsen, P. E.; Egholm, M. An Introduction to Peptide Nucleic Acid. *Curr. Issues Molec. Biol.* **1999**, *1* (2), 89–104.

(29) Kleiner, R. E.; Brudno, Y.; Birnbaum, M. E.; Liu, D. R. DNA-Templated Polymerization of Side-Chain-Functionalized Peptide Nucleic Acid Aldehydes. *J. Am. Chem. Soc* **2008**, *130* (14), 4646–4659. https://doi.org/10.1021/JA0753997.

(30) Loving, G.; Imperiali, B. A Versatile Amino Acid Analogue of the Solvatochromic Fluorophore 4- *N,N* -Dimethylamino-1,8-Naphthalimide: A Powerful Tool for the Study of Dynamic Protein Interactions. *J. Am. Chem. Soc.* **2008**, *130* (41), 13630–13638. https://doi.org/10.1021/ja804754y.

(31) Manna, A.; Rapireddy, S.; Sureshkumar, G.; Ly, D. H. Synthesis of Optically Pure ΓPNA Monomers: A Comparative Study. *Tetrahedron* **2015**, *71* (21), 3507–3514. https://doi.org/10.1016/j.tet.2015.03.052.

(32) Porcheddu, A.; Giacomelli, G.; Piredda, I.; Carta, M.; Nieddu, G. A Practical and Efficient Approach to PNA Monomers Compatible with Fmoc-Mediated Solid-Phase Synthesis Protocols. *European J. Org. Chem.* **2008**, *2008* (34), 5786–5797. https://doi.org/10.1002/ejoc.200800891.

(33) Wu, Y.; Xu, J.-C. Synthesis of Chiral Peptide Nucleic Acids Using Fmoc Chemistry. *Tetrahedron* **2001**, *57* (38), 8107–8113. https://doi.org/10.1016/S0040-4020(01)00789-X.

(34) Ikeda, H.; Nakamura, Y.; Saito, I. Synthesis and Characterization of Naphthalimide-Containing Peptide Nucleic Acid. *Tetrahedron Lett.* **2002**, *43* (32), 5525–5528.

https://doi.org/10.1016/S0040-4039(02)01164-4.

(35) Kollar, J.; Hrdlovic, P.; Chmela, S.; Sarakha, M.; Guyot, G. Synthesis and Transient Absorption Spectra of Derivatives of 1,8-Naphthalic Anhydrides and Naphthalimides Containing 2,2,6,6-Tetramethylpiperidine; Triplet Route of Deactivation. *J. Photochem. Photobiol. A Chem.* **2005**, *170* (2), 151–159. https://doi.org/10.1016/J.JPHOTOCHEM.2004.07.021.

(36) Grimm, J. B.; English, B. P.; Chen, J.; Slaughter, J. P.; Zhang, Z.; Revyakin, A.; Patel, R.; Macklin, J. J.; Normanno, D.; Singer, R. H.; Lionnet, T.; Lavis, L. D. A General Method to Improve Fluorophores for Live-Cell and Single-Molecule Microscopy. *Nat. Methods* **2015**, *12* (3), 244–250. https://doi.org/10.1038/nmeth.3256.

(37) Feagin, T. A.; Shah, N. I.; Heemstra, J. M. Convenient and Scalable Synthesis of Fmoc-Protected Peptide Nucleic Acid Backbone. *J. Nucleic Acids* **2012**, *2012*, 354549. https://doi.org/10.1155/2012/354549.

(38) Pabisch, S.; Feichtenschlager, B.; Kickelbick, G.; Peterlik, H. Effect of Interparticle Interactions on Size Determination of Zirconia and Silica Based Systems - A Comparison of SAXS, DLS, BET, XRD and TEM. *Chem. Phys. Lett.* **2012**, *521*, 91–97. https://doi.org/10.1016/j.cplett.2011.11.049.

(39) Souza, T. G. F.; Ciminelli, V. S. T.; Mohallem, N. D. S. A Comparison of TEM and DLS Methods to Characterize Size Distribution of Ceramic Nanoparticles. In *Journal of Physics: Conference Series*; Institute of Physics Publishing, 2016; Vol. 733, p 012039. https://doi.org/10.1088/1742-6596/733/1/012039.

(40) Domingos, R. F.; Baalousha, M. A.; Ju-Nam, Y.; Reid, M. M.; Tufenkji, N.; Lead, J. R.; Leppard, G. G.; Wilkinson, K. J. Characterizing Manufactured Nanoparticles in the Environment: Multimethod Determination of Particle Sizes. *Enironmental Sci. Technol.* **2009**, *43* (19), 7277–7284. https://doi.org/10.1021/es900249m.

(41) Faccini, A.; Tortori, A.; Tedeschi, T.; Sforza, S.; Tonelli, R.; Pession, A.; Corradini, R.;

Marchelli, R. Circular Dichroism Study of DNA Binding by a Potential Anticancer Peptide Nucleic Acid Targeted Against the MYCN Oncogene. **2008**, *500* (April 2007), 494–500. https://doi.org/10.1002/chir.

(42) Sharma, C.; Awasthi, S. K. Versatility of Peptide Nucleic Acids (PNAs): Role in Chemical Biology, Drug Discovery, and Origins of Life. *Chem. Biol. Drug Des.* **2017**, *89* (1), 16–37. https://doi.org/10.1111/cbdd.12833

Chapter 3

Forced Intercalation Peptide Nucleic Acid Probes for the Detection of an Adenosine-to-Inosine Modification*

3.1 Abstract:

The deamination of adenosine to inosine is an important modification in nucleic acids that functionally recodes the identity of the nucleobase. Current methods to analyze and detect this single nucleotide change, such as sequencing and PCR, typically require laborious and costly procedures. Alternatively, fluorescent "turn-on" probes that result in signal enhancement in the presence of target are useful tools for real-time detection and monitoring of nucleic acid modification. Here a forced-intercalation PNA (FIT-PNA) probe was designed to bind to inosine-containing nucleic acids using thiazole orange (TO), 4-dimethylamino-naphthalimide (4DMN), and malachite green (MG) fluorogenic dyes. We show that incorporation of the dye as a surrogate base negatively affects the duplex stability but does not abolish binding to targets, while the identity of the adjacent nucleobase and temperature affect the overall signal and selectivity for inosine. We determine that TO probes are viable candidates to enable selective inosine detection for biological applications.

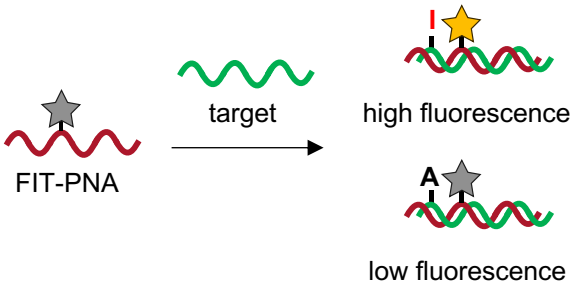

*Authors: Swenson, C.S.; Robichaux, R.; Knutson, S. D.; Heemstra, J. M.

3.2 Introduction:

Genetic information is converted from DNA into protein in a highly regulated manner using RNA as an intermediary. The posttranscriptional modification of RNA is an important cellular mechanism for regulating gene expression. In higher eukaryotes, the predominant type of RNA editing results in a change in the nucleobase identity and base pairing preference, such as the deamination of an adenosine to inosine (A → I) catalyzed by ADAR (adenosine deaminases acting on RNA) enzymes (**Figure 3.1A**).[1] Inosine base pairs with cytosine, essentially recoding and A to a G. Aberrant activity in the ADAR family has been linked to many types of cancer and neurological disorders including glioblastoma, epilepsy and amyotrophic lateral sclerosis (ALS).[2–7]Additionally, inosine can be detected in DNA as a result of oxidative damage that may result in changes to downstream transcription and translation.[8]

While A → I editing is detectable by sequencing, a key challenge is the detection of single nucleotide variations in targeted transcripts. Previously our lab has developed an inosine enrichment technique for use in high-throughput RNA sequencing (RNA-seq) to identify and detect edited sites.[9] While effective, we recognized that this approach is not time or cost-effective and is incapable of real-time analysis of RNA editing due to mulit-step sample preparation. As a simpler method for detecting inosine, we developed a covalent chemical labeling approach to attach reporter molecules to edited transcripts.[10,11] However, the multiple required steps and inability to label inosine in a sequence-defined manner make it difficult to transition to live-cell and real-time applications for specific transcripts. We acknowledged the need for a method that selectively detects inosine-containing nucleic acids with high affinity and low background in a single step to overcome these limitations.

Forced intercalation (FIT) oligonucleotide probes are useful tools for detecting and imaging DNA and RNA targets *in vitro* and *in cellulo*.[12] The replacement of a canonical nucleobase with a fluorogenic dye such as thiazole orange (TO) along the backbone imparts a responsive behavior.[13,14] These probes selectively bind targets *via* complementary Franklin-Watson-Crick

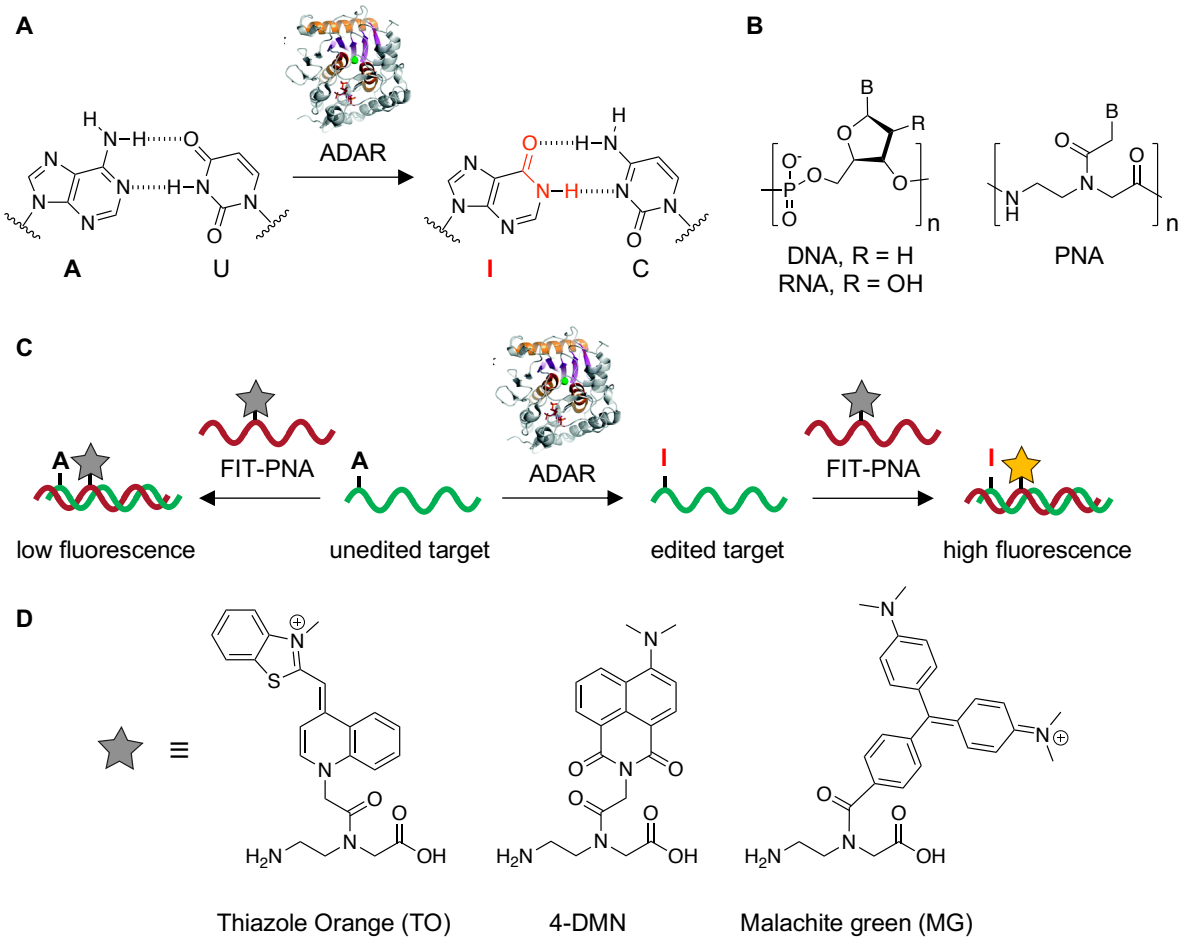

Figure 3.1: FIT-PNA probes target inosine containing nucleic acids. A) Adenosine is deaminated to inosine by ADAR. B) Chemical structures of DNA, RNA, and PNA. C) PNA-FIT probes allow discrimination of edited and unedited targets by a fluorescent signal. D) Chemical structures of fluorogenic dyes used in this study.

hybridization, prompting a fluorescent response from the dye and making them capable of distinguishing single mismatched nucleotides.[15] Because high affinity and specificity are requirements for performance, many research groups have turned to using peptide nucleic acid (PNA) as a convenient scaffold to design and synthesize FIT probes.

PNA is an unnatural nucleic acid mimic wherein a pseudopeptide backbone replaces the sugar phosphate backbone of canonical DNA or RNA (**Figure 3.1B**).[16] This synthetic backbone provides the molecule with stronger hybridization affinity, improved specificity, and increased resistance to enzymatic degradation, all of which are essential properties for FIT probe applications.[16–20] Therefore, it is unsurprising that many FIT-PNA probes have been developed to

detect and image myriad nucleic acid targets *in vitro* and in live cells.[21–28] Kam et. al. demonstrated the ability of a TO-containing FIT-PNA to image the mutated *KRAS* oncogene in live cells with single nucleotide polymorphism resolution.[29] Similarly, Seitz and coworkers exhibited the detection of a cytidine to uridine (C → U) RNA edit using a binary probe system.[30] This was the first example of using a FIT-PNA probe to image a posttranscriptional modification expressed in live cells. However, a FIT-PNA probe has not yet been reported to selectively target inosine-containing nucleic acids for imaging and detection of enzyme activity (**Figure 3.1C**).

Significant advances have also been made to expand the repertoire of fluorogenic dyes available for designing FIT-PNA probes.[31–36] Our group has previously achieved success using the fluorogenic dyes 4-dimethylamino-naphthalimide (4DMN) and malachite green (MG) as reporters for PNA self-assembly and protein labeling, respectively.[37,38] We hypothesized that these dyes could be incorporated into FIT-PNA probes and provide enhanced fluorescence upon binding similar to the well characterized TO dye (**Figure 3.1D**). Here we describe the synthesis and characterization of a novel MG-containing PNA monomer followed by the design, synthesis, and characterization of FIT-PNA probes incorporating TO, 4DMN, and MG dyes to target an inosine-containing oligonucleotide. We demonstrate that the mismatched base identity and temperature effect the overall fluorescence and specificity. Through experimental observation, we conclude that TO-containing FIT-PNA probes are viable candidates for distinguishing adenosine and inosine-containing targets *in vitro* and suggest the use of triplex forming PNAs for targeting edited RNA transcripts.

3.3 Results and Discussion:

3.3.1 Design and Synthesis of Fluorogenic PNA Monomers

FIT-PNA probes utilize fluorogenic dyes that exhibit dramatic changes in fluorescence dependent upon the corresponding environment. Asymmetric cyanine-based dyes such as TO become rotationally constrained by base stacking interactions, resulting in fluorescence

enhancement upon hybridization to complementary nucleic acids.[14,15,31] MG-based dyes possess a similar mechanism of fluorescence but have not yet been explored for intercalation-based signal enhancement. The relative ease of modifying the nucleobase portion of PNA has already produced many different fluorescent analogues.[14,15,44,31,36,37,39–43] We hypothesized that incorporating a MG base surrogate would be a simple and effective process to introduce a new class of dyes for FIT-PNA probes.

In order to synthesize a MG-containing PNA monomer (**Scheme 3.1**), we first produced the leucomalachite green carboxylic acid moiety **1** through the reaction between 4-carboxybenzaldehyde and dimethylaniline in the presence of zinc chloride. This was then coupled to Fmoc-protected benzyl ester PNA backbone (synthesized by previously reported procedures)[45] by employing HATU and *N*-methylmorpholine to produce the protected leucomalachite green PNA monomer **2**. The benzyl group was removed by palladium catalyzed hydrogenation to afford an Fmoc-leucomalachite green PNA monomer **3**. Subsequent oxidation by choranil generated the final MG-containing PNA monomer **4**. This relatively short synthetic route afforded an MG-based PNA monomer in a simple and effective manner.

We were also curious to investigate the use of solvatochromic 4DMN dye in FIT-PNA probes, as we had previously been successful in employing this dye to signal the self-assembly and stimuli-responsive disassembly process of γ-PNA amphiphiles.[37] This dye belongs to the naphthalimide family and experiences altered emission based on an internal charge transfer

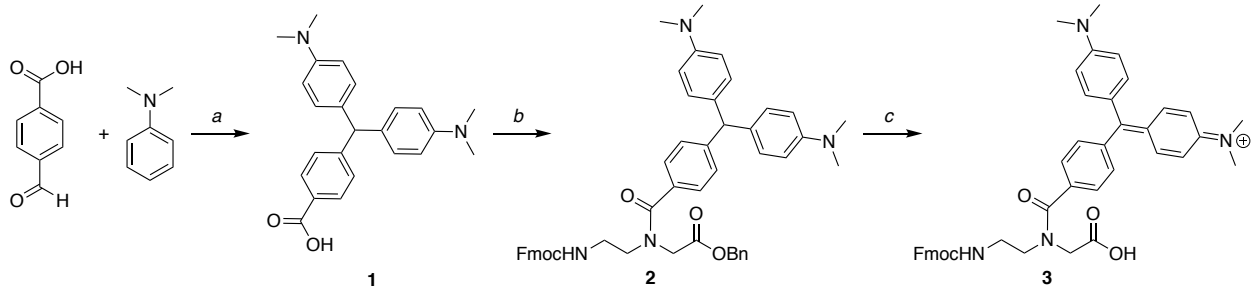

Scheme 3.1: Synthesis of MG-PNA monomer. a) zinc chloride, reflux, 52%. b) Fmoc-(aminoethyl)glycine-benzyl-ester PNA backbone, HATU, NMM, DMF, 68%. c) 2 steps: 1.) H2, Pd/C, MeOH. 2.) chloranil, MeOH, 72% (2 steps).

mechanism that is highly dependent upon the polarity of the environment.[46] We wondered if the change in environment and solvation state between hybridized and single-stranded PNA would induce a similar change in emission intensity or wavelength and if dyes of this family could thus be useful for FIT-PNA probes. PNA monomers containing a 4DMN base surrogate were synthesized as described previously.[37]

Finally, we synthesized TO-containing PNA monomers adapted from previously reported procedures.[15,31] This well-established FIT probe dye has yet to be employed for A→I detection and we predicted that it could be highly effective for distinguishing between edited and unedited transcripts.

3.3.2 Design and Synthesis of FIT-PNA Probes

In order to determine the effectiveness of TO, 4DMN, and MG dyes for detecting inosine-containing targets, we initially designed sequences complementary to a linear RNA target containing either adenosine or inosine at a defined position (**Figure 3.2**). The FIT-PNA probe was synthesized having a cytosine opposite the A/I in the RNA, as A:C mismatches are a common

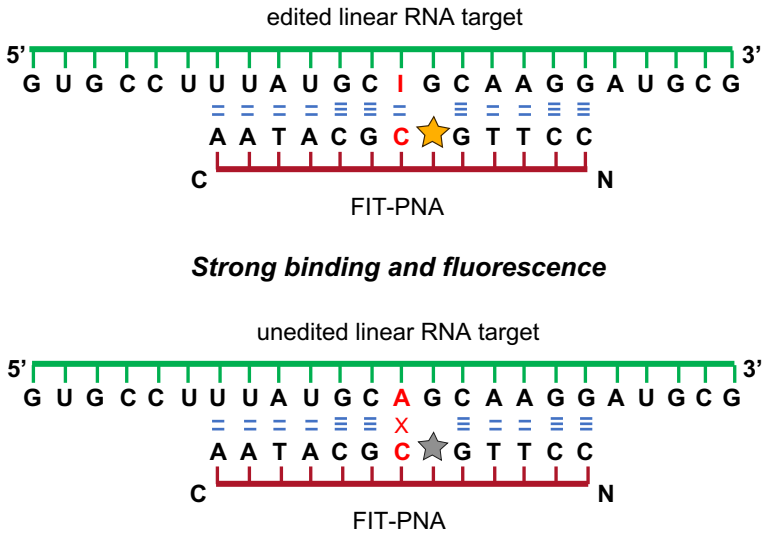

Figure 3.2: FIT-PNA probes hybridize to a linear RNA target and distinguish between edited and unedited targets through increased fluorescence.

Table 3.1: Sequences of FIT-PNA probes and confirmed masses determined by ESI-TOF.

Probe	Sequence	Mass $(M+4)^{4+}$	Found $(M+4)^{4+}$
4DMN (15mer)	C – Lys^+ A A T A C G C D G T T C C T A – N	1070.1879	1070.6957
TO (13mer)	C – Lys^+ A A T A C G C TO G T T C C – N	947.6356	947.8971
MG (13mer)	C – Lys^+ A A T A C G C MG G T T C C – N	953.6582	953.9188
Control (15mer)	C – Lys+ A A T A C G C C G T T C C T A – N	1037.9263	1038.4390
Control (13mer)	C – Lys+ A A T A C G C C G T T C C – N	902.6226	902.8863

motif for ADAR-catalyzed editing. The dye was placed adjacent to the A:C mismatch or I:C base pair to probe the effect of simulated editing hybridization and fluorescence. FIT-PNA probes containing each dye at the specified position were synthesized by solid-phase protocols, purified by HPLC, and confirmed by ESI-TOF (**Table 3.1**; **Appendix B**). The 4DMN probe was extended by two extra bases to ensure binding, as we had previously observed a large decrease in affinity when incorporating this particular dye (data not shown). Control strands complementary to the inosine-containing target were also synthesized to elucidate the change in affinity caused by including the dye.

3.3.3 Characterization of FIT-PNA Probes Binding to Target Transcripts

In order to characterize the change in fluorescence upon hybridization with either edited or unedited targets, we first used a linear RNA target as a proof-of-concept. Initially we confirmed binding to target RNA by thermal denaturation and determined the effect of the internal dye on the binding affinity. FIT-PNA probes were mixed with inosine- or adenosine-containing RNA targets to a final concentration of 2.5 μM PNA and RNA in 1xPBS. The samples were heat denatured at 95°C followed by annealing at 20°C. Absorbance was monitored between 20-95°C and melting temperatures were determined in triplicate (**Table 3.2; Figure B1**). As expected, there was not a significant change in affinity between adenosine and inosine targets for

fluorogenic probes. However, there were large decreases in melting temperature compared to the complementary control strands for all probes, suggesting incorporation of the dye is the major contributor to the loss in affinity. The TO-containing FIT-PNA probe displayed the least significant decrease in affinity, whereas the 4DMN and MG probes significantly perturbed the duplex stability, likely due to the large increase in size as compared to native nucleobases.

Table 3.2: UV melting temperatures of FIT-PNA probes associated with a linear RNA target. Error is represented as SEM (n=3).

Probe	Target	T_m (°C)	ΔT_m (°C)
4DMN (15mer)	RNA-A	54.9 ± 0.6	(-11.9)
	RNA-I	55.5 ± 0.7	(-15.1)
TO (13mer)	RNA-A	60.1 ± 0.3	(-2.4)
	RNA-I	61.6 ± 0.1	(-7.6)
MG (13mer)	RNA-A	56.7 ± 0.1	(-5.9)
	RNA-I	53.3 ± 0.2	(-15.9)
Control (15mer)	RNA-A	66.8 ± 0.5	0
	RNA-I	70.6 ± 0.4	0
Control (13mer)	RNA-A	62.5 ± 0.2	0
	RNA-I	69.1 ± 0.4	0

After confirming the ability of fluorogenic probes to bind to the RNA targets, we characterized the fluorescence in the presence or absence of adenosine- and inosine-containing targets. FIT-PNA probes were mixed with linear RNA-A or RNA-I to a final concentration of 2.5 μM in 1xPBS. After heat denaturation and annealing, samples were incubated at room temperature for 1 hour before analyzing the fluorescence. The TO probe showed a similar

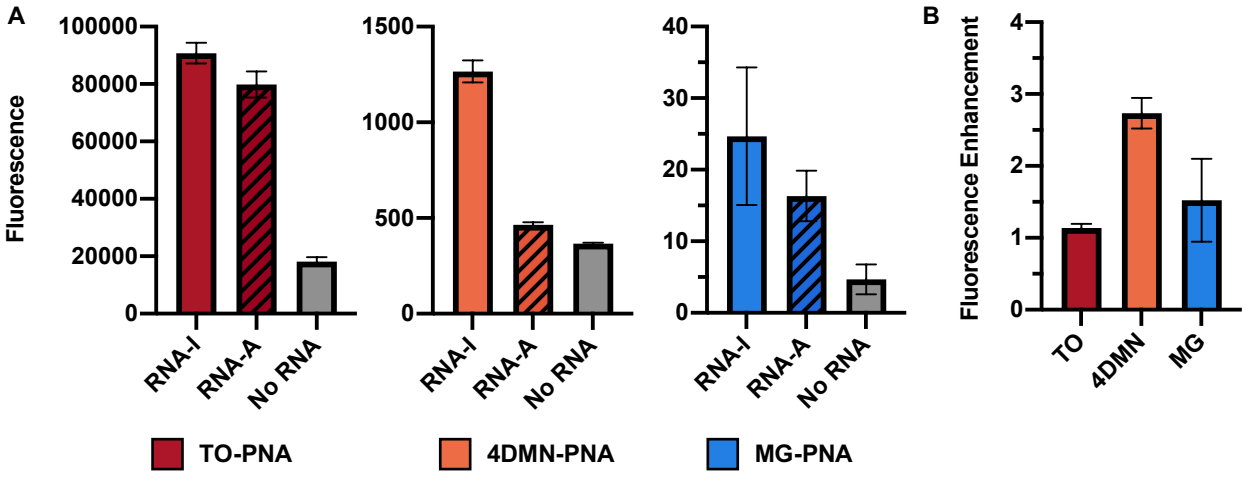

Figure 3.3: A) Fluorescence of FIT-PNA probes in the presence and absence of linear RNA targets containing inosine or adenosine. Error bars represent SEM (n = 3). B) Fluorescence enhancement of PNA in the presence of inosine targets compared to adenosine targets. Error bars represent SEM (n=3).

enhancement in fluorescence over FIT-PNA alone for both targets, whereas the 4DMN probe only displayed an appreciable fluorescence increase in the presence of the inosine target (**Figure 3.3**). However, both probes presented very little selectivity for inosine over adenosine, with the 4DMN probes and TO probes having only 2.7- and 1.2-fold increase in fluorescence, respectively. While the MG probe exhibited some enhancement in fluorescence (1.5-fold over adenosine and 5.6-fold over MG-PNA alone), the fluorescence intensity was extremely low and therefore difficult to accurately confirm the resulting activity. Thus, we decided that the MG probe was not a viable

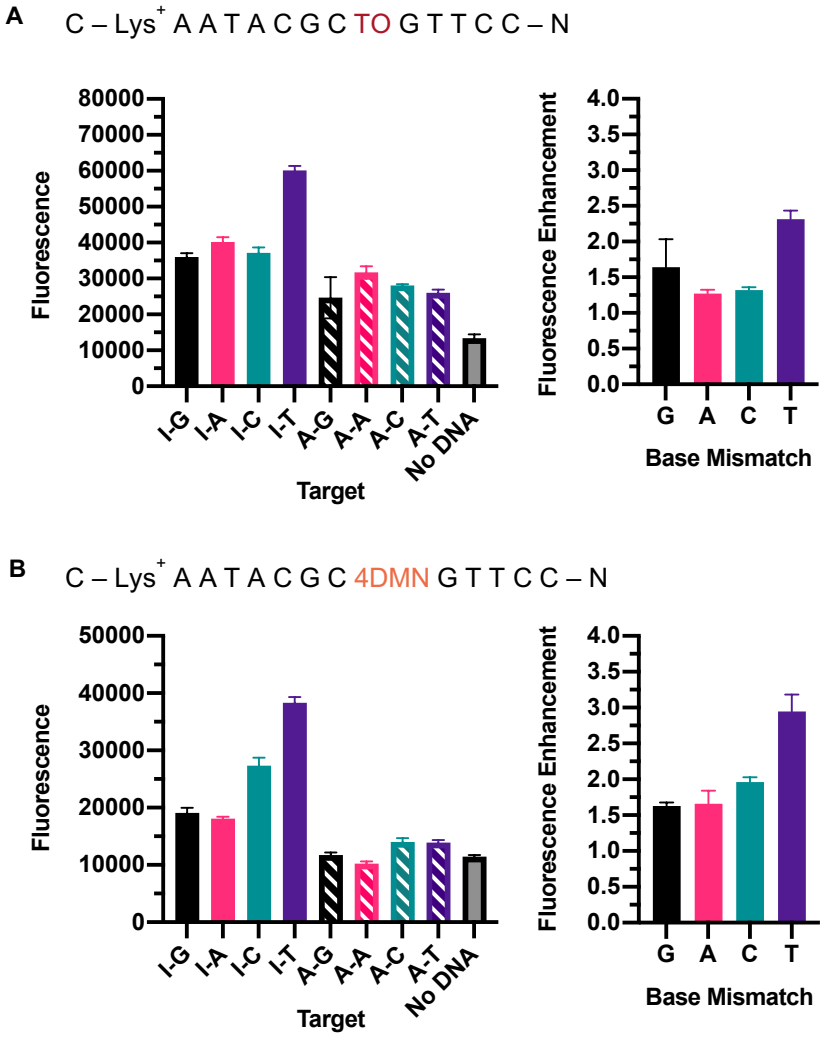

Figure 3.4: FIT-PNA fluorescence in the presence of DNA mismatched targets. (A) TO-PNA fluorescence and enhancement of inosine over adenosine. n=3. (B) 4DMN-PNA fluorescence and enhancement of inosine over adenosine. Error bars represent SEM (n=3).

candidate for forced intercalation fluorescence enhancement and moved forward testing the 4DMN and TO probes.

To further elucidate the fluorescent properties of the FIT-PNAs, we tested the effect of the base identity opposite of the dye within the duplex. FIT probes rely upon local base stacking interactions for intercalation to adopt favorable conformations or environments for fluorescence emission.[14,15] Base stacking interactions are dependent upon the sequence and identity of local H-bonding nucleobase pairs.[47,48] We therefore hypothesized that the affinity, selectivity, and fluorescence properties may be affected by the specific target sequence. We chose to employ DNA for these experiments as it represents a more cost-effective choice and inosine is also found in DNA as a result of oxidative damage. We designed strands containing inosine or adenosine adjacent to each of the four canonical nucleobases: A, C, T, and G (**Figure B2**). TO and 4DMN FIT-PNA probes were hybridized to the DNA and fluorescence enhancement analyzed as described above. We discovered that both probes contain a preference for pairing against thymine with higher specificity for inosine over adenosine (2.9- and 2.3-fold for 4DMN and TO, respectfully) than other nucleobases (**Figure 3.4A and 3.4B**). There is not a significant preference for the other nucleobases, with both probes exhibiting lower than 2-fold specificity for inosine. We then measured the effect of temperature on the fluorescence activity. By monitoring the fluorescence at temperatures from 25-60°C we determined that specificity is dependent upon temperature, increasing from ~2-fold up to 11-fold for TO-PNA at 55°C when adjacent to a thymine residue (**Figure 3.5**). As the melting temperature is approached, the enhancement in fluorescence increases while inversely the fluorescence intensity decreases (**Figure B3**). This is likely due to the slightly more favorable binding to inosine targets over adenosine targets and the reduction in duplexed versus single stranded probes at temperatures approaching the melting point. As the 4DMN dye substitute perturbs binding to a much greater extent than the TO substitute, there is not as significant of an effect on the fluorescence enhancement at higher temperatures. These results indicated that TO-PNA is capable of distinguishing between inosine and adenosine

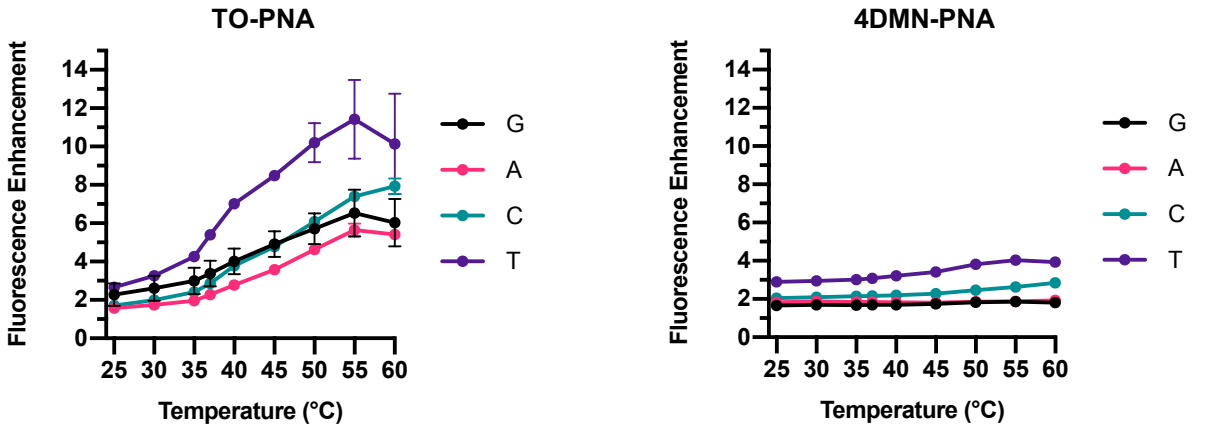

Temperature (°C)	G	A	C	T
25	2.3	1.6	1.7	2.7
30	2.6	1.7	2.0	3.3
35	3.0	2.0	2.4	4.3
37	3.4	2.3	2.9	5.4
40	4.0	2.8	3.8	7.1
45	4.9	3.6	4.8	8.5
50	5.7	4.6	6.1	10.2
55	6.5	5.7	7.4	11.4
60	6.0	5.4	7.9	10.1

Temperature (°C)	G	A	C	T
25	1.6	1.7	2.0	2.9
30	1.7	1.7	2.1	3.0
35	1.6	1.7	2.1	3.1
37	1.7	1.7	2.1	3.1
40	1.6	1.7	2.2	3.3
45	1.7	1.7	2.2	3.5
50	1.8	1.7	2.4	3.9
55	1.8	1.7	2.5	4.0
60	1.8	1.8	2.7	4.0

Figure 3.5: The effect of temperature on fluorescence enhancement and specificity of inosine over adenosine of FIT-PNA probes in the presence of mismatched DNA targets. Error bars represent SEM (n=3).

containing oligonucleotides with up to 11-fold increase in specificity at higher temperatures. We therefore moved forward designing TO probes for targeting inosine containing transcripts.

ADAR enzymes catalyze the deamination of adenosine into inosine to regulate many biological processes including gene expression and translation.[1] To date, millions of editing sites have been identified in the transcriptome with varying editing frequency at each site.[48,49] In order to validate whether a TO FIT-PNA probe can identify sites of A-to-I editing, we targeted a mimic of the HER1 RNA hairpin, a frequent and conserved editing site required for Hmg2p-induced ER remodeling (**Figure 3.6A**).[11,51] We designed and synthesized a probe complementary to the target where the PNA is capable of pairing with a majority of the loop region, which we theorized would improve strand displacement and binding (**Figure 3.6B; Appendix B**). The fluorescence was measured in the presence and absence of HER1-I and HER1-A as described above. We

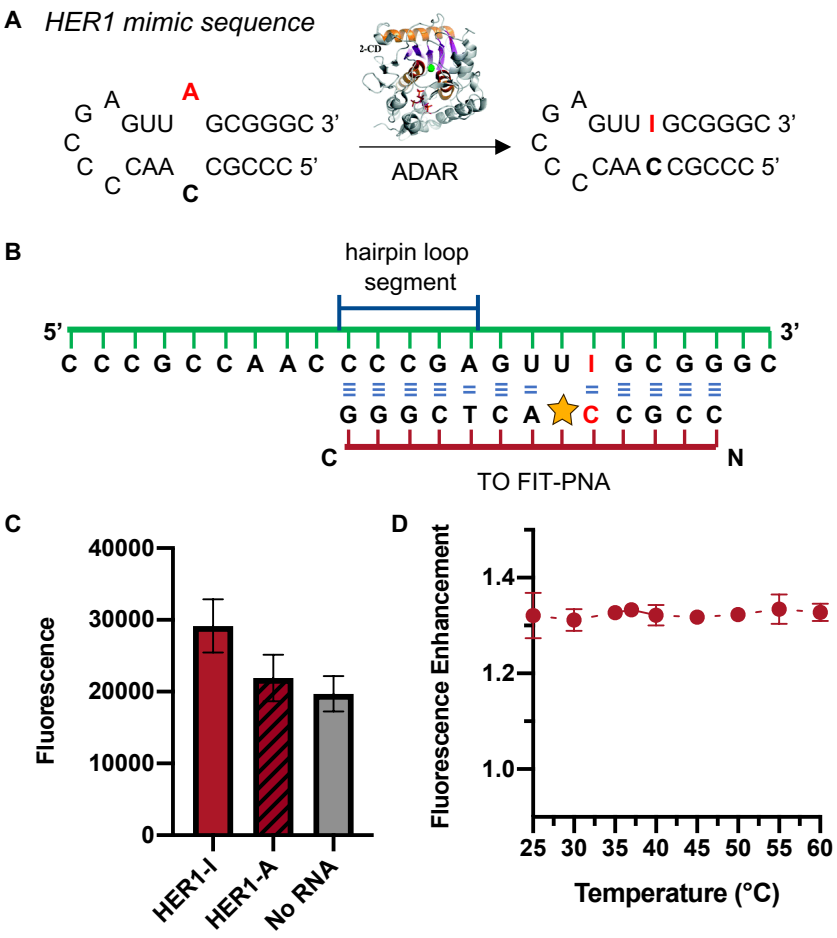

Figure 3.6: TO FIT-PNA targeting a HER1 mimic RNA sequence. (A) Sequence of the HER1 RNA hairpin edited by ADAR. (B) Binding mode of TO FIT-PNA to the HER1-I target. (C) Fluorescence of TO FIT-PNA probe in the presence or absence of targets. Error bars represent SEM (n=3). (D) The change in fluorescence enhancement as an effect of temperature. Error bars represent SD (n=3).

observed a very slight enhancement in fluorescence in the presence of target RNA with only a 1.34-fold increase in specificity for inosine over adenosine (**Figure 3.6C**). We then measured the fluorescence over a range of temperatures to see if we could improve the specificity as before. Again, we observed a decrease in fluorescence at higher temperatures, however it was not accompanied with an increase in specificity (**Figure 3.6D; Figure B4**). Unfortunately, there was no significant effect on fluorescence enhancement with increasing temperature as observed with the linear targets. Due to the strong nature of the RNA hairpin, we hypothesized that the FIT-PNA probe was incapable of binding in a duplex to the targets. Using thermal denaturation, we

determined that there is no significant change or additional inflection in melting temperature when the probe is introduced to the target, suggesting that the probe is not binding (**Table B1; Figure B5**). The innate strong affinity of RNA hairpins makes this a difficult target for duplex forming hybridization-based probes.

In order to bind double-stranded RNA targets, researchers have developed "triplex" binding PNA which incorporate unnatural nucleobase adducts capable of binding to the Hoogsteen face of a Franklin-Watson-Crick duplex.[52] Because adenosine deamination in RNA occurs exclusively to dsRNA, we reasoned that this design could be particularly useful for our desired application. Recently, Sugimoto and coworkers developed a triplex-forming PNA incorporating these unnatural bases capable of recognizing and binding to an inosine-containing RNA hairpin with 100-fold greater affinity than the adenosine counterpart.[53] Using fluorophore-quencher interactions, they showed feasible competition assays for inosine detection. However, this required synthetic quencher labeled RNA and would therefore not be able to work with endogenous samples or as an imaging platform *in cellulo*. Instead, incorporating triplex-forming nucleobases into FIT-PNA probes may provide an avenue for sequence-specific inosine detection and imaging in native environments. This has been shown to be feasible in recent work by Nishizawa and coworkers, wherein including cyanine dye analogs as base surrogates in triplex forming PNAs (tFIT-PNA) resulted in increased fluorescence upon triplex formation.[54,55] We believe that these two approaches could be combined to create tFIT-PNA probes capable of real-time detection and imaging of inosine-containing RNA.

3.4 Conclusions:

The deamination of adenosine to inosine is an important modification in nucleic acids used to regulate numerous cellular functions. Distinguishing this single nucleotide change in a sequence specific manner in real-time remains a challenge. We explored the use of FIT-PNA probes for inosine detection by evaluating three different fluorogenic dyes: thiazole orange, 4-

dimethylamino-naphthalimide, and malachite green. PNA monomers containing each dye as a base surrogate were synthesized and incorporated into oligomers complementary to an inosine-containing target of interest. Thermal melting revealed that the negative contribution on stability from the dye was greater than the mismatch resulting from A-to-I editing. Fluorescence studies showed that both TO and 4DMN resulted in increased signal in the presence of RNA and that each dye contained a preference for an adjacent thymine residue in DNA. Greater selectivity for inosine over adenosine in DNA followed increasing temperature up to 11-fold for TO when paired against a thymine base. Unfortunately, the FIT-PNA probes were incapable of disrupting an innately strong RNA hairpin typically found near edited sites. We suggest the use of triplex forming PNAs as an alternative avenue for targeting such transcripts. In any case, the data presented displays the ability of TO- and 4DMN-containing FIT-PNA probes to distinguish between inosine and adenosine-containing nucleic acids, particularly in DNA. We anticipate that further exploration of dye identity, target selectivity, and sequence design will make these probes useful for a range of inosine detection platforms, including live-cell imaging and real-time enzyme activity monitoring.

3.5 Materials and Methods:

Abbreviations: Fmoc, fluorenylmethyloxycarbonyl; DMF, dimethylformamide; HATU, 1-[Bis(dimethylamino)methylene]-1*H*-1,2,3-triazolo[4,5-*b*]pyridinium 3-oxid hexafluorophosphate; NMM, *N*-methylmorpholine; DIPEA, diisopropylethylamine; TFA, trifluoroacetic acid; DCM, dichloromethane; Boc, tert-butyloxycarbonyl; NMP, N-methyl-2-pyrrolidone; PyBOP, benzotriazol-1-yl-oxytripyrrolidinophosphonium hexafluorophosphate; FCC, flash column chromatography.

Synthesis of Fluorogenic PNA Monomers

Canonical PNA monomers of A, C, T, and G were purchased from PolyOrg, Inc. All other reagents and solvents were acquired from Chem-Impex, Millipore Sigma, or Fisher Scientific and used without further purification unless otherwise stated. All reactions were performed under inert nitrogen gas using dry solvents unless otherwise stated. Dry solvents were dispensed from a J. C. Meyer solvent system prior to use to ensure dryness. Product formation was monitored by thin layer chromatography (TLC) on Merck silica gel 60 F254 glass plates and visualized using UV light and staining with ninhydrin or potassium permanganate followed by heating. Flash column chromatography was performed under pressurized air using SiliaFlash F60 grade silica acquired from SiliCycle, Inc. Final products were confirmed and characterized by proton and carbon nuclear magnetic resonance (NMR) using a Varian Inova 400 MHz spectrometer. Spectra were analyzed using the MestReNova software. An Agilent 6230 electrospray ionization time-of-flight (ESI-TOF) mass spectrometer confirmed mass of products. The (aminoethyl)glycine benzyl ester PNA backbone, thiazole orange, and 4DMN monomers were synthesized by previously reported procedures.[15,31,37,45]

*p-Carboxyl leucomalachite green (**1**)*

To a 100mL round bottom flask was added 4-carboxybenzaldehyde (96.3 mmol), *N,N*-dimethylaniline (6.65 mmol), and zinc chloride (13.4 mmol). The mixture was refluxed for 5 h after which TLC showed complete consumption of starting material. The reaction was cooled to room temperature, filtered, and concentrated under reduced pressure. The crude mixture was recrystallized in methanol to yield the purified product as a light blue solid (3.47 mmol, 52% yield). ^{1}H NMR (400 MHz, DMSO-d6) δ 12.23 (s, 1H), 7.83 (d, 2H), 7.15 (d, 2H), 6.83 (d, 4H), 6.64 (d, 4H), 5.38 (s, 1H) 2.84 (s, 12H). ^{13}C NMR (400 MHz, DMSO-d6) δ 148.84, 131.60, 129.41, 129.26, 128.83, 112.41, 109.58, 54.11, 40.24. HRMS (ESI-TOF) *m/z* 375.1995 (calc'd $[M+H]^+$ = 375.1994)

*Fmoc leucomalachite green (aminoethyl)glycine benzyl ester (**2**)*

Compound **1** (1.52 mmol) was dissolved in DMF (6 mL) in a 100 mL round bottom flask. HATU (2.41 mmol) was added followed by NMM (3.63 mmol) and the reaction was stirred for 30 min. Fmoc benzyl ester PNA backbone (1.21 mmol) dissolved in DMF (2 mL) with 1 eq of NMM was added to the reaction and stirred overnight at RT after which full consumption of backbone was indicated by TLC. The reaction was concentrated under reduced pressure and purified by FCC using a gradient of hexane to ethyl acetate to yield the final product as a light blue solid (0.82 mmol, 68% yield). ^{1}H NMR (400 MHz, DMSO-d6, two rotamers) δ 7.86 (d, 2H) 7.65 & 7.59 (d, 2H minor & major rotamer) 7.40-7.36 (m, 6H) 7.29-7.25 (m, 4H) 7.17 (d, 2H) 7.03 & 6.99 (d, 2H, minor & major rotamer) 6.96 & 6.83 (d, 4H, minor & major rotamer) 6.63 & 6.58 (d, 4H, minor & major rotamer) 5.33 & 5.27 (s, 1H, minor & major rotamer) (5.18 (s, 2H) 4.24 (s, 2H) 4.20 (t, 1H) 4.16 (s, 2H) 3.50;3.25 (m, 2H) 3.12-3.07 (m, 2H) 2.84 & 2.81 (s, 12H, minor & major rotamer) ^{13}C NMR (400 MHz, DMSO-d6) δ 171.46, 169.16, 155.92, 148.78, 143.86, 140.74, 135.87, 133.08, 131.79, 129.40, 128.71, 128.45, 128.11, 127.94, 127.61, 127.02, 126.51, 126.26, 125.07, 120.11, 112.34, 65.98, 65.48, 59.76, 53.97, 46.73, 40.23, 20.77, 14.09. HRMS (ESI-TOF) *m/z* 787.4603 (calc'd $[M+H]^+$ = 787.3781)

*Fmoc malachite green PNA monomer (**3**)*

Compound **2** (0.132 mmol) was dissolved in methanol (2.5 mL) under nitrogen gas. Palladium on activated carbon (~10%/wt. eq.) was added and the nitrogen was replaced with a balloon of hydrogen gas. The reaction was stirred overnight after which TLC indicated full consumption of starting material. The reaction was filtered through celite and concentrated under reduced pressure. The crude material was dissolved in methanol (2 mL) was added chloranil (0.866 mmol). The reaction was stirred overnight and concentrated under reduced pressure. The product was purified by FCC using a gradient of DCM to 15% methanol in DCM to yield the purified monomer

as a dark blue solid (0.107 mmol, 72% yield). ^{1}H NMR (600 MHz, DMSO-d6) δ 12.7 (s, 1H) 7.87-7.84 (m, 2H) 7.67-7.63 (m, 2H) 7.57 (d, 2H) 7.38 (t, 2H) 7.35 (t, 1H) 7.27(t, 2H) 7.23-7.18 (m, 4H) 6.94 (d, 2H) 6.62 (d, 2H) 6.57 (d, 2H) 4.30 (d, 1H) 4.18 (t, 2H) 4.09 (s, 2H) 3.48;3.39 (m, 2H) 3.11-3.07 (m, 2H) 2.86 (s, 6H) 2.62 (s, 6H) ^{13}C NMR (400 MHz, DMSO-d6) δ 171.34, 170.69, 155.88, 150.06, 148.96, 143.83, 140.71, 135.94, 135.80, 133.67, 129.38, 128.53, 128.43, 127.58, 127.49, 127.00, 125.62, 125.33, 125.02, 120.08, 113.99, 111.34, 79.83, 65.45, 46.63, 40.49, 40.16, 40.06 38.25. HRMS (ESI-TOF) *m/z* 695.3150 (calc'd $[M]^{+}$ = 695.3228).

Synthesis of FIT-PNA probes

PNA oligomers were synthesized on a Biotage SP Wave semi-automatic peptide synthesizer under microwave assistance. Synthesis began by downloading 50 mg of a rink amide MBHA (0.52 mmol/g) with 10 μmols of Fmoc-Lys(Boc)-OH using HATU (1.5 eq), DIPEA (1.5 eq) and 2,6-lutidine (1.5 eq) in 200 μL of dry NMP for 1 hour at room temperature. The resin was then capped using a solution of 9% acetic anhydride and 13% 2,6-lutidine in DMF. The resin was washed (5x1mL DMF, 5x1mL DCM, 3x1mL DMF) and deprotected using 25% piperidine in DMF (3x1mL for 2 min). Successive couplings were performed by first mixing Fmoc PNA monomer (5 eq) with HATU (5 eq), DIPEA (5 eq) and 2,6-lutidine (5 eq) in 300 μL dry NMP and pre-activating for 10 min. The activated solution was then added to the resin and coupling proceeded using microwave assistance at 75°C for 6 min. The resin was then washed (5x1mL DMF), capped using capping solution (2x1mL for 5min), washed (5x1mL DMF, 5x1mL DCM, 3x1mL DMF), and deprotected using deprotection solution (3x1mL for 2min). A final washing step (5x1mL DMF, 5x1mL DCM, 3x1mL DMF) completed a coupling cycle. For the thiazole orange PNA monomer, HATU was replaced with PyBOP (5eq) for activation and coupling steps which improved solubility and efficiency. Loading and monomer coupling efficiency was monitored by absorbance at 301nm of the dibenzofulvene-piperidine adduct using a Nanodrop 2000 spectrophotometer. Upon

completion of synthesis, the resin was washed with DCM (3x1mL) and dried under vacuum to prepare for cleavage. Cleavage from the resin was performed three times using 500 μL of a solution of 95% TFA, 2.5% H_2O, and 2.5% triisopropylsilane for 1 hour. The crude oligomer was precipitated by addition of ether and centrifuged to a pellet. The pellet was washed with ether (3x) and dissolved in 50% acetonitrile in H_2O for purification. The crude oligomer was purified by reverse-phase HPLC using an Agilent Eclipse XDB-C18 5 μm, 9.4 x 250 mm column at 60°C with a flow rate of 2 mL/min, monitored at 260 nm using a 15 min linear gradient (10-40%) of 0.1% TFA/acetonitrile in 0.1% TFA/water. FIT-PNA probes containing 4DMN was also monitored at 420 nm, while thiazole orange and malachite green were monitored at 510 nm and 620 nm, respectively. Identity and retention time were confirmed by ESI-TOF mass spectrometry.

Melting temperature analysis of FIT-PNA probes with RNA and DNA

Samples of FIT-PNA probe and RNA or DNA at 2.5μM in 1xPBS were prepared from stock solutions and annealed by heating to 95°C for 5 min, followed by incubation at 20°C for 1 hr. A 100μL volume of each sample was transferred to an 8-cell quartz microcuvette with a 1 cm pathlength. Absorbance was monitored at 260 nm from 20-95°C at a rate of 0.5°C/min using a Shimadzu UV-1800 spectrophotometer equipped with a temperature controller and Julabo CORIO CD water circulator. Melting temperatures were determined by the first derivate method using a total of three independent trials. Molar absorptivity values at 260 nm for the dye-containing PNA monomers are as follows: 4DMN = 8507 $M^{-1}cm^{-1}$; TO = 6600 $M^{-1}cm^{-1}$; MG = 4900 $M^{-1}cm^{-1}$.

Fluorescence enhancement of FIT-PNA probes

Samples were prepared in triplicate from stock solutions in 1xPBS composed of 2.5 μM FIT-PNA probe alone, 2.5 μM FIT-PNA with 2.5 μM inosine-containing RNA or DNA target, 2.5 μM FIT-PNA probe with 2.5 μM adenosine-containing RNA or DNA target, and a 1xPBS blank. The

samples were heated to 95°C for 5 min followed by incubation at room temperature for 1 hour for annealing. A 60 μL volume of each sample was transferred to a 384 microwell plate and covered with a clear lid. Fluorescence was measured using a Biotek Cytation 5 Plate Reader (excitation/emission = 450/515nm for 4DMN; 500/541nm for TO; 620/680nm for MG). Fluorescence spectra were also measured for each probe (excitation/emission = 450/480-700 nm for 4DMN; 500/532-700 nm for TO). Fluorescence enhancement for inosine over adenosine was determined by dividing the fluorescence values from samples with inosine-containing targets by samples with adenosine-containing targets. Fluorescence enhancement over background was determined by dividing the fluorescence values by that of the sample composed of FIT-PNA probe alone. Values were calculated using a total of three independent trials.

Thermal evaluation of fluorescence enhancement of FIT-PNA probes

Samples prepared from determining fluorescence enhancement were used to elucidate the effect of temperature on fluorescence. Samples were placed in a 384 microwell plate using a Biotek Cytation 5 Plate Reader, fluorescence was measured every 5°C from 25-60°C, including a reading at 37°C (excitation/emission = 450/515nm for 4DMN; 500/541nm for TO; 620/680nm for MG). Fluorescence enhancement at each temperature was determined as previously described. Values were calculated using a total of three independent trials.

3.6 References:

(1) Meier, J. C.; Kankowski, S.; Krestel, H.; Hetsch, F. RNA Editing—Systemic Relevance and Clue to Disease Mechanisms? *Front. Mol. Neurosci.* **2016**, *9*, 124. https://doi.org/10.3389/fnmol.2016.00124.

(2) Maas, S.; Patt, S.; Schrey, M.; Rich, A. Underediting of Glutamate Receptor Glur-B MRNA in Malignant Gliomas. *Proc. Natl. Acad. Sci. U. S. A.* **2001**, *98* (25), 14687–14692.

https://doi.org/10.1073/pnas.251531398.

(3) Chen, L.; Li, Y.; Lin, C. H.; Chan, T. H. M.; Chow, R. K. K.; Song, Y.; Liu, M.; Yuan, Y. F.; Fu, L.; Kong, K. L.; Qi, L.; Li, Y.; Zhang, N.; Tong, A. H. Y.; Kwong, D. L. W.; Man, K.; Lo, C. M.; Lok, S.; Tenen, D. G.; Guan, X. Y. Recoding RNA Editing of AZIN1 Predisposes to Hepatocellular Carcinoma. *Nat. Med.* **2013**, *19* (2), 209–216. https://doi.org/10.1038/nm.3043.

(4) Brusa, R.; Zimmermann, F.; Koh, D. S.; Feldmeyer, D.; Gass, P.; Seeburg, P. H.; Sprengel, R.; Sakmann, B. Early-Onset Epilepsy and Postnatal Lethality Associated with an Editing-Deficient GluR-B Allele in Mice. *Science (80-.).* **1995**, *270* (5242), 1677–1680. https://doi.org/10.1126/science.270.5242.1677.

(5) Krestel, H. E.; Shimshek, D. R.; Jensen, V.; Nevian, T.; Kim, J.; Geng, Y.; Bast, T.; Depaulis, A.; Schonig, K.; Schwenk, F.; Bujard, H.; Hvalby, Ø.; Sprengel, R.; Seeburg, P. H. A Genetic Switch for Epilepsy in Adult Mice. *J. Neurosci.* **2004**, *24* (46), 10568–10578. https://doi.org/10.1523/JNEUROSCI.4579-03.2004.

(6) Kwak, S.; Kawahara, Y. Deficient RNA Editing of GluR2 and Neuronal Death in Amyotropic Lateral Sclerosis. *J. Mol. Med.* **2005**, *83*, 110–120. https://doi.org/10.1007/s00109-004-0599-z.

(7) Kawahara, Y.; Ito, K.; Sun, H.; Aizawa, H.; Kanazawa, I.; Kwak, S. RNA Editing and Death of Motor Neurons. *Nature* **2004**, *427* (6977), 801–801. https://doi.org/10.1038/427801a.

(8) Alseth, I.; Dalhus, B.; Bjørås, M. Inosine in DNA and RNA. *Current Opinion in Genetics and Development*. Elsevier Ltd June 1, 2014, pp 116–123. https://doi.org/10.1016/j.gde.2014.07.008.

(9) Knutson, S. D.; Arthur, R. A.; Johnston, H. R.; Heemstra, J. M. Selective Enrichment of A-to-I Edited Transcripts from Cellular RNA Using Endonuclease V. *J. Am. Chem. Soc.* **2020**, *142*, 5241–5251. https://doi.org/10.1021/jacs.9b13406.

(10) Knutson, S. D.; Ayele, T. M.; Heemstra, J. M. Chemical Labeling and Affinity Capture of

Inosine-Containing RNAs Using Acrylamidofluorescein. *Bioconjug. Chem.* **2018**, *29* (9), 2899–2903. https://doi.org/10.1021/acs.bioconjchem.8b00541.

(11) Knutson, S. D.; Korn, M. M.; Johnson, R. P.; Monteleone, L. R.; Dailey, D. M.; Swenson, C. S.; Beal, P. A.; Heemstra, J. Chemical Profiling of A-to-I RNA Editing Using a Click-Compatible Phenylacrylamide. *Chem. – A Eur. J.* **2020**, *26* (44), 9874–9878. https://doi.org/10.1002/chem.202001667.

(12) Tomoike, F.; Abe, H. RNA Imaging by Chemical Probes. *Adv. Drug Deliv. Rev.* **2019**, *147*, 44–58. https://doi.org/10.1016/j.addr.2019.08.001.

(13) Seitz, O.; Bergmann, F.; Heindl, D. A Convergent Strategy for the Modification of Peptide Nucleic Acids: Novel Mismatch-Specific PNA-Hybridization Probes. *Angew. Chem. Int. Ed.* **1999**, *38*(15), 2203-2206.

(14) Köhler, O.; Seitz, O. Thiazole Orange as Fluorescent Universal Base in Peptide Nucleic Acids. *Chem. Commun.* **2003**, *3* (23), 2938–2939. https://doi.org/10.1039/b308299g.

(15) Köhler, O.; Jarikote, D. V.; Seitz, O. Forced Intercalation Probes (FIT Probes): Thiazole Orange as a Fluorescent Base in Peptide Nucleic Acids for Homogeneous Single-Nucleotide-Polymorphism Detection. *ChemBioChem* **2005**, *6* (1), 69–77. https://doi.org/10.1002/cbic.200400260.

(16) Nielsen, P. E.; Egholm, M.; Berg, R. H.; Buchardt, O. Sequence-Selective Recognition of DNA by Strand Displacement with a Thymine-Substituted Polyamide. *Science (80-.).* **1991**, *254* (5037), 1497–1500. https://doi.org/10.1126/science.1962210.

(17) Demidov, V. V; Potaman, V. N.; Frank-Kamenetskii, M. D.; Egholm, M.; Buchardt, O.; Sonnichsen, S. H.; Nlelsen, P. E. Stability of Peptide Nucleic Acids in Human Serum and Cellular Extracts. *Biochem. Pharmacol.* **1994**, *48* (6), 1310–1313.

(18) Egholm, M.; Buchardt, O.; Christensen, L.; Behrens, C.; Freier, S. M.; Driver, D. A.; Berg, R. H.; Kim, S. K.; Norden, B.; Nielsen, P. E. PNA Hybridizes to Complementary Oligonucleotides Obeying the Watson–Crick Hydrogen-Bonding Rules. *Nature* **1993**, *365*,

566–568. https://doi.org/10.1038/365566a0.

(19) Uhlmann, E.; Peyman, A.; Breipohl, G.; Will, D. W. PNA: Synthetic Polyamide Nucleic Acids with Unusual Binding Properties. *Angew. Chemie Int. Ed.* **1998**, *37* (20), 2796–2823. https://doi.org/10.1002/chin.199909294.

(20) Nielsen, P. E.; Egholm, M.; Buchardt, O. Peptide Nucleic Acid (PNA). A DNA Mimic with a Peptide Backbone. *Bioconjug. Chem.* **1994**, *5* (1), 3–7. https://doi.org/10.1021/bc00025a001.

(21) Kam, Y.; Rubinstein, A.; Naik, S.; Djavsarov, I.; Halle, D.; Ariel, I.; Gure, A. O.; Stojadinovic, A.; Pan, H. G.; Tsivin, V.; Nissan, A.; Yavin, E. Detection of a Long Non-Coding RNA (CCAT1) in Living Cells and Human Adenocarcinoma of Colon Tissues Using FIT-PNA Molecular Beacons. *Cancer Lett.* **2014**, *352* (1), 90–96. https://doi.org/10.1016/j.canlet.2013.02.014.

(22) Torres, A. G.; Fabani, M. M.; Vigorito, E.; Williams, D.; Al-Obaidi, N.; Wojciechowski, F.; Hudson, R. H. E.; Seitz, O.; Gait, M. J. Chemical Structure Requirements and Cellular Targeting of MicroRNA-122 by Peptide Nucleic Acids Anti-MiRs. *Nucleic Acids Res.* **2012**, *40* (5), 2152–2167. https://doi.org/10.1093/nar/gkr885.

(23) Kummer, S.; Knoll, A.; Socher, E.; Bethge, L.; Herrmann, A.; Seitz, O. Fluorescence Imaging of Influenza H1N1 MRNA in Living Infected Cells Using Single-Chromophore FIT-PNA. *Angew. Chemie Int. Ed.* **2011**, *50* (8), 1931–1934. https://doi.org/10.1002/anie.201005902.

(24) Kummer, S.; Knoll, A.; Socher, E.; Bethge, L.; Herrmann, A.; Seitz, O. PNA FIT-Probes for the Dual Color Imaging of Two Viral MRNA Targets in Influenza H1N1 Infected Live Cells. *Bioconjug. Chem.* **2012**, *23* (10), 2051–2060. https://doi.org/10.1021/bc300249f.

(25) Tonelli, A.; Tedeschi, T.; Germini, A.; Sforza, S.; Corradini, R.; Medici, M. C.; Chezzi, C.; Marchelli, R. Real Time RNA Transcription Monitoring by Thiazole Orange (TO)-Conjugated Peptide Nucleic Acid (PNA) Probes: Norovirus Detection. *Mol. Biosyst.* **2011**,

7 (5), 1684–1692. https://doi.org/10.1039/c0mb00353k.

(26) Sonar, M. V.; Wampole, M. E.; Jin, Y. Y.; Chen, C. P.; Thakur, M. L.; Wickstrom, E. Fluorescence Detection of KRAS2 MRNA Hybridization in Lung Cancer Cells with PNA-Peptides Containing an Internal Thiazole Orange. *Bioconjug. Chem.* **2014**, *25* (9), 1697–1708. https://doi.org/10.1021/bc500304m.

(27) Socher, E.; Jarikote, D. V.; Knoll, A.; Röglin, L.; Burmeister, J.; Seitz, O. FIT Probes: Peptide Nucleic Acid Probes with a Fluorescent Base Surrogate Enable Real-Time DNA Quantification and Single Nucleotide Polymorphism Discovery. *Anal. Biochem.* **2008**, *375* (2), 318–330. https://doi.org/10.1016/j.ab.2008.01.009.

(28) Hashoul, D.; Shapira, R.; Falchenko, M.; Tepper, O.; Paviov, V.; Nissan, A.; Yavin, E. Red-Emitting FIT-PNAs: “On Site” Detection of RNA Biomarkers in Fresh Human Cancer Tissues. *Biosens. Bioelectron.* **2019**, *137*, 271–278. https://doi.org/10.1016/j.bios.2019.04.056.

(29) Kam, Y.; Rubinstein, A.; Nissan, A.; Halle, D.; Yavin, E. Detection of Endogenous K-Ras MRNA in Living Cells at a Single Base Resolution by a PNA Molecular Beacon. *Mol. Pharm.* **2012**, *9* (3), 685–693. https://doi.org/10.1021/mp200505k.

(30) Fang, G.; Chamiolo, J.; Kankowski, S.; Hövelmann, F.; Friedrich, D.; Löwer, A.; Meier, J. C.; Seitz, O. A Bright FIT-PNA Hybridization Probe for the Hybridization State Specific Analysis of a C → U RNA Edit *via* FRET in a Binary System. *Chem. Sci.* **2018**, *9* (21), 4794–4800. https://doi.org/10.1039/C8SC00457A.

(31) Bethge, L.; Jarikote, D. V. New Cyanine Dyes as Base Surrogates in PNA: Forced Intercalation Probes (FIT-Probes) for Homogeneous SNP Detection. *Bioorg. Med. Chem.* **2008**, *16* (1), 114–125. https://doi.org/10.1016/J.BMC.2006.12.044.

(32) Kolevzon, N.; Hashoul, D.; Naik, S.; Rubinstein, A.; Yavin, E. Single Point Mutation Detection in Living Cancer Cells by Far-Red Emitting PNA–FIT Probes. *Chem. Commun.* **2016**, *52* (11), 2405–2407. https://doi.org/10.1039/C5CC07502E.

(33) Socher, E.; Knoll, A.; Seitz, O. Dual Fluorophore PNA FIT-Probes - Extremely Responsive and Bright Hybridization Probes for the Sensitive Detection of DNA and RNA. *Org. Biomol. Chem.* **2012**, *10* (36), 7363–7371. https://doi.org/10.1039/c2ob25925g.

(34) Tedeschi, T.; Tonelli, A.; Sforza, S.; Corradini, R.; Marchelli, R. A Pyrenyl-PNA Probe for DNA and RNA Recognition: Fluorescence and UV Absorption Studies. *Artif. DNA PNA XNA* **2010**, *1* (2), 83–89. https://doi.org/10.4161/adna.1.2.13899.

(35) Mansawat, W.; Boonlua, C.; Siriwong, K.; Vilaivan, T. Clicked Polycyclic Aromatic Hydrocarbon as a Hybridization-Responsive Fluorescent Artificial Nucleobase in Pyrrolidinyl Peptide Nucleic Acids. *Tetrahedron* **2012**, *68* (21), 3988–3995. https://doi.org/10.1016/j.tet.2012.03.062.

(36) Okamoto, A.; Tanabe, K.; Saito, I. Synthesis and Properties of Peptide Nucleic Acids Containing a Psoralen Unit. *Org. Lett.* **2001**, *3* (6), 925–927. https://doi.org/10.1021/ol015549x.

(37) Swenson, C. S.; Velusamy, A.; Argueta-Gonzalez, H. S.; Heemstra, J. M. Bilingual Peptide Nucleic Acids: Encoding the Languages of Nucleic Acids and Proteins in a Single Self-Assembling Biopolymer. *J. Am. Chem. Soc.* **2019**, *141* (48), 19038–19047. https://doi.org/10.1021/jacs.9b09146.

(38) Ayele, T. M.; Knutson, S. D.; Ellipilli, S.; Hwang, H.; Heemstra, J. M. Fluorogenic Photoaffinity Labeling of Proteins in Living Cells. *Bioconjug. Chem.* **2019**, *30* (5), 1309–1313. https://doi.org/10.1021/acs.bioconjchem.9b00203.

(39) Gangamani, B. P.; Kumar, V. A.; Ganesh, K. N. 2-Aminopurine Peptide Nucleic Acids (2-ApPNA): Intrinsic Fluorescent PNA Analogues for Probing PNA-DNA Interaction Dynamics. *Chem. Commun.* **1997**, No. 19, 1913–1914. https://doi.org/10.1039/a705539k.

(40) Ikeda, H.; Yoshida, K.; Ozeki, M.; Saito, I. Synthesis and Characterization of Flavin-Tethered Peptide Nucleic Acid. *Tetrahedron Lett.* **2001**, *42* (13), 2529–2531. https://doi.org/10.1016/S0040-4039(01)00228-3.

(41) Cichon, M. K.; Haas, C. H.; Grolle, F.; Mees, A.; Carell, T. Efficient Interstrand Excess Electron Transfer in PNA:DNA Hybrids. *J. Am. Chem. Soc.* **2002**, *124* (47), 13984–13985. https://doi.org/10.1021/ja0277733.

(42) Marcus Wilhelmsson, L.; Holmén, A.; Lincoln, P.; Nielsen, P. E.; Nordén, B. A Highly Fluorescent DNA Base Analogue That Forms Watson-Crick Base Pairs with Guanine. *Journal of the American Chemical Society*. **2001**, *123*(10), 2434–2435. https://doi.org/10.1021/ja0025797.

(43) Ikeda, H.; Nakamura, Y.; Saito, I. Synthesis and Characterization of Naphthalimide-Containing Peptide Nucleic Acid. *Tetrahedron Lett.* **2002**, *43* (32), 5525–5528. https://doi.org/10.1016/S0040-4039(02)01164-4.

(44) Okamoto, A.; Tainaka, K.; Saito, I. Clear Distinction of Purine Bases on the Complementary Strand by a Fluorescence Change of a Novel Fluorescent Nucleoside. *J. Am. Chem. Soc.* **2003**, *125* (17), 4972–4973. https://doi.org/10.1021/ja034090u.

(45) Feagin, T. A.; Shah, N. I.; Heemstra, J. M. Convenient and Scalable Synthesis of Fmoc-Protected Peptide Nucleic Acid Backbone. *J. Nucleic Acids* **2012**, *2012*, 354549. https://doi.org/10.1155/2012/354549.

(46) Zhang, W.; Wang, Y.; Xu, Y.; Qian, X. New Fluorescent Conjugates of Uridine Nucleoside and Substituted 1,8-Naphthalimide: Synthesis, Weak Interactions and Solvent Effects on Spectra. *Monatshefte fur Chemie* **2003**, *134* (3), 393–402. https://doi.org/10.1007/s00706-002-0525-4.

(47) Riley, K. E.; Hobza, P. On the Importance and Origin of Aromatic Interactions in Chemistry and Biodisciplines. *Acc. Chem. Res.* **2013**, *46* (4), 927–936. https://doi.org/10.1021/ar300083h.

(48) Karabiyik, H.; Sevinçek, R.; Karabiyik, H. π-Cooperativity Effect on the Base Stacking Interactions in DNA: Is There a Novel Stabilization Factor Coupled with Base Pairing H-Bonds? *Phys. Chem. Chem. Phys.* **2014**, *16* (29), 15527–15538.

https://doi.org/10.1039/c4cp00997e.

(49) Ramaswami, G.; Li, J. B. RADAR: A Rigorously Annotated Database of A-to-I RNA Editing. *Nucleic Acids Res.* **2014**, *42* (109–113). https://doi.org/10.1093/nar/gkt996.

(50) Picardi, E.; D'Erchia, A. M.; Giudice, C. Lo; Pesole, G. REDIportal: A Comprehensive Database of A-to-I RNA Editing Events in Humans. *Nucleic Acids Res.* **2017**, *45*, D750–D757. https://doi.org/10.1093/nar/gkw767.

(51) Wang, Y.; Park, S. H.; Beal, P. A. Selective Recognition of RNA Substrates by ADAR Deaminase Domains. *Biochemistry* **2018**, *57* (10), 1640–1651. https://doi.org/10.1021/acs.biochem.7b01100.

(52) Zengeya, T.; Gupta, P.; Rozners, E. Triple-Helical Recognition of RNA Using 2-Aminopyridine-Modified PNA at Physiologically Relevant Conditions. *Angew. Chemie Int. Ed.* **2012**, *51* (50), 12593–12596. https://doi.org/10.1002/anie.201207925.

(53) Annoni, C.; Endoh, T.; Hnedzko, D.; Rozners, E.; Sugimoto, N. Triplex-Forming Peptide Nucleic Acid Modified with 2-Aminopyridine as a New Tool for Detection of A-to-I Editing. *Chem. Commun.* **2016**, *52* (51), 7935–7938. https://doi.org/10.1039/c6cc02164f.

(54) Sato, T.; Sato, Y.; Nishizawa, S. Triplex-Forming Peptide Nucleic Acid Probe Having Thiazole Orange as a Base Surrogate for Fluorescence Sensing of Double-Stranded RNA. *J. Am. Chem. Soc.* **2016**, *138* (30), 9397–9400. https://doi.org/10.1021/jacs.6b05554.

(55) Chiba, T.; Sato, T.; Sato, Y.; Nishizawa, S. Red-Emissive Triplex-Forming PNA Probes Carrying Cyanine Base Surrogates for Fluorescence Sensing of Double-Stranded RNA. *Org. Biomol. Chem.* **2017**, *15* (37), 7765–7769. https://doi.org/10.1039/c7ob02077e.

Chapter 4

Single-Molecule Investigation and Thermoreversible Control of PNA:DNA Hybridization*

4.1 Abstract:

Peptide nucleic acid (PNA) is a unique synthetic nucleic acid analog that has been adopted for use in many biological applications. These applications rely upon the robust Franklin-Watson-Crick base pairing provided by PNA, particularly at lower ionic strengths. However, our understanding of the relationship between the kinetics of PNA:DNA hybridization and ionic strength is incomplete. Here we measured the kinetics of association and dissociation of PNA with DNA across a range of ionic strengths and temperatures at single-molecule resolution using TIRF. PNA:DNA duplexes displayed significantly higher thermostability at lower ionic strengths, which we found can be attributable to an increase in the rate of association. Conversely, the dissociation rate remained largely unaffected by ionic strength. In comparison to a similar DNA:DNA duplex, however, it was found that the higher thermostability of PNA:DNA duplexes is due to a much slower dissociation rate at lower ionic strengths. We then report the thermoresponsive control of PNA:DNA hybridization through glyoxal caging. We show that this straightforward, scarless, and robust method is capable of thoroughly abolishing duplex formation, and hybridization can be completely restored following thermal decaging. This investigation into the kinetics of PNA:DNA hybridization and use of glyoxal to control structure provides a framework towards better understanding and design of future PNA probes for diverse applications.

---

*Authors: Swenson, C. S.; Lackey, H. H.; Reece, E. J.; Peterson, E. M.; Knutson, S. D.; Harris, J. M.; Heemstra, J. M. Adapted from Ref. 27 with permission from Knutson, S. D.; Sanford, A. A.; Swenson, C. S.; Korn, M. M.; Manuel, B. M., Heemstra, J. M. *Journal of the American Chemical Society*. **2020**, *142*(41), 17766-17781. Copyright 2020 American Chemical Society.

4.2 Introduction:

Nucleic acids are virtually unrivaled in their ability to store information and translate sequence into structure via Franklin-Watson-Crick base pairing. Through the rules of complementary hybridization, interactions and structures can be predicted with a high degree of accuracy. This has led to uses in many applications ranging from therapeutics and diagnostics to materials and programming.[1–4] Researchers have also attempted to improve the properties of nucleic acids through artificial analogues, or xeno nucleic acids (XNAs).[5–7] An interesting and promising XNA that provides unique properties is peptide nucleic acid (PNA).

PNA is an entirely synthetic nucleic acid analogue wherein the nucleobases are arrayed along a neutral *N*-(2-aminoethyl)-glycine backbone in place of the negatively charged phosphate backbone of canonical DNA and RNA (**Figure 4.1**).[8] This unique pseudopeptide backbone is responsible for dramatically altering the interactions of nucleic acids and proteins with PNA. For example, PNA is unrecognized by hydrolases resulting in much slower degradation in complex biological environments.[9,10] Additionally, PNA is capable of Franklin-Watson-Crick base-pairing similar to canonical nucleic acids, however the formed heteroduplexes exhibit much higher thermal stability than observed for natural nucleic acids.[11,12] These properties have made PNA an attractive choice for numerous applications involving antisense agents, duplex-invasion gene editing, nucleic acid biosensors, stimuli-responsive materials, and tools for cellular imaging. [13–21]

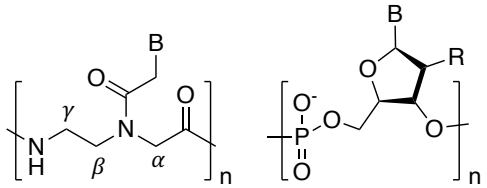

Figure 4.1: Structures of DNA, RNA, and PNA

Since the increased thermostability of PNA hybridization with DNA or RNA is a key attribute for many applications, understanding these interactions is of critical importance. PNA hybridization surprisingly demonstrates a negative salt dependence wherein lower ionic strength results in increased duplex stability.[12,22,23] This is the inverse of the trend for natural nucleic acid duplexes, and has led to studies of PNA:DNA and PNA:RNA duplex stability predominantly being

performed at ionic strengths far below physiological levels.[24] Moreover, the mechanism by which ionic strength governs PNA duplex formation remains unknown. However, the effect of ionic strength on the mechanism of natural nucleic acids duplex formation has been extensively studied at the single-molecule level using kinetic measurements.[25,26] These investigations detail how changes in ionic strength affect the energy barrier between single-stranded DNA and duplex through a change in the transition state energy. We envisioned using a similar approach to reveal how ionic strength affects the kinetics of PNA:DNA duplex formation.

Herein we applied a previously described single-molecule kinetics measurement technique to measure the effect of ionic strength on the kinetics of PNA:DNA duplex formation.[26] By employing an anchor DNA attached to a glass slide to immobilize a DNA capture strand that binds a diffusible TAMRA-labeled PNA probe, we measured the kinetics of duplex formation at the single-molecule level over a range of ionic strengths (50-450mM NaCl) and temperatures (22.5-30°C) using total internal reflectance (TIRF) spectroscopy (**Figure 4.2**). We report that the increase in stability at lower ionic strengths stems from a faster association rate, while the dissociation rate remains largely unaffected. This is in contrast to a comparable DNA:DNA duplex, wherein both association and dissociation rates are significantly affected by ionic strength. When used in biological and nanotechnology applications, the association rate of PNA with complementary nucleic acids is expected to have significant impact on function. To demonstrate, we report the control of PNA:DNA duplex association through a covalent thermoreversible interaction using a small molecule, glyoxal (**Figure 4.3**).[27] This

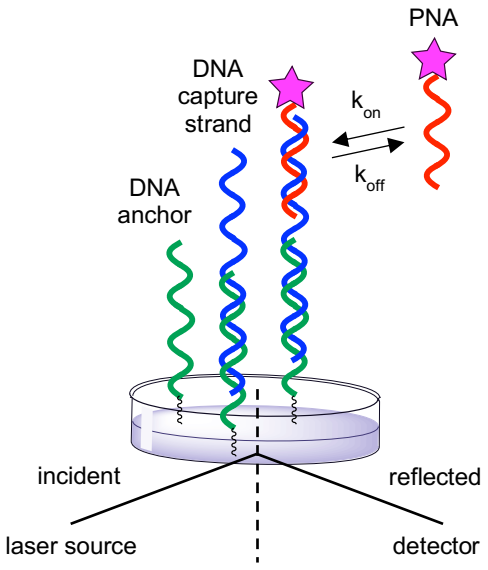

Figure 4.2: Schematic of experimental setup illustrating the interaction between the anchor DNA, immobilized DNA capture strand, and diffusing PNA probe.

modification blocks the Franklin-Watson-Crick face of PNA and greatly diminishes duplex formation. Increased temperature under mild alkaline conditions results in removal of the glyoxal adducts and rescues hybridization. This investigation of ionic strength dependence and application of glyoxal to elucidate and control the mechanism of PNA:DNA duplex formation provides a good framework for fundamental understanding and design of future PNA probes for myriad applications ranging across physics, chemistry, and biology.

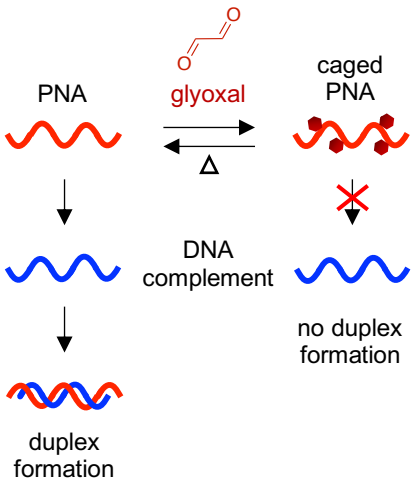

Figure 4.3: Thermally reversible glyoxal treatment inhibits hybridization of PNA:DNA duplexes.

4.3 Results and Discussion:

In order to determine the effect of temperature and ionic strength on the kinetics of PNA:DNA duplex formation, we employed a previously reported single-molecule platform for observing nucleic acid hybridization.[26] Glass slides were covalently functionalized with DNA anchor strands through an amine-epoxide reaction (**Table C1**). Unreacted sites were capped using an amine-biotin to reduce nonspecific adsorption to the surface. A DNA capture probe was immobilized through hybridization to the anchor DNA. This probe contains an anchoring sequence and a sequence complementary to a target PNA separated by a short polypyrimidine linker (**Table C1**). We chose to observe the kinetics of a 9mer PNA sequence, as we expected the rates of hybridization affinity to be within the range of our experimental setup (**Table C1**).[28] A longer complementary sequence would require very long acquisition times due to a slow duplex dissociation rate, whereas a shorter sequence would dissociate quickly, making hybridization events difficult to detect. The target PNA oligomer was functionalized with a rhodamine dye and a thin volume of sample at the interface was imaged using a TIRF microscope to observe single-

molecule hybridization events with the immobilized DNA capture probe. Time-lapse fluorescence images were acquired and analyzed to determine the locations of DNA probe molecules on the surface. We observed a significant number of repeated events at specific locations on the substrate, indicating that PNA is capable of specifically interacting with the DNA probe. These locations with repeated hybridization events were not observed when using non-complementary scrambled oligonucleotides, nor on substrates lacking immobilized DNA capture probe. From this, the duration of repeated hybridization events can be accurately determined, whereas sites of nonspecific adsorption or photobleaching can be discarded (**Figure C1**). The average interval times between dissociation (t_{off}) and association (t_{on}) events at single molecule sites was measured and used to calculate the rates of association and dissociation.[26]

4.3.1 Effect of Ionic Strength and Temperature on PNA:DNA Hybridization Kinetics

Using the described experimental procedure, the association and dissociation rates of PNA:DNA hybridization were determined over a range of salt concentrations (50-450 mM NaCl) and temperatures (22.5-30°C) (**Table C2**). We observed a 3.5-fold decrease in association rate (k_{on}) with increasing ionic strengths from 50 mM to 450 mM at 22.5°C (**Figure 4.4A**). In contrast, the dissociation rate (k_{off}) displayed little dependence on ionic strength with only a slight increase (~1.4-fold) at higher ionic strengths (**Figure 4.4B**). As expected, increasing temperature resulted

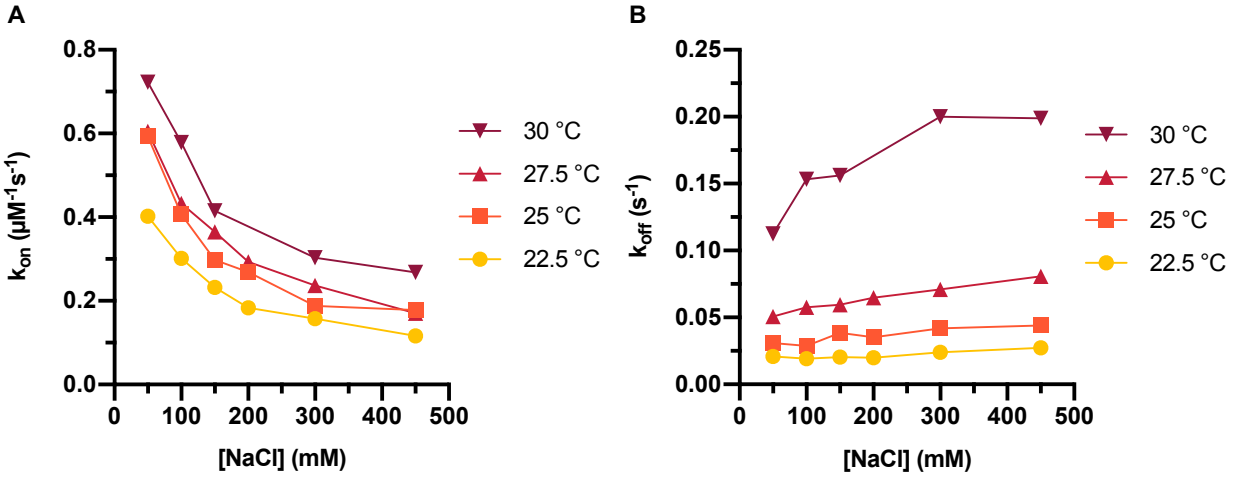

Figure 4.4: Plots of association (A) and dissociation (B) rates of PNA:DNA hybridization with increasing ionic strength at different temperatures.

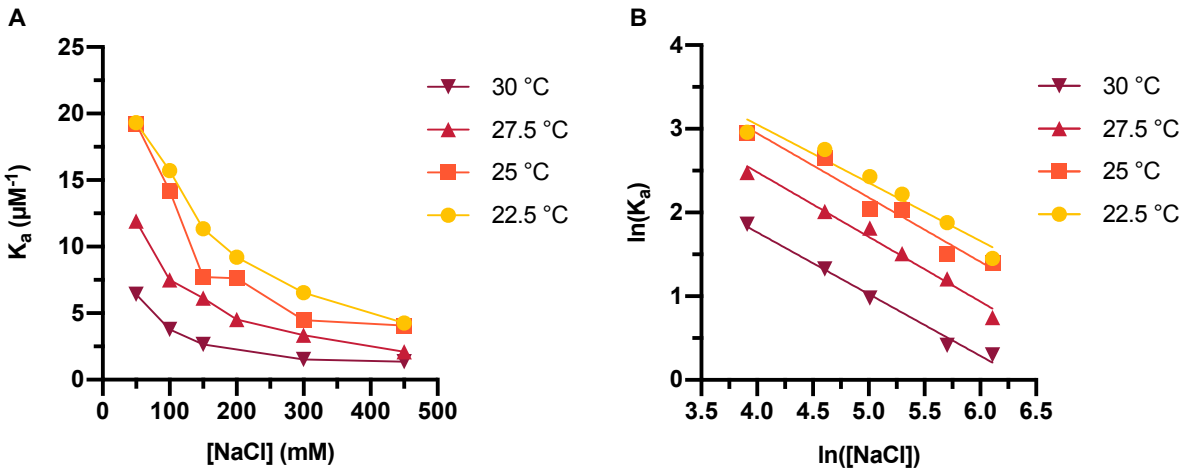

Figure 4.5: Association constant and Leipply analysis. A) Plot of association constant of PNA:DNA hybridization with increasing ionic strength at different temperatures. B) Leipply type analysis of PNA:DNA hybridization displaying a negative slope to indicate that ions are ejected into the bulk solution upon duplex formation.

in increasing association and dissociation rates across all ionic strengths. We then calculated the association constant, K_a, from the kinetic rate constants at each salt concentration and temperature using the relationship $K_a = k_{on}/k_{off}$ (**Figure 4.5A; Table C2**). These calculations determined that the stability of the duplex increased at lower ionic strengths and temperatures in agreement with previous thermal melting studies.[12,22] The data shown indicate that the previously observed increase in PNA:DNA duplex stability at lower ionic strengths can be mainly attributed to a much faster association rate. This is possibly due to an ionic stabilization of the single stranded oligomers in the bulk solution, similar to "salting in" effects observed with proteins.[29] Increasing salt concentration may improve the solubility and decrease the free energy of the unbound PNA, thus increasing the barrier to duplex formation. Another possibility is that the single-stranded DNA adopts a more elongated structure due to increased electrostatic repulsion between negatively charged phosphate groups. This could make the DNA more accessible and decrease the energy barrier for duplex formation with PNA.

In order to further elucidate the role of ionic strength on PNA:DNA hybridization, we performed a Leipply type analysis from the calculated K_a values.[30] This analysis relates the association constant to the concentration of ions in solution to understand the relationship

between duplex formation and ions either ejected or absorbed upon hybridization. A plot of the ln(K_a) vs ln([NaCl]) fit to a simple linear regression provides a magnitude of the slope (**Figure 4.5B**). This magnitude relates to the change in the number of ions involved in duplex formation, with a negative slope suggesting ions are ejected into the bulk solution and a positive slope suggesting that ions are incorporated into the duplex. The analysis for PNA:DNA hybridization displayed a negative slope at all temperatures, indicating that ions are ejected into the bulk solution upon hybridization. The requirement of ejecting ions for duplex formation may explain the decrease in association rate and affinity for PNA:DNA duplexes, as this process is less favorable at high salt concentration.

4.3.2 Comparison of PNA:DNA and DNA:DNA Hybridization Kinetics

Due to the inverse relationship between affinity and ionic strength for PNA:DNA duplexes compared to native nucleic acid duplexes, we sought to compare the hybridization kinetics across similar sequences at a range of ionic strengths. Initially we used a 9mer DNA of the same sequence as the PNA target (**Table C1**). However, due to the increased affinity of PNA:DNA duplexes compared to native duplexes, this sequence displayed very short hybridization event times even at higher ionic strengths that made identifying DNA probe sites extremely difficult (data not shown). Instead, for this comparison we designed an 11mer DNA-2A that contained two

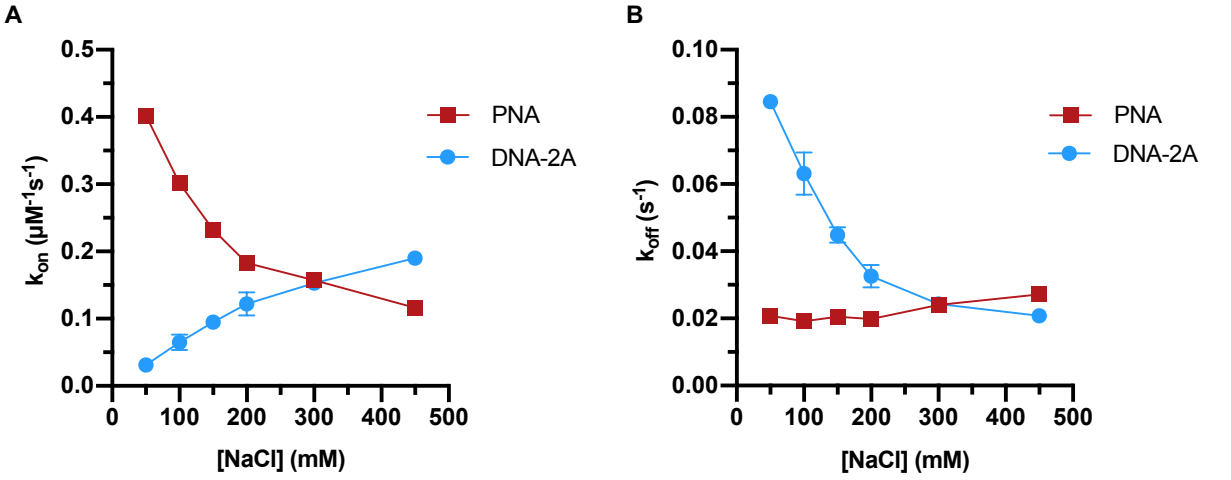

Figure 4.6: Plots of association (A) and dissociation (B) rates of PNA or DNA-2A hybridization to DNA capture probe with increasing ionic strength. Error bars represent 2*SEM (n=3).

additional adenosine bases complementary to the DNA capture probe linker to provide a similar stability to the PNA target when hybridized to the probe capture region across all ionic strengths (**Table C1**). The hybridization kinetics of DNA-2A were measured across the range of salt concentrations (50-450 mM NaCl) at 22.5°C (**Table C3**). Both the association and dissociation rates of DNA-2A:DNA hybridization were strongly affected by the ionic strength (**Figure 4.6A and 4.6B**). The association rate (k_{on}) decreased 6-fold with decreasing ionic strength from 450 mM to 50 mM. This is larger than the 3.5-fold change in PNA:DNA hybridization, suggesting a greater effect of ionic strength on native DNA:DNA duplexes. The trend is also the opposite, with PNA:DNA hybridization exhibiting an inverse relationship between association rate and increasing ionic strength. Conversely, the dissociation rate (k_{off}) of DNA-2A:DNA hybridization increased 4-fold with decreasing ionic strength over the same range. Again, the larger change in rate compared to the PNA:DNA duplex suggests a greater effect of ionic strength on duplex stability.

The association constants (K_a) for DNA-2A:DNA hybridization were calculated using the measured rate constants and a Leipply type analysis was performed to determine the relationship

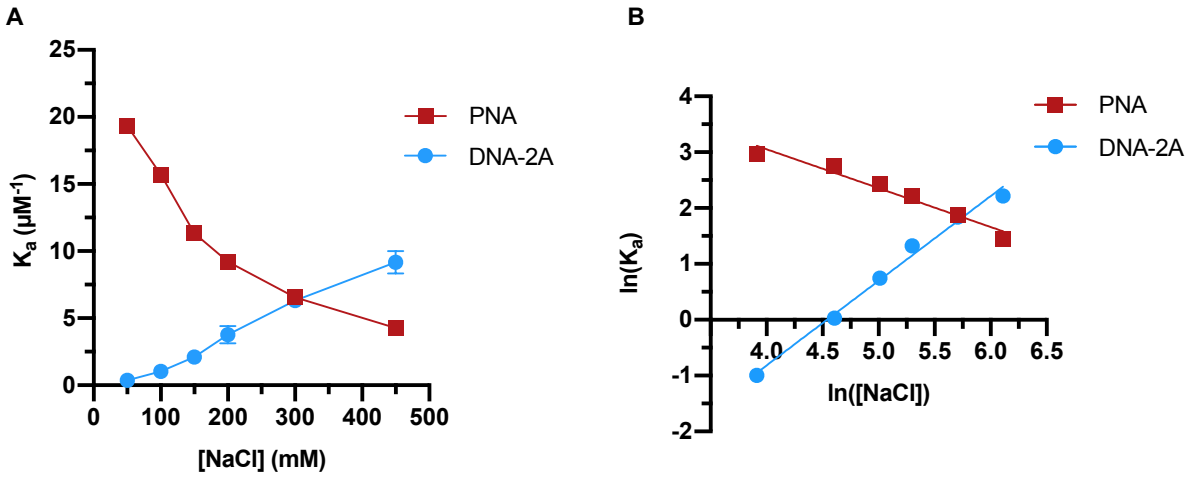

Figure 4.7: Comparison of association constant and Leipply analysis of PNA and DNA. A) Plot of association constant of PNA or DNA-2A hybridization to DNA capture probe with increasing ionic strength. Error bars represent 2*SEM (n=3). B) Leipply type analysis of PNA or DNA-2A hybridization at 22.5°C. Negative slope indicates ions are ejected upon duplex formation; positive slope indicates ions are absorbed.

of the ions with duplex formation (**Figure 4.7**). As expected, the association constant increased with increasing ionic strength as reported previously.[24] However, unlike PNA:DNA hybridization, this change in stability is dependent upon both the association and dissociation rate changes. The Leipply type analysis resulted in a linear fit with a positive slope, indicating ions are incorporated into the duplex upon hybridization. The larger magnitude of the slope compared to PNA:DNA also demonstrates that a greater number of ions are involved in duplex formation, likely adding to the larger change in kinetic rates observed for DNA-2A:DNA hybridization. This may also help explain the inverse trends observed between PNA and DNA hybridization rates and stability dependent on the change in ionic strength, as ions are ejected during PNA:DNA duplex formation but absorbed upon DNA:DNA hybridization.

In order to draw a more distinct comparison, we measured the kinetics of the 9mer DNA with the same sequence as the PNA target at the highest ionic strength (450 mM) at 22.5°C. As we mentioned previously, lower ionic strengths resulted in extremely fast interaction kinetics for

Table 4.1: PNA and DNA hybridization kinetics.

Sample	Temperature (°C)	[NaCl] (mM)	k_{off} (s^{-1})	k_{on} ($\mu M^{-1}s^{-1}$)	K_a (μM^{-1})
DNA	22.5	450	0.34	0.44	1.3
PNA	22.5	450	0.020	0.18	9.1

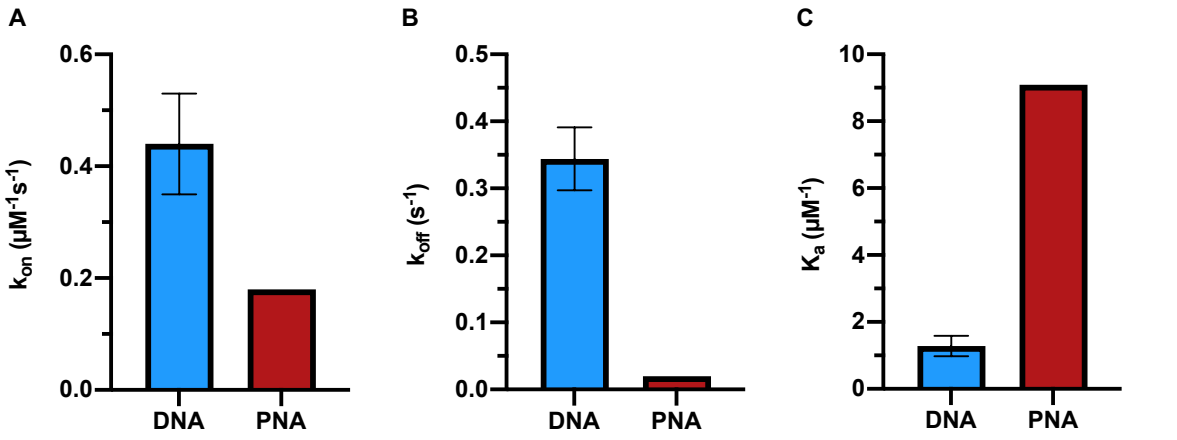

Figure 4.8: Comparison of association and rate constants of PNA and DNA. A) Assocation rate comparison of DNA and PNA hybridization. B) Dissociation rate comparison of DNA and PNA. C) Association constant comparison of DNA and PNA. All data was measured at 450 mM NaCl at 22.5°C. Error bars represent 2*SEM (n=3).

this DNA sequence, which made data collection and accurate analysis particularly difficult. However, we were able to collect quality data at 450 mM NaCl for a direct comparison of PNA and DNA hybridization (**Table 4.1**; **Table C4**). We observed significantly faster overall association and dissociation kinetics for DNA:DNA hybridization (**Figure 4.8A and 4.8B**). However, the association constant for PNA:DNA was much larger than the equivalent DNA:DNA duplex, in agreement with other studies of PNA duplex stability (**Figure 4.8C**). [8,10,11] This can be mostly attributed to the very slow dissociation rate of PNA when hybridized to DNA, which is ~17x slower than that of the comparable DNA.

As our data suggests, the main driver for increased stability of PNA:DNA duplexes at lower ionic strengths is the association rate. This is immensely important for many applications which utilize PNA hybridization such as antisense therapeutics, nucleic acid diagnostics, and gene editing. If we can regulate the hybridization, we can add additional control to fine-tune these specific interactions and subsequent activity between native and non-native nucleic acids.

4.3.3 Thermoreversible Control of PNA:DNA Hybridization

In order to control hybridization, we sought to reversibly disrupt the base pairing through blocking or altering the donor-acceptor pairs of the nucleobases. Several approaches have been developed which incorporate small molecule “protecting” groups that rely upon chemical or UV triggers to reversibly prevent duplex formation.[31–36] While effective for a number of applications, these methods require complex and often costly synthesis of monomers to include nucleobase protecting groups. The use of chemical or light triggers can also alter native environments and result in structural changes to certain nucleobases. Alternatively, we envisioned the use of temperature as a trigger for reversibly controlling hybridization, as heat is relatively easy to control and introduce into myriad experimental settings. We and others have previously reported that glyoxal is capable of disrupting nucleic acid structure by “caging” the nitrogen groups on the Franklin-Watson-Crick face, reacting to produce stable *bis*-hemiaminal adducts (**Figure 4.9A**).[27,37] Subsequent treatment with heat under mild alkaline conditions removes the glyoxal adducts,

"decaging" the nucleobases back to their native structures (**Figure 4.9B**).[38] Because glyoxal reacts directly with the nucleobases, we hypothesized that it could disrupt PNA hybridization regardless of the neutral pseudopeptide backbone.

We synthesized a FAM-labeled PNA oligomer based on the "Nielsen decamer" sequence (**Table C1**).[11,22] This sequence was treated with glyoxal over a range of time (5-240 min) and analyzed by HPLC and PAGE to determine caging efficiency (**Figure C2A and C2C**). After 10 minutes we observed three distinct bands on PAGE, indicating different levels of caging. The PNA appeared to be fully caged after ~2 hours. Interestingly, we observed an unexpected apparent size decrease by a downward shift of electrophoretic mobility on the gel. However, we confirmed through mass spectrometry that glyoxal attachment occurred on full-length PNA (**Figure C3**). While uncertain, we hypothesize that the addition of glyoxal may impart transient negative charge to the PNA through cooperative hydrogen bonding between hydroxyl adducts, which would explain the downward shift based on additional charge instead of a change in size. In any case, subsequent treatment with heat (95°C at pH 7.5) over a range of time (1-20 min) resulted in decaging of the PNA strand, proceeding to complete removal of adducts after ~5 minutes and restoration of electrophoretic mobility similar to untreated PNA (**Figure 4.10A; Figure C2B**).

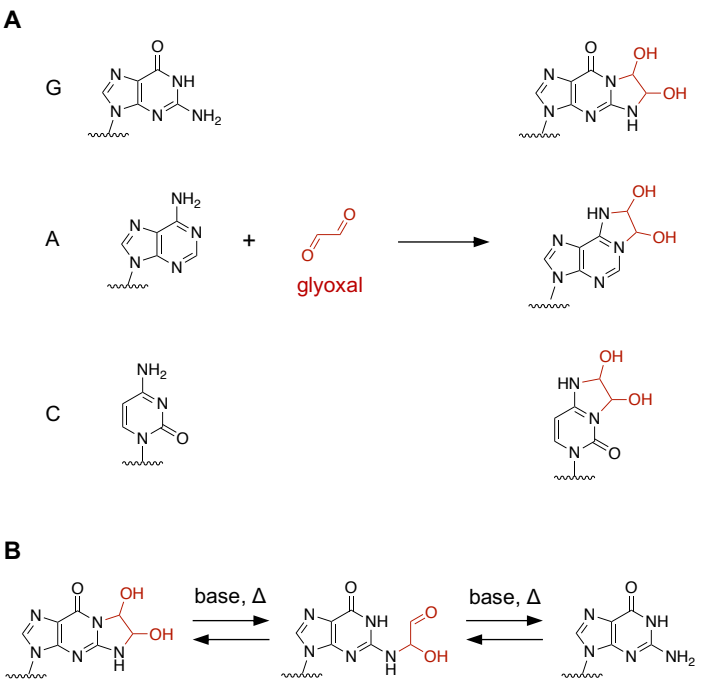

Figure 4.9: Glyoxal reactivity with nucleobases. A) Glyoxal reacts with nitrogen groups on G, A, and T to form *bis*-hemiaminal adducts. B) Glyoxal is removed by heat under mild alkaline conditions.

To better understand how the extent of caging effects hybridization, we utilized a microscale thermophoresis (MST) binding assay over the range of caging times using a

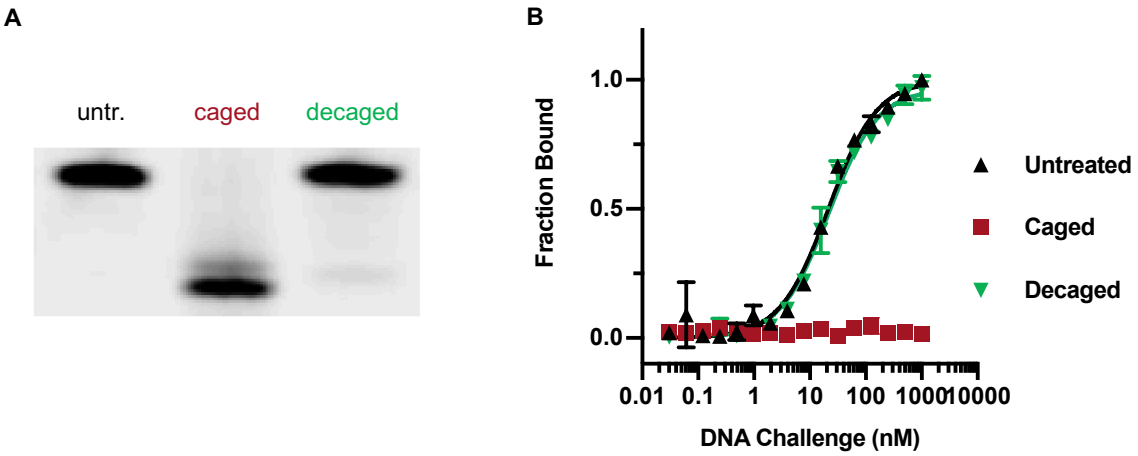

Figure 4.10: Glyoxal caging and decaging of PNA. A) 20% PAGE analysis of untreated, caged, and decaged PNA. Decaging restores electrophoretic mobility. B) MST analysis of untreated, caged, and decaged PNA binding to complementary DNA. Decaging rescues hybridization.

complementary or scrambled DNA sequence (**Table C1**). We observed a significant decrease in binding from 5 to 10 minutes and complete disruption after 20 minutes of caging (**Figure C4**). There was no observable binding to the scrambled DNA target and the untreated PNA was capable of hybridization, suggesting that the lack of binding upon glyoxal treatment is due to the caging of the nucleobases. We then compared untreated, caged, and decaged PNA for binding to the complementary DNA target. While caging resulted in disrupted binding, we clearly observed full restoration of hybridization following decaging conditions (**Figure 4.10B**). Together, these results indicate that glyoxal caging is a simple and robust method for providing an external level of control over PNA:DNA hybridization and is the first example of functional caging of PNA.

4.4 Conclusions:

The ability to store and accurately predict information through complementary hybridization of nucleic acids is a major driving force for biology and technology. In particular, PNA exhibits desirable properties for applications including powerful and specific base pairing to complementary targets, even at ionic strengths much lower than physiological levels.[12,22,23] Proper design and utilization of PNA probes in applications such as nucleic acid diagnostics and

materials requires discrete knowledge about the mechanisms behind hybridization. We wanted to determine the less-studied relationship between the rates of PNA:DNA duplex formation and ionic strength at the single-molecule level. We employed a single-molecule imaging technique to measure the association and dissociation events of a PNA probe with a complementary DNA capture strand. We discovered that the dissociation rate is mainly unaffected by ionic strength, whereas the association rate significantly decreases at higher salt concentrations. We propose that it is this change in the association rate that is the main contributor for the increased duplex stability, possibly due to a “salting in” effect on single stranded PNA or decreased DNA accessibility at higher ionic strengths. When compared to a similar DNA:DNA duplex, rate constants for PNA:DNA duplexes were less affected by ionic strength and the difference in association constant thus duplex stability was attributed to a major difference in the dissociation rate of PNA:DNA duplexes vs DNA:DNA.

A major benefit of using PNA probes as nucleic acid detection devices and therapeutics is the capability for strong hybridization over ranges of ionic strengths. In this model system, we measured the kinetics using NaCl. However, we recognize that complex environments can contain a plethora of different ions including different concentrations of mono- and divalent types. Further studies will include additional salts to better represent the effect of different ions on PNA:DNA hybridization. These ions will include the Hofmeister series, which is a series of anions that are commonly studied for protein purification through a “salting out” effect.[39,40] Because the neutral backbone of PNA is similar to that of proteins, we will investigate how these anions and the role of hydration affects the kinetics of PNA duplex formation.

The kinetics of PNA hybridization play pivotal roles in applications for nucleic acid sensors, antisense interactions, and gene editing among others. In order to provide another layer of control over the association of duplex formation, we utilized a thermoreversible glyoxalation reaction to cage the Franklin-Watson-Crick face of PNA. This small molecule was capable of thoroughly depleting PNA:DNA duplex formation after only 20 minutes caging reaction. Subsequently,

complete restoration of PNA:DNA association was achieved upon treatment with heat. We anticipate this robust and scarless method of functional control over PNA activity to be greatly useful for antisense gene regulation and other nucleic acid therapeutics.

Fundamental understanding of the kinetic rates of hybridization and the ability to reversibly control duplex formation provide a framework for the efficient design and prediction of activity for diverse PNA probes. We believe our findings offer a basis for future experiments to investigate PNA:DNA hybridization kinetics in varying environments as well as the optimization of existing PNA-based applications.

4.5 Materials and Methods:

Abbreviations: Fmoc, fluorenylmethyloxycarbonyl; DMF, dimethylformamide; HATU, 1-[Bis(dimethylamino)methylene]-1*H*-1,2,3-triazolo[4,5-*b*]pyridinium 3-oxid hexafluorophosphate; NMM, *N*-methylmorpholine; DIPEA, diisopropylethylamine; TFA, trifluoroacetic acid; DCM, dichloromethane; NMP, N-methyl-2-pyrrolidone; NHS, *N*-hydroxysuccinimide; FAM, 5,6-carboxyfluoroscein; MST, microscale thermophoresis.

PNA oligomer synthesis:

PNA was synthesized using a standard solid-phase synthesis protocol on a Biotage SP wave semi-automatic synthesizer. Synthesis began by loading ~50 mg of a rink amide MBHA resin (0.52 mmol/g) with 5 μmols of the first Fmoc-PNA monomer or Fmoc-amino acid using 1.5 eq. HATU, 1.5 eq. DIPEA, and 1.5 eq. 2,6-lutidine in 200 μL dry NMP for 1 hour followed by capping using a solution of 9% acetic anhydride and 13% 2,6-lutidine in DMF. The resin was then deprotected with a solution of 25% piperidine in DMF. For monomer couplings, 5 eq. of monomer was pre-activated for 10 minutes with 5 eq. HATU, 5 eq. DIPEA, and 5 eq. 2,6-lutidine in 400 μL NMP before addition to the resin. Coupling proceeded with microwave-assistance at 75°C for 6

min. The resin was then washed (5x1 mL DMF), capped using the capping solution (2x5 min with 1 mL each), washed (5x1 mL DMF, 3x1 mL DCM, 3x1 mL DMF), deprotected with deprotection solution (3x2 min with 1mL each), and washed (5x1 mL DMF, 3x1 mL DCM, 3x1 mL DMF) to complete a coupling cycle. NHS-Rhodamine or FAM-COOH was coupled to the resin using DIPEA or HATU/DIPEA in DMF following the final PNA monomer. Upon completion of synthesis, the resin was washed with DCM and dried before cleavage using a solution of 2.5% H_2O and 2.5% TIS in TFA. The crude oligomer was ether precipitated, washed with ether, and dried for purification. Purification was performed by reverse-phase HPLC using an Agilent Eclipse XDB-C18 5 μm, 9.4x250 mm column at 60°C with a flow rate of 2 mL/min, monitored at 260 nm using a linear gradient (10%-40% in 15 min) of 0.1% TFA/acetonitrile in 0.1% TFA/H_2O. Identity of pure oligomer was confirmed using an Agilent 6230 elctrospray ionization time-of-flight (ESI-TOF) mass spectrometer.

DNA substrate preparation:

DNA oligonucleotides were synthesized and purified by HPLC by the University of Utah Health Sciences Center DNA/Peptide Core Facility. DNA and PNA were resuspended in ultrapure water and, for unlabeled oligonucleotides, their concentration was determined using absorbance at 260 nm. In the case of carboxytetramethylrhodamine labeled DNA and PNA, concentration was quantified using light absorption at 555 nm with a molar absorptivity of $9.0x10^4$ reported by the reagent vendor. Stock solutions were stored at -20°C, and were thawed shortly before experiments and stored at 4°C.

Glass substrates used to anchor probe DNA and resist nonspecific adsorption were prepared using previously described protocols.[41] Briefly, float glass coverslips were cleaned by first rinsing twice in ultrapure water and methanol. Coverslips were then cleaned for 20 minutes using RCA solution[42] (a 1:1:5 mixture of 30% hydrogen peroxide, 30% ammonium hydroxide solution, and water) at 75°C. Coverslips were then rinsed 3 times with ultrapure water, and dried

for 30 minutes at 120°C. Coverslips were then sealed in a jar containing 250 µL of 3-glycidyloxypropyl-trimethoxysilane in a small vial and held at 80°C for 90-120 minutes to deposit a silane layer on the glass. Coverslips were removed from the jar and heated at 120°C in air for 90 minutes to drive off the unreacted silane and allow for cross-linking of the deposited silane layer.

The coverslips were then cooled and a 15 µL droplet of 100 µM amine-modified capture ssDNA in 100 mM pH 10.0 carbonate buffer was placed on a coverslip. Another coverslip was placed on top of this one to form a thin solution layer between them. This coverslip stack was placed in a small beaker and nested inside a larger jar containing the same carbonate buffer to prevent the thin solution layer between the coverslips from evaporating. This assembly was sealed and incubated at 40°C for 4-8 h to allow the amine-modified DNA to react with the epoxide surface. Coverslips were then separated under water, rinsed with ultrapure water, and placed in a solution of 20 mM 3-amino1-propanesulfonic acid in 100 mM carbonate buffer for 8 hours at 40°C to passivate unreacted epoxide groups on the surface. Substrates were then rinsed in water and stored for up to 21 days at 4°C before use in imaging experiments.

Fluorescence imaging:

Solutions used for imaging experiments were prepared with 10 mM Tris buffer at pH 8.0 with 1 mM EDTA and varying amounts of sodium chloride, as noted in the text. Buffers were filtered with a 0.2 µm filter and stored at 4°C. Stock solutions of DNA and PNA were diluted into the appropriate buffers and vortexed shortly before injecting into the imaging flow cell for kinetics measurements.

Coverslips with capture DNA were loaded into an imaging microfluidics cell. This microfluidics cell uses a double-stick gasket (3M 9495MP) to form a channel and seal coverslip to a PMMA top plate with ports for sample injection. The flow cell was imaged using an Olympus

IX-71 microscope configured for objective-based total internal reflection fluorescence microscope (TIRF).[26,43] Illumination was provided by a 532 nm laser (BWTek) coupled into a single-mode optical fiber (Thorlabs). Light from the fiber was collimated by an achromatic doublet lens (Thorlabs), passed through an aperture, quarter wave plate (Thorlabs), and a shutter (Uniblitz), reflected from a dichroic mirror (Semrock), and finally focused onto the back-focal plane of the microscope objective (60x, 1.45NA, Olympus) with an achromatic doublet (Thorlabs) to illuminate the sample. Fluorescence emission from individual molecules is collected by the objective and sent through the dichroic mirror, emission filter (Semrock), and a 1.6x magnifier (for a total magnification of 96x) and imaged with an Andor iXon DU897 electron-multiplying charge-coupled device camera. The microscope system and sample were enclosed in a fiberboard incubator and the temperature was controlled to within $\pm 0.2^{\circ}C$ using a proportional-integral-derivative controlled heater-fan assembly (Omega HVL14900) calibrated with a NIST-traceable thermometer (VWR).

Image acquisition and analysis:

Fluorescence images were collected with exposure times designed to minimize photobleaching, while still sampling the hybridization kinetics. Hybridization was monitored using time-lapse videos with 100 ms exposures and interval times between 0.3 s and 5 s intervals. The excitation laser exposure experienced by fluorophores on target DNA bound at the interface before dissociation has been shown to result in minimal photobleaching.[26,43] Images were collected in 300x300 pixel sub-regions of the sensor, corresponding to 50x50μm in the sample. The sensor readout was at 1MHz to minimize read noise, and the electron-multiplying amplifier was deactivated to avoid additional EM photon-counting noise.[44] Images were acquired as 15-60 min 16-bit monochrome FITS-image stacks using Andor SOLIS software version 4.27.30001.0.

Images were analyzed using a super-resolution imaging scheme previously described.[26] First, we locate all fluorescent spots in each image, and track them to determine locations of probe DNA molecules on the surface that experience repeat hybridization visits by fluorescently tagged

target DNA molecules. The duration of each hybridization event, and the interval time between events are used to determine the association and dissociation rate of each probe molecule on the surface. Probe molecules with anomalous kinetics and spurious nonspecific adsorption sites are discarded. Hybridization events from the remaining filtered probe molecules are pooled and fit to a first-order kinetics model to determine the association rate constant, k_{on}, the dissociation rate constant, k_{off}, and the association constant, K_a.

PNA glyoxal caging:

1 nmol of PNA oligonucleotide was mixed with 14.5 µL of a 40% glyoxal solution (Sigma Aldrich) and brought to a final volume of 100 µL with nuclease-free water. Samples were reacted at 50 ºC for 0 minutes, 5 minutes, 10 minutes, 20 minutes, 30 minutes, 1 hour, 2 hours, and 4 hours. At each time point, reactions were purified with reverse-phase HPLC using an Agilent Eclipse Plus C18 3.5 µm, 4.6x150 mm column at 60°C with a flow rate of 1 mL/min, monitored at 260 nm using a linear gradient (10% - 50% in 20 min) of 0.1% TFA/acetonitrile in 0.1% TFA/H2O. Collected fractions were dried under vacuum and then resuspended in 50 µl phosphate buffered saline (137 mM NaCl, 2.7 mM KCl, 8 mM Na2HPO4, 2 mM KH2PO4, pH 7.5). 10 pmol of each reaction was analyzed by 20% denaturing PAGE.

PNA glyoxal decaging:

250 pmol of caged (2 h glyoxal treatment) PNA strand was added to a final volume of 50 µL of phosphate buffered saline (137 mM NaCl, 2.7 mM KCl, 8 mM Na2HPO4, 2 mM KH2PO4, pH 7.5). Samples were incubated in a thermal cycler at 95 ºC for 0 minutes, 1 minutes, 2 minutes, 5 minutes, 10 minutes and 20 minutes. 5 pmol of each reaction was then analyzed by 20% denaturing PAGE.

PNA hybridization assays:

To test hybridization, a full complement and scrambled DNA oligonucleotide was purchased from Integrated DNA Technologies. PNA complement: 5' AGTGATCTAC 3'; PNA scrambled: 5' CTATGGTACA 3'. For each hybridization test, a 20 nM solution of untreated, caged, or decaged FAM-labeled PNA strand was prepared in 1X binding buffer (40 mM HEPES, 100 mM KCl, 1 mM MgCl2, 0.05% Tween 20, pH 7.4). A 1 μM solution of complement and scrambled DNA was prepared in 1X binding buffer and serially diluted 1:1 several times. Dilutions were combined with an equal volume of 10 nM PNA solution to yield final conditions in all samples of 5 nM PNA strand, 1X binding buffer, and DNA challenge (complement or scramble) ranging from ~152 pM to 500 nM in a final volume of 100 μL. Samples were incubated at room temperature for 30 minutes and then loaded into NT.115 standard glass capillaries. MST experiments were performed using a Nanotemper Monolith NT.115 Pico instrument. All measurements were analyzed using the Pico-RED filter with 20% LED intensity and low laser power.

4.6 References:

(1) Li, L.; Xu, S.; Yan, H.; Li, X.; Yazd, H. S.; Li, X.; Huang, T.; Cui, C.; Jiang, J.; Tan, W. Nucleic Acid Aptamers for Molecular Diagnostics and Therapeutics: Advances and Perspectives. *Angew. Chemie Int. Ed.* **2020**. https://doi.org/10.1002/anie.202003563.

(2) Seeman, N. C.; Sleiman, H. F. DNA Nanotechnology. *Nat. Rev. Mater.* **2018**, *3* (1), 17068. https://doi.org/10.1038/natrevmats.2017.68.

(3) Lakin, M. R.; Phillips, A. Domain-Specific Programming Languages for Computational Nucleic Acid Systems. *ACS Synth. Biol.* **2020**, *9* (7), 1499–1513. https://doi.org/10.1021/acssynbio.0c00050.

(4) O'donoghue, P.; Heinemann, I. U. Synthetic DNA and RNA Programming. *Genes*. **2019**, *10*(7), 523. https://doi.org/10.3390/genes10070523.

(5) Anosova, I.; Kowal, E. A.; Dunn, M. R.; Chaput, J. C.; Horn, W. D. V.; Egli, M. The Structural

Diversity of Artificial Genetic Polymers. *Nucleic Acids Res.* **2016**, *44* (3), 1007–1021. https://doi.org/10.1093/nar/gkv1472.

(6) Morihiro, K.; Kasahara, Y.; Obika, S. Biological Applications of Xeno Nucleic Acids. *Mol. Biosyst.* **2017**, *13* (2), 235–245. https://doi.org/10.1039/c6mb00538a.

(7) Ma, Q.; Lee, D.; Tan, Y. Q.; Wong, G.; Gao, Z. Synthetic Genetic Polymers: Advances and Applications. *Polym. Chem.* **2016**, *7* (33), 5199–5216. https://doi.org/10.1039/c6py01075j.

(8) Nielsen, P. E.; Egholm, M.; Berg, R. H.; Buchardt, O. Sequence-Selective Recognition of DNA by Strand Displacement with a Thymine-Substituted Polyamide. *Science (80-.).* **1991**, *254* (5037), 1497–1500. https://doi.org/10.1126/science.1962210.

(9) Demidov, V. V; Potaman, V. N.; Frank-Kamenetskii, M. D.; Egholm, M.; Buchardt, O.; Sonnichsen, S. H.; Nlelsen, P. E. Stability of Peptide Nucleic Acids in Human Serum and Cellular Extracts. *Biochem. Pharmacol.* **1994**, *48* (6), 1310–1313.

(10) Nielsen, P. E.; Egholm, M.; Buchardt, O. Peptide Nucleic Acid (PNA). A DNA Mimic with a Peptide Backbone. *Bioconjug. Chem.* **1994**, *5* (1), 3–7. https://doi.org/10.1021/bc00025a001.

(11) Egholm, M.; Buchardt, O.; Christensen, L.; Behrens, C.; Freier, S. M.; Driver, D. A.; Berg, R. H.; Kim, S. K.; Norden, B.; Nielsen, P. E. PNA Hybridizes to Complementary Oligonucleotides Obeying the Watson–Crick Hydrogen-Bonding Rules. *Nature* **1993**, *365*, 566–568. https://doi.org/10.1038/365566a0.

(12) Tomac, S.; Sarkar, M.; Ratilainen, T.; Wittung, P.; Nielsen, P. E.; Norden, B.; Graslund, A. Ionic Effects on the Stability and Conformation of Peptide Nucleic Acid Complexes. *J. Am. Chem. Soc.* **1996**, *118* (24), 5544–5552. https://doi.org/10.1021/ja960495l.

(13) Pellestor, F.; Paulasova, P. The Peptide Nucleic Acids (PNAs), Powerful Tools for Molecular Genetics and Cytogenetics. *European Journal of Human Genetics*. **2004**, *12*(9), 694–700. https://doi.org/10.1038/sj.ejhg.5201226.

(14) D'Agata, R.; Giuffrida, M. C.; Spoto, G. Peptide Nucleic Acid-Based Biosensors for Cancer

Diagnosis. *Molecules*. **2017**, *22*(11), 1951. https://doi.org/10.3390/molecules22111951.

(15) Gambari, R. Peptide Nucleic Acids: A Review on Recent Patents and Technology Transfer. *Expert Opin. Ther. Pat.* **2014**, *24* (3), 267–294. https://doi.org/10.1517/13543776.2014.863874.

(16) Gupta, A.; Mishra, A.; Puri, N. Peptide Nucleic Acids: Advanced Tools for Biomedical Applications. *J. Biotechnol.* **2017**, *259*, 148–159. https://doi.org/10.1016/j.jbiotec.2017.07.026.

(17) Wu, J.-C.; Meng, Q.-C.; Ren, H.-M.; Wang, H.-T.; Wu, J.; Wang, Q. Recent Advances in Peptide Nucleic Acid for Cancer Bionanotechnology. *Acta Pharmacol. Sin.* **2017**, *38*, 798–805. https://doi.org/10.1038/aps.2017.33.

(18) Narenji, H.; Gholizadeh, P.; Aghazadeh, M.; Rezaee, M. A.; Asgharzadeh, M.; Kafil, H. S. Peptide Nucleic Acids (PNAs): Currently Potential Bactericidal Agents. *Biomed. Pharmacother.* **2017**, *93*, 580–588. https://doi.org/10.1016/j.biopha.2017.06.092.

(19) Saarbach, J.; Sabale, P. M.; Winssinger, N. Peptide Nucleic Acid (PNA) and Its Applications in Chemical Biology, Diagnostics, and Therapeutics. *Curr. Opin. Chem. Biol.* **2019**, *52*, 112–124. https://doi.org/10.1016/j.cbpa.2019.06.006.

(20) Swenson, C. S.; Velusamy, A.; Argueta-Gonzalez, H. S.; Heemstra, J. M. Bilingual Peptide Nucleic Acids: Encoding the Languages of Nucleic Acids and Proteins in a Single Self-Assembling Biopolymer. *J. Am. Chem. Soc.* **2019**, *141* (48), 19038–19047. https://doi.org/10.1021/jacs.9b09146.

(21) Swenson, C. S.; Heemstra, J. M. Peptide Nucleic Acids Harness Dual Information Codes in a Single Molecule. *Chem. Commun.* **2020**, *56* (13), 1926–1935. https://doi.org/10.1039/c9cc09905k.

(22) De Costa, N. T. S.; Heemstra, J. M. Evaluating the Effect of Ionic Strength on Duplex Stability for PNA Having Negatively or Positively Charged Side Chains. *PLoS One* **2013**, *8* (3), e58670. https://doi.org/10.1371/journal.pone.0058670.

(23) Park, H.; Germini, A.; Sforza, S.; Corradini, R.; Marchelli, R.; Knoll, W. Effect of Ionic Strength on PNA-DNA Hybridization on Surfaces and in Solution. *Biointerphases* **2007**, *2*, 80–88. https://doi.org/10.1116/1.2746871.

(24) Tan, Z. J.; Chen, S. J. Nucleic Acid Helix Stability: Effects of Salt Concentration, Cation Valence and Size, and Chain Length. *Biophys. J.* **2006**, *90* (4), 1175–1190. https://doi.org/10.1529/biophysj.105.070904.

(25) Dupuis, N. F.; Holmstrom, E. D.; Nesbitt, D. J. Single-Molecule Kinetics Reveal Cation-Promoted DNA Duplex Formation through Ordering of Single-Stranded Helices. *Biophys. J.* **2013**, *105* (3), 756–766. https://doi.org/10.1016/j.bpj.2013.05.061.

(26) Peterson, E. M.; Harris, J. M. Identification of Individual Immobilized DNA Molecules by Their Hybridization Kinetics Using Single-Molecule Fluorescence Imaging. *Anal. Chem.* **2018**, *90* (8), 5007–5014. https://doi.org/10.1021/acs.analchem.7b04512.

(27) Knutson, S. D.; Sanford, A. A.; Swenson, C. S.; Korn, M. M.; Manuel, B. A.; Heemstra, J. M. Thermoreversible Control of Nucleic Acid Structure and Function with Glyoxal Caging. *J. Am. Chem. Soc.* **2020**, *142* (41), 17766–17781. https://doi.org/10.1021/jacs.0c08996.

(28) Giesen, U.; Kleider, W.; Berding, C.; Geiger, A.; Ørum, H.; Nielsen, P. E. A Formula for Thermal Stability (T(m)) Prediction of PNA/DNA Duplexes. *Nucleic Acids Res.* **1998**. https://doi.org/10.1093/nar/26.21.5004.

(29) Arakawa, T.; Timasheff, S. N. Mechanism of Protein Salting In and Salting Out by Divalent Cation Salts: Balance between Hydration and Salt Binding. *Biochemistry* **1984**, *23* (25), 5912–5923. https://doi.org/10.1021/bi00320a004.

(30) Leipply, D.; Lambert, D.; Draper, D. E. Ion-RNA Interactions Thermodynamic Analysis of the Effects of Mono- and Divalent Ions on RNA Conformational Equilibria. *Methods Enzymol.* **2009**, *469*, 433–463. https://doi.org/10.1016/S0076-6879(09)69021-2.

(31) Höbartner, C.; Mittendorfer, H.; Breuker, K.; Micura, R. Triggering of RNA Secondary Structures by a Functionalized Nucleobase. *Angew. Chemie Int. Ed.* **2004**, *43* (30), 3922–

3925. https://doi.org/10.1002/anie.200460068.

(32) Ikeda, M.; Kamimura, M.; Hayakawa, Y.; Shibata, A.; Kitade, Y. Reduction-Responsive Guanine Incorporated into G-Quadruplex-Forming DNA. *ChemBioChem* **2016**, *17* (14), 1304–1307. https://doi.org/10.1002/cbic.201600164.

(33) Govan, J. M.; Young, D. D.; Lusic, H.; Liu, Q.; Lively, M. O.; Deiters, A. Optochemical Control of RNA Interference in Mammalian Cells. *Nucleic Acids Res.* **2013**, *41* (22), 10518–10528. https://doi.org/10.1093/nar/gkt806.

(34) Lucas, T.; Schäfer, F.; Müller, P.; Eming, S. A.; Heckel, A.; Dimmeler, S. Light-Inducible AntimiR-92a as a Therapeutic Strategy to Promote Skin Repair in Healing-Impaired Diabetic Mice. *Nat. Commun.* **2017**, *8*, 15162. https://doi.org/10.1038/ncomms15162.

(35) Lu, J.; Koo, S. C.; Li, N. S.; Piccirilli, J. A. Synthesis of 2′-O-Photocaged Ribonucleoside Phosphoramidites. *Nucleosides, Nucleotides and Nucleic Acids* **2015**, *34* (2), 114–129. https://doi.org/10.1080/15257770.2014.965256.

(36) Matsushita-Ishiodori, Y.; Ohtsuki, T. Photoinduced RNA Interference. *Acc. Chem. Res.* **2012**, *45* (7), 1039–1047. https://doi.org/10.1021/ar200227n.

(37) McMaster, G. K.; Carmichael, G. G. Analysis of Single- and Double-Stranded Nucleic Acids on Polyacrylamide and Agarose Gels by Using Glyoxal and Acridine Orange. *Proc. Natl. Acad. Sci. U. S. A.* **1977**, *74* (11), 4835–4838. https://doi.org/10.1073/pnas.74.11.4835.

(38) Burnett, W. V. Northern Blotting of RNA Denatured in Glyoxal without Buffer Recirculation. *Biotechniques* **1997**, *22* (4), 668–671. https://doi.org/10.2144/97224st01.

(39) Leberman, R. The Hofmeister Series and Ionic Strength. *FEBS Lett.* **1991**, *284* (2), 293–294. https://doi.org/10.1016/0014-5793(91)80707-A.

(40) Duong-Ly, K. C.; Gabelli, S. B. Salting out of Proteins Using Ammonium Sulfate Precipitation. In *Methods in Enzymology*. **2014**, *541*, 85-94. https://doi.org/10.1016/B978-0-12-420119-4.00007-0.

(41) Peterson, E. M.; Manhart, M. W.; Harris, J. M. Single-Molecule Fluorescence Imaging of

Interfacial DNA Hybridization Kinetics at Selective Capture Surfaces. *Anal. Chem.* **2016**, *88* (2), 1345–1354. https://doi.org/10.1021/acs.analchem.5b03832.

(42) Kern, W.; Poutinen, D. A. Cleaning Solution Based on Hydrogen Peroxide for Use in Silicon Semiconductor Technology. *RCA Rev.* **1970**, *31* (2), 187.

(43) Peterson, E. M.; Reece, E. J.; Li, W.; Harris, J. M. Super-Resolution Imaging of Competitive Unlabele DNA Hybriization Reveals the Influence of Fluorescent Labels on Duplex Formation an Dissociation Kinetics. *J. Phys. Chem. B* **2019**, *123* (50), 10746–10756. https://doi.org/10.1021/acs.jpcb.9b09736.

(44) Robbins, M. S.; Hadwen, B. J. The Noise Performance of Electron Multiplying Charge-Coupled Devices. *IEEE Trans. Electron Devices* **2003**, *50* (5), 1227–1232. https://doi.org/10.1109/TED.2003.813462.

Chapter 5

Conclusions and Future Perspectives

Nearly three decades have passed since Nielsen and coworkers first invented PNA and described it as the "molecule with two identities".[1,2] Since then, researchers have leveraged organic, biological, and analytical chemistry to develop and implement technologies using the unique properties of PNA. For example, PNA has been used in nucleic acid therapeutics and diagnostics for antisense interactions, gene editing platforms, drug delivery vehicles, detection devices, and imaging probes.[3–9] While these techniques have garnered widespread use and attention, the focus has primarily been on the base pairing capability of the nucleobases. Looking beyond the Franklin-Watson-Crick hybridization properties of PNA, we wanted to highlight the ability to incorporate amino acid-like functionality and underscore the alternative "peptide" identity described by Nielsen et. al. to open the door for PNA to be used both a nucleic acid and peptide analogue.

In Chapter 1, we described the many ways in which researchers have incorporated amino acid functional groups into PNA in order to improve properties such as solubility, cell permeability, and hybridization affinity.[10–13] These ways include appending single or chains of amino acids to the terminal ends of PNA, or direct inclusion of side chains within the PNA backbone.[14] The ability to integrate functional groups at defined positions along the backbone provides an underexplored avenue for encoding information through the peptide nature of PNA. The Heemstra Lab is particularly interested in leveraging this information towards the design of new PNA materials and probes for diverse applications in chemical biology.

5.1 Expanding the Repertoire of Bilingual PNA

Our lab has demonstrated an example of a PNA capable of simultaneously encoding information from amino acid and nucleic acid sources, wherein an embedded amino acid

sequence drives intermolecular assembly while disassembly can be attained through sequence-specific complementary hybridization (**Chapter 2**). This initial exploration provides the framework for future studies involving more complex sequences and side chains. Specifically, we envision establishing design rules that allow for predictable structural or functional outcomes dependent on the PNA sequence, length, and identity of the embedded amino acid modifications. For example, does increasing the hydrophobicity of the side chains alter the size, critical assembly concentrations, or morphology of amphiphilic assemblies? Are total charge and amino acid/nucleic acid identity important for assembly, stability, and subsequent activity? Can we access peptide-like structural motifs such as coils and sheets through incorporation of different amino acid sequences? In order to begin answering some of these questions, we have expanded our synthesis of γ-modified PNA monomers to include leucine and glutamic acid side chains and are currently undergoing structural analyses with representative amphiphiles. With the multitude of natural and unnatural amino acid side chains available for precise placement along the PNA scaffold, the capabilities of this dual information coding biopolymer are limited only by our imagination.

5.2 Applications of Bilingual PNA Amphiphiles

Along with determining the effect of amino acid identity and sequence on assembly properties, we envision these amphiphiles to be useful in a range of applications. Initially we are exploring these materials as smart drug delivery platforms, wherein the PNA targets an oncomiRNA (miRNA-21), thus acting as both delivery vehicle and therapeutic in one package. On top of antisense delivery, the encapsulation of small molecules into PNA assemblies for stimuli-responsive administration of drugs is also being explored. Expanding beyond drug delivery therapeutics, we anticipate uses as small molecule detection and activation platforms. A unique property of our PNA amphiphiles over alternative scaffolds is the information-rich hydrophobic

portion as the nucleic acid sequence can be leveraged for control over assembly. We envision the design of assays wherein the hydrophobic portion is duplexed with a complementary nucleic acid such as an aptamer. Displacement of the strand by a small molecule or nucleic acid target "deprotects" the hydrophobic portion, resulting in spontaneous self-assembly of PNA amphiphiles. Outfitting the PNA with reactive moieties could take advantage of the increase in effective concentration to result in small molecule activation of either a fluorescent dye or pro-drug. This would provide a useful and generic method for diagnostics and utilize the unique information storage properties of the PNA scaffold. Finally, we anticipate through the simultaneous encoding and interpretation of amino acid and nucleic acid information, we can extend beyond stimuli-responsive assemblies and create precise adaptors capable of interacting with specific protein and nucleic acid targets. Such a design could provide a user-defined mediator for the precise interactions between proteins and nucleic acids in a range of chemical biology applications.

5.3 Utilization of FIT-PNA Probes for A → I Detection

The deamination of adenosine to inosine is an important modification that occurs in DNA and RNA that regulates many biological processes. Current methods for sequence-specific detection such as PCR and sequencing are often costly and time-consuming. We recognized an unmet need for the simple and low background imaging of inosine-containing nucleic acids in a sequence-defined manner, which we sought to accomplish using PNA. In Chapter 3, we described the synthesis and incorporation of 4-dimethylamino-naphthalimide (4DMN), malachite green (MG), and thiazole orange (TO) forced-intercalation PNA (FIT-PNA) probes for the detection of an adenosine to inosine (A → I) modification in DNA and RNA. While we were able to achieve an appreciable 11-fold specificity for I over A with TO in DNA, the enhancement for RNA targets was not significant enough for our purposes. We determined that the FIT-PNA was incapable of binding to the targeted RNA hairpin due to the innate affinity of the hairpin interaction. For future designs, we are looking to target the RNA duplex over the single strand using previously

described triplex forming PNA nucleobases.[15] Incorporating fluorogenic dyes with triplex forming nucleobases in the PNA scaffold for forced intercalation fluorescence would allow the simple, robust, and sequence-specific detection and imaging of inosine-containing transcripts in native environments, providing a yet unmet need for this particular epitranscriptomic modification. Beyond imaging and detection, we also envision FIT-PNA probes to be capable of measuring the activity of adenosine deaminases acting on RNA (ADAR) enzymes to further elucidate the impact and mechanistic roles of sequence selection, as well as provide simple fluorescent assays for screening therapeutic candidates against ADAR activity.

5.4 Single-Molecule Exploration of PNA:DNA Hybridization

The Franklin-Watson-Crick base pairing properties of PNA benefit from stronger affinity and specificity for DNA and RNA compared to native nucleic acids, particularly at lower ionic strengths. This has made PNA a desirable candidate for improving hybridization-based applications. An understanding of the relationship between environment (i.e. ionic strength) and hybridization is important for the proper design and optimization of activity for PNA probes. We employed a single molecule imaging technique to explore the effect of ionic strength on the kinetics of PNA:DNA duplex formation (**Chapter 4**). Our findings indicate that the association rate is much faster at lower ionic strengths while the dissociation rate is mainly unaffected. We also determined that the higher affinity of PNA:DNA duplexes as compared to DNA:DNA is due to a significantly slower dissociation rate. We anticipate this information to be useful in the future design of PNA probes for applications including antisense regulation and gene editing, where therapeutic activity is related to the kinetics of hybridization. We also believe these experiments provide a protocol for future exploration of PNA:DNA hybridization. For example, we can use this method to probe more complex environments and the effect of different ions such as the Hofmeister series.[16] Additionally, we can evaluate the kinetics of hybridization using backbone modified PNA described in Chapter 1. Through a systematic exploration, we can help determine

what the identity, position, and number of side chain modifications provide towards the hybridization properties, as well as elucidate the mechanism behind the unique duplex invasion properties of γ-modified and tail-clamp PNAs.[17] The wealth of information on PNA activity that can be obtained through single-molecule experiments would greatly benefit the field and provide basic information to assist the improvement of PNA hybridization-based applications.

5.5 References:

(1) Nielsen, P. E.; Egholm, M.; Berg, R. H.; Buchardt, O. Sequence-Selective Recognition of DNA by Strand Displacement with a Thymine-Substituted Polyamide. *Science (80-.).* **1991**, *254* (5037), 1497–1500. https://doi.org/10.1126/science.1962210.

(2) Nielsen, P. E. Peptide Nucleic Acid. A Molecule with Two Identities. *Acc. Chem. Res.* **1999**, *32* (7), 624–630. https://doi.org/10.1021/ar980010t.

(3) Pellestor, F.; Paulasova, P. The Peptide Nucleic Acids (PNAs), Powerful Tools for Molecular Genetics and Cytogenetics. *Eur. J. Hum. Genet.* **2004**, *12* (9), 694–700. https://doi.org/10.1038/sj.ejhg.5201226.

(4) D'Agata, R.; Giuffrida, M. C.; Spoto, G. Peptide Nucleic Acid-Based Biosensors for Cancer Diagnosis. *Molecules* **2017**, *22* (11), 1951. https://doi.org/10.3390/molecules22111951.

(5) Gambari, R. Peptide Nucleic Acids: A Review on Recent Patents and Technology Transfer. *Expert Opin. Ther. Pat.* **2014**, *24* (3), 267–294. https://doi.org/10.1517/13543776.2014.863874.

(6) Gupta, A.; Mishra, A.; Puri, N. Peptide Nucleic Acids: Advanced Tools for Biomedical Applications. *J. Biotechnol.* **2017**, *259*, 148–159. https://doi.org/10.1016/j.jbiotec.2017.07.026.

(7) Wu, J.-C.; Meng, Q.-C.; Ren, H.-M.; Wang, H.-T.; Wu, J.; Wang, Q. Recent Advances in Peptide Nucleic Acid for Cancer Bionanotechnology. *Acta Pharmacol. Sin.* **2017**, *38*, 798–805. https://doi.org/10.1038/aps.2017.33.

(8) Narenji, H.; Gholizadeh, P.; Aghazadeh, M.; Rezaee, M. A.; Asgharzadeh, M.; Kafil, H. S. Peptide Nucleic Acids (PNAs): Currently Potential Bactericidal Agents. *Biomed. Pharmacother.* **2017**, *93*, 580–588. https://doi.org/10.1016/j.biopha.2017.06.092.

(9) Saarbach, J.; Sabale, P. M.; Winssinger, N. Peptide Nucleic Acid (PNA) and Its Applications in Chemical Biology, Diagnostics, and Therapeutics. *Curr. Opin. Chem. Biol.* **2019**, *52*, 112–124. https://doi.org/10.1016/j.cbpa.2019.06.006.

(10) Swenson, C. S.; Heemstra, J. M. Peptide Nucleic Acids Harness Dual Information Codes in a Single Molecule. *Chem. Commun.* **2020**, *56* (13), 1926–1935. https://doi.org/10.1039/c9cc09905k.

(11) Braasch, D. A.; Corey, D. R. Synthesis, Analysis, Purification, and Intracellular Delivery of Peptide Nucleic Acids. *Methods* **2001**, *23* (2), 97–107. https://doi.org/10.1006/meth.2000.1111.

(12) Díaz-Mochón, J. J.; Bialy, L.; Watson, J.; Sánchez-Martín, R. M.; Bradley, M. Synthesis and Cellular Uptake of Cell Delivering PNA-Peptide Conjugates. *Chem. Commun.* **2005**, No. 26, 3316–3318. https://doi.org/10.1039/b503777h.

(13) Tedeschi, T.; Sforza, S.; Corradini, R.; Marchelli, R. Synthesis of New Chiral PNAs Bearing a Dipeptide-Mimic Monomer with Two Lysine-Derived Stereogenic Centres. *Tetrahedron Lett.* **2005**, *46* (48), 8395–8399. https://doi.org/10.1016/j.tetlet.2005.09.157.

(14) Moccia, M.; Adamo, M. F. A.; Saviano, M. Insights on Chiral, Backbone Modified Peptide Nucleic Acids: Properties and Biological Activity. *Artif. DNA PNA XNA* **2016**, *5* (3), e1107176. https://doi.org/10.1080/1949095X.2015.1107176.

(15) Zengeya, T.; Gupta, P.; Rozners, E. Triple-Helical Recognition of RNA Using 2-Aminopyridine-Modified PNA at Physiologically Relevant Conditions. *Angew. Chemie Int. Ed.* **2012**, *51* (50), 12593–12596. https://doi.org/10.1002/anie.201207925.

(16) Leberman, R. The Hofmeister Series and Ionic Strength. *FEBS Lett.* **1991**, *284* (2), 293–294. https://doi.org/10.1016/0014-5793(91)80707-A.

(17) Faruqi, A. F.; Egholm, M.; Glazer, P. M. Peptide Nucleic Acid-Targeted Mutagenesis of a Chromosomal Gene in Mouse Cells. *Proc. Natl. Acad. Sci. U. S. A.* **1998**, *95* (4), 1398–1403. https://doi.org/10.1073/pnas.95.4.1398.

Appendix A

Spectral and Omitted Data of Chapter 2

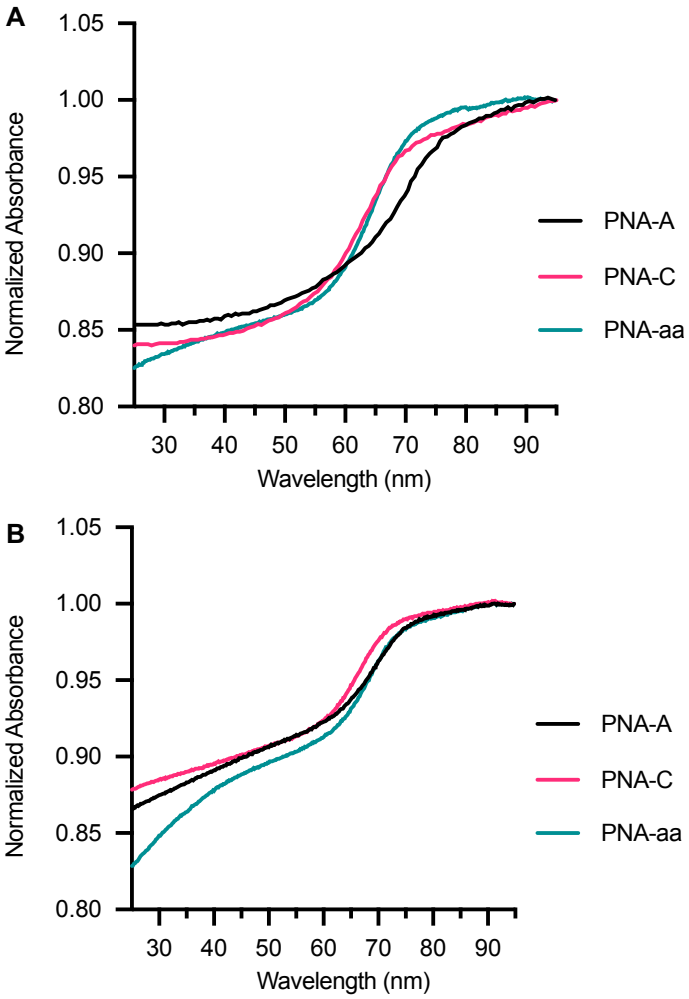

Figure A1: Melting curves of PNA with DNA and RNA targets. A) UV melting curves of PNA-A and PNA-C with complementary DNA. Concentration of PNA and DNA is 5 μM in 1xPBS. T_m of PNA-A = 69.5 ± 0.1 °C. T_m of PNA-C = 63.03 ± 0.1 °C. T_m of PNA-aa = 64.5 ± 0.1 °C. B) UV melting curves of PNA-A, PNA-C and PNA-aa with target miRNA-21. Concentration of PNA and RNA is 5 μM in 1xPBS. T_m of PNA-A = 68.6 ± 0.3 °C. T_m of PNA-C = 65.8 ± 0.2 °C. T_m of PNA-aa = 67.5 ± 0.2 °C.

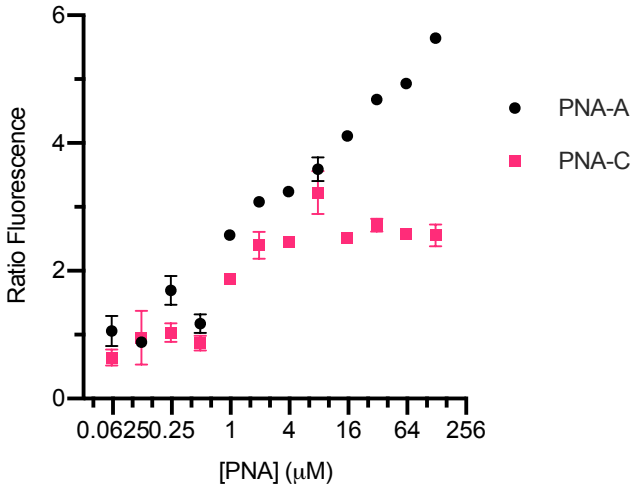

Figure A2: Plot of the fluorescence ratio of PNA-A and PNA-C to the 4-DMN monomer as a function of concentration. Error bars represent SEM (n=3).

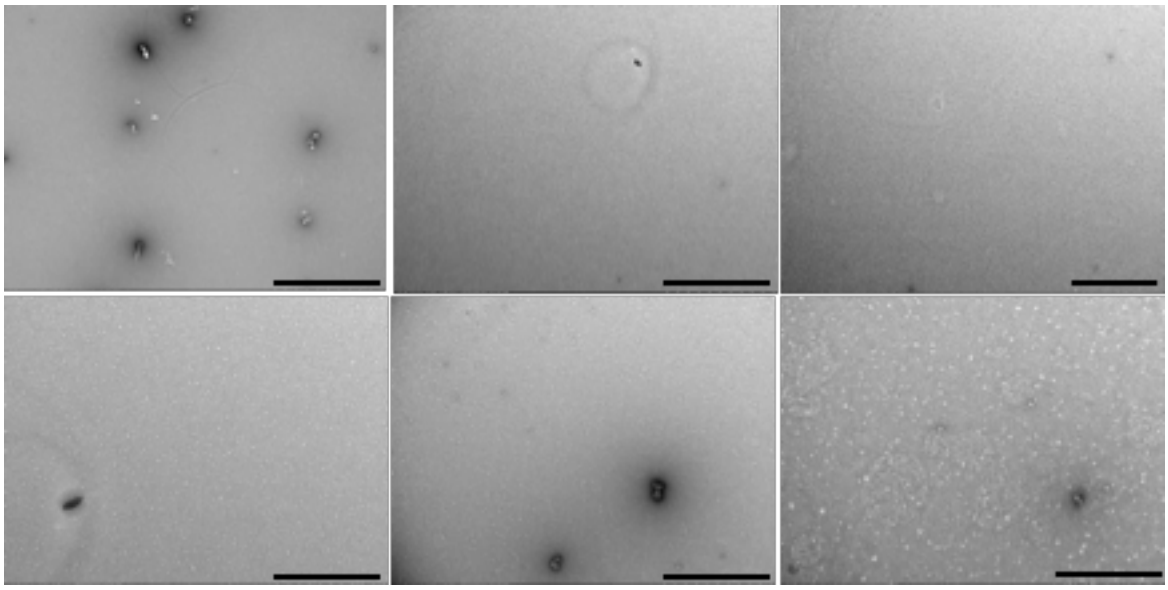

Figure A3: TEM images of control PNA-C showing few amorphous assemblies. Scale bars = 5 μm (top left); 2 μm (top middle); 2 μm (top right); 1 μm (bottom left); 1 μm (bottom middle); 500 nm (bottom right). [PNA-C] in top left image is 1mM. All other images were taken at 100 μM.

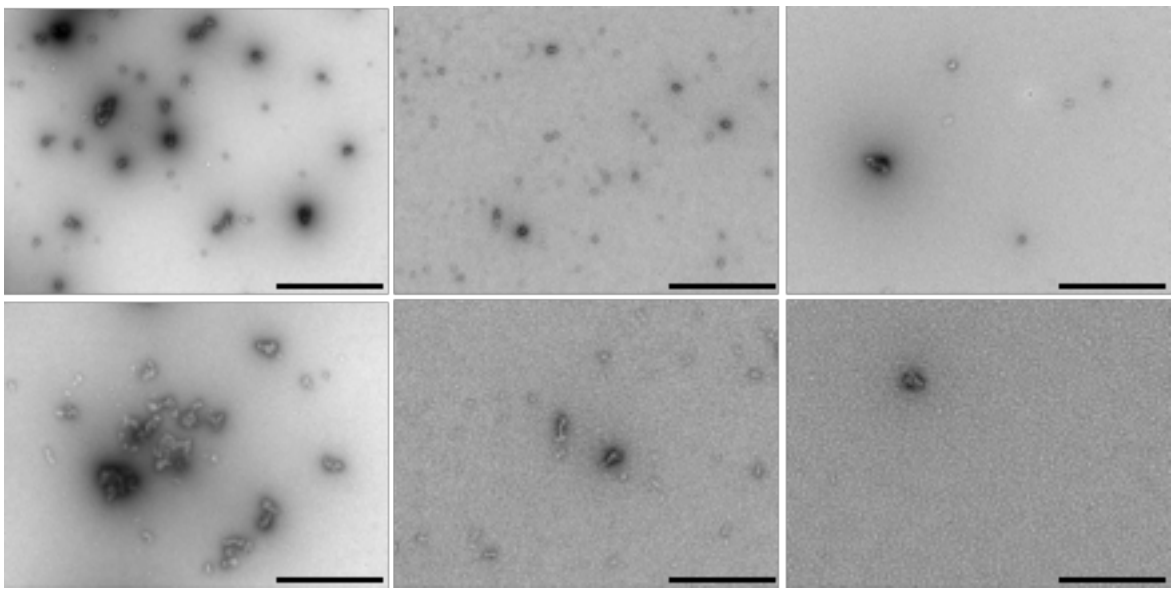

Figure A4: TEM images of amino acid amphiphile PNA-aa showing amorphous assemblies of varying sizes. [PNA-aa] = 1 mM. Scale bars = 2 μm (top left); 1000 nm (top middle, top right, bottom left); 500 nm (bottom middle, bottom right).

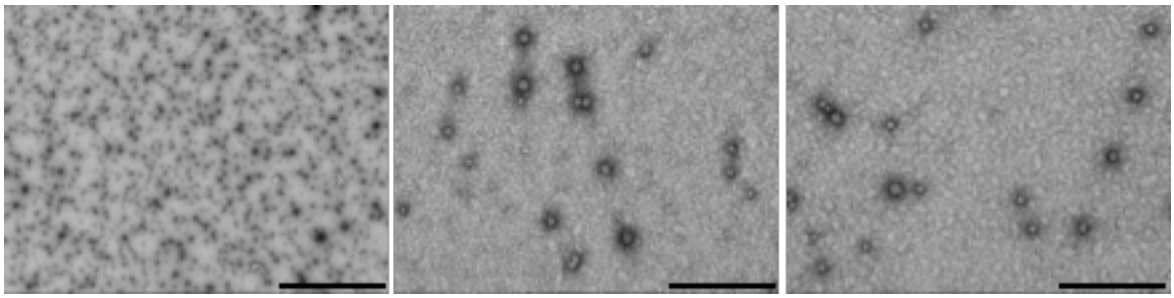

Figure A5: Additional TEM images of amphiphile PNA-A at 1 mM. Scale bars = 2 μm (left); 500 nm (middle); 500 nm (right).

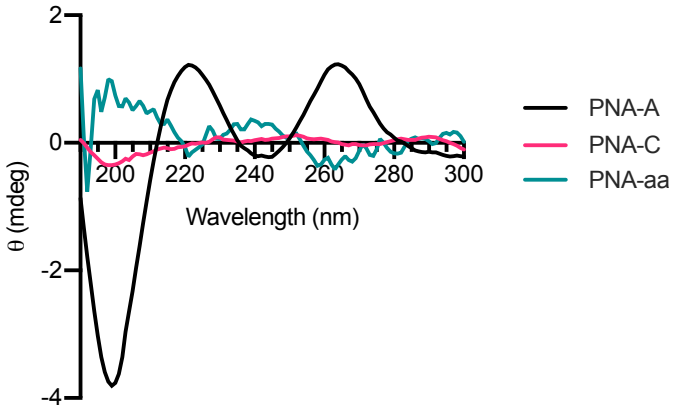

Figure A6: Circular dichroism traces of amphiphile PNA-A, control PNA-C, and amino acid-containing amphiphile PNA-aa. Samples are all 100 μM in 1xPBS.

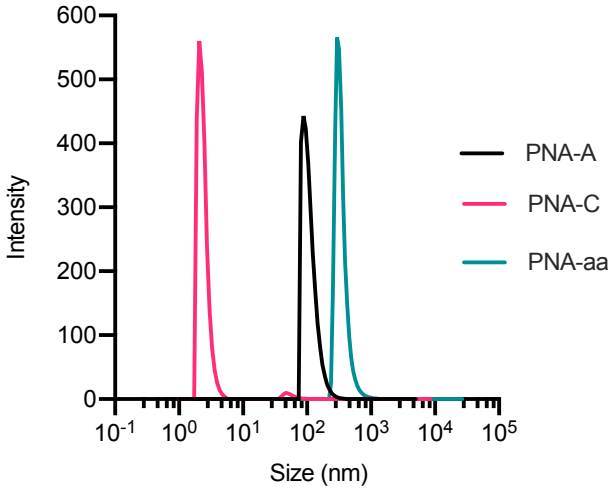

Figure A7: DLS normalized number distribution of assemblies of PNA-A, PNA-C and PNA-aa. Samples are all 500 μM in water. Average diameter of particles of PNA-A = 110.2 ± 31.9 nm, PNA-C = 2.4 ± 0.5 nm and 54.9 ± 15.4 nm, and PNA-aa = 344.7 ± 92.3 nm.

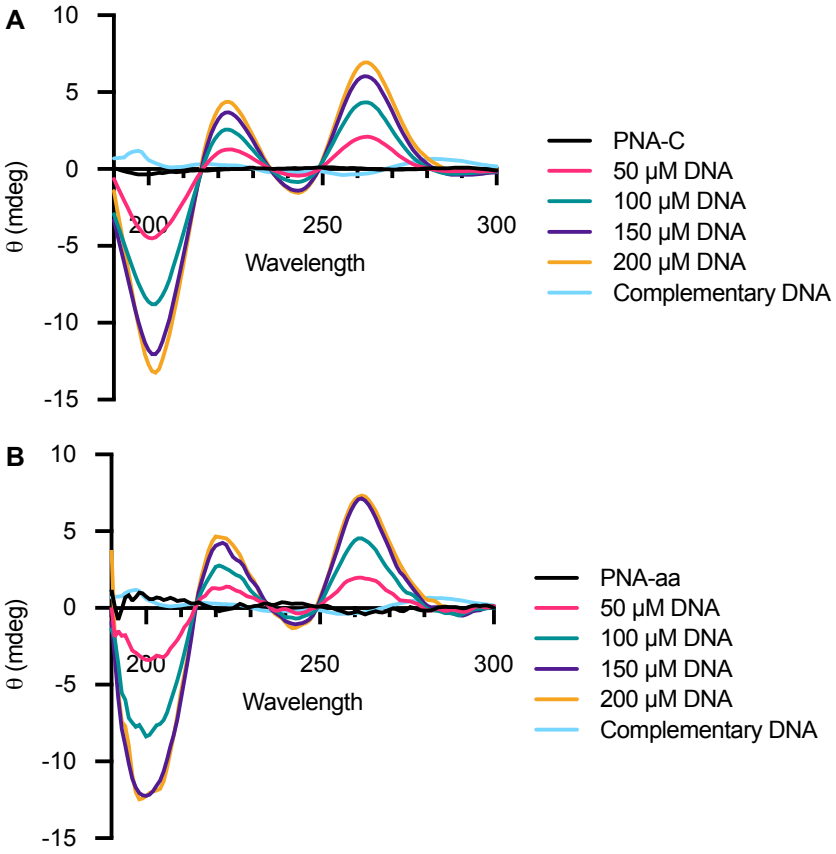

Figure A8: Circular dichroism traces showing the ability of control PNA-C and amino acid containing amphiphile PNA-aa to bind complementary DNA. (A) PNA-C binding to various concentrations of complementary DNA at 100 μM in 1xPBS. (B) PNA-aa binding to various concentrations of complementary DNA at 100 μM in 1xPBS.

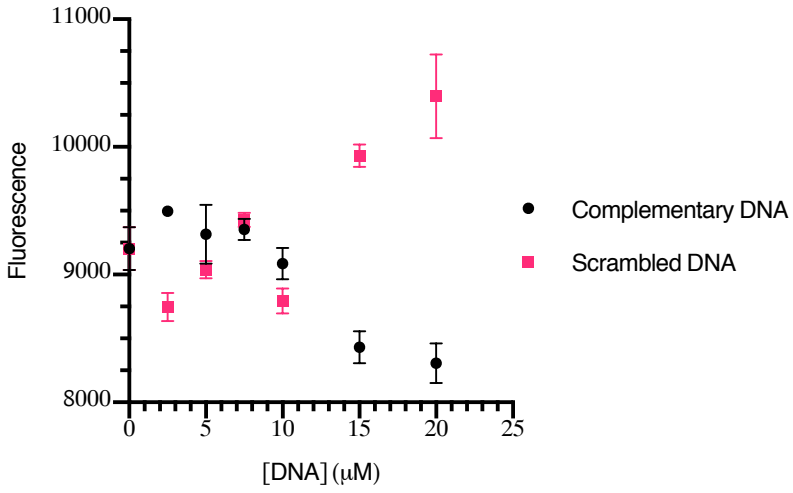

Figure A9: Fluorescence response of PNA-A upon addition of complementary and scrambled DNA. [PNA-A] = 10 μM in 1xPBS. Error bars represent SEM (n=3).

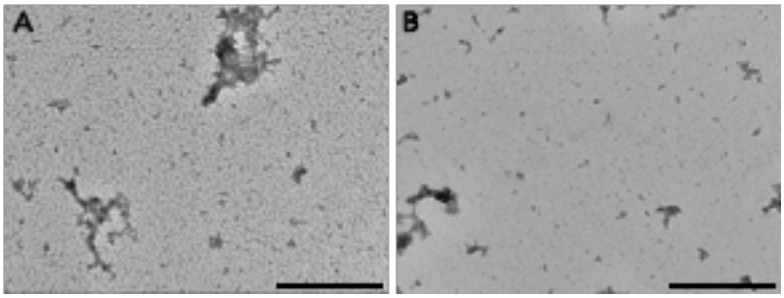

Figure A10: Additional images of PNA-A with (A) complementary DNA or (B) miRNA-21 at 100 μM in 1xPBS displaying the disappearance of small spherical assemblies. Scale bars = 500 nm.

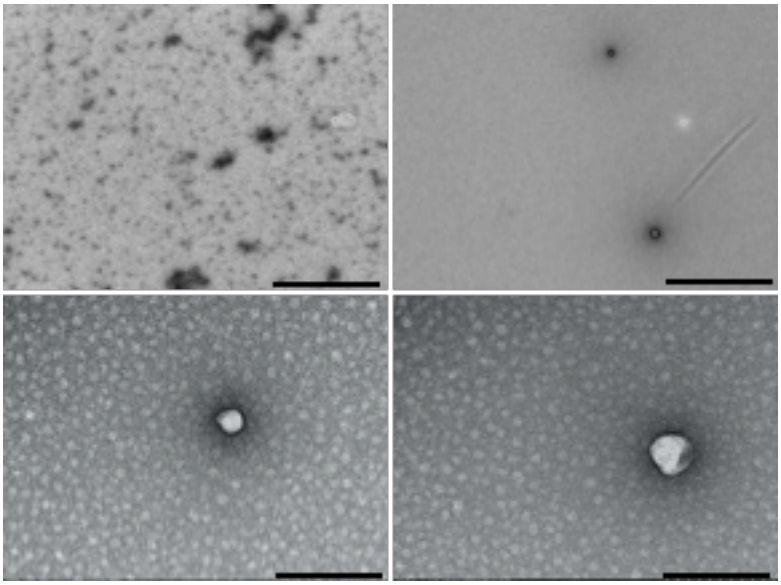

Figure A11: Additional images of PNA-A with scrambled DNA at 100 μM in 1xPBS displaying the retention of small spherical assemblies. Scale bars = 500 nm (top left), 2000 nm (top right), and 200 nm (bottom images).

Structure, HPLC, and ESI-TOF of PNA-A:

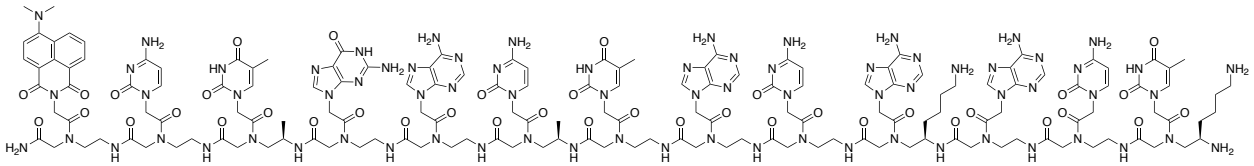

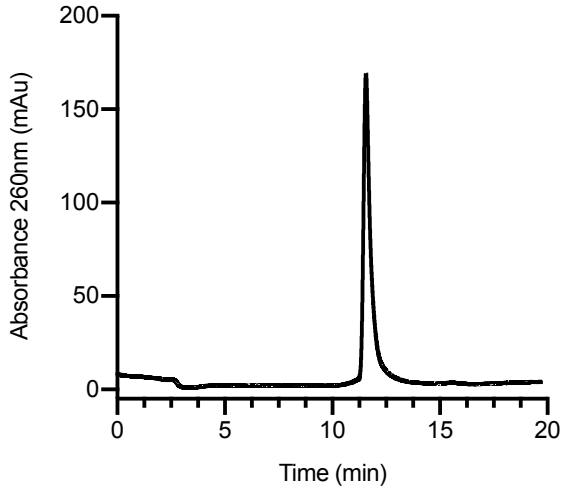

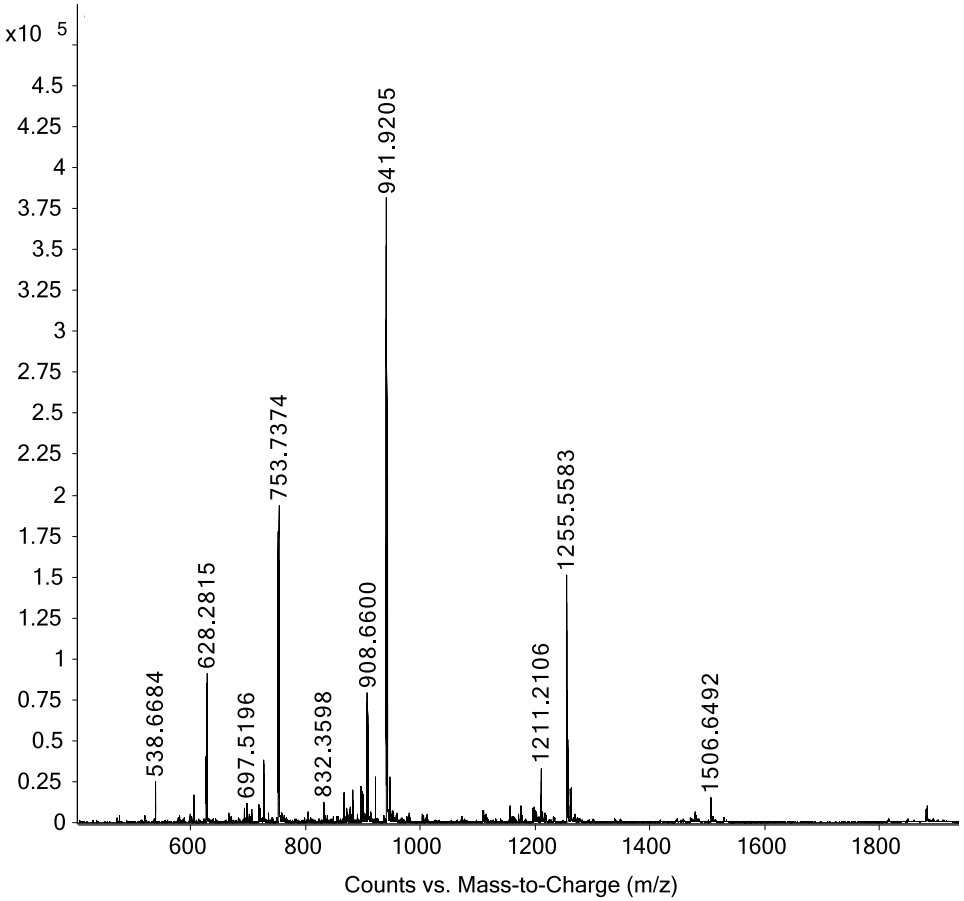

Structure, HPLC, and ESI-TOF of PNA-C:

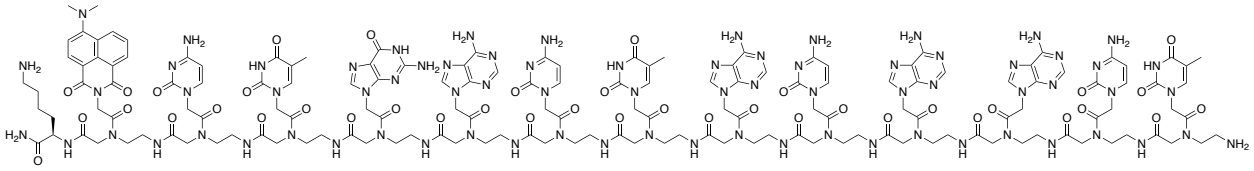

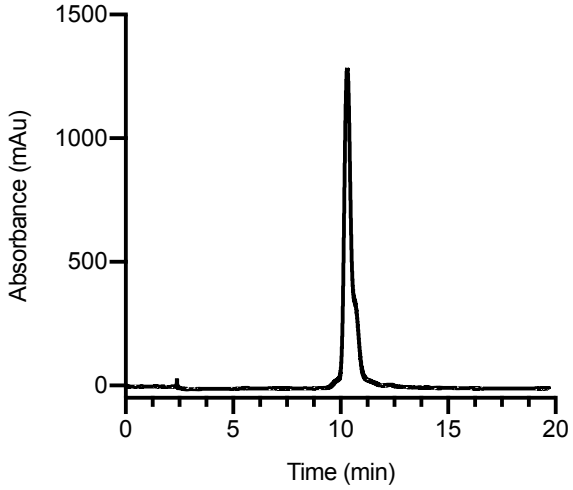

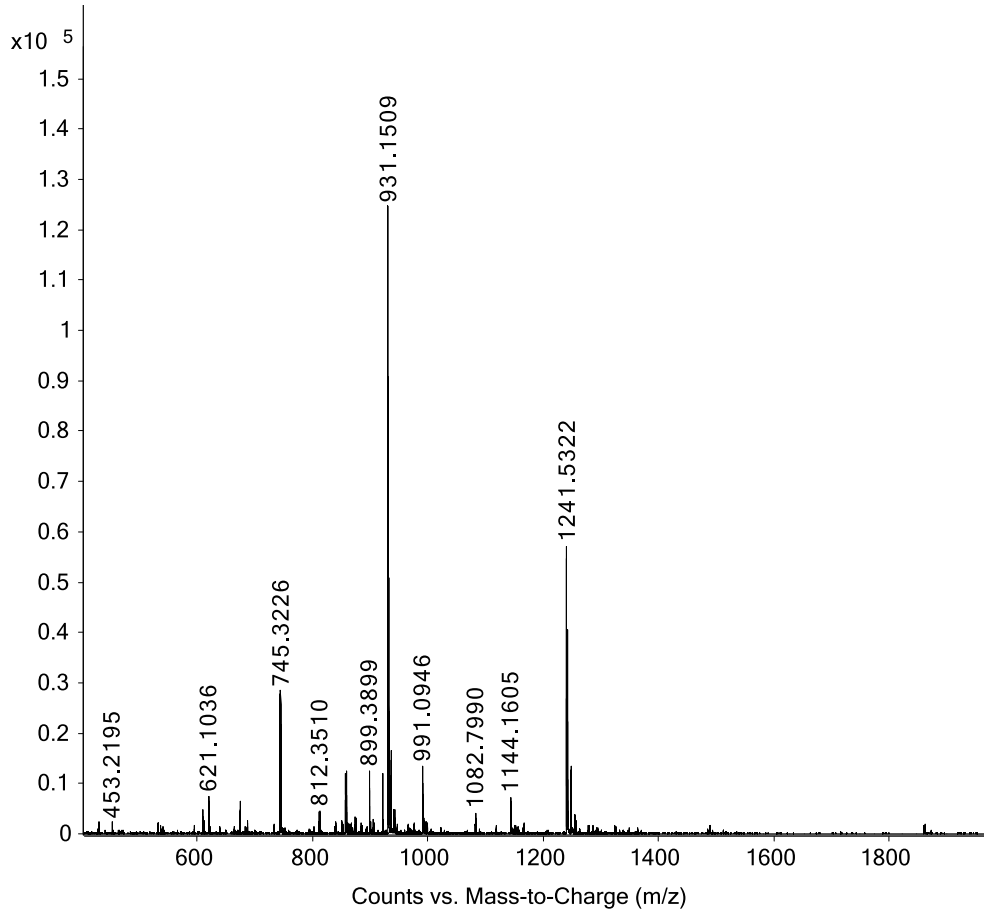

Structure, HPLC, and ESI-TOF of PNA-aa:

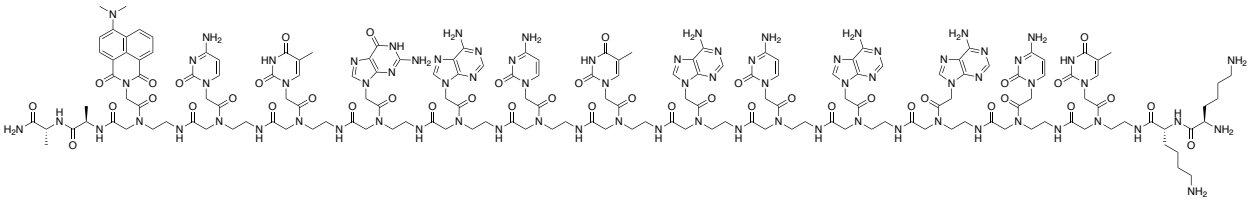

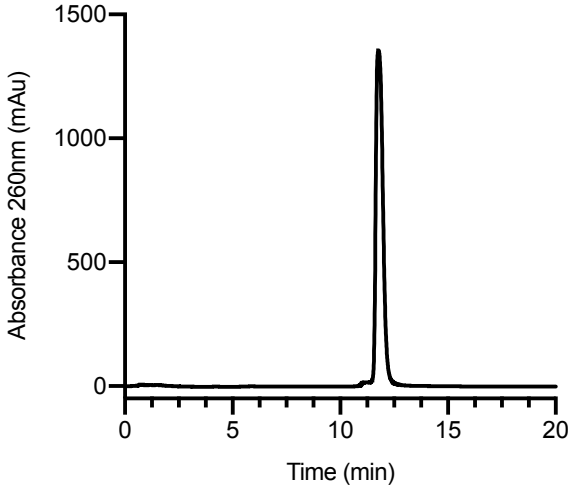

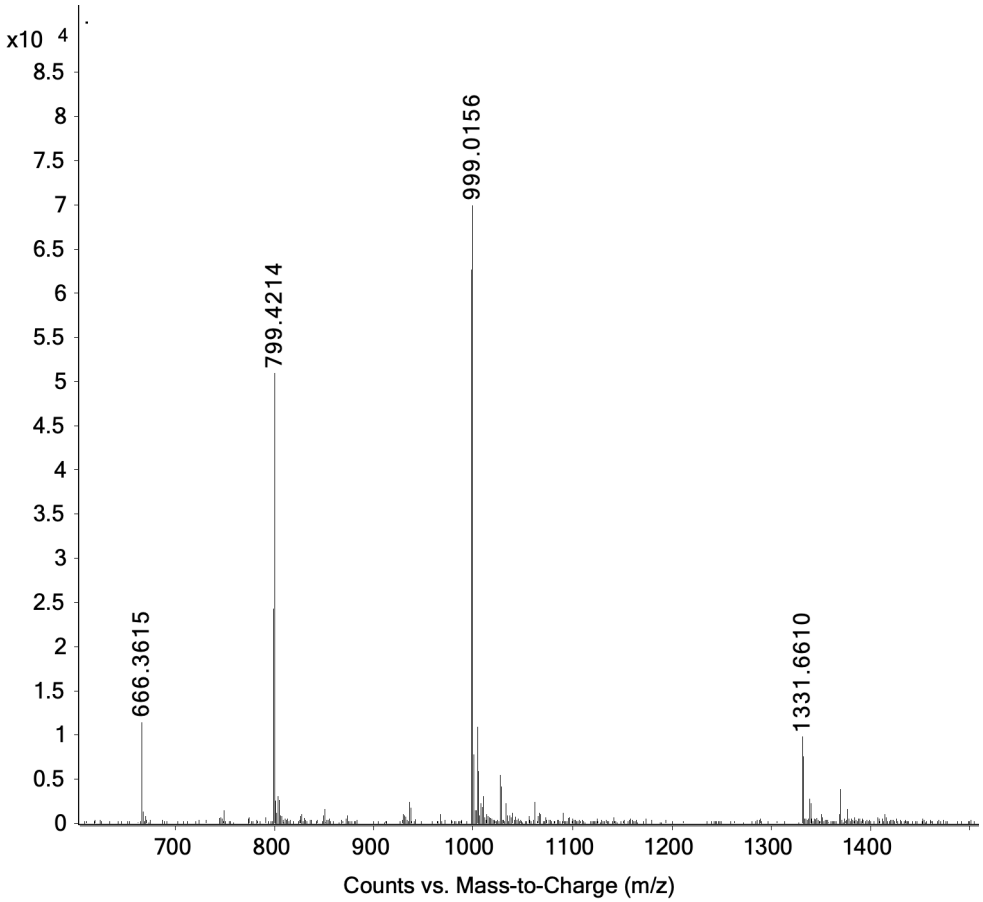

^{1}H- and ^{13}C-NMR of 1:

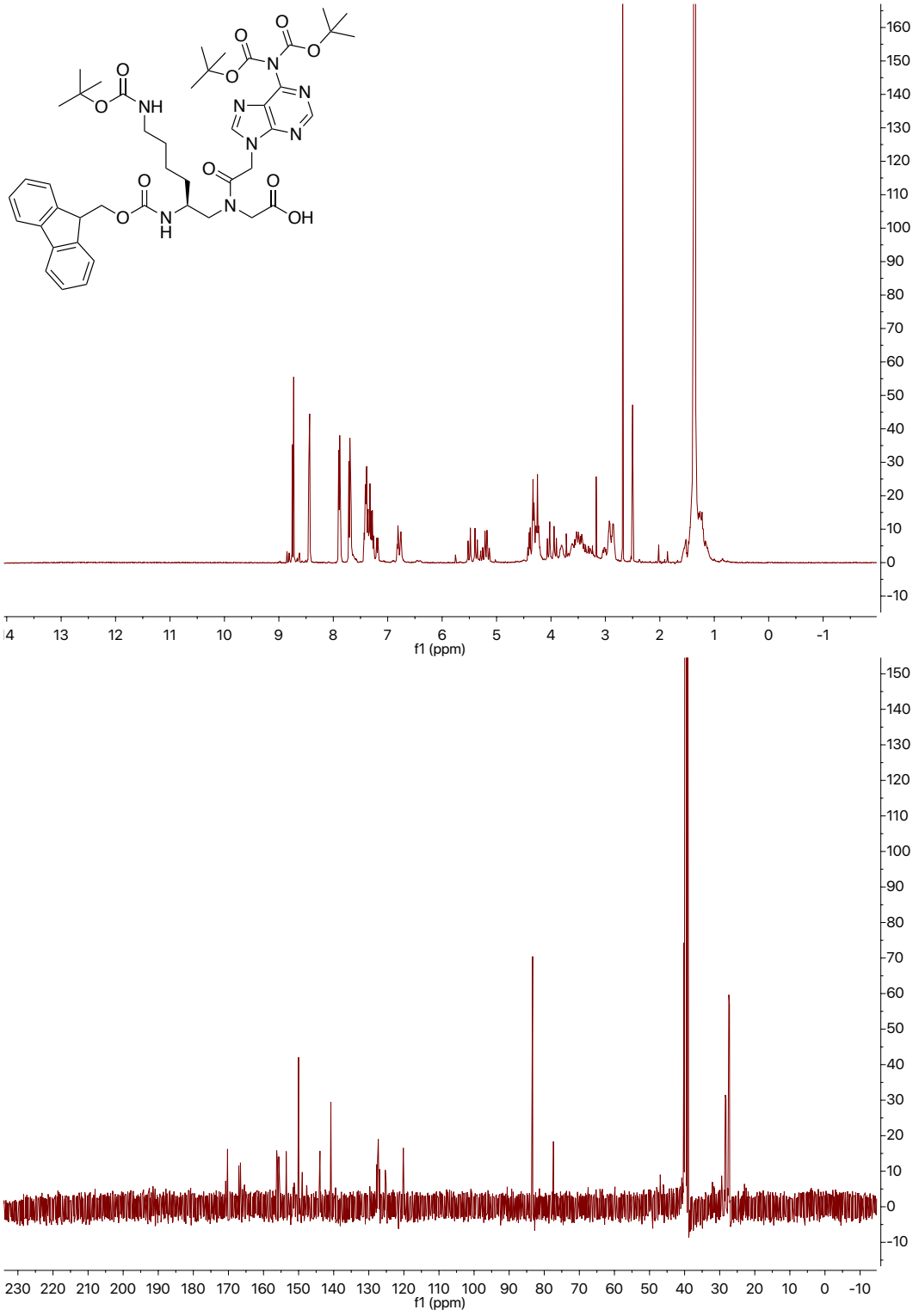

^{1}H- and ^{13}C-NMR of 2:

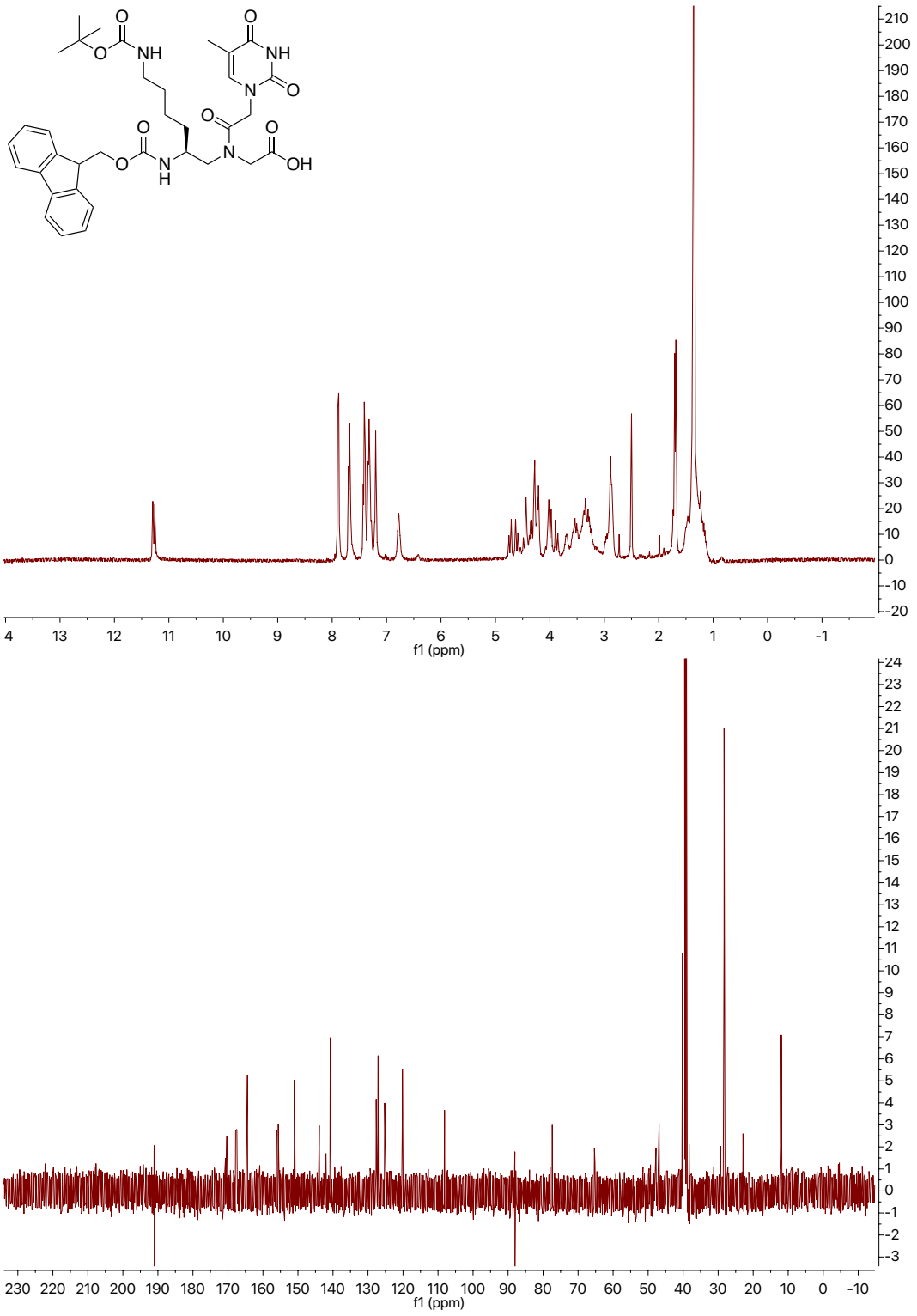

^{1}H- and ^{13}C-NMR of 3:

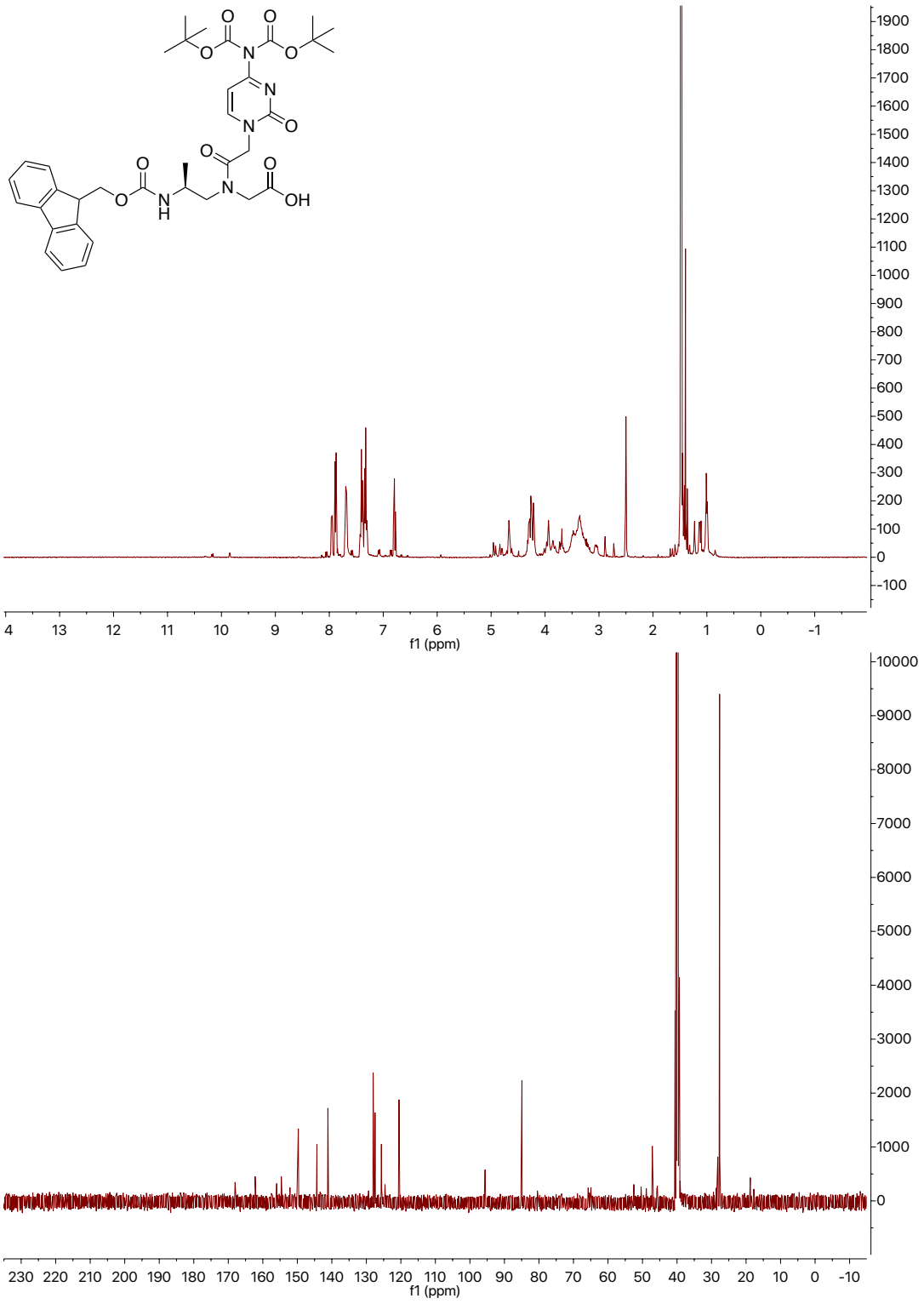

^{1}H- and ^{13}C-NMR of 4:

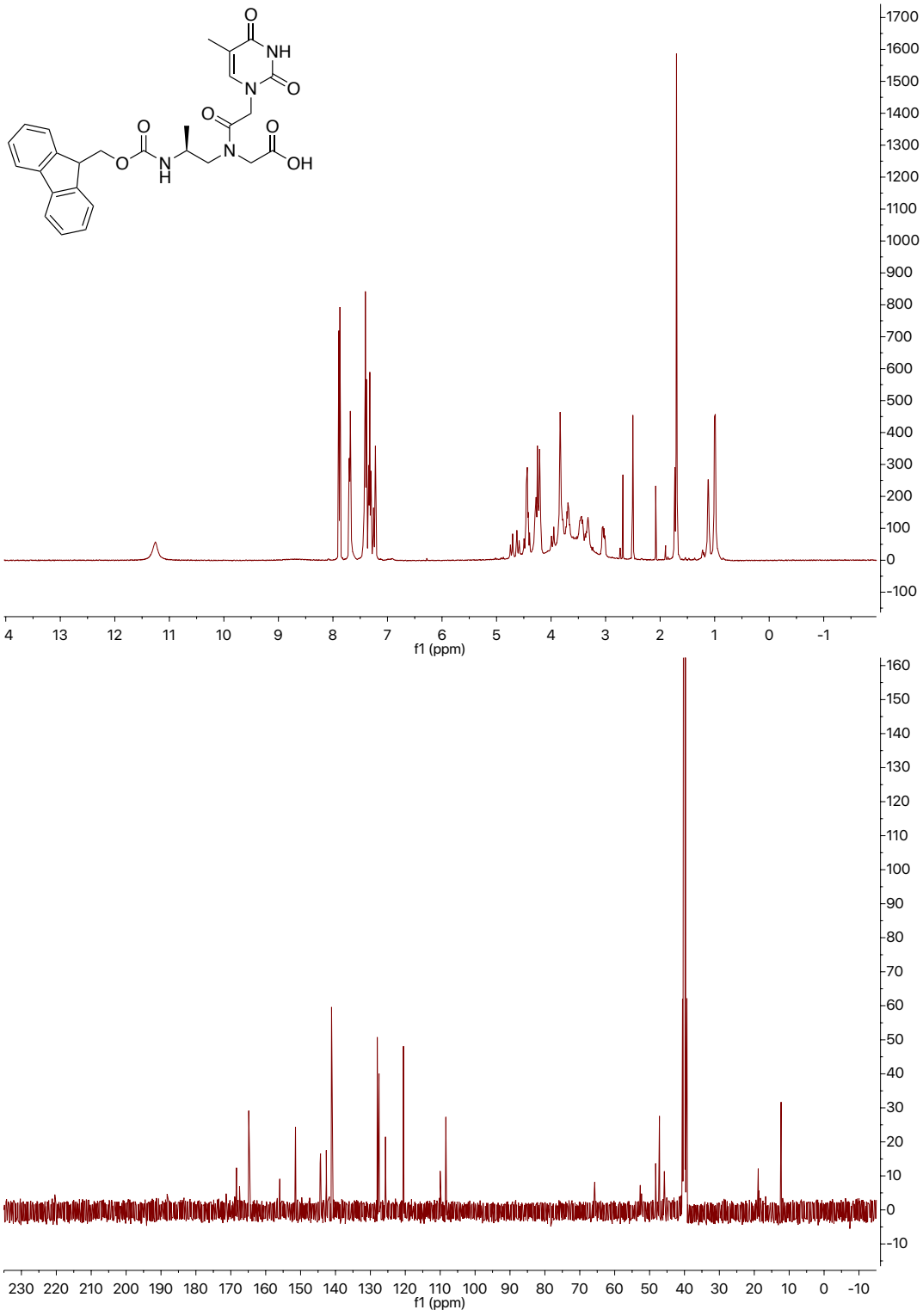

^{1}H- and ^{13}C-NMR of 5:

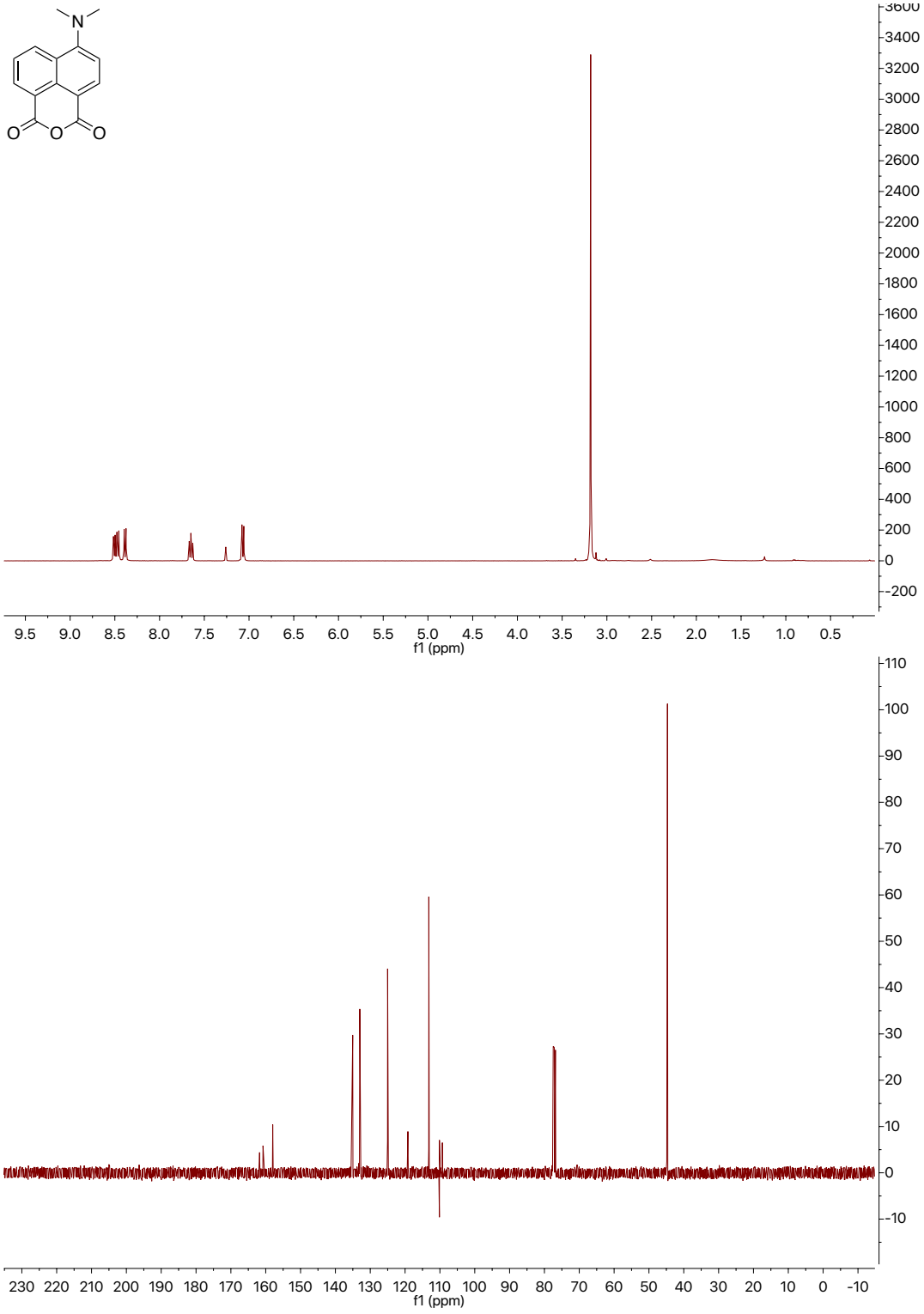

^{1}H- and ^{13}C-NMR of 6:

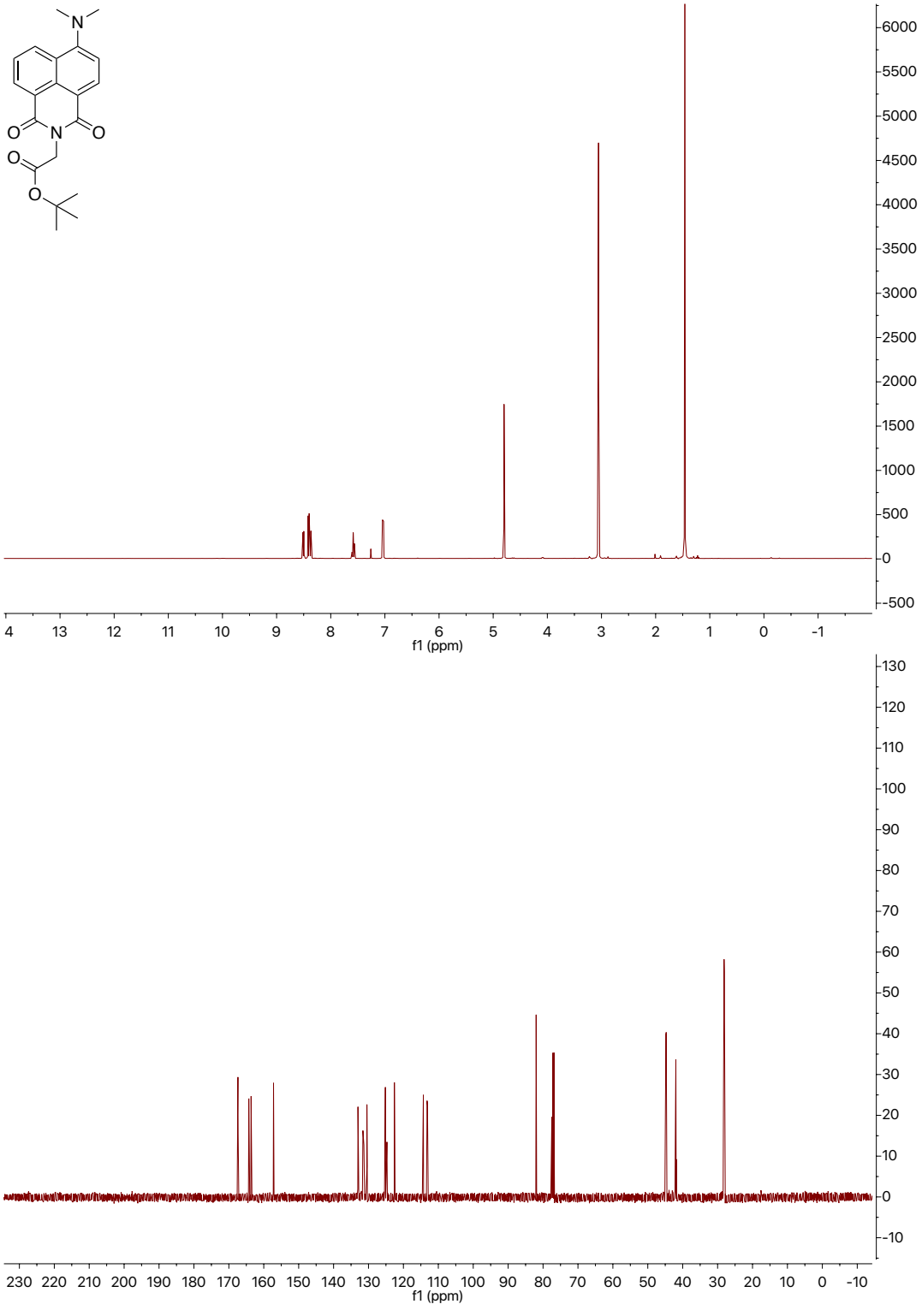

^{1}H- and ^{13}C-NMR of 7:

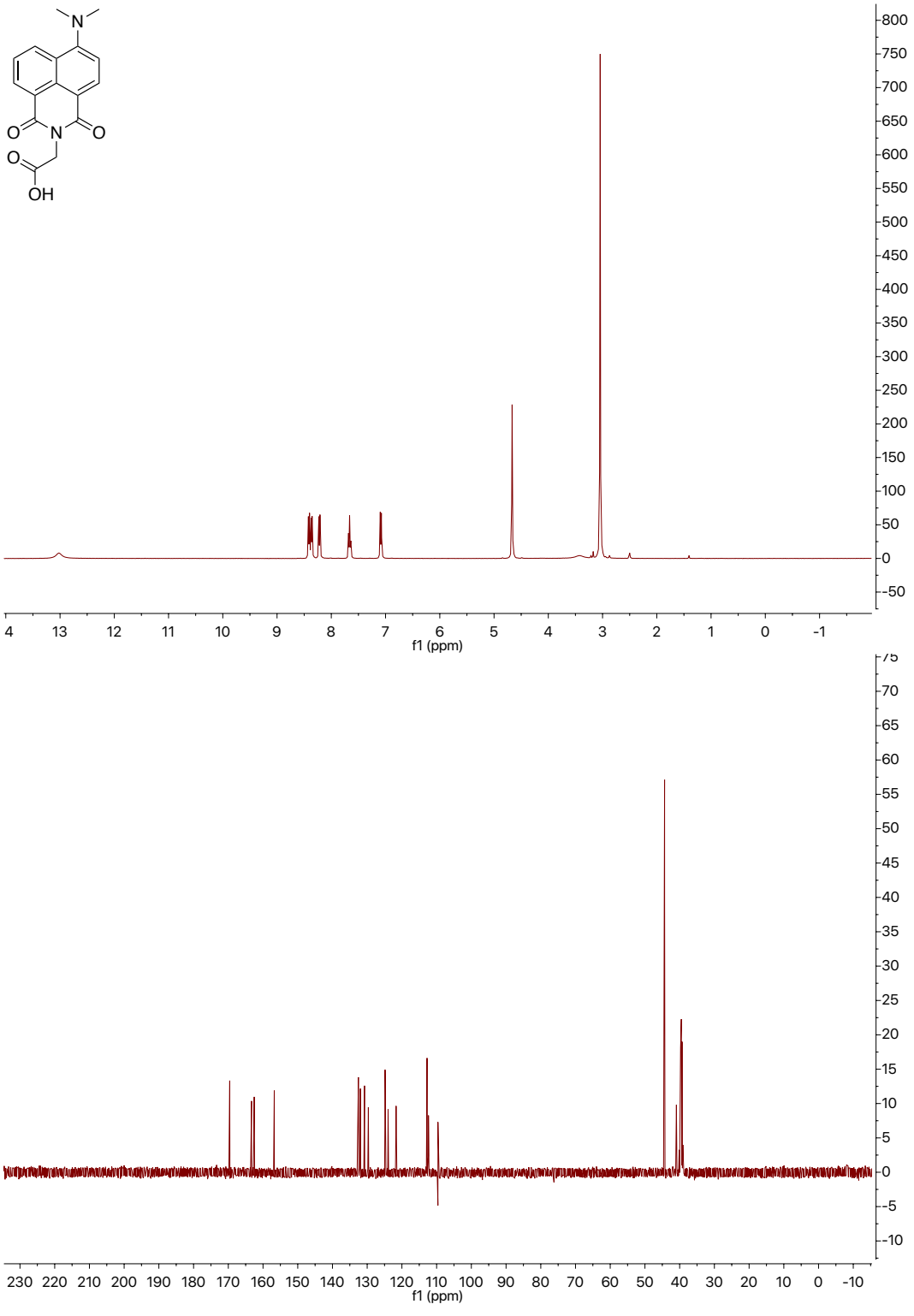

^{1}H- and ^{13}C-NMR of 8:

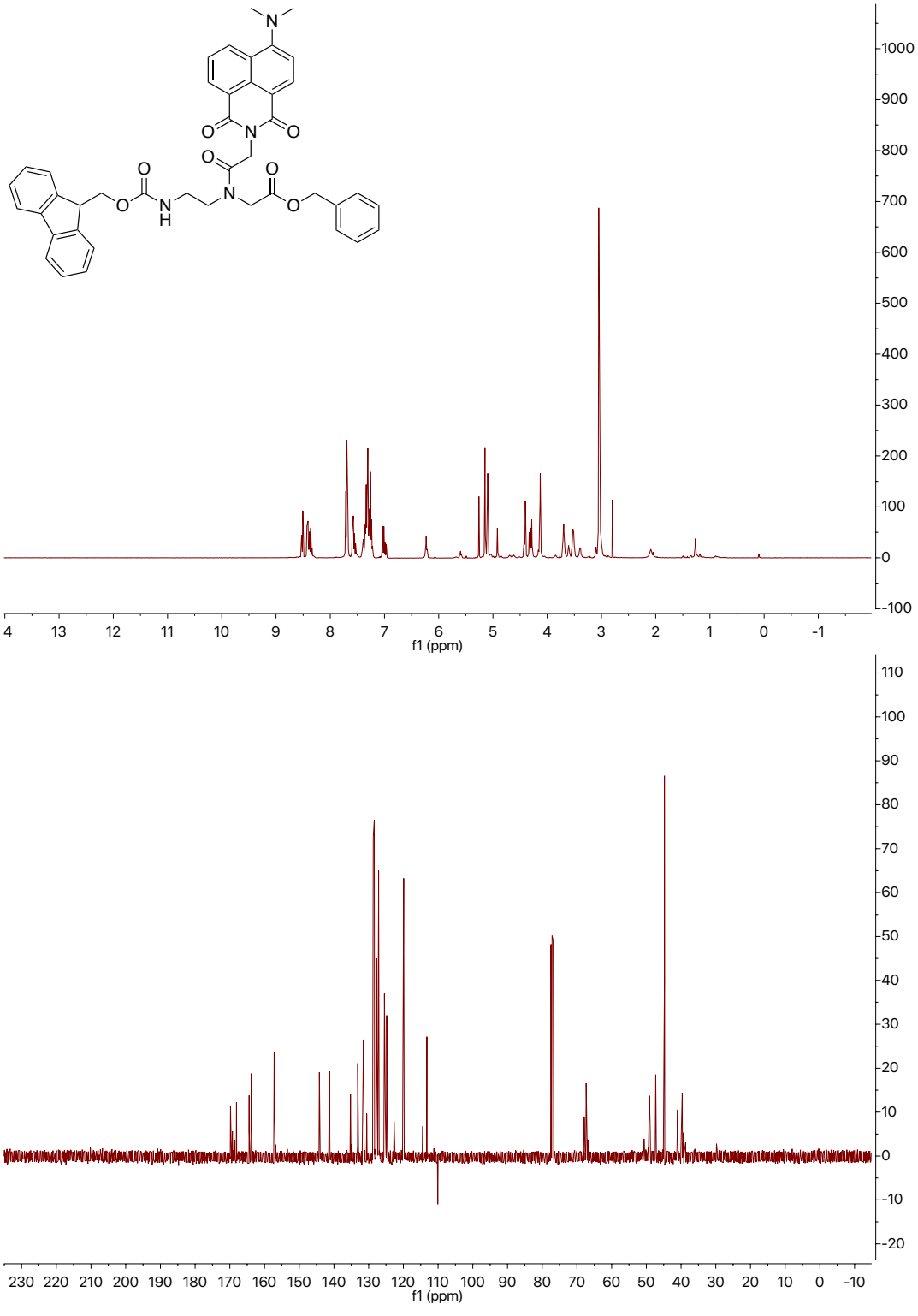

^{1}H- and ^{13}C-NMR of 9:

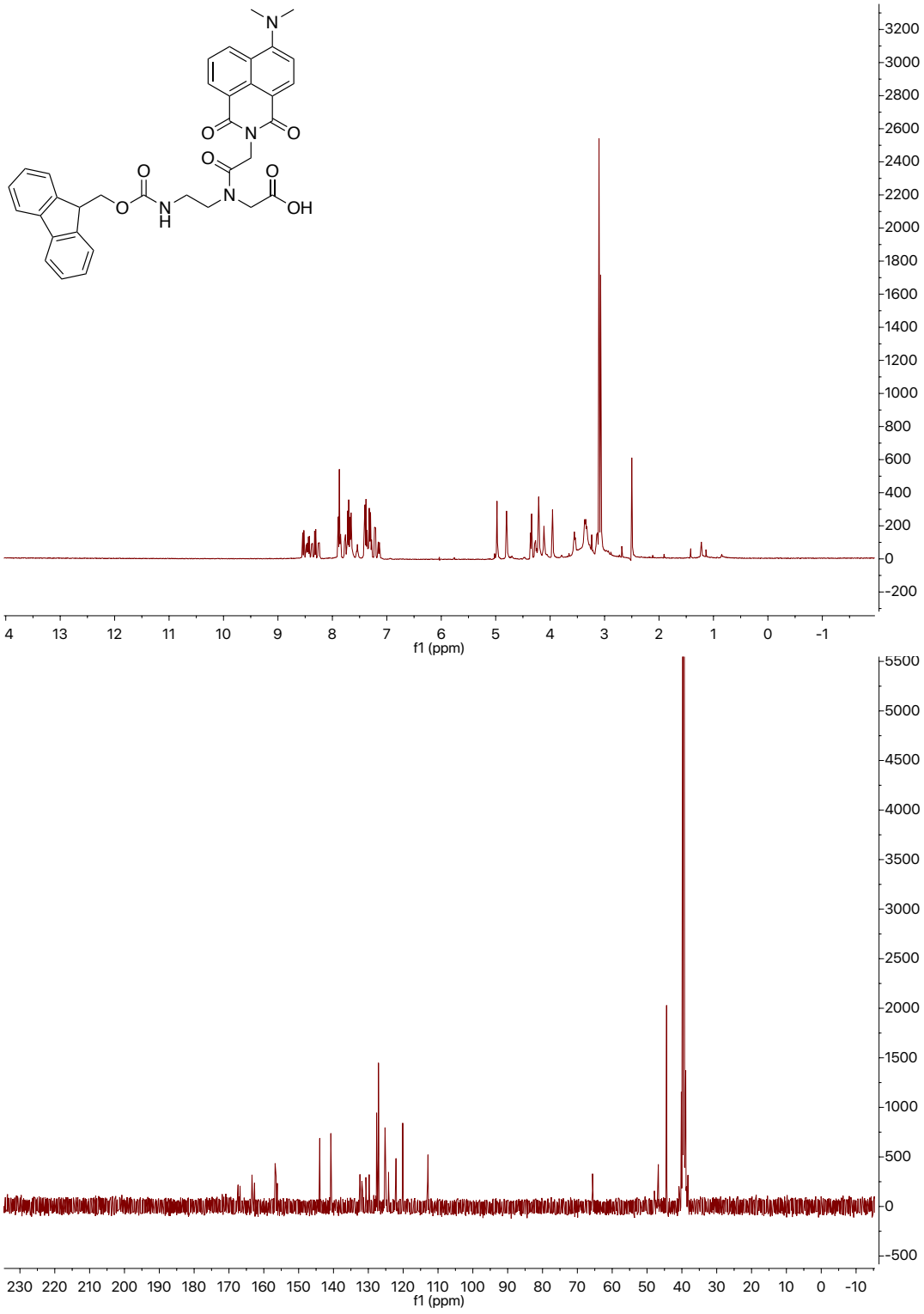

Appendix B

Tabular, Spectral, and Omitted Data of Chapter 3

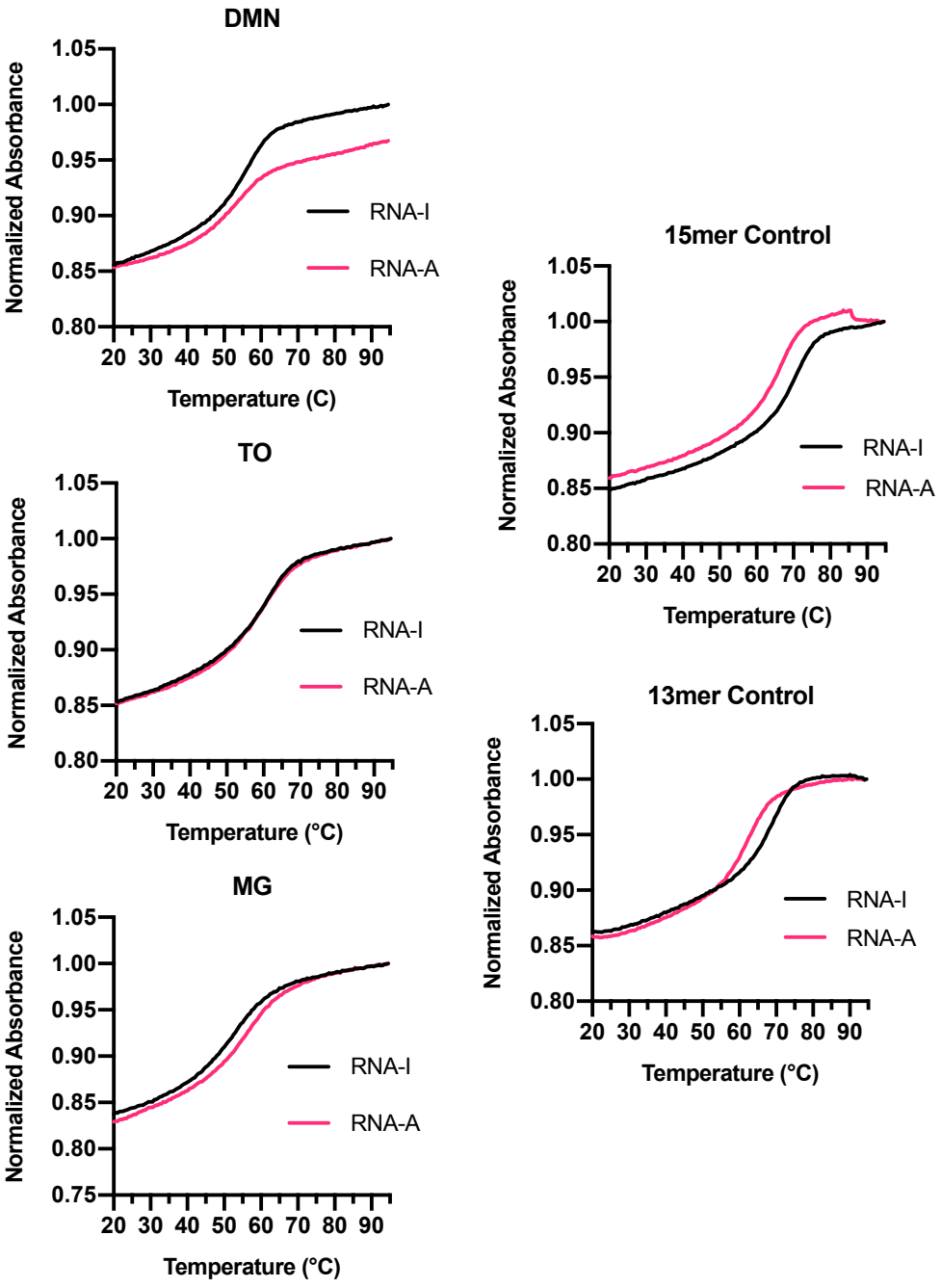

Figure B1: Melting curves of FIT-PNA and control probes in presence of linear inosine or adenosine-containing RNA targets.

Inosine-containing (edited):

5’ – GTG CCT TTA TGC **I** -G- C AAG GAT GCG – 3’

5’ – GTG CCT TTA TGC **I** -A- C AAG GAT GCG – 3’

5’ – GTG CCT TTA TGC **I** -C- C AAG GAT GCG – 3’

5’ – GTG CCT TTA TGC **I** -T- C AAG GAT GCG – 3’

Adenosine-containing (unedited):

5’ – GTG CCT TTA TGC **A** -G- C AAG GAT GCG – 3’

5’ – GTG CCT TTA TGC **A** -A- C AAG GAT GCG – 3’

5’ – GTG CCT TTA TGC **A** -C- C AAG GAT GCG – 3’

5’ – GTG CCT TTA TGC **A** -T- C AAG GAT GCG – 3’

Figure B2: Sequences of linear DNA targets. Underlined portion represents FIT-PNA binding site. Hyphenated nucleobases represent the residue opposite the dye in a duplex adjacent to the site of editing (bold).

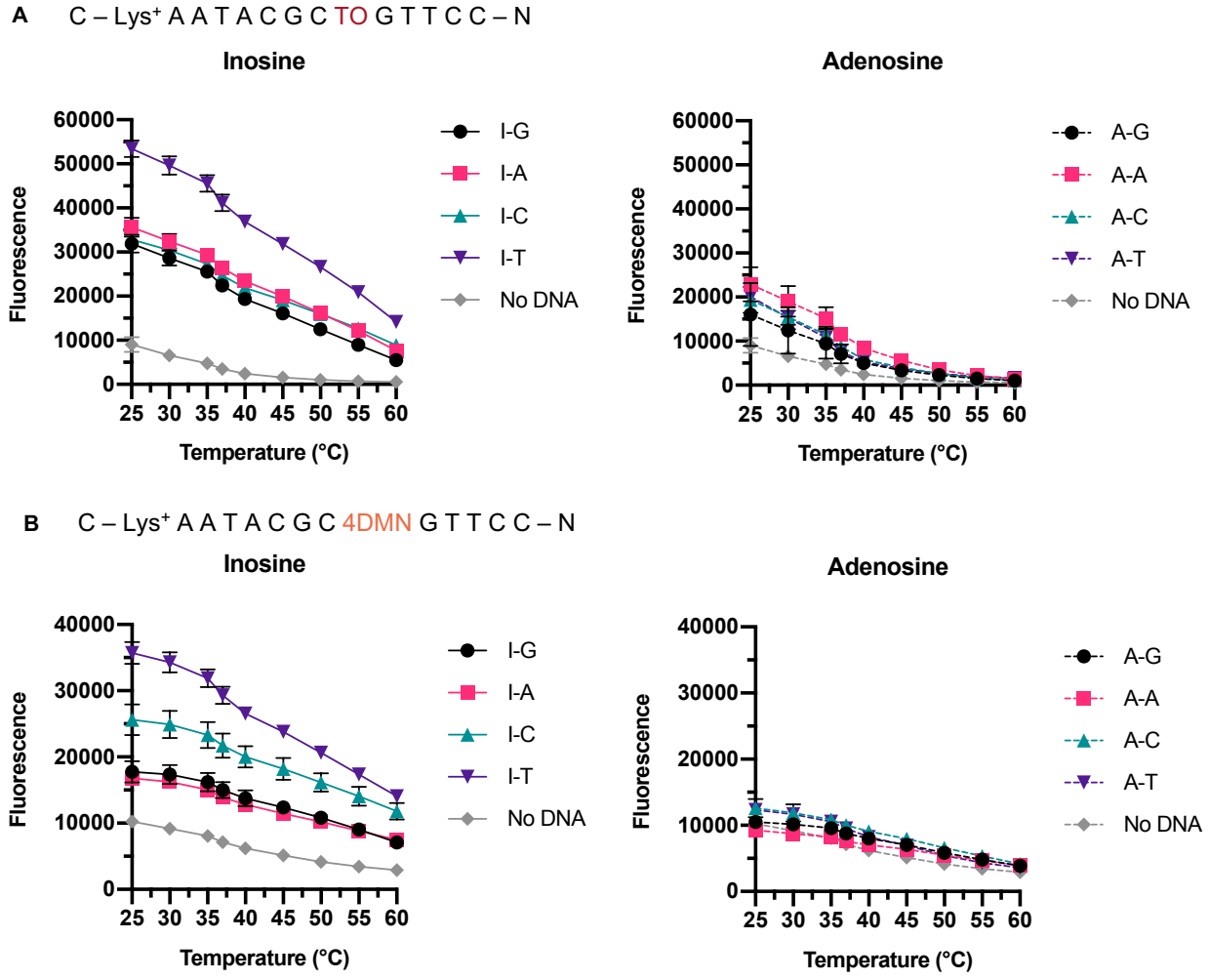

Figure B3: The effect of temperature on fluorescence intensity of FIT-PNA probes in the presence of DNA targets containing either inosine or adenosine.

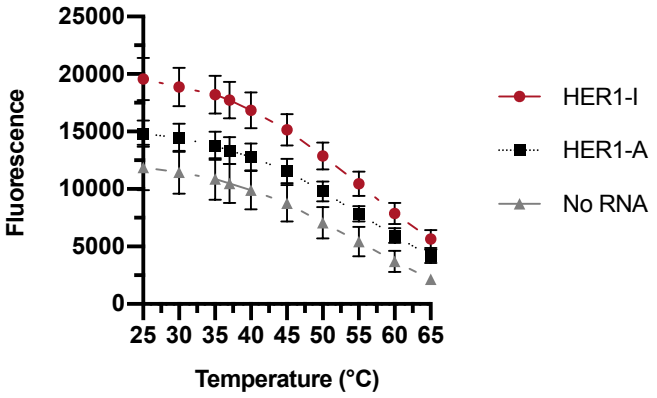

Figure B4: The effect of temperature on fluorescence intensity of FIT-PNA probes in the presence of "edited" or "unedited" HER1 RNA.

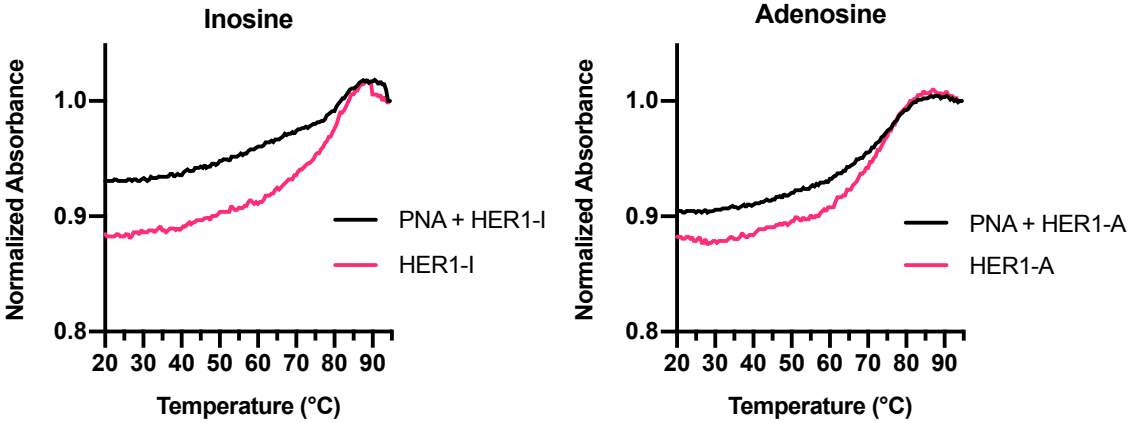

Figure B5: Melting curves of HER1-I and HER1-A targets in the absence and presence of TO FIT-PNA.

Table B1: UV melting temperatures of HER1-I and HER1-A targets in the absence and presence of TO FIT-PNA. Error is represented as SEM (n=3).

Sample	Tm (°C)	ΔT_m (°C)
PNA + HER1-I	80.4 ± 0.7	0.8 ± 0.8
HER1-I	81.1 ± 0.4	
PNA + HER1-A	76.5 ± 0.4	0.9 ± 0.8
HER1-A	75.6 ± 0.6	

Structure, HPLC, and ESI-TOF of TO FIT-PNA:

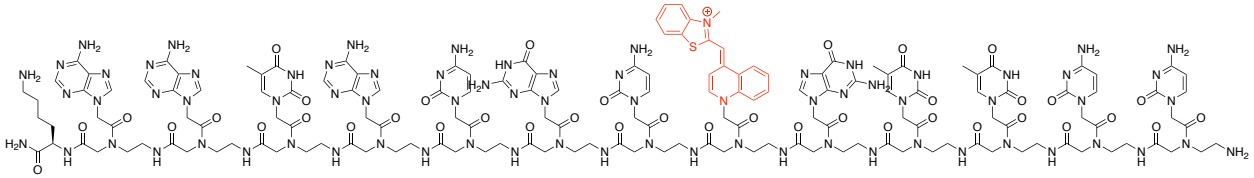

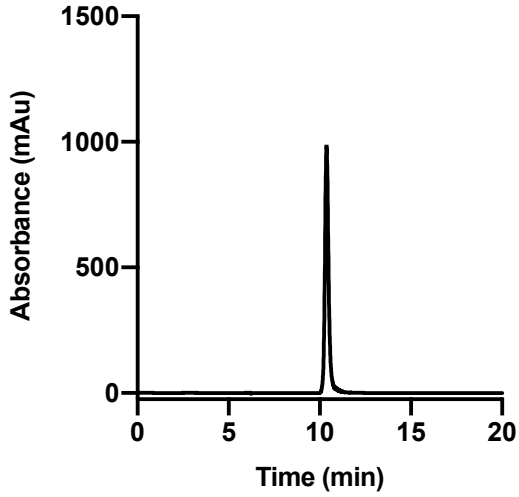

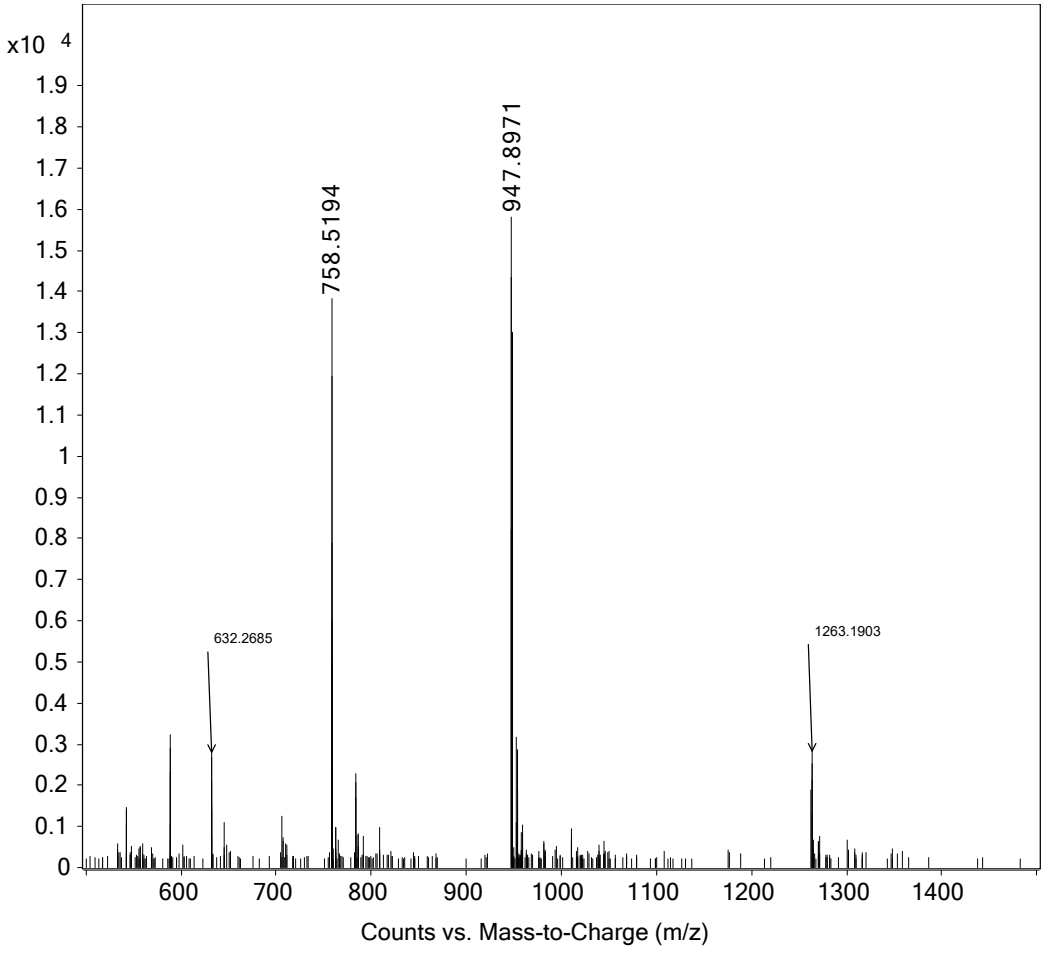

Structure, HPLC, and ESI-TOF of 4DMN FIT-PNA:

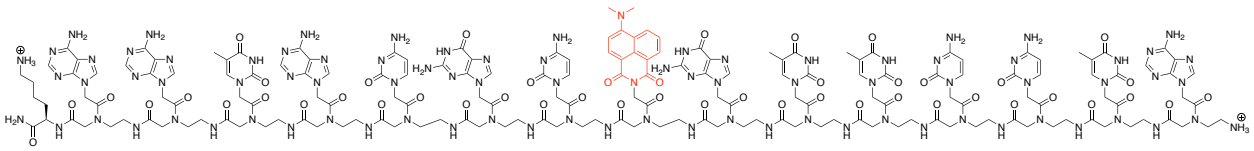

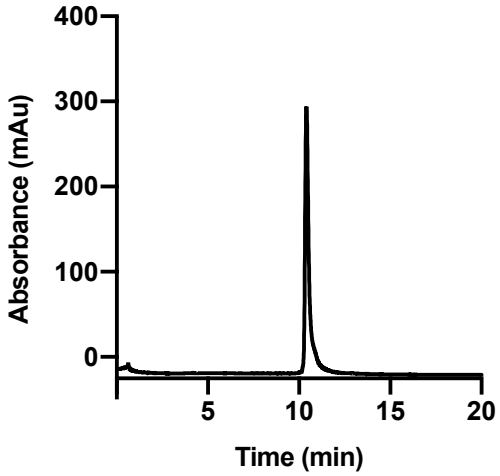

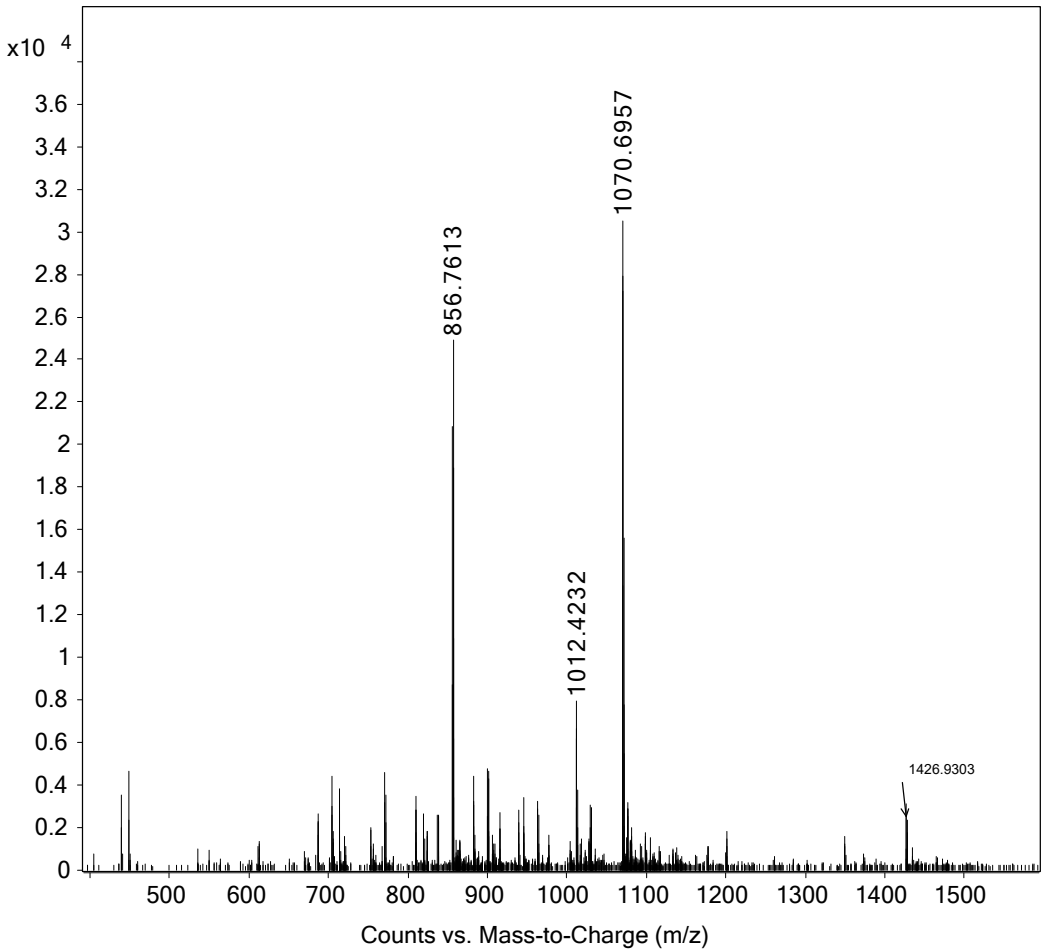

Structure, HPLC, and ESI-TOF of MG FIT-PNA:

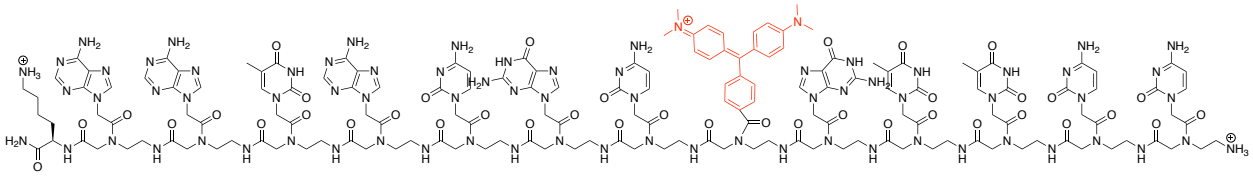

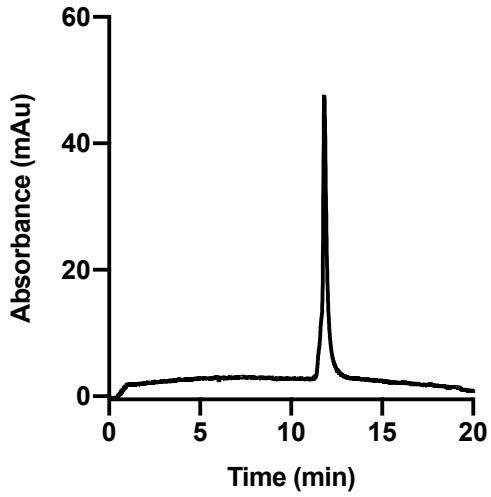

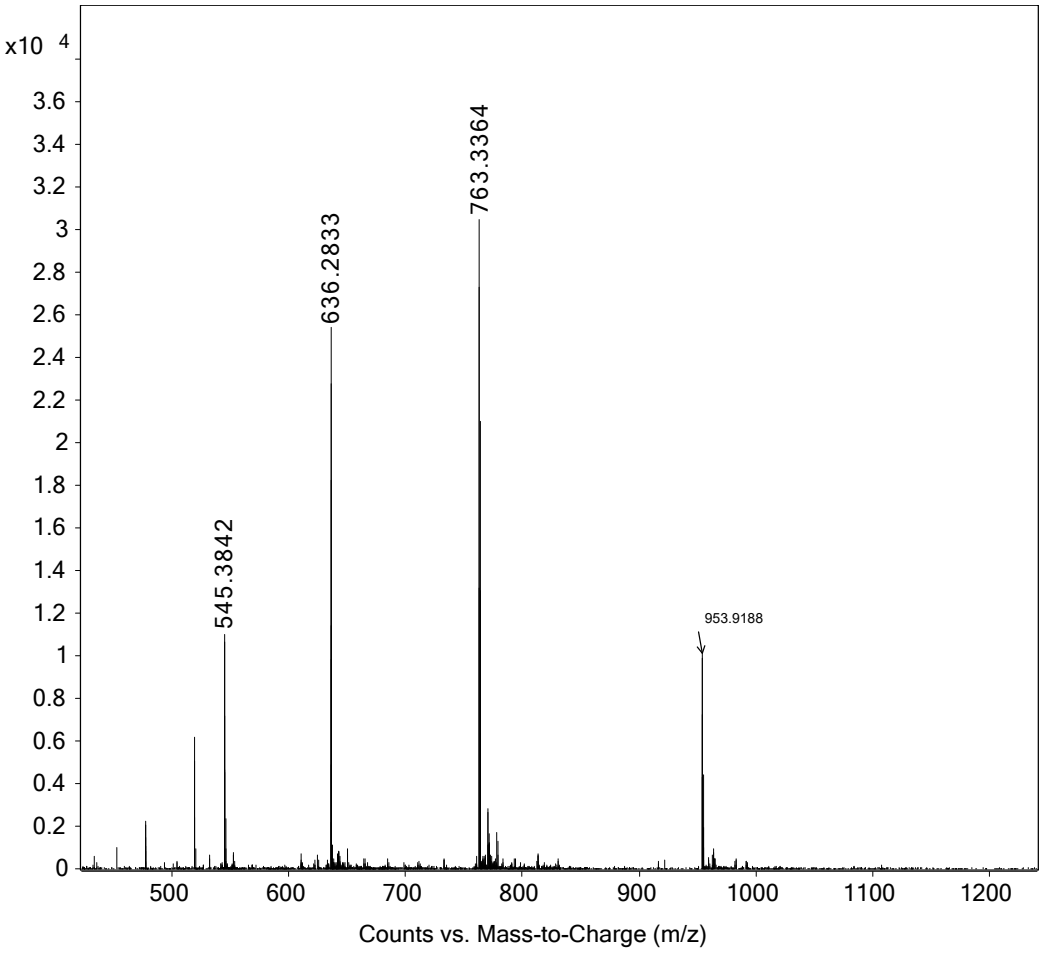

Structure, HPLC, and ESI-TOF of 15mer Control PNA:

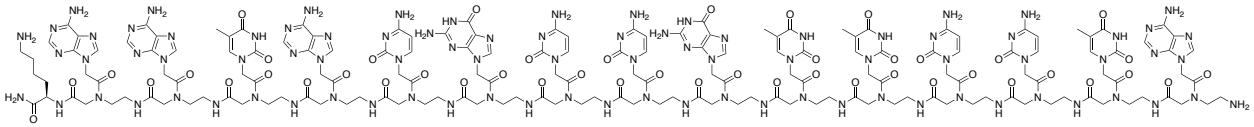

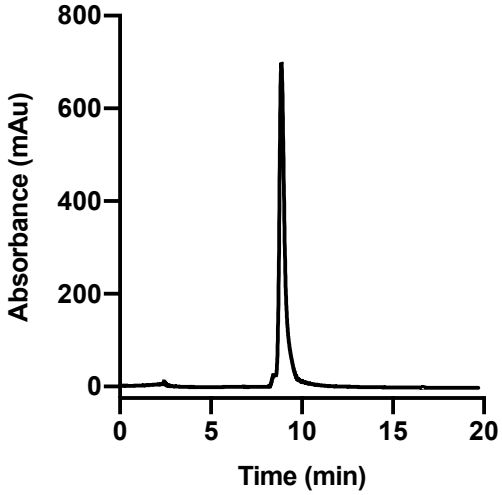

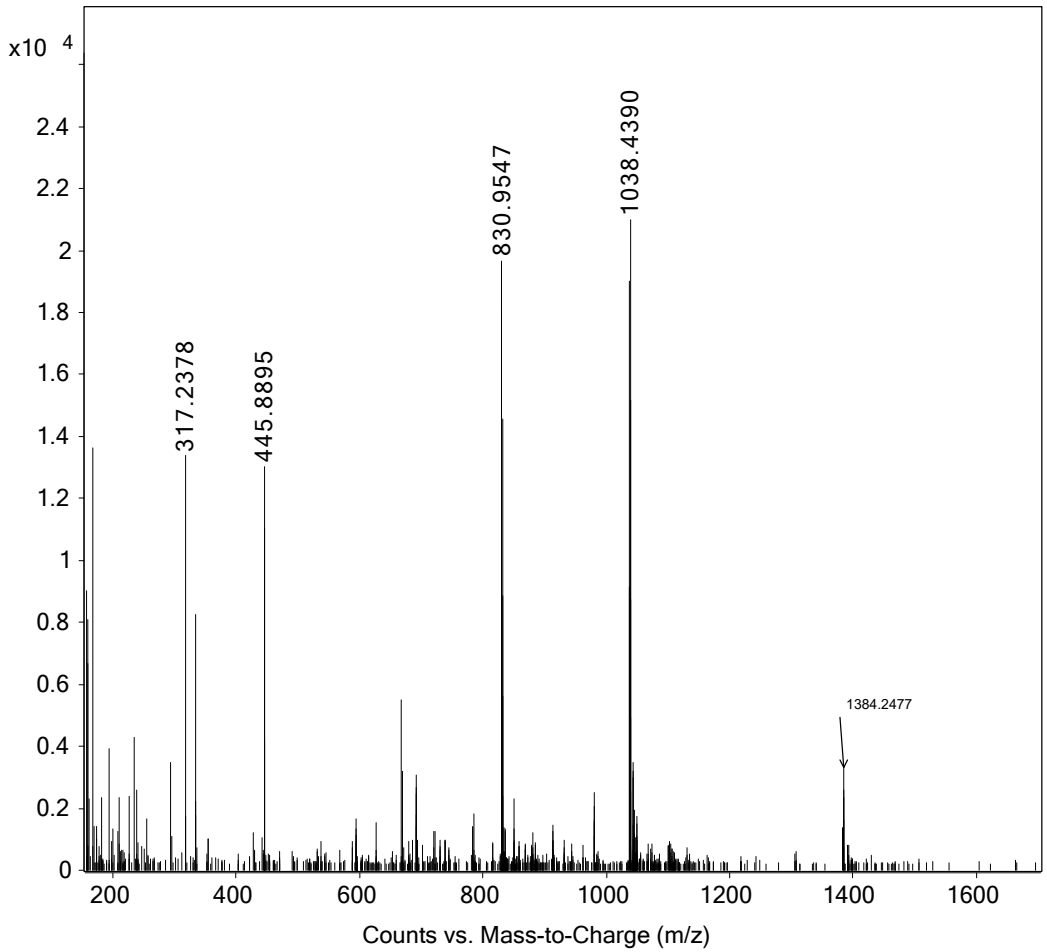

Structure, HPLC, and ESI-TOF of 13mer Control PNA:

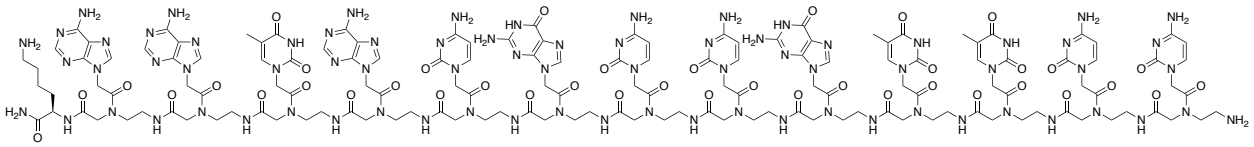

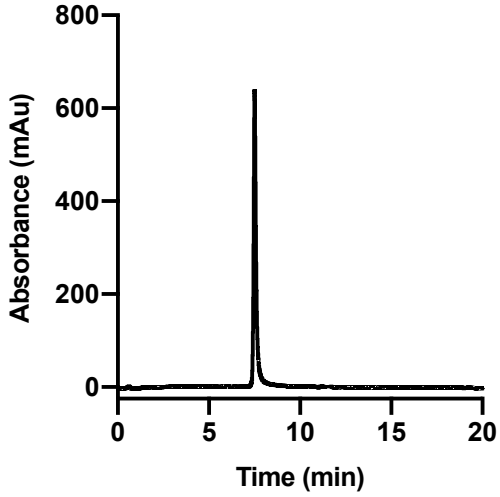

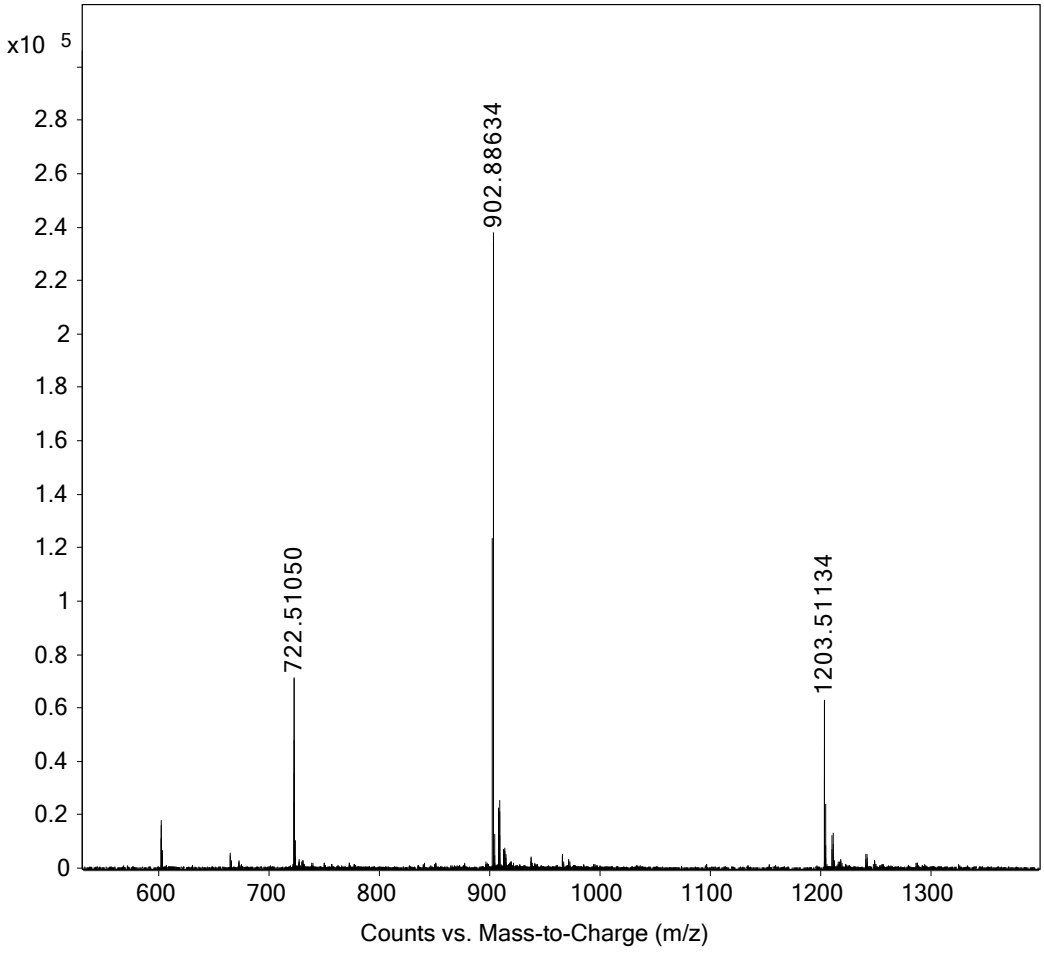

Structure, HPLC, and ESI-TOF of HER1 TO FIT-PNA:

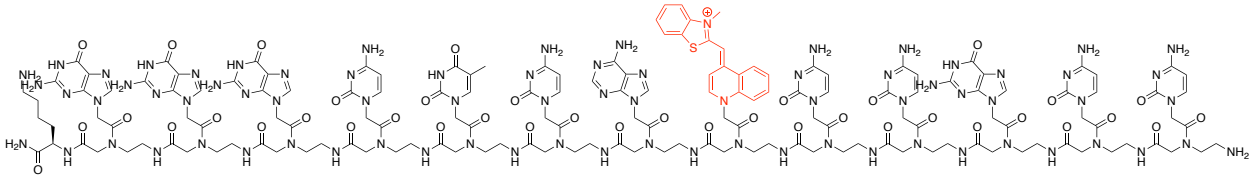

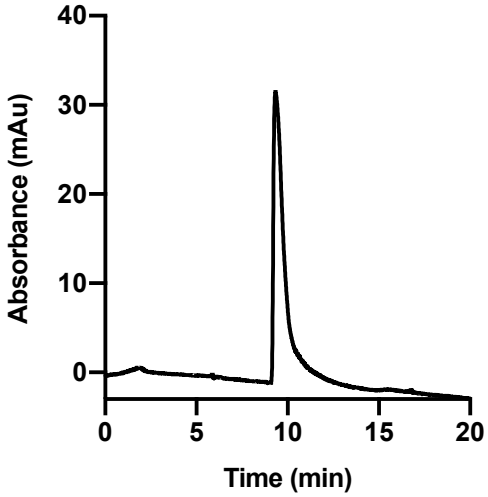

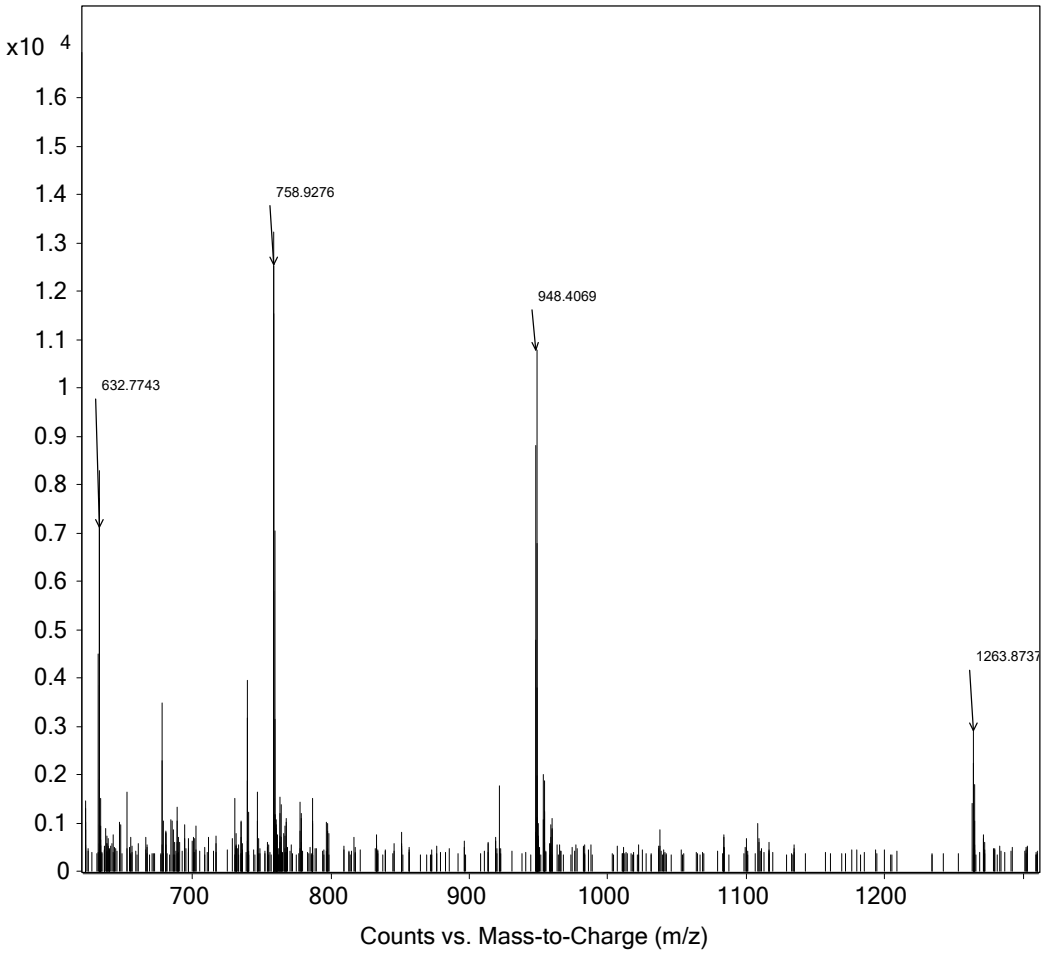

^{1}H- and ^{13}C-NMR of 1:

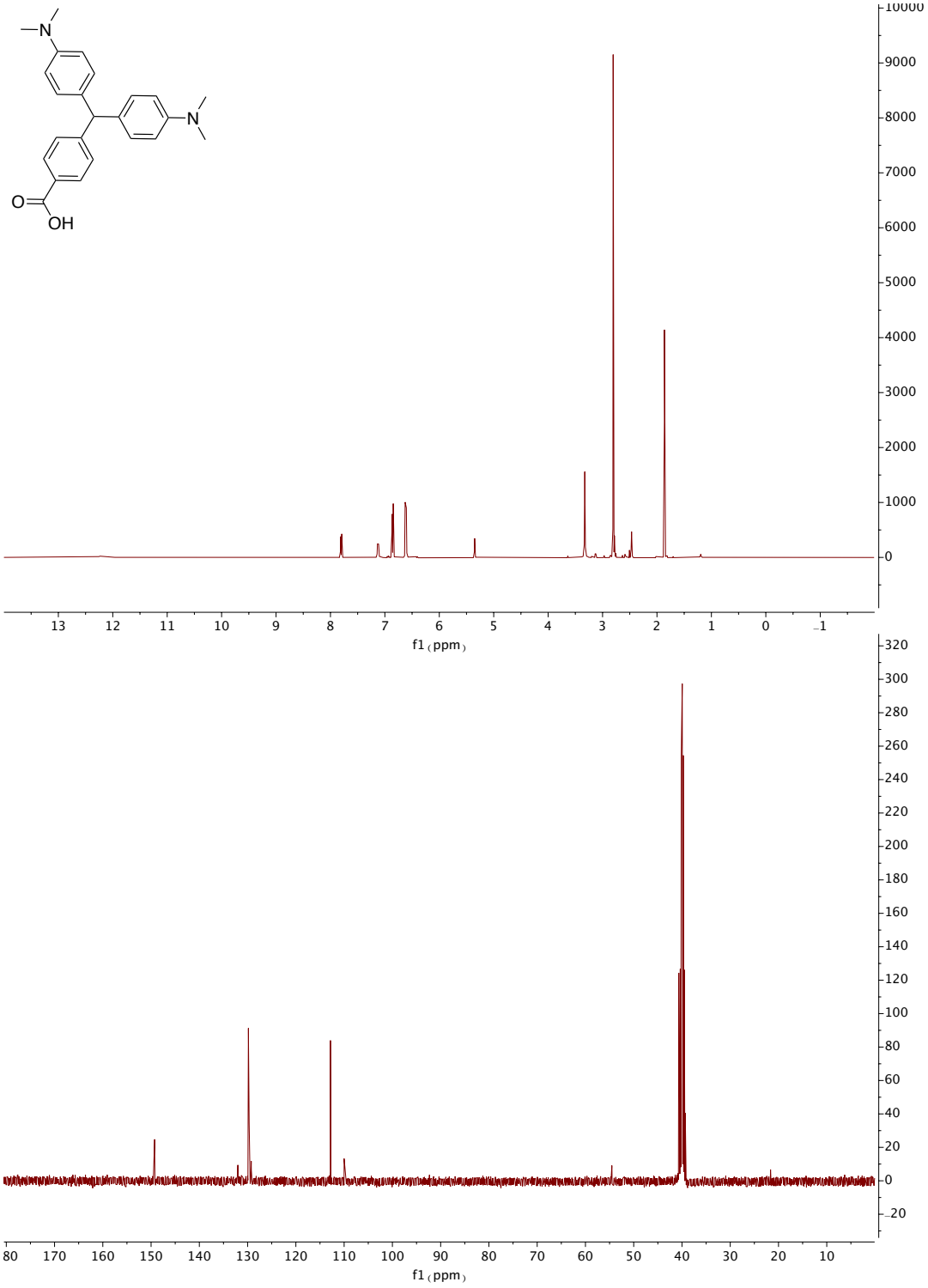

^{1}H- and ^{13}C-NMR of 2:

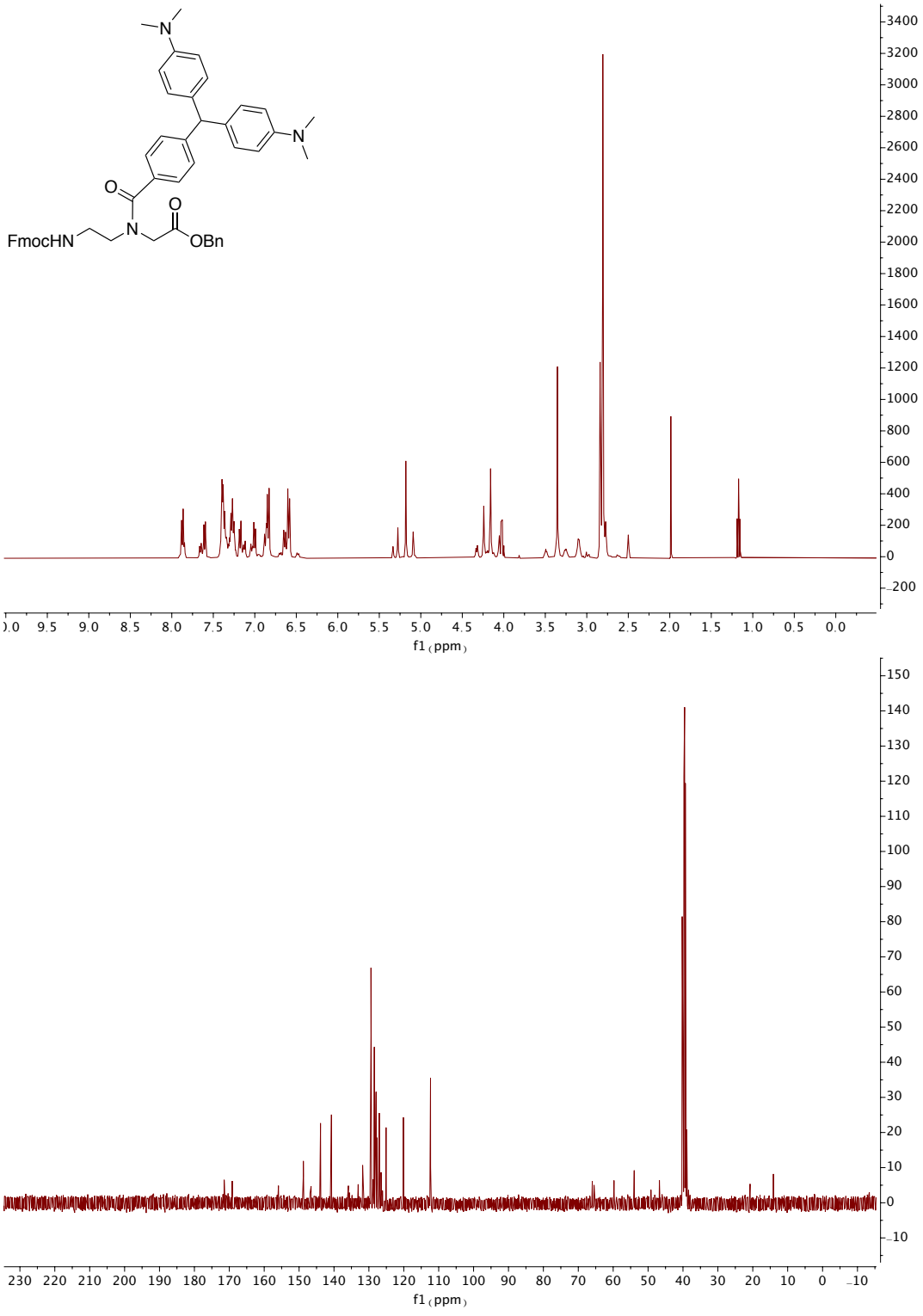

^{1}H- and ^{13}C-NMR of 3:

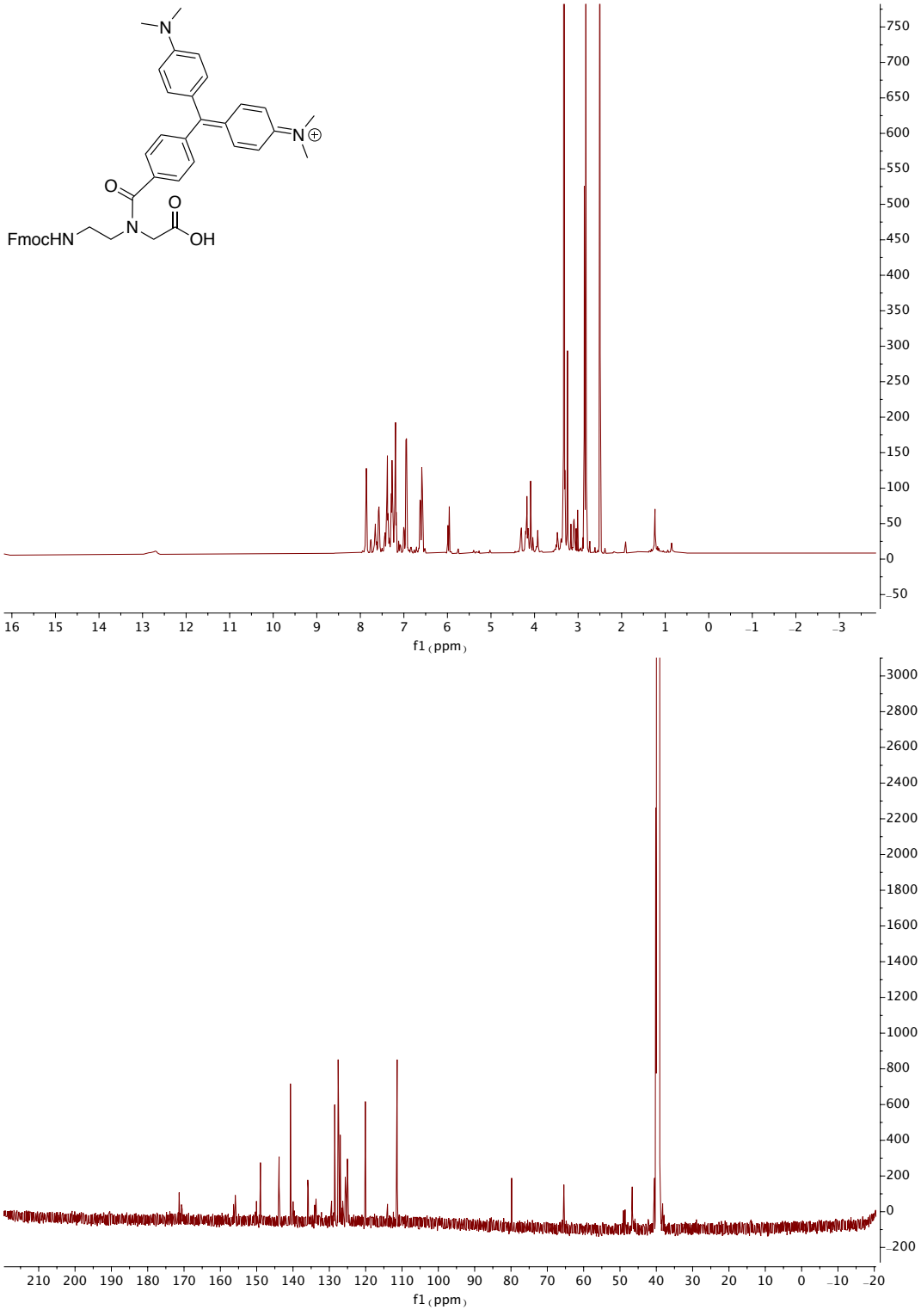

Appendix C

Tabular, Spectral, and Omitted Data of Chapter 4

Table C1: Sequences of nucleic acids used in Chapter 4.

Oligomer	Sequence
DNA Anchor	5' – ACA CAC ACA CAC ACA CAC – 3' – NH_2
DNA Capture	5' – GTG TGT GTG TGT GTG TGT TTT CCC CCC TTT ACA TAG GTA – 3'
PNA Target	^{C}TGT ATC CAT^{N} – TAMRA
DNA Target	3' – TGT ATC CAT – TAMRA – 5'
DNA-2A Target	3' – AAT GTC TCC AT – TAMRA – 5'
PNA Glyoxal	Glu^{-} – ^{C}TCA CTA GAT G^{N} – FAM
Glyoxal DNA Complement	5' – AGT GAT CTA C – 3'
Glyoxal DNA Scramble	5' – CTA TGG TAC A – 3'

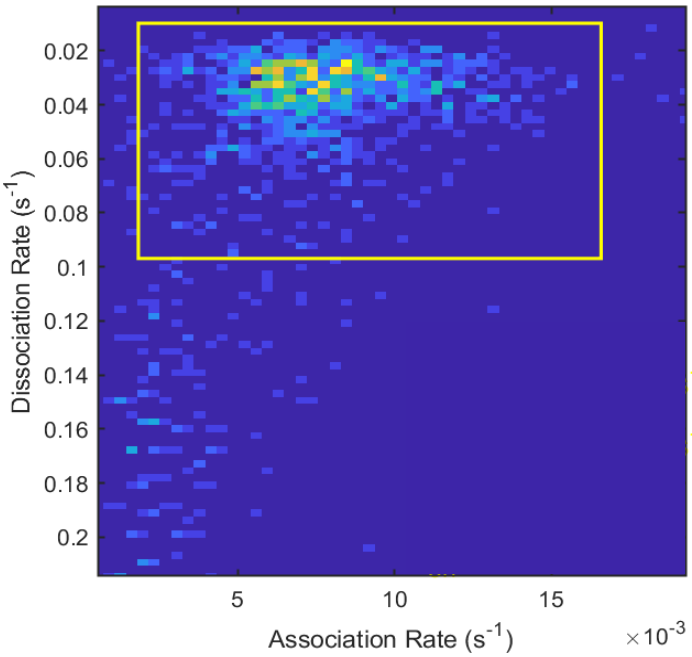

Figure C1: Plot of dissociation and association rates of single molecule sites imaged using TIRF. Lighter colors indicate a greater density of hybridization events in that range. Data from these areas were analyzed to determine kinetic parameters.

Table C2: Values of PNA:DNA hybridization as determined by single-molecule hybridization events.

Temperature (°C)	[NaCl] (mM)	T_{off} (s)	T_{on} (s)	k_{off} (s^{-1})	k_{on} ($\mu M^{-1}s^{-1}$)	K_a (μM^{-1})
22.5	50	48.04	87.82	0.021	0.40	19
	100	52.13	117.20	0.019	0.30	15
	150	48.85	152.20	0.021	0.23	11
	200	50.31	193.00	0.020	0.18	9.2
	300	41.61	224.70	0.024	0.16	6.5
	450	36.75	304.20	0.027	0.12	4.3
25	50	32.46	59.61	0.031	0.59	19
	100	34.90	86.77	0.029	0.41	14
	150	25.94	118.70	0.039	0.30	7.7
	200	28.36	131.50	0.035	0.27	7.6
	300	23.82	187.80	0.042	0.19	4.5
	450	22.77	198.23	0.044	0.18	4.1
27.5	50	19.70	58.42	0.051	0.61	12
	100	17.33	81.69	0.058	0.43	7.5
	150	16.81	96.81	0.056	0.37	6.1
	200	15.46	120.60	0.065	0.29	4.5
	300	14.11	149.20	0.071	0.24	3.3
	450	12.37	207.50	0.081	0.17	2.1
30	50	8.90	48.92	0.11	0.72	6.4
	100	6.52	61.09	0.15	0.58	3.8
	150	6.40	85.02	0.16	0.42	2.7
	300	5.00	116.53	0.20	0.30	1.5
	450	5.03	131.82	0.20	0.27	1.4

Table C3: Values of DNA-2A:DNA hybridization as determined by single-molecule hybridization events at 22.5°C.

Trial	[NaCl] (mM)	t_{on} (s)	t_{off} (s)	k_{off} (s^{-1})	k_{on} ($\mu M^{-1}s^{-1}$)	K_a (μM^{-1})
1	50	1144	11.84	0.085	0.031	0.37
	100	486	14.74	0.068	0.074	1.1
	150	418.3	23.2	0.043	0.085	2.0
	200	256.2	33.74	0.030	0.14	4.7
	300	223.1	41.28	0.024	0.16	6.6
	450	198.5	50.54	0.020	0.18	9.1
2	100	494.2	15.53	0.064	0.068	1.1
	150	319.6	22.42	0.045	0.10	2.3
	200	293.7	30.64	0.033	0.11	3.5
	300	212.8	43.38	0.023	0.16	6.8
	450	168.9	49.39	0.020	0.20	9.8
3	100	620.7	17.49	0.057	0.054	0.94
	150	528.2	21.29	0.047	0.095	2.0
	200	291.8	28.26	0.035	0.11	3.2
	300	212.8	43.38	0.023	0.16	6.8
	450	258.8	44.95	0.022	0.19	8.7

Table C4: Values of DNA:DNA hybridization as determined by single-molecule hybridization events at 22.5°C.

Trial	[NaCl] (mM)	t_{on} (s)	t_{off} (s)	k_{off} (s^{-1})	k_{on} ($\mu M^{-1}s^{-1}$)	K_a (μM^{-1})
1	450	95.33	3.280	0.31	0.53	1.7
2	450	87.22	2.589	0.39	0.38	0.99
3	450	79.92	2.932	0.34	0.42	1.2

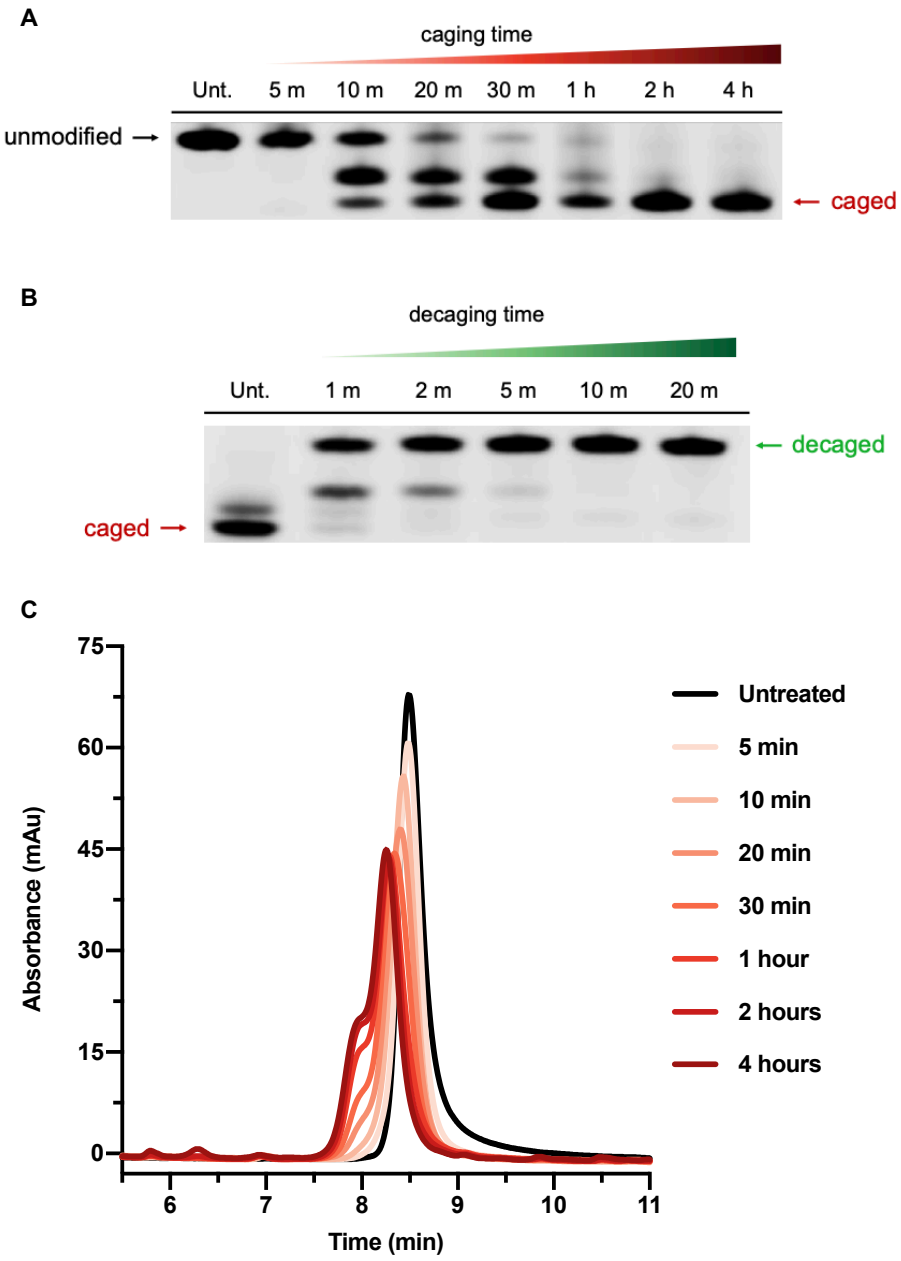

Figure C2: 20% PAGE and HPLC analysis of PNA caging and decaging. A) PAGE analysis with increasing caging times, illustrating downward mobility shift. B) PAGE analysis with increasing decaging times at 95°C pH 7.5. C) HPLC analysis with increasing caging times, illustrating small upfield peak forming with caging.

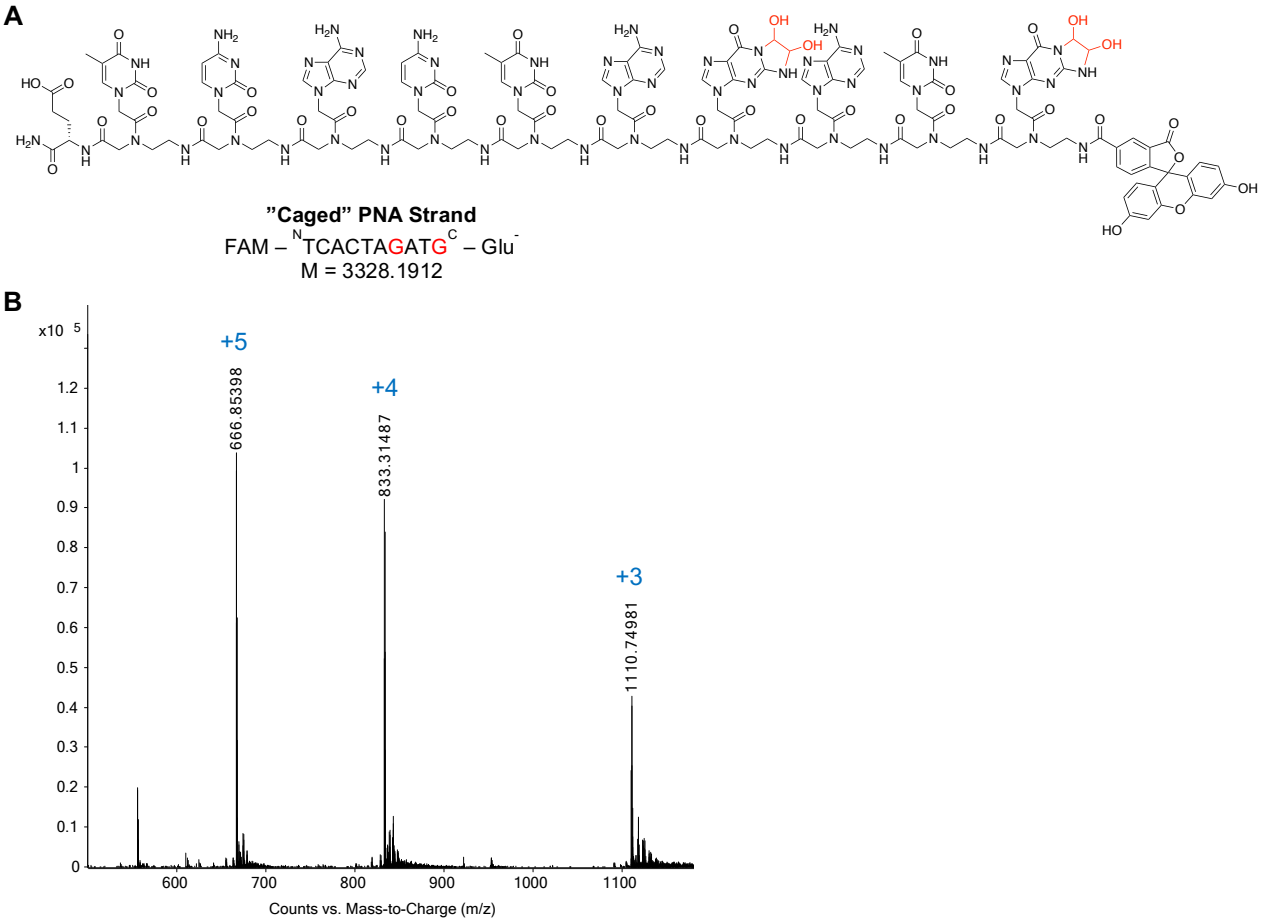

Figure C3: Sequence of "caged" PNA strand after glyoxal treatment. A) Putative glyoxal adducts (red) on nucleobases in PNA sequence. B) ESI-TOF mass spectra of purified caged PNA representing two *bis*-hemiaminal adducts.

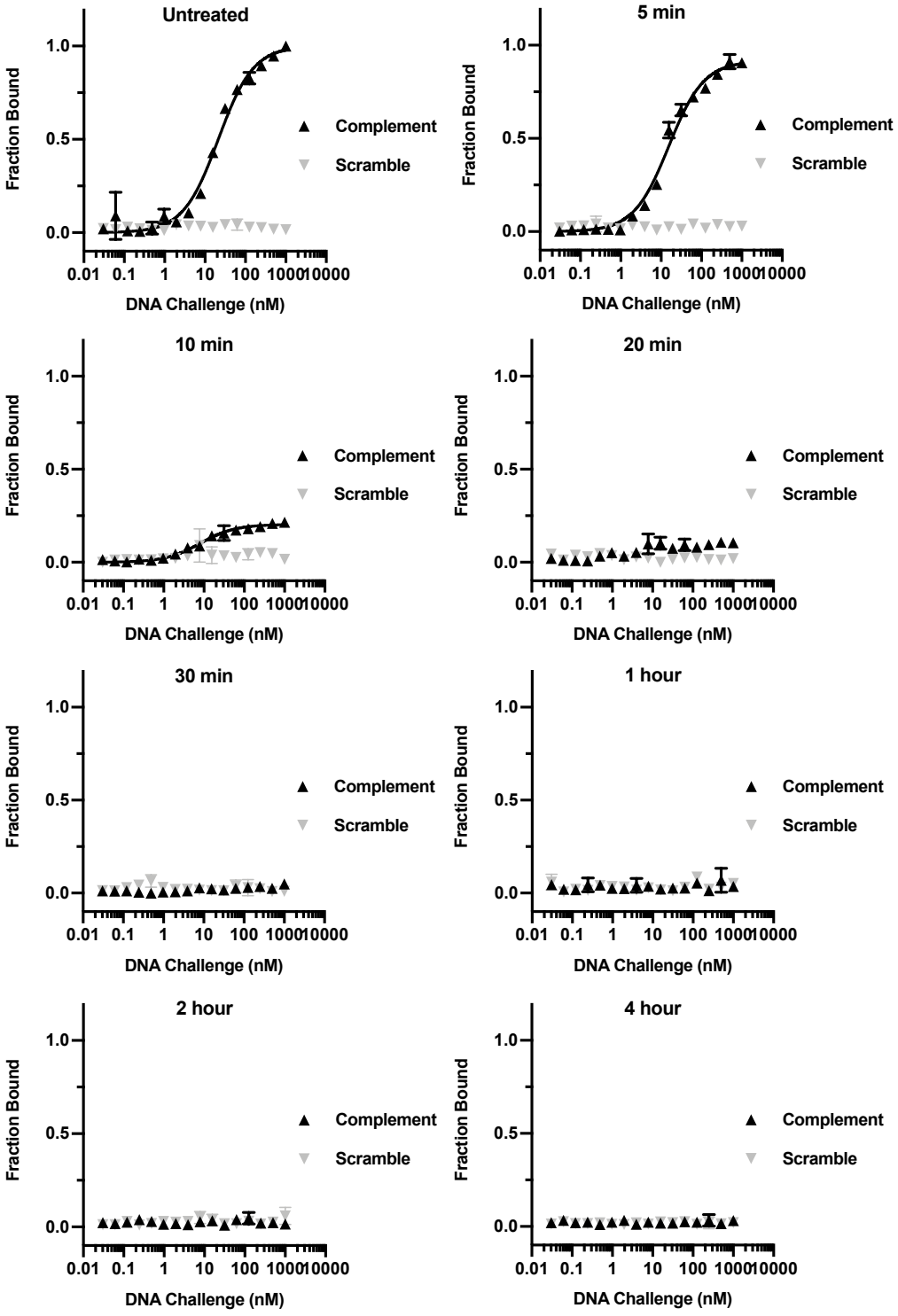

Figure C4: MST analysis of PNA hybridization with complementary (black) or scrambled (grey) DNA with increasing caging times. Error bars represent SEM (n=3).

Structure, HPLC, and ESI-TOF of PNA Target:

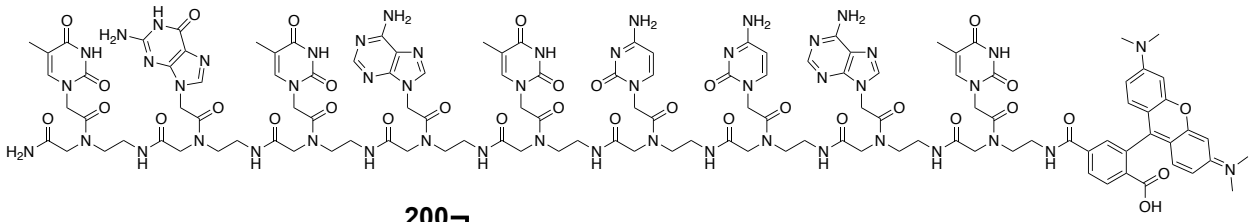

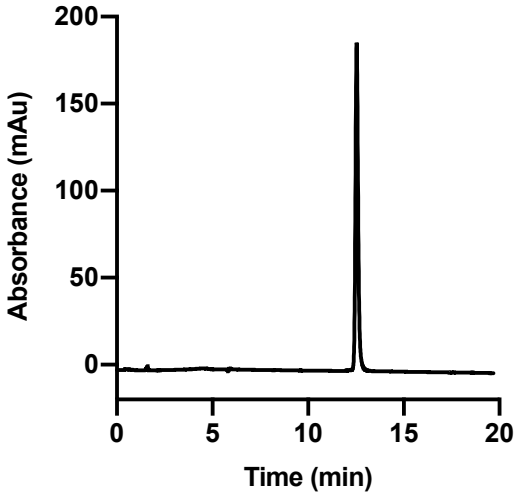

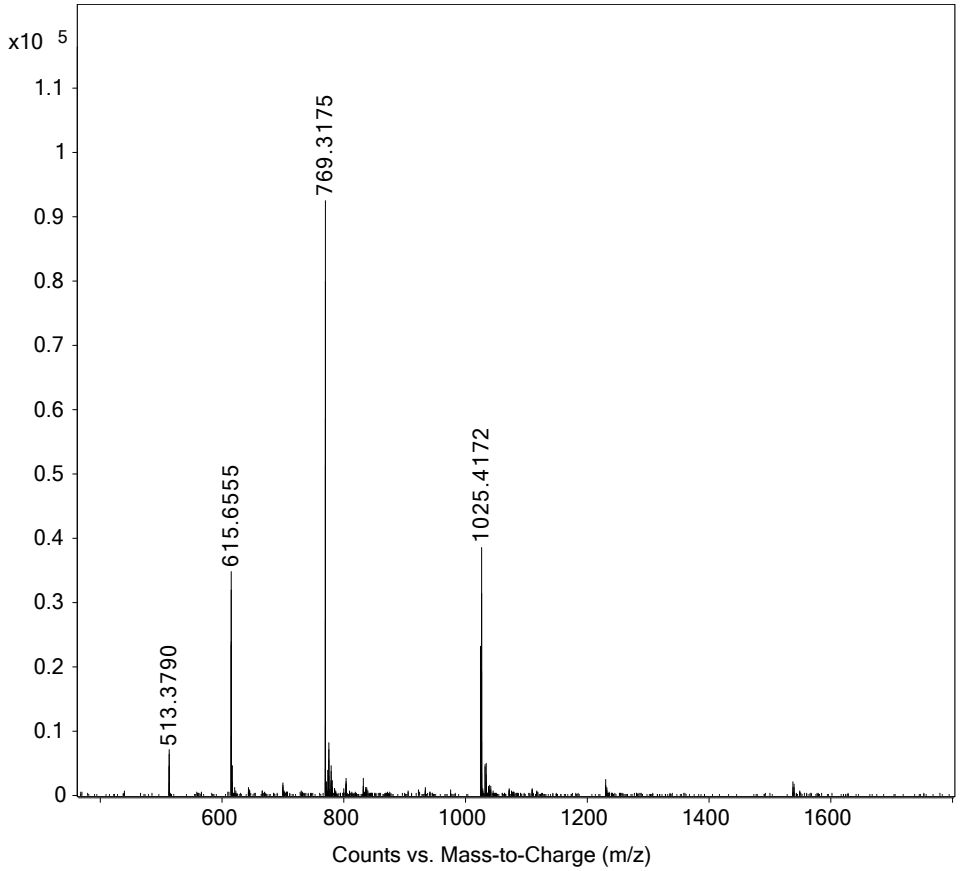

Structure, HPLC, and ESI-TOF of PNA Glyoxal:

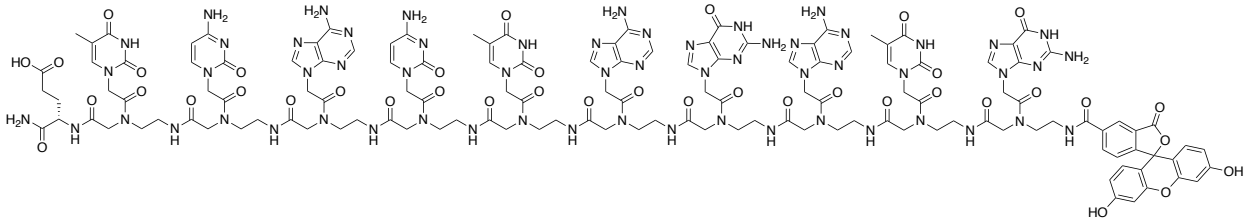

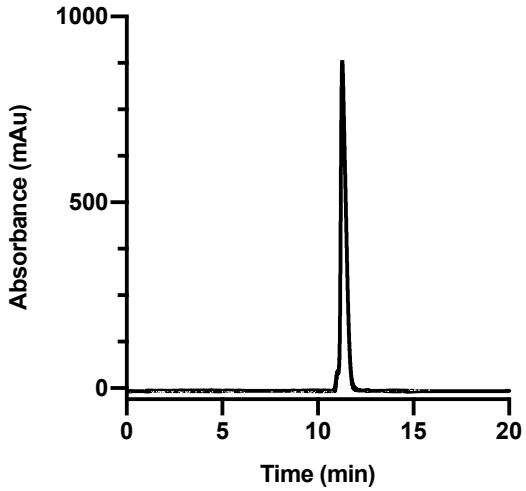

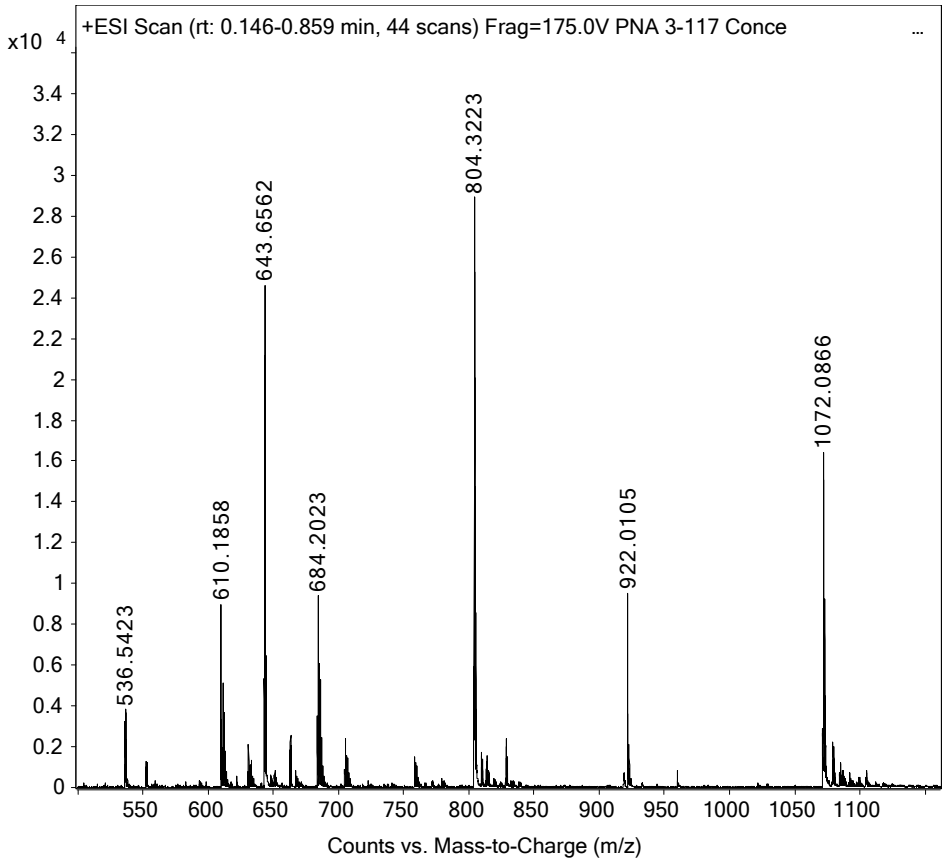

Appendix D

Optimization of PNA Oligomer Synthesis and Purification

Methods and Results:

All abbreviations for chemicals can be found in Chapter 2. G, Fmoc-guanine(Bhoc) PNA monomer; A, Fmoc-adenine(Bhoc) PNA monomer; T, Fmoc-thymine(Bhoc) PNA monomer; C, Fmoc-cytosine(Bhoc) PNA monomer.

Optimization of HPLC Purification

In order to optimize PNA oligomer synthesis, I first synthesized a 9mer PNA strand with sequence ^{C}TGTATCCAT^{N} and optimized the HPLC purification protocol. The 9mer PNA was synthesized using the SP wave synthesizer as described in chapter 2 using slightly different conditions: monomers were coupled for 7 min at 70°C and deprotected for 5 min (optimized later). Optimization of the purification method was carried out using an Agilent Eclipse XDB-C18 5 µm, 9.4 x 250 mm column at 60°C monitoring at 260nm using linear gradients of solvent A (0.1% TFA in acetonitrile) in solvent B (0.1% TFA in water). Optimization conditions can be found in **Table D1**. Injection volume was 10µL for each condition.

After applying the conditions, it can be seen that increasing the time of the linear gradient results in increased retention time and a broadening of the peaks (**Figure D1**). Due to the broadening of the peaks, there is not a significant difference between each condition on the ability to isolate the full-length product. For this reason, I decided to proceed with a 15min gradient of 10-30% solvent A for the most efficient purification method.

I then tested this condition over a range of flow rates (**Table D1**). As the flow rate increases, the retention time significantly decreases, and the peaks sharpen (**Figure D2**). However, this sharpening of the peaks resulted in poor separation and difficult full-length isolation. Flow rates of 1 and 2 mL/min of solvent resulted in peaks that were easily separated by the fraction collector and I proceeded to use 2 mL/min for future purification as the most efficient method.

The most efficient method determined by these optimization conditions resulted in a linear gradient of 10-30% solvent A in 15 min with a flow rate of 2 mL/min. It is important to note that I later changed to a gradient of 10-40% solvent A for future purifications as I found this to be an even more efficient separation method, though I did not optimize this gradient through a similar evaluation. I next proceeded to test the loading, coupling, capping, and deprotection conditions for each monomer on the SP wave synthesizer to optimize solid-phase PNA oligomer synthesis.

Optimization of Solid-Phase PNA Synthesis

In order to optimize coupling conditions without depleting our stocks of PNA monomers, I chose to synthesize 5mer sequences of ^{C}GTCAG^{N} to evaluate all conditions. Conditions for optimization of the coupling cycle can be found in **Table D2**. For each oligomer I synthesized on a ~5 μmol scale using ~25 mgs of a rink amide MBHA resin (0.52 mmol/g) swelled for 30min in DMF and deprotected (3x5min with 25% piperidine in DMF). I synthesized four separate PNA oligomers to explore different conditions for loading, capping, coupling, and deprotection in parallel for each monomer. The loading for each oligomer proceeded using G with HATU (1.5eq), DIPEA (1.5eq), and 2,6-Lutidine (1.5eq) in 200μL dry NMP for times of 1, 2, 3, or 4 hours. The resins were then washed according to the method in Chapter 2. Capping was then performed using 1mL of a solution of 9% Acetic anhydride and 13% 2,6-Lutidine in DMF for 5, 10, 15, and 20 min. A Kaiser test was used to determine the presence of free primary amines following capping. Deprotection of the loaded resin was performed (3x5min with 1mL of 25% piperidine in DMF) and the loading was determined by measuring the absorbance at 301nm of the consecutive deprotection solutions. The total μmols were determined by Beer's law using the cumulative absorbances determined from three deprotection reactions and an extinction coefficient of 7800$M^{-1}cm^{-1}$ for the dibenzofulvene-piperidine adduct produced. The percent yield was determined by the ratio of measured μmols loaded to the calculated μmols for each monomer amount weighed. The results of loading and capping are summarized in **Table D3**. Increasing

loading times did not result in greater loading yields. Increased capping time from 5 to 10 minutes resulted in reaction completion by Kaiser test.

I next optimized the coupling of the monomers to each of the loaded resins. The monomer (25μmol) was activated for 10 min using HATU (1 eq), DIPEA (1 eq), and 2,6-Lutidine (1 eq.) in 200μL dry NMP before applying to the resin. The activated monomers were coupled to the resin at 75°C for 6, 7, 8, or 15 minutes. The resin was then washed as described in Chapter 2. Deprotection proceeded in triplicate using 1mL of 25% piperidine in DMF for 1, 2, 3, or 4 minutes. Coupling efficiency was determined by absorbance as described above. The calculated percent yield was determined by the ratio of the measured μmols to the measured μmols from the previous coupling for each individual oligomer. The results of coupling and deprotection for each monomer are summarized in **Table D4-D7**. It is noted that the G monomer consistently displayed greater than theoretical yields over all conditions. This is likely due to leftover unreacted monomer on the resin following washing steps. For future G couplings, washing times were increased to mitigate the carryover. In any case, increased coupling times did not result in greater coupling efficiency for all monomers. Increased deprotection times also did not significantly affect coupling efficiency and complete deprotection was apparent for all conditions.

After coupling and deprotection, the resins were washed as described and cleaved for HPLC analysis of full-length product. Cleavage proceeded using 2.5% H_2O and 2.5% TIS in TFA for 2 hours. The product was precipitated with ice cold ether (10 eq), washed with ice cold ether, and dried under vacuum. The resulting precipitate was dissolved in 200μL of 50% acetonitrile in H_2O and purified by HPLC using a gradient of 10-40% solvent A with a flow rate of 2 mL/min as determined above. The retention time of full-length product was confirmed using matrix-assisted mass spectrometry (MALDI). The percent purity of full-length product was calculated using the Agilent software by determining the area under each curve as compared to the total area (**Table D1**). The final purity of the produced 5mer PNAs was not affected by increasing reactions times across loading, capping, coupling, or deprotection. From these results, I proceeded to synthesize

PNA using the minimal amount of reaction times for the greatest efficiency. However, I elected to use the 10-minute capping and 2-minute deprotection times to ensure reaction completion as incomplete capping or deprotection can potentially lead to significant truncation and complex impurities during synthesis. The optimized reaction conditions are summarized in **Table D8** and all PNA oligomers in this dissertation were produced using these conditions on the Biotage SP wave synthesizer as seen in Chapters 2, 3, and 4.

Table D1: HPLC conditions tested to optimize PNA purification. Injection volume 10µL. PNA Sequence: ^{C}TGTATCCAT^{N}

HPLC Conditions	Linear Gradient	Flow Rate	Retention Time (min)	Peak Isolation
1	10-30% solvent A in 15 min	2 mL/min	11.766	Good
2	10-30% solvent A in 18 min	2 mL/min	12.695	Good
3	10-30% solvent A in 20 min	2 mL/min	13.239	Good
4	10-30% solvent A in 23 min	2 mL/min	13.980	Good
5	10-30% solvent A in 25 min	2 mL/min	14.351	Good
6	10-30% solvent A in 15 min	1 mL/min	18.811	Good
7	10-30% solvent A in 15 min	3 mL/min	9.148	Poor
8	10-30% solvent A in 15 min	4 mL/min	7.736	Poor

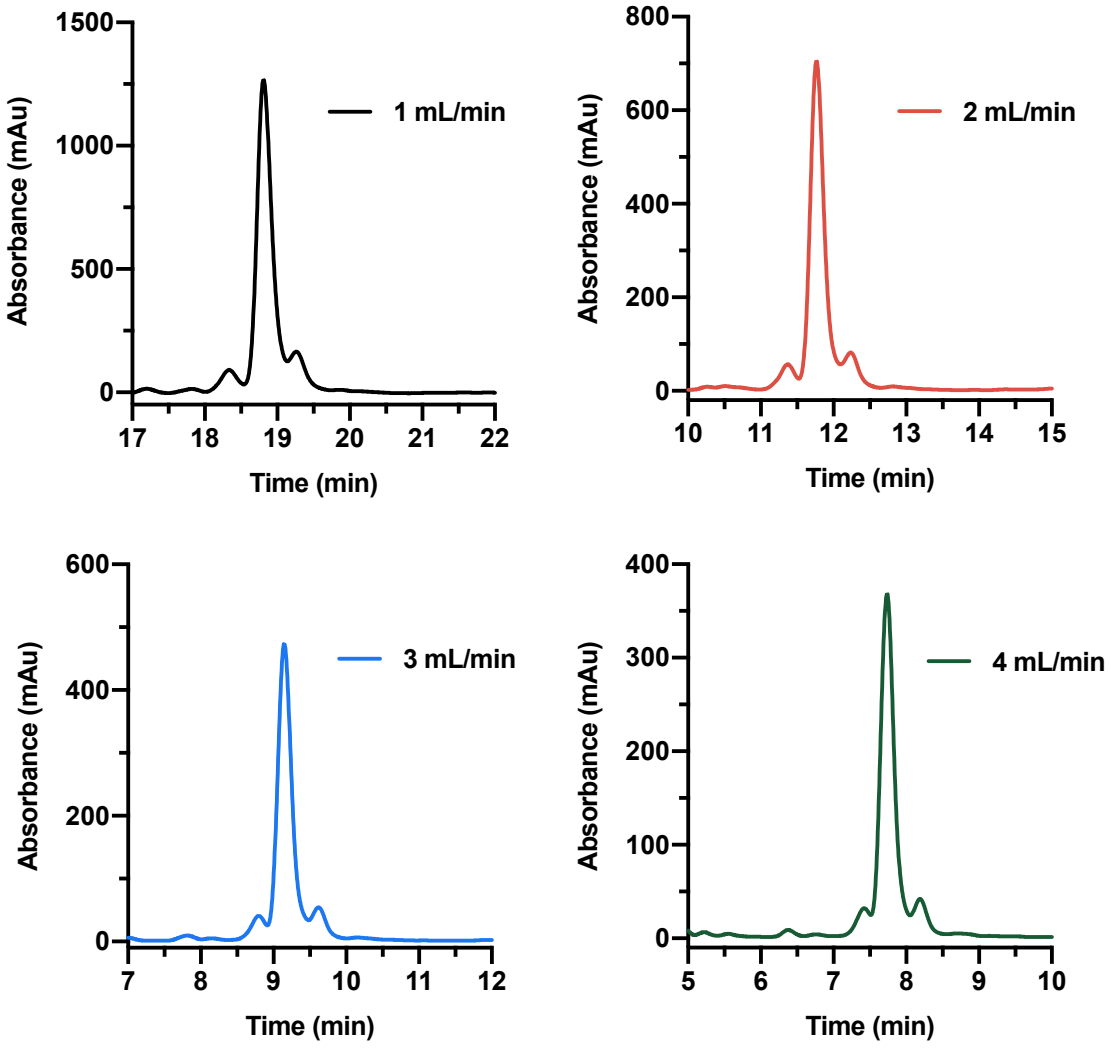

Figure D2: HPLC traces of optimized flow rate. Flow rates of 1 (black) and 2 (blue) mL/min were most capable of isolating full-length product from surrounding truncated products.

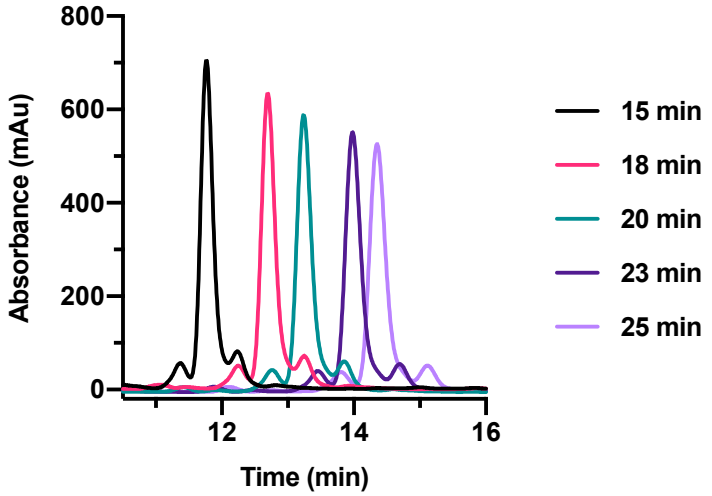

Figure D2: HPLC traces of optimized linear gradient time. Gradient was a constant 10-30% solvent A and flow rate of 2 mL/min. Increasing gradient time did not result in significantly improved separation.

Table D2: Reaction conditions tested to optimize solid-phase PNA synthesis. Each condition was tested using a sequence of ^{C}GTCAG^{N} on a 5μmols scale using 25mgs of resin.

Coupling Cycle Conditions	Loading	Capping	Coupling	Deprotection	% Purity
1	1 hour	5 min	6 min	3x1 min	74
2	2 hours	10 min	7 min	3x2 min	72
3	3 hours	15 min	8 min	3x3 min	73
4	4 hours	20 min	15 min	3x4 min	76

Table D3: Optimization of loading and capping. Positive Kaiser test indicates presence of free primary amines. Absorbance is the cumulative amount over three separate deprotection reactions.

Coupling Cycle Conditions	Amount Monomer G	Loading	Capping	Kaiser Test	Absorbance (301nm)	Total µmols	% Yield
1	3.6 mg	1 hour	5 min	Positive	2.788	3.574	74
2	3.2 mg	2 hours	10 min	Negative	2.256	2.893	67
3	3.3 mg	3 hours	15 min	Negative	2.166	2.777	62
4	3.4 mg	4 hours	20 min	Negative	2.645	3.391	74

Table D4: Optimization of coupling and deprotection for PNA T monomer. All couplings proceeded at 75°C using microwave assistance. Absorbance is the cumulative amount over three separate deprotection reactions.

Thymine PNA Monomer	Coupling	Deprotection	Absorbance (301nm)	Total µmols	% Yield
1	6 min	3x1 min	2.776	3.559	99.6
2	7 min	3x2 min	2.361	3.027	105
3	8 min	3x3 min	2.142	2.747	99
4	15 min	3x4 min	2.629	3.370	99

Table D5: Optimization of coupling and deprotection for PNA C monomer. All couplings proceeded at 75°C using microwave assistance. Absorbance is the cumulative amount over three separate deprotection reactions.

Cytosine PNA Monomer	Coupling	Deprotection	Absorbance (301nm)	Total µmols	% Yield
1	6 min	3x1 min	1.888	2.421	68
2	7 min	3x2 min	1.619	2.076	69
3	8 min	3x3 min	1.675	2.148	78
4	15 min	3x4 min	1.930	2.474	73

Table D6: Optimization of coupling and deprotection for PNA A monomer. All couplings proceeded at 75°C using microwave assistance. Absorbance is the cumulative amount over three separate deprotection reactions.

Adenine PNA Monomer	Coupling	Deprotection	Absorbance (301nm)	Total µmols	% Yield
1	6 min	3x1 min	1.677	2.149	89
2	7 min	3x2 min	1.533	1.966	95
3	8 min	3x3 min	1.591	2.040	95
4	15 min	3x4 min	1.745	2.237	90

Table D7: Optimization of coupling and deprotection for PNA G monomer. All couplings proceeded at 75°C using microwave assistance. Absorbance is the cumulative amount over three separate deprotection reactions.

Guanine PNA Monomer	Coupling	Deprotection	Absorbance (301nm)	Total µmols	% Yield
1	6 min	3x1 min	1.935	2.482	115
2	7 min	3x2 min	1.788	2.292	117
3	8 min	3x3 min	1.650	2.160	104
4	15 min	3x4 min	2.037	2.612	117

Table D8: Optimized conditions for solid-phase PNA oligomer synthesis.

Optimized Conditions	Loading	Capping	Coupling	Deprotection	HPLC Purification
	1 hour	10 min	6 min	3x2 min	Linear gradient of 10-40% solvent A in 15 min with a flow rate 2 mL/min